Dynamics of *E. coli* genome and cytosol under antibiotics

Michal Wlodarski

Department of Physics
University of Cambridge

This dissertation is submitted for the degree of
Doctor of Philosophy

Selwyn College

30 September 2017

Declaration

I hereby declare that:

- except where specific reference is made to the work of others, the contents of this dissertation are original and have not been submitted in whole or in part for consideration for any other degree or qualification in this, or any other university;
- this dissertation is my own work and contains nothing which is the outcome of work done in collaboration with others, except as specified in the text and Acknowledgements;
- this dissertation contains fewer than 60,000 words including abstract, tables, footnotes and appendices, but excluding table of contents, photographs, diagrams, figure captions, bibliography and acknowledgements, and has fewer than 150 figures.

In addition, I declare that parts of the Introduction and most of the contents of Chapter 3 of this dissertation were published previously as a peer-reviewed scientific paper (refer to Publications).

Finally, I declare that some contents of Section 1.3.1 of Chapter 1 of this dissertation were published previously as part of popular science articles (refer to Publications).

Michal Wlodarski
30 September 2017

Acknowledgements

Completion of this work would not be possible without help of many people. First and foremost, I am very grateful to Professor Pietro Cicuta for believing in me and giving me an opportunity to take on this journey; for his timely support and thoughtful guidance, no matter how challenging the circumstances. I also thank Dr Gillian Fraser who encouraged me to apply for this PhD position and who offered important advice on the direction of this research at multiple occasions during the last four years.

I also owe thanks to many talented scientists whose work made this project possible or whose insights offered significant improvements. Dr Avelino Javer had completed the ground work on loci tracking and his programmes were applied here. Dr Marco Cosentino Lagomarsino and Dr Bianca Sclavi offered extensive, very useful discussions at almost all stages of the project; and about almost all aspects of the work. Dr Jurij Kotar built and customised the microscopy set-up and continuously provided excellent technical support. Professor Kevin Dorfman and Dr Julian Struksheats offered a gift of multiple silicon wafers and helpful support on microfluidics work. Bianca Raciti contributed two summers of meticulous work on cell size analysis, strengthening interpretations of many results. Mia Panlilio developed excellent cell segmentation and tracking programme used here.

Many thanks go also to former and current members (some of whom are mentioned above) of our research group: Joachim, Tommaso, Andrew, Viola, Sho, Nicola, Omar, Ryan, Evelyn, Cornelius, Weichao, Yen-Chun, Eileen, Maurizio, Lucia, Eugenia, Emma, Tim, and Simone for creating a friendly, fun, and supportive environment. In addition, I am especially grateful to Luigi and Estelle, who at multiple occasions offered patient help at improving analysis programmes and at explaining intricacies of biology, respectively. My thanks extend beyond the group to many members of the Biological and Soft Systems division, and especially to Di, Theresa, Darshana, Fiona, Lorenzo, Otti, Karolis, Mykolas, Elisa, Anna-Lena, Ben, Michal, Dale, Siri, Atipat, Alex O., Jinglin, Kerstin, Jerome, and Jehangir with whom I shared much time at the laboratory and elsewhere, and who made this time very enjoyable. In addition, I want to thank Kim, Nora, Will, Daniel, and Richard, Suresh, and Pete for their invaluable and seamless administrative work and their supportive attitude throughout my time at the Cavendish.

I am also grateful to Professor Sabine Bahn and members of her research group, especially Santi and Jakub, who helped me build foundations for my research work at Cambridge during one of my Maser of Research degree rotation projects. In addition, I am thankful for the

academic support I received from my Director of Studies, Dr Martin Welch, my first year *viva* examiners, Dr Jim Ajioka and Dr Kevin Chalut, and my College Tutors, Dr Gavin Jarvis and Dr David Smith. I also thank Professor Ulrich Keyser and Professor Jamie Hobbs who kindly served as the PhD *viva* examiners and offered many thoughtful improvements to this work.

This effort would not be possible without amazing support from my dearest friends: Jessica, Marcos, Alex LZ, and Kyndy; and from many other fantastic friends, especially: Islam, Alex D., Agata, Jon, Migle, Ele, Eleonora, Natalia, Ola, Andrzej, Pinar, Jeroen, Tadas, Deesh, and Dirk. Finally, I am infinitely grateful to my family, and especially to my Parents and Grandparents, for their unconditional love and support.

Publications

Peer-reviewed

Wlodarski M, Raciti B, Kotar J, Cosentino Lagomarsino M, Fraser GM, Cicuta P. Both genome and cytosol dynamics change in *E. coli* challenged with sublethal rifampicin. *Phys. Biol.* 14(1). 2017. Published online.

In preparation

Wlodarski M, Raciti B, Cosentino Lagomarsino M, Fraser GM, Cicuta P. Both genome and cytosol dynamics change in *E. coli* challenged with sublethal antibiotics and sorbitol. Manuscript in preparation.

Popular science

1. Wlodarski, M. The State of the World's Antibiotics in 2015. *The Science in Society Review* by The Triple Helix Society. 25. pp. 8–10. 2016. Cambridge, UK. Published online.

2. Wlodarski, M. Outsmarted by Bacteria: The battle against antibiotic resistance. *The Science in Society Review* by The Triple Helix Society. 23. pp. 8–12. 2014. Cambridge. UK, Published online.

Abstract

In light of an urgent need for improved antimicrobial diagnostics and therapeutics, understanding bacterial behaviour, and bacterial responses to treatments in particular, is one of the key objectives of modern medical research. While the molecular mode of action of antibiotics is usually well known, their effect on the cell at a "systems" level (on the regulatory networks, metabolism, *etc*.) is only beginning to be quantitatively understood. We address some of these response phenotypes in *Escherichia coli* testing different antibiotic classes and growth conditions. We study the short ($<$15 s) time-scale fluctuation dynamics of fluorescently-tagged chromosomal loci and cytosolic aggregates, which report for the state of locus ”compaction” and the levels of macromolecular crowding of the cytosol, respectively. We improve the precision of those measurements developing a novel data treatment procedure and discover that sub-lethal doses of ciprofloxacin, rifampicin, and vancomycin as well as hyperosmotic shock conditions cause small but consistent changes (unique to each treatment agent) to the physical organisation of chromosomal Ori2 and Ter3 loci and the cytosol. We reveal, among other findings, strong correlations between the effects in different parts of the chromosome and between the chromosome and cytosol. In addition, we complement the marker dynamics work with single-cell level gene expression measurements during sub-lethal translation inhibition. Specifically, we compare responses to tetracycline and chloramphenicol from constitutive and ribosomal promoters in Ori3 and Ter3 chromosomal positions over long (7 h) treatment times in exponentially growing bacteria. We reveal, for the first time, the kinetics of cellular resource allocation and provide novel insights on globally regulated transcription, relevant to the three-component proteome partitioning model, gene-length dependent effects of the processivity of translation, and ”reversibility” of ribosome-binding antibiotics. In addition, we discover a strong correlation between the timing of responses from promoters in the Ori3 and Ter3 positions, and a small but consistent difference in the response magnitude between the two positions.

Initial remarks

Motivation and context for this work

Over the last 10-20 years, the premise that physical organisation of the nucleoid can directly influence its biological function has grown in importance, particularly in areas of chromosomal segregation [1–4] and gene expression [5–8]. In parallel, despite vast improvements in medicine such as the success of complex biologic therapeutics and the emergence of advanced gene-editing therapies and cell-based medicines against increasingly challenging diseases, untreatable bacterial infections remain one of the main causes of death and pose an increasing threat to public health worldwide [9]. Consequently, we motivate our work with the urgent necessity for improved antimicrobial diagnostics and therapeutics, and a need for more complete systems-level understanding of how antibiotics affect bacterial physiology. Through this research work we aim to improve understanding of the effects that antibiotic treatments have on the physical organisation of the *E. coli* chromosome and cytosol, and how these properties can affect biological functions of these components.

Bacterial nucleoid is now understood to show significant structural complexity and dynamics [10–12]. In recent years, a picture of the bacterial chromosome has emerged where the chromosome can be seen as as a polymer molecule suspended in a viscolelastic medium (the cytosol), where individual parts of such polymer (*e.g.*, genetic loci) sub-diffuse through a crowded environment of macromolecules, some of which (*e.g.*, nucleic acids and cytoskeletal filaments) show significant elasticity [13–15]. It follows that changes to the elastic moduli of macromolecules or to the viscosity of the surrounding medium (for example, modulated by local enzymatic processes or altered by stressors such as antibiotics) will affect the energy states of individual polymer parts [16, 17]. Given the important role of the nucleoid-associated proteins at DNA supercoil stabilisation and gene regulation, and the role of DNA topology and local energy states at transcription initiation, physical properties of genetic loci are now thought to have a significant influence on the activity of genes [16, 5].

Despite these important advancements, the exact nature of the physical interplay between the chromosome and cytosol and how they affect each other's dynamics and biological function, including response to treatments, remain subjects of study and debate [18–20]. In this work, we gain insight into the physical properties of the chromosome and cytosol of live antibiotic-challenged bacteria, using a "microrheology" technique that allows us to track intracellular

fluorescent markers, whose short time-scale displacements report for – we speculate – the local state of "compaction" of genetic loci and the level of molecular crowding of the cytosol. The majority of work involving tracking of chromosomal markers so far have focused on the segregation dynamics (*e.g*, [3]), with only a limited number of studies characterising the physical structure of the chromosome at the local level [21, 13, 14, 22]. Of those, several used antibiotics but only at relativity high doses and limited exposure times to shut down specific cellular processes but none provided systematic analysis of the physical effects excreted by antibiotics.

In response to these critical gaps in understanding of antibiotic effects, we first improve the precision of our measurements developing a crucial data treatment procedure and then perform a systematic study of how sub-lethal doses of clinically important classes of antibiotics and hyperosmotic shock conditions alter these physical properties in bacteria cultured in different growth conditions. Finally, we complement the biophysical measurements with gene expression experiments: by combining microscopy and microfluidics methods, we measure high-throughput single-cell level kinetic responses in gene activity under translation inhibition in populations of exponentially growing bacteria. We investigate how the position of a gene in the chromosome affects its activity depending on what type of promoter (constitutive of regulated) controls its expression. As a result we offer a number of novel insights about the kinetics of the compensatory cellular resource allocation during treatment with different translation inhibitors, and about position-dependent differences in gene expression responses to treatment.

Overview of individual chapters

Chapter 1 serves as an introduction to this PhD work and presents current state of knowledge on the *E. coli* nucleoid, its physical properties and biological function, antibiotics, single-cell level microscopy, and chromosomal and cytosolic dynamics. It also outlines gaps in our understanding of these areas and explains how this work attempts to improve our understanding of these topics.

Chapter 2 presents the methods employed to answer the research questions set out in this work. Specifically, it outlines the details about the bacterial strains, laboratory techniques, experimental set-ups, and image processing and data analysis protocols.

Chapter 3 explains our data treatment developments which account for fluorescent marker photo-bleaching and size-displacement dependence. This empirical data correction procedure serves as a foundation for the next chapter providing a precise way to quantify marker displacements over time, critical for investigating effects of antibiotics.

Chapter 4 presents and discusses our systematic study of how various sub-lethal antibiotic treatments and hyperosmoic shock conditions affect the short time-scale dynamics of the chromosomal and cytosolic markers, and discusses relationship between effects in different parts of the chromosome and between the genome and the cytosol.

Chapter 5 complements the biophysical measurements of previous two chapters with a high-throughput single-cell level study on how chromosomal positions of genes affect kinetic responses in gene activity to different translation inhibitors.

Chapter 6 draws conclusions from the previous chapters and outlines possible directions of future work.

Appendices A-C contain supplementary materials to chapters 3-5, respectively, Appendix D presents key findings gathered after the submission of this dissertation (added after the PhD *viva* examination), and Appendix E outlines past communications of this research work and attended educational events.

Table of contents

Chapter 1

Introduction

1.1 *E. coli* and its nucleoid

1.1.1 *E. coli* bacterium

Bacteria form a separate domain of life and belong to prokaryotic microorganisms [23]. They are simpler than eukaryotes: for example, do not have distinct organelles and intracellular membranes, and are three orders of magnitude smaller in volume than a typical mammalian cell. At the same time, bacteria present extensive complexity of life and show an extraordinary ability to adapt to the changing environment adjusting their biology to the varying metabolic requirements [24, 25].

E. coli is a model organism in cell biology and by far the most comprehensively characterised bacterium with many details of its structural, genetic, and molecular biology relatively well understood. This rod-shaped, Gram-negative, facultative anaerobic bacterium reproduces asexually through binary fission to produce, in principle, two genetically identical daughter cells from each mother cell [26]. Typically, it follows logistic growth dynamics, consisting of the lag, exponential, stationary, and death growth phases – with the reduction in the growth rate and the cell death occurring primarily due to nutrient depletion and toxic metabolite accumulation. Its growth rate can vary widely, for example in a bulk liquid culture, the doubling time ranges between 20 minutes and several hours, depending on the strain cultured, nutrient composition, temperature of the medium, and degree of culture aeration [25].

The relatively well understood biology and short doubling times are some of the reasons why we chose *E. coli* for this work. Other important reasons include its ease of handling, culturing, and manipulating in laboratory conditions, relevance to clinical practice, and compatibility with existing image processing protocols. Moreover, the majority of the genome and cytosol dynamics studies, including the work of A. Javer *et al.* – whose project directly preceded this one and provided many of the methods applied here (refer to Section 2.6) – were completed using *E. coli* as the model organism [14, 22].

Formation of colonies and multi-species communities are important aspects of bacterial growth affecting physiology of individual bacteria and the speed of evolutionary adaptation.

As *E. coli* uses horizontal gene transfer to exchange genetic material, its denser communities, characterised by spatially inhomogeneous metabolic requirements (*e.g.*, as in biofilms [27, 28]), promote genetic variation and differentiated gene expression as well as provide mechanical protection for the colony and limit the population exposure to toxins. The growth complexities outlined above make eradication of infections more challenging. With bacterial physiology depending heavily on growth conditions, we studied *E. coli* in two different conditions: as standard microcolonies on agarose pads and as planktonic cultures in a customised microfluidic device (refer to Section 2.3, Methods). The latter condition also provided a crucial advantage of long (13 h) experiments, important in studying bacterial responses to antibiotics (refer to Chapter 5).

While invaluable in the laboratory, *E. coli* is also important in the clinic. Although most *E. coli* strains are non-pathogenic and constitute beneficial human flora, several pathotypes exist and can cause acute and traveller's diarrhoea [29], urinary tract infections (UTIs) [30], and contribute to Crohn disease development [29]. While many *E. coli* infections are self-limiting, some – such as the UTIs – need to be controlled with antibiotics (usually ciprofloxacin or trimethoprim [30]), and some – such as those caused by the multi-drug resistant extended-spectrum beta-lactamase *E. coli* – may require surgical interventions [31].

In light of an urgent need for improved antimicrobial diagnostics and therapeutics [32–34], understanding bacterial behaviour and bacterial responses to treatments is one of the key objectives of modern medical research. Despite many attempts to provide a more complete picture of antibiotic effects (*e.g.*, [35]), systems-level physiological responses such as effects on gene regulatory networks and on the macromolecular composition of cells (*e.g.*, the concentration of ribosomes, protein-DNA ratio) remain largely unexplored. In this work, we study some of such responses in *E. coli* by exploring effects of a variety of antibiotics on the organisation of the genome and the cytosol, and how physical properties of those components may affect expression of genes.

1.1.2 Levels of nucleoid organisation

In the last 40-50 years, enormous amount of evidence has emerged that the bacterial chromosome has a remarkable level of spatial and temporal organization (reviewed in [36]). *E. coli* bacterium stores most of its genetic code in a form of a single circular chromosome. The chromosome consists of about 4.7 million base pairs and has a total length of approximately 1.5 mm [37]. The chromosome structure shows multiple levels of organisation starting at the level of the DNA strands which interact with themselves, RNA, and associated proteins: first locally – forming bends and loops, then at intermediate length scales – giving rise to numerous supercoil domains, and then globally – forming several million base-pair long macro domains.

Plectonemic and toroidal loops The helical nature of DNA [38], its closed circular form, and the under-wound state (fewer helical loops than expected for given DNA piece in a relaxed state) cause the bacterial DNA to bend and form plectonemic and toroidal loops (supercoils)

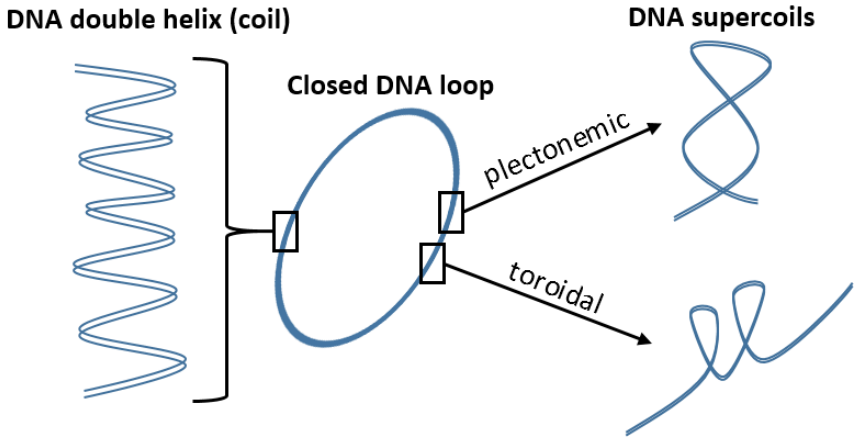

Fig. 1.1 **Schematic representation of DNA supercoiling.** The helical nature of DNA, its closed circular form, and the under-wound (thermodynamically strained) state cause the DNA molecule to bend forming plectonemic and toroidal supercoils. DNA supercoils (stabilised by active processes) constitute the basic level of chromosomal organisation and generally allow for improved access to genetic information stored in DNA.

(Figure 1.1) [39]. This thermodynamically strained supercoiled state (stabilised by active processes) generally allows for improved access to genetic information stored in DNA and constitutes the basic level of chromosomal organisation.

DNA supercoil domains Torsionally constrained chromosomal DNA forms approximately 500 supercoiling domains [40]. Consequently, the *E. coli* chromosome is generally a negatively supercoiled structure, meaning its linking number – the number of times each single strand of DNA winds around the other – is lower than in the relaxed configuration. This widespread negative supercoiling is critical to its function: expression of hundreds of *E. coli* genes depends on suitable negative supercoiling levels [40].

Chromosomal macrodomains Macrodomains govern the global organisation of the bacterial chromosome and were first identified as parts of the chromosome localised in specific intracellular locations [41]. There are four macrodomains (Ori, Right, Ter, Left) which do not interact with each other and two non-structured (NSR, NSL) regions which can interact with its neighbouring macrodomains. By fluorescently tagging specific chromosomal loci, macrodomains were shown to have lower loci motilities compared to the non-structured regions [42]. In addtion, MatP, SeqA and SlmA proteins were demonstrated to be macrodomain-specific [43].

Nucleoid-associated proteins Key architectural component are the nulecoid associated proteins (NAPs) (Figure 1.2). Twelve distinct NAPs were identified in *E. coli* [44] and include the major 'exponential growth phase' NAPs (Fis, H-NS, IHF, and HU), starvation-induced protein (Dps) which is important in the stationary phase of the population growth curve [45],

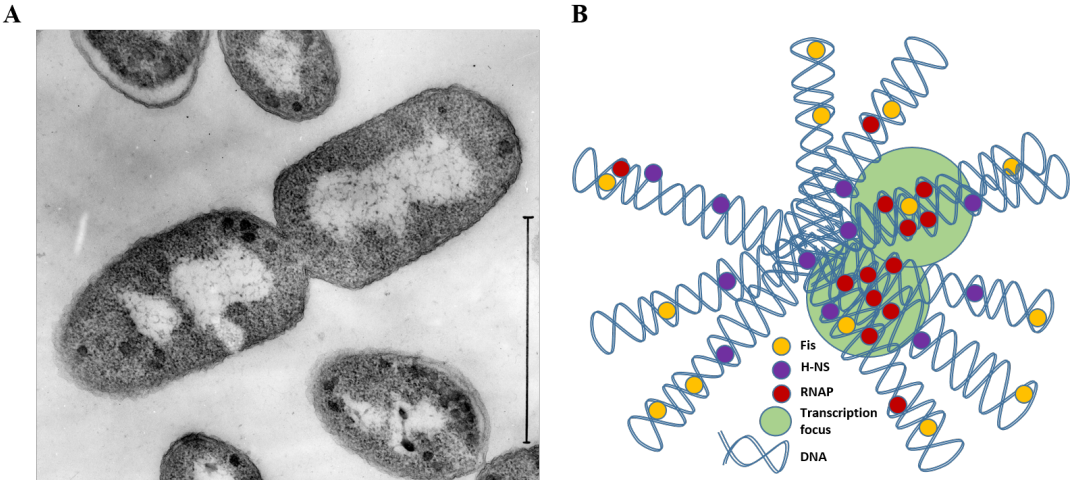

Fig. 1.2 ***E. coli* nucleoid and a schematic model of its organisation by the nucleoid-associated proteins (NAPs) and RNAP.** (**A**) An electron micrograph of a longitudinal thin section of a dividing *E.coli* bacterium. The centrally located (white) nucleoid is prominent. Original magnification $\times$12,000; vertical bar represents the length of 1 μm. Image is available under a Creative Commons Attribution (Non-Commercial Share Alike License; CIL: 37254). (**B**) Folded chromosome is organised into negatively supercoiled looped domains (and stabilised) by NAPs such as the exponential phase Fis and H-NS. In addition, at fast growth, RNAP forms superstructures (transcription factories).

and also Lrp, MukB, StpA,CbpA, CbpB, EbfC, and MvaT [18, 46, 47]. These proteins not only contribute to maintenance of the under-wound state of DNA critical for information access but are also responsible for DNA wrapping (*e.g.*, HU, Fis), bridging (*e.g.*, Fis H-NS, StpA), bending (*e.g.*, HU, Fis, IHF), and ultimately can bring together geographically distant genes into co-regulated clusters, and contribute to chromosomal macrodomain formation [19, 47, 46]. In addition, at fast growth, RNAP organises superstructures termed transcription factories (or foci) where active transcription of rRNA genes occurs [48].

1.1.3 Importance of nucleoid compaction

As the *E. coli* DNA is several orders of magnitude longer than the cell length, it must be organised and packaged with associated proteins and RNA into a compact structure called the nucleoid [37, 18]. The strong compaction of nucleoid arises from a combination of forces generated by cellular confinement, macromolecular crowders, interactions with proteins (*e.g.*, NAPs and enzymes), self-adherence, DNA supercoiling, and transcription [16, 49].

Cellular confinement Packing of the chromosomal material into a small volume of a cell produces strong forces which compact and reduce the size of the nucleoid [16]. However, confinement occurs in the radial and not the longitudinal dimension. This is implied by non-septating cells containing discrete nucleoid structures as well the pre-replication ('G1') nucleoid in normally dividing cells not extending to the end of the cells but extending into the cell periphery in the radial direction [10].

Macromolecular crowding The intracellular concentrations of macromolecules tend to be much higher in bacteria than in eukaryotes. In the crowded environment of the bacterial cytosol (refer to Section 1.5.4), proteins and larger protein-nucleic acid structures such as ribosomes cannot diffuse freely due to significant steric hindrance. In such conditions, entropic forces cause the chromosome material to reduce its size through depletion-attraction interactions for other molecules to have more space and less steric constrain [20, 19, 18].

Self-adherence There is a tendency for coalescence of chromosomal material [10]. Imaging reveals that virtually all of the chromosomal DNA is part of the nucleoid [50, 1] and also, that during the replication and segregation processes, the newly replicated material can be observed to protrude in elongated shapes [1]. Moreover, the relative fixed positions of chromosomal loci and pairs of loci also imply self-adherence of the chromosome.

DNA-protein interactions The activity of type II DNA topoisomerases determines the torsional constraint of the chromosome as explained previously. The nuceloid shape modulation by the NAPs can add to the mechanical forces acting on the chromosome with DNA bending and wrapping. Finally, transcription and translation processes contribute to the modulation of the physical structure of the nucleoid – locally with multiple copies of RNA polymerase enzymes forming transcription foci [51] and globally as a consequence of transcription-translation coupling mechanisms [37].

Transcription In bacteria, the processes of transcription and translation are physically linked. As RNAP transcribes DNA into messenger RNA (mRNA), the newly synthesised mRNA molecule elongates away from the nucleoid surface into the cytoplasm where it is simultaneously translated in by polysomes (ribosome complexes). If the synthesised protein is transmembrane, the resultant DNA–RNAP–mRNA–polysome–protein–membrane chain exerts an expanding 'transertion' force on the nucleoid (Figure 1.3). Transertion can be viewed as a highly dynamic process in which multiple membrane-DNA tethers are constantly formed and broken modulating the overall shape and degree of compaction of the nucleoid [52, 53, 48, 17].

As part of the 'DNA-ribsome mixing' theory, transertion is also important for ensuring optimal use of RNAP and ribosomes. In exponentially growing cells, the expanding force of transertion allows the 30S and 50S ribosome components to enter the nucleoid and initiate translation and thus to contribute to the nucleoid expanding forces in a positive feedback loop [54]. Co-transcriptional translation is thought to provide protection of nascent mRNA from degradation by ribonucleases and to increase translation efficiency. It is also evident that under favourable growth conditions, the majority of ribosomes form polysome complexes that do not mix with the nucleoid material. Following translation initiation, the 70S ribosomes diffuse out of the nucleoid into ribosome-rich regions. This dynamic picture of the DNA-ribosome mixing model implies circulation of ribosome components and presents gene expression as

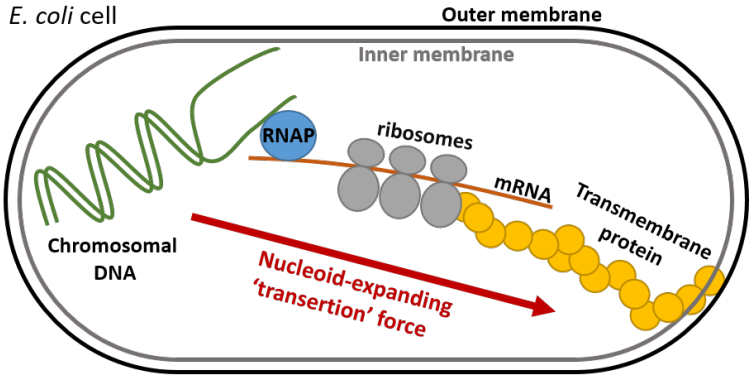

Fig. 1.3 **Schematic representation of the origins of the nucleoid-expanding 'transertion' force.** In bacteria, transcription and translation are physically linked. The newly synthesised mRNA molecule elongates away from the nucleoid surface and is simultaneously translated. If the synthesised protein is transmembrane, the resultant DNA–RNAP–mRNA–polysome–protein–membrane chain exerts an expanding 'transertion' force (*red arrow*), which can be viewed as a highly dynamic process in which multiple membrane-DNA tethers are constantly formed and broken modulating the shape and degree of compaction of the nucleoid.

highly interlinked with the physical system of the cell [17].

In addition to those introduced above, numerous other factors such as signalling and alarmone [55] molecules play a role in altering the local DNA topology and the levels of local DNA physical compaction. By modulating these parameters, the cell must ensure sufficient energy (level of negative supercoiling) is available to enable key biological processes such as DNA replication and transcription. In this picture, the local physical properties of a bacterial chromosomal locus reflect the nature of its nucleo-protein environment and can directly influence its biological activity.

1.2 Gene expression in *E. coli*

1.2.1 Growth-rate dependent gene regulation

Regulation of *E. coli* genes in response to environmental clues can be achieved with transcription factors binding directly to the DNA and thus blocking access of transcription machinery to the promoter (reviewed in [56]). Transcription factors 'sense' changes in the surroundings by direct binding to ligands or protein, by covalent modification, or by changes in their intracellular availability. These regulatory proteins achieve binding specificity with structural motifs that are 'cognate' to the DNA base sequences. Specificity can be further enhanced with a number of mechanisms including multimerisation of the transcription factor.

In addition to regulation with transcription factors, expression of a large number of genes can be intrinsically regulated by the global physiological state of a bacterium [25]. For *E. coli*, a variety of parameters such as gene copy number and transcription rate, the macromolecular

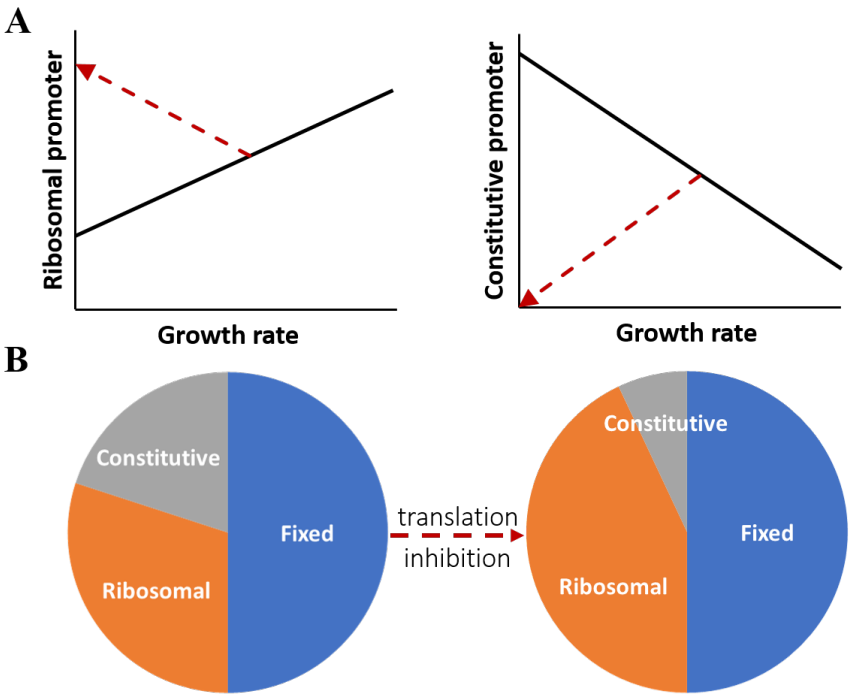

Fig. 1.4 **Global transcription regulation enables efficient resource allocation to achieve balanced growth in changing environment.** **(A)** Schematic representation of how the activity of ribosomal (*left*) and constitutive (*right*) promoters changes as a function of growth rate. As nutrient conditions improve and the growth rate increases, the activity of ribosomal promoters is stimulated (*e.g.*, through the decrease in the (p)ppGpp concentration – refer to Section 1.2.1) to meet the high demand for protein synthesis. At the same time, as cellular resources are allocated to ribosomal promoters, expression of constitutive proteins decreases. **(B)** Schematic representation of the three-component proteome partition model at translation inhibition. The simplest constraint to cellular resources includes three protein fractions: fixed (*blue*; estimated at 50% for *E. coli* and invariant to growth-rate dependent regulation), ribosome and ribosome-affiliated (*orange*), and constitutive (*gray*). Dose-dependent effects of translation inhibition on both promoters operating at fixed nutrient conditions are depicted in **(A)** as *dashed red arrows*, with the inhibitor's dose increasing in the arrow's direction. Translation inhibition causes compensatory production of ribosomes at an expense of constitutive protein synthesis. Adapted from [60].

composition of the cytosol (including protein-to-DNA ratio and the number of RNAP molecules and ribosomes), and the total cell mass and size, were shown to depend strongly on the growth conditions, with strong correlations between individual gene expression levels and the growth rate rather than specific nutrient concentrations [57–59, 25]. Such global gene regulation can have significant population effects. For example, in case of toxic (growth-limiting) gene products, growth-rate dependent regulation can constitute a positive feedback mechanism and even without specific regulation lead to bistability and emergence of antibiotic-tolerant sub-populations (Section 1.3.4). Similarly, growth-promoting expression of constitutive antibiotic resistance conferring genes can result in bistability in the presence of antibiotics [25, 24].

Global gene regulation provides efficient and highly sophisticated mechanism of response to, for example, stressors such as antibiotics or changes in metabolic requirements. One key example is the regulatory action of an alarmone molecule, guanosine tetraphosphate and pentaphosphate, collectively termed (p)ppGpp, which exerts differential gene regulation depending on the promoter type [61–63]. The ribosome-associated RelA protein senses amino acid scarcity by synthesising (p)ppGpp, which then interacts with RNAP but affects transcription from only a subset of promoters. Different kinetic properties of promoters determine differential outcomes of (p)ppGpp action: as (p)ppGpp decreases stability of the open complex (melted, RNA-bound promoter region), it reduces transcription of intrinsically unstable complexes [63].

Such mechanism enables efficient resource allocation to achieve balanced growth in changing environment: if nutrient conditions improve and the growth rate increases, the (p)ppGpp concentration will decrease, stimulating the activity of ribosomal promoters to meet the high demand for protein synthesis. At the same time, as cellular resources such as RNAP and transcription factors are allocated to ribosomal promoters, expression of constitutive proteins will decrease (Figure 1.4A) [64, 60, 65, 66]. Globally regulated transcription also helps bacteria face antibiotic-induced translation inhibition, which – similarly to improved nutrient conditions – causes a build-up of intracellular amino acids and results in a compensatory production of ribosomes at an expense of constitutive protein synthesis [60] (Figure 1.4B).

1.2.2 Role of the nucleo-protein environment of a genetic locus

While highly condensed, the physical organisation of the nucleoid must allow for efficient and flexible gene expression [44, 16] as well as protein diffusion, and DNA replication and segregation [67, 16]. Recent evidence suggests that changes to the local chromosome organisation can directly affect the accessibility of genes and the activity of regulatory proteins [16]. A variety of gene expression regulators capable of modulating local DNA organisation and energy levels have been identified and include: action of specific NAPs, nature of local DNA topology and changes to the supercoiling levels, and fluctuations in the concentration of metabolites such as (p)ppGpp.

NAPs binding heterogeneity Most bacterial NAPs show preference for binding to curved or AT-rich DNA regions. For example, HU, H-NS, and IHF all have higher binding affinity to curved DNA [68] while Fis, StpA, MvaT and also H-NS and IHF bind strongly to AT-rich regions [46]. When DNA-bound, NAPs can act as typical transcription factors, either stabilising or inhibiting RNAP-promoter interactions [44]. In addition, NAPs can affect gene expression by modulating local DNA supercoiling levels and changing DNA strand topology [49]. Specific examples of NAP binding patterns and NAP-dependent regulation include: the compacting and regulatory HU activity correlated with levels of negative superhelicity [69] and DNA gyrase binding [69]; Fis activating activity of stable RNA promoters at low negative supercoiling regions [70]; and formation of extended binding domains by H-NS in

high affinity binding sites to silence transcription via plectoneme stabilisation and RNAP trapping [71, 46, 72, 73].

Normal bacterial growth depends heavily on NAPs activity. A number of specific NAP-coding gene null mutants showed significant changes in the cellular motility, metabolism, and virulence [74]. Antibiotic sensitivity was also affected, with *infA* and *fis* null mutants displaying hypersensitivity to ciprofloxacin and with the *hns* null mutant displaying hypersensitivity to rifampicin, vancomycin, and other antibiotics [75]. In addition, large scale gene silencing mediated by IHF and other global regulators, combined with the nucleoid condensation controlled by the Dps protein is thought to underpin some of the bacterial survival 'bet-hedging' strategies [76, 77].

DNA supercoiling The level of DNA supercoiling has a global effect on gene expression [78, 49]. More than 300 supercoiling-sensitive genes were identified with approximately one-third of these genes increasing their activity if the level of negative supercoiling is reduced, while the remaining two-thirds having the opposite response [79]. TopoIV and DNA gyrase enzymes control the level of supercoiling [80]. This is important for gene expression as the mechanical stress carried by the supercoiled configuration can locally weaken the attraction between the DNA strands. The resultant breaking of base-pair bonds between the two strands is required for the transcription machinery to reach relevant gene regions in order to initiate transcription [16]. In addition, as protein discriminate between different spacing between DNA strands, the level of supercoiling is important for the protein-DNA interactions [46], which in turn have an influence on the chromosome organisation and on the gene expression regulation [81].

Small molecule metabolites Small molecule metabolites such as nucleoside triphosphates (NTPs) [82, 83] and (p)ppGpp can affect RNAP-promoter interactions exerting global regulatory effects described earlier (refer to Section 1.2.1). In addition to its widespread effects on transcription, (p)ppGpp contributes to replication, translation, and metabolism regulation to allow stress survival; coordinates these processes to prevent conflict during stress; and contributes to emergence of antibiotic 'tolerance' (or 'persistence') and resistance [84].

Among promoters strongly affected by regulatory factors introduced in this Section are those involved in growth rate modulation, growth phase-dependent adaptation, and stress responses to nutrient alterations and toxins (*e.g.*, the SOS response, refer to Section 1.3.4). One of the promoters studied in this work is the *rrnB*P1 (refer to Chapter 5), a well characterised ribosomal promoter regulated by the global regulators introduced above. Conversely, in this work we also include a constitutive P5 promoter which is not regulated and whose activity depends on availability of gene expression machinery components such as RNAP and transcription initiation (sigma) factors (refer to Section 1.2.1).

1.2.3 Importance of the genomic position

Locus distance from the origin of replication is an important factor affecting expression of a gene [6]. There are at least four reasons why occupying a specific position along the chromosome will influence the activity of a genetic promoter.

First, at fast growth, when the doubling time is shorter than the duration of chromosome replication, new rounds of DNA replication begin before the previous ones terminate. In cells undertaking such 'multifork DNA replication' [85, 26], the gene copy number is larger for genes closer to the origin of replication, generally leading to a higher gene product yield for these genes.

Second, DNA gyrase binding site density is higher in regions closer to the origin of replication [78]. As gyrase plays a crucial role of relieving topological tension formed by the transcription machinery moving down the double-stranded DNA ahead of the transcribing RNAP [86], it can reduce high levels of positive supercoiling arising in the Ori half of the genome during increased gene expression (in the exponential growth phase) in that part of the chromosome [87].

Next, heterogeneous distribution of NAPs along the chromosome can contribute to the formation of co-regulated gene clusters, as outlined earlier (refer to Section 1.2.2). Consequently, the same gene, acquired via intra-/inter-genomic or horizontal gene transfer [88], may experience, depending on its position in the genome: high expression levels making use of existing regulatory mechanisms or low expression levels, for example being silenced in an extended binding domain formed by H-NS.

Finally, position in the genome is important due to local effects resulting from the orientation of neighbouring genes. Convergent transcription can lead to transcription interference (TI) where the RNAP transcribing a neighbouring gene does not stop and clashes head-on with the incoming transcription complex [89]. Depending on the promoter strengths (and thus the number of RNAP molecules at a gene and transcription initiation frequency) of the two convergently transcribed genes, the probability of successfully transcribing the whole gene without interference may vary considerably [90]. Conversely, divergent transcription of a neighbouring gene can result in increased gene expression rates due to the local negative supercoiling build-up behind the transcription complex [91]. Interestingly, divergent gene orientation is more common in *E. coli* genome that the convergent one [92, 90]. Remarkably, presence of Fis and H-NS binding sites near the promoter region can effectively insulate promoters from the effects from neighbouring genes [*private conversation with Dr Bianca Sclavi, ENS Cachan, Université Paris-Saclay*].

Although gene expression regulation mechanisms, gene cluster formation and activity, NAPs binding site distributions across the genome, and even some physical properties of individual chromosomal loci were studied previously, it remains unknown whether exposure to antibiotics can affect the physical organisation of the genome and how these effects vary for different

genomic positions. Further, it is currently unclear whether the widespread antibiotic-induced changes to gene expression reported previously are chromosomal position- and promoter type-dependent.

1.3 Antibacterial treatments

1.3.1 Importance of antibiotics and the problem of resistance

Antibiotics revolutionised medicine by providing accessible, non-invasive means of combating previously untreatable and often highly contagious infectious diseases. These agents have been in use for more than 70 years and saved countless lives [93]. However, their use was associated with a rapid development of resistant bacterial strains rendering many of antibiotics ineffective [93, 94]. First cases of ineffective therapies were observed soon after the introduction of antibiotics with resistance to important antibiotic classes reported in 1930–50s. Nowadays, each of the major groups of antibiotics, including penicillin derivatives, tetracycline, quinolones, and glycopeptides, confronted clinically significant organisms exhibiting resistance, with some microbes presenting multi-drug resistance [94].

The diminishing arsenal of antibiotics available to clinicians is now a widely recognised global problem [32–34]. Local guidelines on effective prescribing [95] and patients' adherence to anti-infective treatments as well as reports addressing global problems associated with the antibiotic use in animal husbandry and agronomy [96] were publicised. In line with these recommendations and warnings, the need for novel antimicrobial agents or more effective delivery strategies is widely expressed [97, 98]. The most recent years have seen an encouraging revival in antibiotic development, partly due to the Generating Antibiotic Incentives act and the Innovative Medicines Initiative scheme, with three first-in-class antibiotics discovered in 2011, 2012, and 2017 [99] (Figure 1.5). However, given that in Europe alone 25,000 people die every year of antibiotic resistant bacteria the need for improvement is vast [9].

It is recognised that the gaps in understanding of microbial biology and especially the limited insight into the genetic and functional basis of resistance development fundamentally hinder the long-awaited progress [32, 98]. It is the scientific progress in the understanding of the biology of microbes that has a chance to propel the industrial innovation towards novel more accessible means of antimicrobial therapies, provide policy makers with more manageable solutions, and therefore facilitate the disease management for the prescribers and their patients.

1.3.2 Modes of action of antibiotics

Clinically successful antibiotics must show selective toxicity, meaning they must be toxic to the pathogen and innocuous to the host. Selective toxicity relies on the ability to exploit the differences between the pathogen and the host biochemistry. Three broad classes of reactions can be distinguished representing potential targets for antibiotics [100]: utilisation of a carbon source material for the production of ATP and simple precursor carbon compounds; utilisation

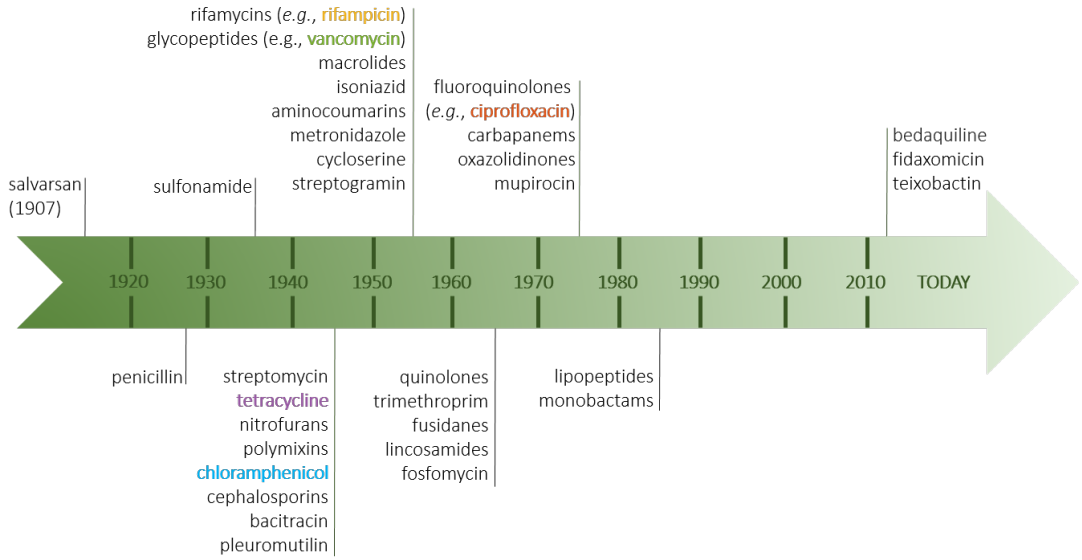

Fig. 1.5 **Timeline of antibiotic discovery.** Schematic not-to-scale representation of when some of the distinct classes of clinically used antibiotics were discovered. Discovery or patent dates were used and rounded to nearest decade. Antibiotic "discovery void" starting in 1980s is prominent. After 2010, encouraging revival in antibiotic development has seen the discovery of three first-in-class antibiotics. Antibiotics used in this work are shown in colour.

of those precursors in synthesis of small molecules necessary for cell growth (*e.g.*, amino acids, phospholipids, carbohydrates, growth factors); assembly of those small molecules into macromolecular structures (*e.g.*, proteins, RNA, DNA, polysaccharides, peptidoglycan). Drugs used in this work are clinically important antibiotics that interact with with bacteria-specific enzymes or structures to inhibit assembly of macromolecules (Figure 1.6): DNA (ciprofloxacin; targets DNA gyrase), mRNA (rifampicin; targets RNA polymerase), protein (tetracycline and chloramphenicol; target the ribosome), and peptidoglycan (vancomycin; targets peptide subunits of peptidoglycan). Their pharmacology is characterised below.

Ciprofloxacin Ciprofloxacin is an example of a fluoroquinolone (a group of clinically significant quinolones) and is active against Gram-positive and Gram-negative bacteria (broad spectrum). It acts by inhibiting the bacterial type II topoisomerases activity. In *E. coli* its primary target is DNA gyrase [101], however, it also affects the activity of topoIV [102]. By inhibiting topoisomerases, it prevents DNA replication (and thus segregation) and transcription [100, 103].

Rifampicin Rifampicin is classified as an antimycobacterial agent due to its prominent role in the treatment of infections caused by mycobacteria (*e.g.*, tuberculosis) [104]. However, it is active against most Gram-positive and many Gram-negative bacteria. It binds to and inhibits the activity of bacterial RNAP and thus inhibits transcription and indirectly prevents protein synthesis [100].

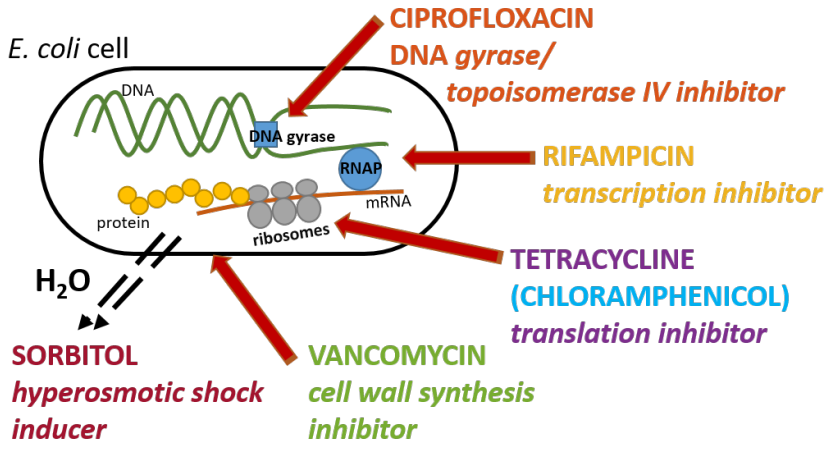

Fig. 1.6 **We test effects of sub-lethal doses of antibiotics from four major antibiotic classes and a hyperosmotic shock inducing agent, sorbitol.** Tested antibiotic classes include: DNA replication (ciprofloxacin), transcription (ciprofloxacin and rifampicin), translation (tetracycline and chloramphenicol), cell wall synthesis (vancomycin) inhibitors. Figure shows a schematic representation of primary modes of action of each agent. Red arrows point to the main molecular targets. Dashed lines represent movement of water. RNAP, RNA polymerase; mRNA, messenger RNA.

Tetracycline Tetracycline is a broad spectrum polyketide antibiotic which exerts its bacteriostatic effects primarily by binding reversibly to the 16S rRNA of the bacterial 30S ribosomal subunit. As a result, it inhibits peptide elongation as incoming aminoacyl tRNA cannot bind to the ribosome acceptor site [105]. Another broad spectrum antibiotic, **chloramphenicol** (refer to Chapter 5) has a similar mode of action to tetracycline, however, its main binding site is in the 23S rRNA of the 50S ribosomal subunit [106].

Vancomycin Vancomycin belongs to a group of glycopeptide antibiotics and although used clinically to treat Gram-positive infections, at high concentrations it can exert bactericidal effects also in Gram-negative bacteria. It acts by inhibiting the bacterial cell wall synthesis. Specifically, it binds to D-alanyl-D-alanine moieties of the side peptides of the NAM and NAG residues of peptidoglycan. Binding prevents the NAM-NAG strands from cross-linking [107]. As a result, the strong polymeric lattice is not formed and the cell cannot maintain its internal osmotic pressure [100]. Notably, at concentrations used in the clinic, vancomycin does not penetrate into the cytoplasm [108].

1.3.3 Effects of antibiotics on bacterial growth

Treatment-induced change to the bacterial growth rate constitutes the most basic and clinically most relevant effect and it has been studied extensively since the discovery of these agents (*e.g.*, [109]). Effects of antibiotics are traditionally divided into bacteriostatic – when the bacterial growth rate is inhibited, and bactericidal – when the treatment results in cell death. In reality, assigning antibiotics to one of these two groups is not feasible as any antibiotic

will kill bacteria if given at a high enough dose. In clinical practice, so called 'bactericidal' drugs usually fail to kill every organism within the standard 18–24 h after the test, and most of so called 'bacteriostatic' agents do kill some bacteria within that period of time. The effects on growth of individual strains are usually reported in terms of the minimal bactericidal concentration (MBC) at which $\geq 99.9\%$ of bacteria are killed and the minimal inhibitory concentration (MIC) at which visible growth is inhibited. Formally, an effect against a specific bacterial strain as measured under standardised conditions is classified as bacteriostatic when its MBC to MIC ratio is > 4 [110].

Treatment efficacy can be largely affected by environmentally induced changes to the bacterial physiology, for example through biofilm structure formation [28], phenotypic switching to 'persister' states [111, 112] (Section 1.3.4), and responses to metabolic stimuli [113]. On the molecular level, the nature of the drug-target interaction was recently proposed to be a basis (in conjunction with the physiochemical properties of the drug molecule) of growth-rate dependent efficacy of ribosome-targeting drugs. Faster growing cells were less susceptible to bactericidal antibiotics, the opposite being true for bacteriostatic antibiotics [114].

Antibiotics used in this work are typically classified as bactericidal (with the exception of tetracycline and chloramphenicol). However, how exactly their action results in the reduction of growth rate or death is debated.

1. For **ciprofloxacin**, the net effect is the formation of DNA breaks covalently bound to topoisomerases, whose drug-induced inhibition prevents DNA replication and transcription leading to the cell division and protein synthesis inhibition, respectively. In addition, given that gyrase is distributed roughly every 100 kilobases along the chromosome, the number of resultant DNA breaks is thought to lead to substantial problems with the cell's ability to deal with the widespread DNA damage [103]. Erroneous protein synthesis is also thought to play a role in quinolone killing as protein synthesis was demonstrated as necessary for the bacteriocidal effects of several quinolones while inhibition of the SOS response (below) significantly enhanced the killing effects.

2. For **tetracycline**, reversible binding to ribosomes causes inhibition of peptide elongation and results in reduced protein production rates. As a result, bacteria remain viable, however, their growth rate is reduced [105]. The same is true for **chloramphenicol** [106]. At very high doses, secondary mechanisms may become dominant leading to bacteriocidal effects. For example, tetracycline can alter cytoplasmic membrane properties (lower membrane polarisation values) and cause leakage of intracellular components [115].

3. For **rifampicin**, its high affinity binding to RNAP suggests that at sufficiently high drug concentrations the cell death occurs as a result of insufficient protein synthesis. Given the non-reversible interaction with the target, the fact that there are approximately only 5,000 RNAP actively transcribing molecules in a cell at any moment and that mRNA

molecules experience a short 5–10 min lifetime [17], even relatively low rifampicin concentrations can prove potent and escape the compensatory RNAP production.

4. For **vancomycin**, the lytic and non-lytic cell death mechanisms were identified. Interestingly, cell lysis is thought to occur as a result of peptidoglycan synthesis inhibition and necessarily also as a consequence of active degradation of peptidoglacan by (in *E. coli*) murein hydrolyses. The non-lytic mechanisms can also lead to cell death though at lower rates and were demonstrated to involve the activation of the two-component systems controlling autolysin expression [103].

In addition to growth-inhibiting and killing mechanisms outlined above, hydroxyl radical formation was suggested as a possible common killing mechanisms of three distinct antibiotics (a quinolone, a β-lactam, and a aminoglacoside). Hydroxyl radicals are extremely toxic and readily damage proteins, membrane lipids, and DNA. Regardless of their molecular targets, the drugs stimulate hydroxyl radical formation in bacteria and contribute to the killing efficiency of these bacteriocidal drugs. It was further suggested that there is a common mechanism of cellular death underlying all classes of bactericidal antibiotics whereby harmful hydroxyl radicals are formed as a function of metabolism-related NADH depletion, leaching of iron from iron-sulfur clusters, and stimulation of the Fenton reaction [116].

1.3.4 Complexity of bacterial response to antibiotics

In addition to adjustments in the growth rate, bacteria respond to antibiotics by changing their morphology, macromolecular composition, metabolism, gene expression patterns, and even DNA mutation rates [117]. The nature and dynamics of such responses is incredibly complex and will depend on the antibiotic class, dose, exposure time, as well as bacterial growth phase, rate, and environment. The fact that bacteria can use antibiotics as signalling molecules to coordinate multicellular processes within a population, for example in antibiotic-induced biofilm growth [118, 119], exemplifies both the complexity and elegance of such responses. Their multi-factorial nature points toward the network- and systems-like character of responses to antibiotics, where a number of distinct (*e.g.*, genetic, metabolic, structural) cellular processes interact over time to adjust global physiology in order to ultimately avoid death or even to make use of the antibiotic.

Different facets of antibiotic effects have been studied in the past. It is known, for example, that exposure to an antibiotic may change the expression rate of a specific gene or gene cluster to directly compensate for the drug's action, for example by increasing the number of target protein to compensate for its inhibition or to synthesise machinery to repair antibiotic-induced damage [120, 121, 35]. Also, through global changes to the physiology (*e.g.*, effects on the growth rate), antibiotics alter global gene expression patterns [120, 121, 35], with the total number of genes affected varying significantly for different antibiotics [35]. Further, some antibiotics affect macromolecular composition, including protein-to-DNA ratio [122], and the RNAP [64] and ribosome concentrations [60], among other, while some were reported

to change concentrations of second messengers (*e.g.*, [119]) and (p)ppGpp [61], further contributing to widespread gene expression changes.

Despite attempts to provide a more holistic picture of antibiotic effects, systems-level physiological responses such as effects on gene regulatory networks and on the macromolecular composition of cells remain largely unexplored, especially on the quantitative level. It is believed that combined theoretical and experimental efforts are necessary to more fully understand bacterial responses to antibiotics (and their combinations), and to ultimately devise more effective antibacterial treatments [117].

In addition to various changes in physiology, bacteria have evolved efficient damage-mitigating mechanisms. For example, the SOS response is a global DNA-repair response in which RecA protein is activated by DNA damage and promotes auto-cleavage of the LexA repressor protein, inducing expression of SOS-response genes, for example, 'bypass' DNA polymerases (*e.g.*, Pol II) capable of replicating across lesions [123]. Ciprofloxacin activates the SOS response as explained earlier, while rifampicin – due to its irreversible transcription inhibition – can effectively shut it [116]. Vancomycin – in contrary to other cell wall synthesis inhibiting antibitoics such as β-lactams – does not induce the SOS response [124]. Interestingly, the response not only contributes to the normal cell functioning following an episode of DNA damage-inducing stress, it also increases DNA mutation rates providing greater genetic variability, necessary for rapid resistance acquisition [123].

In addition to the relatively quick (minutes–hours) types of responses to antibiotics, bacteria show an extraordinary ability to adapt to even the most hostile conditions by acquiring and inheriting resistance-conferring genes over generations [125]. Molecular mechanisms of resistance include those which minimise intracellular concentration of antibiotic (through either reduced outer membrane penetration or efflux), modify antibiotic target (through either genetic mutation in target-encoding gene or post-translational modification of the target protein), and inactivate the antibiotic (through either its hydrolysis or chemical modification). In addition to acquired resistance, bacteria may show intrinsic resistance to specific antibiotics, for example Gram-negative species show high intrinsic resistance to many compounds due to an inability of these agents to cross the outer membrane (absent in Gram-positive species) [126]. Despite the relatively well characterised biochemistry of antibiotic resistance, current understanding of how resistance spreads across populations and time is limited. Defining and quantifying the determinants of the evolutionary dynamics of resistance to individual drugs and their combinations is necessary to predict resistance spreading patterns and represents one of the more challenging and urgent research questions of our time [127, 125].

Besides the vast challenges presented by antibiotic resistance, antibiotic 'tolerance' (or 'persistence') to treatments remains at least an equally important and clinically relevant but, until recently, somewhat neglected problem [128, 129]. 'Tolerant' bacteria have the ability (inherited or not) to survive transient exposure to high concentrations of an antibiotic, often achieved not by genetically-encoded molecular mechanisms (as in resistance) but by slowing down an essential cellular process (and the growth rate) [111]. While tolerance is thought to

cause the relapse of many bacterial infections [130], current understanding of the origins of tolerant bacteria, how 'tolerance' interlinks with the emergence of resistance [128, 131, 132], and our ability to study this phenomenon (only $<1\%$ of bacteria switch to the 'tolerant' state) remain limited [129, 132].

1.4 Importance of quantitative investigation at single-cell level

1.4.1 Phenotypic heterogeneity of bacterial populations

Studying bacteria is associated with an inherent challenge of high intra-population heterogeneity, displayed even by isogenic populations investigated under controlled environmental conditions [133]. Making use of recently developed automated microscopy technologies combined with established bioengineering techniques and computational methods of analysis, it has recently become possible to observe the phenotypes of individual cells and investigate the genetic and environmental basis of these differences. It was demonstrated that the gene expression of individual bacteria as measured for clonal populations presents significant variation with both the stochasticity in the gene expression processes and fluctuations in the cellular components contributing to the overall phenotypic variation. As a result, population-averaged measurements may lead to the loss of potentially important aspects of cell biology [133].

There are at least two – not mutually exclusive – beneficial population-level consequences of phenotypic heterogeneity. First, from a survival point of view, phenotypic differences between the members of a population are beneficial due to the 'bet-hedging' strategy. That is, a heterogeneous bacterial population is more likely to survive unfavourable environmental conditions compared to a homogeneous one as there is a greater probability that some of its members will not be – by chance – affected by the harmful stimulus. A special type of such survival technique is presented by 'persisters' (refer to Section 1.3.4. Second, from a functional point of view, phenotypic differences can contribute to new population functionalities [134]. In some cases, genetically identical bacteria can complement each other by specialising in distinct metabolic capabilities or collectively display pathogenicity as a result of the division of labour between members of the population [135].

It follows that the nature of the response of individual bacterial cells to treatment, including acquisition of resistance-conferring genes and the degree of their expression may all vary significantly. Consequently, to gain a more complete understanding of the population response to antibiotics exposure, measurements resolved at the single-cell level are necessary to account for the inter-cellular variability [133].

1.4.2 The challenge of high-throughput imaging of live bacteria

Recent advancements in time-lapse microscopy combined with established biotechnology techniques have led to the development of quantitative fluorescence time-lapse microscopy. Tested strains are engineered to emit fluorescent signals in order to report on specific cellular

events, structure morphologies and locations, and gene expression levels. Fluorescent proteins (FPs) are either directly fused or co-expressed with the proteins of interest [136]. FPs offer advantages over traditional fluorescent staining [137]: high molecular specificity (via direct fusion proteins), high spatial resolution (allowing single-cell and intra-cell imaging), and temporal sampling over long time-scales in live cells. In addition, FPs show practical advantages of their relative stability, pH insensitivity, and low cytotoxicity levels. Genetic modifications of FPs can alter their spectral properties, stability, and folding time, among other [138]. Flexibility of FP-encoding gene insertion allows to report on a large range of molecule levels and process rates, while the possibility to use multiple reporters in a single-cell, allows to monitor and quantify several events in overlapping spatial and temporal dimensions [139, 136]. Emitted fluorescent signals are detected and recorded with an automated fluorescence microscope, typically equipped with a computer-controlled autofocus, stage, and high-sensitivity camera.

Combined with automated image acquisition and processing, the technique enables a high-throughput analysis, where fluorescence levels from multiple cells (or multiple intracellular structures from each cell) and multiple fields of view are collected over virtually undefined time-scales (hours–days). Cell lineages can be established for multiple generations providing, for example, information on the nature and rates of phenotypic trait spread within a population. While several processing software packages are available, the processing algorithms can often be customised to the species and experimental settings of interest [140, 136].

In order to study bacterial behaviour with single-cell level microscopy techniques, bacteria need to be cultured in two dimensional microcolonies on the focal plane of the microscope. This can be achieved either by growing bacteria on a solid pad, where bacteria grow in two dimensions for several hours before they start buckling up and grow out of the focal plane, or in a customised microfluidic device where bacteria grow immobilised in micro-channels. Use of microfluidic device allows for an exquisite control of the environment, including the spatial dimensions available for growth, extent of intercellular communication, nutrient availability, and flow rates. In addition, control of the growth environment provides a possibility of precise cell stimulation across spatial and temporal dimensions. Moreover, immobilising cells in suitably sized microchannels allows for tracking of intracellular structure movement. Finally, stable growth conditions in the device allow for long (over several hounded hours, if needed) measurements [141].

One of the challenges associated with fluorescence imaging of live cells is autofluorescence. Most viable cells exhibit some levels of inherent fluorescence originating from endogenous molecules such as aromatic amino acids, NAD(P)H, flavins, and lipofuscins. Autofluorescence can increase the apparent signal intensity and decrease the signal-to-noise (SNR) ratio, decreasing the sensitivity of fluorescence microscopic imaging by interfering with or even precluding the detection of low-level specific fluorescence [142]. Consequently, use of media of minimal fluorescence profiles is advised to ensure minimal background signal. In addition, fluorophores photo-bleach when exposed to light. As a result, samples exposed to different intensity illumination levels or for different imaging times may show varied SNRs or, in case

of biological samples, show differences in physiology due to the detrimental effects of high intensity light on cell viability [143].

1.5 Dynamics of the genome and cytosol

1.5.1 Global nucleoid-wide dynamics

The nucleoid experiences dynamic motions at short (main focus of this work; refer to Section 1.5.2, below) and long time-scales, with the latter displaying two distinct types of dynamics [1]. Firstly, throughout the cell cycle total nucleoid density fluctuates along its length with a 1–2 min periodicity. Roughly 5% of nucleoid material displaces every 5 s. Secondly, the length of the nucleoid changes discontinuously in a cyclic pattern with a 5 min period of nucleoid shortening followed by a 20 min period of elongation. This is contrary to cell length elongation which is monotonic throughout the cell cycle. The nucleoid elongation rate increases for 10 min reaching a maximum and then starts to decline, ultimately turning negative during the shortening phase. The periodicity implies existence of mechanical stress cycles as the kinetics is consistent with visco-elastic stress accumulation, release, and dissipation [10].

This global dynamic behaviour is implicated in chromosome segregation. As described previously, DNA replication and segregation occur simultaneously in bacteria. However, splitting of individual replicated loci occurs with delays, with most loci transiting from one spot to two separate spots about 7–10 min after passage of the replication fork [144]. Insights into the loci splitting dynamics do not explain, however, how bacteria segregate entire chromosome with no need for spindle-like structures used by eukaryotes. The exact mechanisms are not known, however, all proposed models involve removal of inter-segment tethers along or between sisters that contribute to the increase of nucleoid 'fluidity' [10, 145]. This fluidity makes the local motions possible allowing for co-translational transcription, movement of the transcribed regions to the nulecoid periphery, as well as the local dynamics of DNA replication and segregation.

1.5.2 Short time-scale chromosomal dynamics

Tracking intra-cellular movement of biological molecules has been performed in prokaryotes [146] and eukaryotes [147]. Only recently however this approach has been applied to study local physical properties of the chromosome [14, 22, 42, 21, 13]. High-frequency dynamics (fluctuations) of chromosomal loci can be followed with high time-resolution microscopy [14, 42, 21], while recent developments in automation enable long (several hours) time-lapse microscopy imaging.

At time-scales over a minute, chromosomal movement is dominated by segregation, showing up as directed (ballistic) motion [42, 67]. However, on time-scales much shorter than this, displacements are interpreted as fluctuations in a complex environment; in physical systems this is commonly referred to as "microrheology" [148, 149]. The properties of a medium

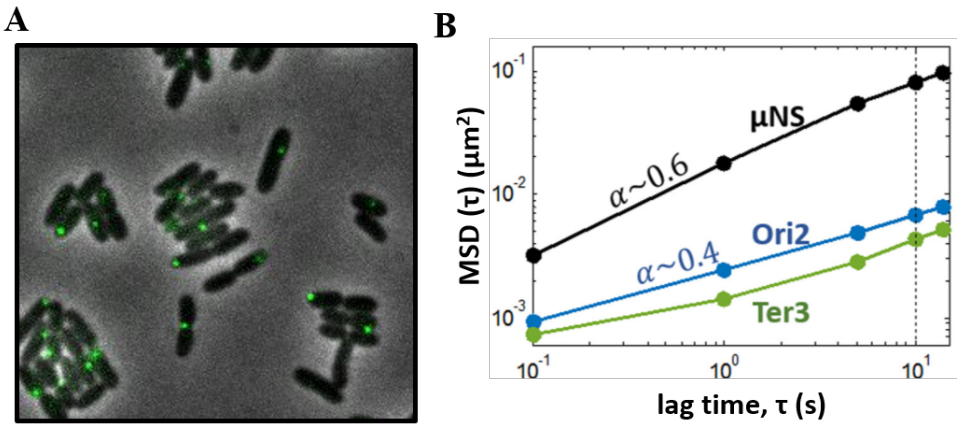

Fig. 1.7 **Single-cell level investigation of fluorescent intracellular marker dynamics.** (**A**) Example phase contrast image of live *E. coli* cells (*black*) with fluorescently-tagged chromosomal loci (*green*). High-frequency dynamics (fluctuations) of chromosomal (and cytosolic) loci is followed with high time-resolution microscopy. On short time-scales (<1 min), displacements are interpreted as fluctuations in a complex environment; in physical systems this is commonly referred to as "microrheology". (**B**) The properties of a medium are measured by tracking and quantifying the mean square displacement (MSD) of a tracer travelling through the medium. MSD scales as τ^{α} with the amplitude proportional to driving forces and inversely proportional to the viscoelastic resistance of the surrounding medium. Chromosomal Ori2 and Ter3 loci explore space slower ($\alpha \simeq 0.4$) than the cytosolic μNS aggregates ($\alpha \simeq 0.6$).

are measured by tracking and quantifying the mean square displacement (MSD) of a tracer travelling through the medium.

The MSD is defined as:

$$MSD(\tau) = \langle (\mathbf{x}(t+\tau) - \mathbf{x}(\tau))^2 \rangle, \tag{1.1}$$

where $\mathbf{x}$ is the position of a particle at a given time, t is the initial time of observation, and τ is the observation time scale (lag time) [150]. The average in Eq. 1.1 can be either a 'time average' of the initial times t for a single locus track, or an 'ensemble average' of multiple tracks at the fixed initial time t, or both, as used in this work. In complex viscoelastic fluids, such as the bacterial nucleoid and cytosol, random motion is subdiffusive, with the MSD scaling as τ^{α} with the exponent $0 < \alpha < 1$ (for diffusion, $\alpha = 1$) [21] with the amplitude proportional to driving forces and inversely proportional to the viscoelastic resistance of the surrounding medium [151] (Figure 1.7).

By measuring MSD of chromosomal loci at short (< 100 s) time-scales, Weber *et al.* [21] revealed that the 'jiggling' motion of chromosomal loci is subdiffusive with the power law exponent $\alpha \simeq 0.4$, as well as superthermal, meaning it is characterised by much stronger temperature dependence than predicted by the Stokes-Einstein relation [13, 151]. The latter suggested a significant contribution from active (ATP-dependent) processes resulting in motion by active diffusion, potentially capable of speeding up diffusion-limited reactions [13]. Supporting

these observations, Javer *et al.* [22] reported that a small fraction (typically 2-5%) of tracked chromosomal loci display super-diffusive dynamics and seemingly directed, near-ballistic trajectories again pointing to the presence of non-trivial active or stress-release contributions to chromosomal motion. The amplitude of this motion varies as a function of the chromosomal coordinate, with regions located closer to the origin of replication (Ori macrodomain)lam showing MSD up to 4-fold larger compared to regions near the terminus of replication (Ter macrodomain) [14]. The latter is likely due to MatP-mediated condensation [43] and possible tethering of the Ter region at certain stages of the cell cycle [152]. Previous work suggested an Ori-Ter gradient in supercoiling, which corresponds to the uneven distribution of DNA gyrase and HU sites [7] and is likely to also contribute to these differences. Functionally, varying local dynamics of the genetic loci can potentially contribute to differential expression of groups of genes as indicated by higher expression of genes (during the exponential phase of growth) belonging to the Ori-proximal region compared to the more distal regions.

1.5.3 Effects of antibiotics on genome organisation and dynamics

In this work, we contribute to the much needed improved understanding of systems-level bacterial responses to antibiotics, introduced earlier. Specifically, we study localisation and fluctuation dynamics of fluorescently-tagged chromosomal loci (and cytosolic markers; refer to Section 1.5.4) under sub-lethal antibiotic treatments. This way, we report on antibiotic-induced changes to genome organisation and cytosol properties (Chapters 3 and 4) and attempt to link those to gene expression responses (Chapter 5). These are very important and novel insights as to date, only few studies investigated effects of antibiotics on the chromosomal organisation and dynamics. In addition, with antibiotic concentrations several times larger than the predicted MICs and short drug exposure times ($\leq$ 30 min), these studies provided limited understanding of such biophysical responses to antibiotics. We summarise these finds below.

Weber *et al.* reported no change in loci dynamics upon treatment with mecillinam (penicillin-binding protein 2 inhibitor) suggesting that effects of inhibition of the motion of MreB do not penetrate into the nucleoid. Rifampicin excreted non-monotonic effects on loci motility. After 1 min of treatment, motility decreased slightly but significantly and consistently. After longer treatment times (up to 30 min), motility increased, plateauing to approximately two-fold greater magnitude. Rifampicin was suggested to have opposing effects on different timescales. Inhibited RNA polymerase activity results in decreased locus motion and remains low during the lifetime of RNA molecules. At longer times, the cellular pool of mRNA decays and contributes to the decrease in the effective viscosity of the cytoplasm, which may result in faster loci motion.

Cabrera *et al.* observed RNA polymerase form ”transcription foci” which disappear following treatment with rifampicin. They used their findings to develop a descriptive model of transcription-dependent nucleoid condensation in line with the trasertion theory. They concluded the process of transcription contributes to nucleoid compaction through the formation

of RNA polymerase foci in the nucleoid's periphery in actively growing cells [53]. Authors proposed that through RNA polymerase inhibition rifampicin can relax the nucleoid as a direct result of RNA polymerase foci dissociation. This effect was assigned to RNA polymerase activity inhibition as the nucloids of rifampicin-resistant mutant cells did not expand following treatment. Conversely, by inhibiting translation (but not transcription), chloramphenicol can reduce the nucleoid-expanding transertion force and consequently compact the nucloid. Moreover, by subjecting cells to rifampicin and chloramphenicol treatments sequentially, they observed that active transcription is necessary for the chlormaphenicol-induced nucleoid compaction [48, 11].

Bakshi *et al.* added to those findings by proposing the DNA-ribosome mixing model (refer to Section 1.3.3) [12]. Effects of rifampicin and choramphenicol on global nuceloid organisation were explained with ribosomal subunits movements between the non-mixing nucloid and polysome structures and without the need to refer to nucleoid-condensing effects of the RNA polymerase foci. At short (0–5 min) timescales, both drugs contract the nucleoid in both length and width by interfering with the expanding force of transertion. At longer (5–20 min) timescales, rifampicin-induced RNA polymerase inhibition results in the mRNA pool depletion and the subsequent polysome structure and 70S ribosome dissociation into 30S and 50S subunits. Free ribosomal subunits mix with the nucleoid contributing to its expansion. Conversely, chloramphenicol-induced translation inhibition leads to further association of ribosomal subunits into 70S ribosomes and polysome structures resulting in even stronger nucleoid compaction. It worth noticing that the non-monotonic global-scale effects of rifampicin are in agreement with the findings of Weber *et al.* on chromosomal loci motility discussed earlier [13].

1.5.4 Cytoplasm composition and cytosol dynamics

The interior of a typical *E. coli* cell (0.5–2 μm^3 in volume, depending on growth conditions) is filled with the cytosol, which constitutes water ($\sim$70% of the total cell mass), crowded with a variety of macromolecules (which occupy 15-20% of the total cytoplasmic space) such as protein ($\sim$55% of the total dry mass) and ribosomal RNA (rRNA; $\sim$15% of the total dry mass), among other [153]. Even though the highly compacted nucleoid spans across $\sim$75% of the cytoplasmic space [1], it accounts for only $\sim$3% of the total dry mass (at fast growth), with other nucleic acids such as mRNA and tRNA accounting for $\sim$1% and $\sim$3% of the total dry mass, respectively [153]. All these components, excluding the nucleoid, comprise the bacterial cytoplasm. In addition to cytoplasm, Gram-negative bacteria such as *E. coli* possess periplasm, which fills the space between the outer and inner cell membranes (30 nm apart along the long cell axis) and can be as crowded as the cytoplasm [154].

Remarkably, at a macromolecular volume fraction (volume occupied by macromolecules relative to the total volume of the cytoplasm) of 0.2 (average value reported for *E. coli*), homogeneously distributed particles of 5 nm in diameter would experience an average intra-particulate

distance of only <2 nm. Consequently, cytoplasmic (and periplasmic) macromolecules produce high levels of 'excluded volume' (volume inaccessible for tracer molecules in the presence of crowders), causing significant steric hindrance and reduced ability to move for intracellular particles [153]. Despite such incredibly crowded cellular environment, processes such as DNA replication and transcription depend on a highly crowded cytoplasm as indicated by the inability to complete (or much lower rates of these processes) *in vitro*, without the presence of synthetic crowders at high concentrations [155].

Given the apparent importance of crowding, bacterial cells are thought to actively maintain a constant range of macromolecule density (and thus a crowding level), presumably to ensure optimal reaction rates. Several osmosensing mechanisms [156] and 'homeocrowding' models [153] have been proposed. Such regulation is important for an enteric bacterium such as *E. coli*, which regularly experiences changes in its osmotic environment, for example at entry and exit from the intestine. Bacterial functioning is typically not affected by small changes to environment osmolarity, however, exposure to a severe osmotic upshift (hyperosmotic shock) can disturb *E. coli* cell function and lead to growth inhibition or even arrest [157]. At such conditions, water is rapidly removed from the cell causing instantaneous cell shrinkage, reduction in cytoplasmic volume (up to $\sim$50%), and plasmolysis (contraction of the protoplast) [158].

Similarily to chromosomal loci, tracer objects in the cytosol also display subdiffusive motions (Figure 1.7), with non-trivial size dependence [15]. In a recent study, genetically encoded size-calibrated cytosolic μNS-GFP aggregates foreign to *E. coli* showed, similarly to chromosomal loci, metabolism-dependent motion. The size of cytosolic aggregates accentuated the effects of metabolism, with the difference in the MSD between metabolically active and inactive cells increasing with aggregate size [15]. The same study, and to date the only one, considered use of an antibiotic, rifampicin, in context of the cytosol dynamics. A relatively high dose was used to switch off transcription and caused a small reduction of cytosolic μNS-GFP aggregates motility. The study measured MSD for long (minutes-hours) lag times [15]. In another study, hyper-osmotic shock conditions of >0.3 osmol caused a decrease in the cytosol dynamics (quantified as change in the diffusion coefficient of GFP). The change was proportional to the magnitude of the osmotic upshift [159].

Despite the well characterised structures and functions of the *E. coli* nucleoid and cytoplasm, the exact nature of the physical interplay between the two and how they affect their biological functions remain subjects of study and debate [18–20]. It is thus currently an open question whether one or other of the chromosome or the crowded cytosol (or both jointly) is causing the complex dynamics observed in the other. Consequently, in order to fully characterise genome dynamics and provide improved systems-level understanding of responses to antibiotics, it is necessary to measure both motions.

Chapter 2

Materials and Methods

2.1 Strains

We used two *E. coli* MG1655 strains with the GFP-ParB/*parS* fluorescent labelling system (provided by Dr Olivier Espéli and Dr Frédéric Boccard [81]) to investigate chromosomal dynamics. Each of these strains has a P1 *parS* site inserted at either Ori2 or Ter3 positions on the chromosome (3,928,826 and 1,341,067 chromosomal coordinates, respectively). Loci have names assigned according to the MD they belong to. Expression of the ParB-GFP fusion protein is driven by the pALA2705 plasmid. No isopropyl β-D-1-thiogalactopyranoside (IPTG) induction was required to produce the ParB-GFP levels necessary to visualize and track loci.

We used the *E. coli* CJW4617 strain (provided by Christine Jacobs-Wagner's laboratory) of a MG1655 background capable of expressing μNS-GFP fusion protein to investigate cytosolic dynamics. The avian reovirus protein μNS is a self-assembling protein [160] and its C-terminal fragment can form globular cytoplasmic particles, even when fused to GFP [161]. μNS-GFP synthesis is under control of the chromosomal IPTG-inducible promoter lac. In this strain, the lactose/IPTG permease-encoding, lacY gene is deleted from the lac operon. Crucially, μNS-GFP aggregates are unlikely to make specific interactions with components of the bacterial cytoplasm, given the evolutionary divergence between bacteria and the avian reovirus. We induced the synthesis of the aggregates with 1 mM IPTG for 3.5-4 h, centrifuged the pre-culture at 4,000 rpm for 10 min, and stopped induction by washing the pellet with the growth medium (refer to Section 2.2) directly before experiments. Induction of GFP-μNS synthesis usually resulted in a single fluorescent focus per cell.

In gene expression experiments, we used *E. coli* BW25113 strains where the GFP production was under control of either the ribosomal *rrnB*P1 or the constitutive P5 promoter inserted in either Ori or Ter region of the genome (strains provided by Dr Bianca Sclavi). The promoter-*gfp* KanR cassette construct fragment was amplified by PCR from the pDoc-K plasmid [162] and inserted at either Ori3 or Ter3 positions (4,413,930 and 1,395,689 chromosomal coordinates, respectively) using λ Red recombination [163]. The insertion positions

were chosen to correspond to the positions of ParS sites in the work by Espeli *et al.* [42]. Ter3 position corresponds directly, while Ori3 was chosen as the closest possible position to Ori2. All inserts were within intragenic regions, as defined by the gene positions in the Ecocyc Genome browser [164].

2.2 Culture conditions

All chemical reagents were obtained from Sigma-Aldrich unless otherwise stated. For all microscopy experiments, we used the "minimal medium" consisting of M9 minimal salts (BD) supplemented with complementary salts (CS; $MgSO_4$ 2 mM, $CaCl_2$ 100 μM, tryptophan 4 μg/mL, and thymidine 5 μg/mL), 0.4% glucose (Glu), and 0.5% casamino acids (CAAs; BD). Experiments testing chloramphenicol did not use CAAs (refer to Chapter 5). Strains were stored at -80°C in lysogeny broth (LB) + 25% glycerol stocks and were streaked on LB plates (containing relevant antibiotic for selection: ampicillin 100 μg/mL and chloramphenicol 25 μg/mL, or kanamycin 50 μg/mL). From each plate, bacteria from 3-4 distinct colonies were selected to inoculate medium and strains were grown overnight at 37°C in LB (with ampicillin 100 μg/mL; for dynamics experiments) or the minimal medium (with kanamycin 50 μg/mL; for gene expression experiments) with shaking at 200 rpm at a 45° angle. Overnight cultures were diluted 200:1 into 2 mL of fresh minimal medium (with no antibiotic) and grown at either 30°C (dynamics experiments) or 37°C (gene expression experiments) to the optical density at a 600 nm wavelength (OD_{600}) of 0.2-0.3 (early exponential growth phase) and transferred either onto agarose pads or loaded into the microfluidic device for image acquisition. Doubling times in bulk (at 37°C in the minimal medium with CAAs) were 65 min, Ori2 and Ter3 MG1655; 80 min, CJW4617; 68 min, BW25113 P1-Ori; 65 min, BW25113 P1-Ter; 72 min, BW25113 P1-Ori; and 68 min, BW25113 P5-Ter.

2.3 Sample preparation for microscopy experiments

Agarose pads contained 1.5% w/v agarose dissolved in the minimal medium and (if required) a fixed concentration of an antibiotic. Pads were approximately 8 mm in diameter and 0.5 mm in thickness. 2.5 μL of the pre-culture were deposited on a pad under aseptic conditions. The pad was then sealed between a cover slip and a glass slide with a stack of 3 frame seals (Fisher Scientific) to ensure access to excess of oxygen (Figure 2.1). Under the microscope, the sample was maintained at 30°C during image acquisition for 2 hours, waiting for 20 min before acquiring the first image.

Microfluidic polydimethylsiloxane (PDMS) device (provided by Prof. Kevin Dorfman) consisted of two main channels supplying fresh medium to and removing waste from submicron-sized channels capable of immobilising bacteria while allowing for balanced exponential growth (Figure 2.1). Device was plasma-cleaned and bonded to a previously sonicated (10 min in acetone and 10 min in isopropanol) and plasma-cleaned cover slip. Bonded device was

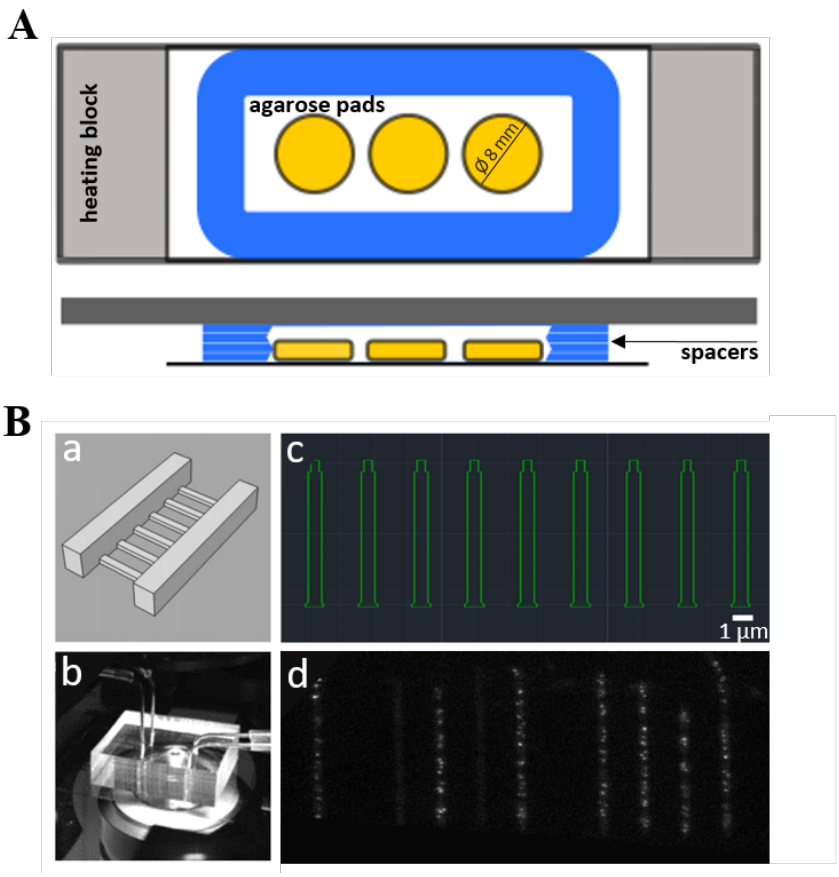

Fig. 2.1 **Experimental set-ups used at microscopy experiments.** (**A**) Agarose pads (*yellow*) are sealed between a cover slip and a glass slide with spacers (*blue*) and sit on a heating block (*gray*) for temperature control. (**B**) Customised microfluidic device consists of (**a**) 2 main channels supplying and removing media from perpendicularly positioned micro-channels (schematic, not-to-scale representation); (**b**) media is supplied and removed via tubing while device sits under the microscope; (**c**) micro-channels are tapered on one end for improved bacteria loading; and (**d**) fluorescent markers inside live bacteria loaded into the micro-channels are shown.

passivated for at least 1 h with a 2 mg/mL bovine serum albumin (BSA) solution at 30°C and then manually loaded (using a syringe connected to device with a tube) with the pre-culture to ensure suitable loading of bacteria (assessed visually under the microscope). The minimal medium containing 0.1 mg/mL BSA was supplied at 4 μL/min using an automated syringe pump (KD Scientific) throughout the experiment. Bacteria were allowed to equilibrate and populate channels for 6 h prior to a media switch (if required) to introduce antibiotic. Image acquisition started 5 h after loading (1 h before the switch). The time of medium arrival at the microfludic device varied by $\pm$ 8 min (as measured 6 times for fluorescein-containing medium, arriving at microfluidic devices loaded with bacteria).

For temperature control, we used a custom built proportional–integral–derivative (PID) temperature controller with two output channels, developed by Dr Jurij Kotar. One channel is used for heating a microscope objective with a heating collar, the other channel is used for

heating either a Fluorine doped Tin Oxide (FTO) glass plate or an aluminium chamber. A sample sits either on the glass plate (agarose pad experiments) or in the chamber (microfluidic experiments). Temperature is measured with K-type thermocouples.

2.4 Determining sub-lethal antibiotic concentrations

In all experiments, we treated bacteria with antibiotic concentrations capable of affecting significantly the cellular physiology but allowing for normal growth. For agarose experiments (loci tracking), the minimal inhibitory concentration (MIC) range for each antibiotic was determined for each of the three strains (MG1655 Ori2, MG1655 Ter3, and CJW4617 μNS) using a standard agar dilution MIC determinaton method [165]. Determined MIC ranges did not differ between different strains. Tested sublethal concentrations were $\sim$75% of the MIC (Table 2.1). Sorbitol was tested at a 400 mM concentration, capable of inducing a hyperosmotic shock in *E. coli* as reported previously [157]. As agarose pads can absorb liquid, it is possible that dissolved antibiotic was diluted after loading the pad with pre-culture. Volume of an agarose pad was about 25 μL and loaded pre-culture volume was 2.5 μL, resulting in a 10% decrease in the antibiotic concentration. However, smaller dilution is likely as some of the loaded pre-culture evaporated rather then was absorbed into the pad.

For loci tracking experiments in the microfluidic device, dose-response curves were constructed using a FLUOstar OMEGA 96-well plate reader (BMG Labtech) growing bacteria at 30°C after diluting overnight cultures 200:1 into 300 μL of minimal medium containing a range of antibiotic concentrations, and measuring the OD_{600} every 30 min for 12 h with shaking at 200 rpm. Slopes of the linear parts of the growth curves from at least 4 biological replicates were calculated and the means used to construct the dose-response curves (Figure 2.2), fitted with Equation 2.1:

$$g(c) = \frac{g_0}{1 + \frac{c}{IC_{50}}}, \tag{2.1}$$

where g is growth rate, g_0 is the growth rate without antibiotic, c is antibiotic concentration, and IC_{50} is the fitted IC_{50} concentration, selected for experiments (Table 2.1). For gene expression experiments, a separate dose-response curve for tetracycline for the P5-Ori strain was constructed (method as above, with growth at 37°C) and the determined IC_{50} concentration of 0.4 μg/mL (0.9 μM) and its ten-fold dilution, 0.04 μg/mL (0.09 μM; approximately IC_8), were used as the "high" and 'low" tetracycline doses, respectively (refer to Chapter 5). Different strains showed a small variability (within one order of magnitude) in the determined IC_{50} concentrations. Chloramphenicol was tested at a 4 μg/mL (12 μM) concentration, one of the concentrations used by Scott *et al.* [60], who measured ribosomal genes activity under chloramphenicol (through determination of the RNA concentration in treated bulk cultures) and proposed the three component proteome allocation model we refer to in this work.

	Agarose pads		Microfluidic device (IC_{50})
	Determined MIC range	Tested concentration (~75% of MIC)	
ciprofloxacin	0.012-0.014 µg/mL	0.01 µg/mL (0.3 µM)	Ori2: 0.011 µg/mL (0.033 µM) Ter3: 0.016 µg/mL (0.048 µM) µNS: 0.013 µg/mL (0.039 µM)
rifampicin	1.2-1.4 µg/mL	1.0 µg/mL (1.2 µM)	Ori2: 2.7 µg/mL (3.3 µM) Ter3: 2.4 µg/mL (2.9 µM) µNS: 2.9 µg/mL (3.5 µM)
tetracycline	0.8-1.0 µg/mL	0.7 µg/mL (1.6 µM)	Ori2: 0.47 µg/mL (1.1 µM) Ter3: 0.75 µg/mL (1.7 µM) µNS: 0.57 µg/mL (1.3 µM)
vancomycin	32-36 µg/mL	25 µg/mL (17.3 µM)	Ori2: 20.3 µg/mL (14.0 µM) Ter3: 25.7 µg/mL (17.7 µM) µNS: 12.8 µg/mL (8.8 µM)
sorbitol	N/A	72.8 mg/mL (400 mM)	72.8 mg/mL (400 mM)

Table 2.1 **Antibiotic concentrations used at loci tracking experiments.** For agarose pad experiments, the MIC range for each antibiotic was determined for each of the three strains (MIC ranges did not differ between different strains). Tested sublethal concentrations were ~75% of the MIC. For the microfluidic device experiments, dose-response curves were constructed (Figure 2.2) and fitted IC_{50} concentrations were selected for experiments.

2.5 Image acquisition and processing

2.5.1 Equipment specifications

We used a Nikon Eclipse TiE inverted microscope with a 60× oil immersion objective (NA 1.45). Images were further magnified with a 2.5× TV adapter before detection on an Andor iXon EM-CCD camera, capable of detecting single fluorophores and yielding a high signal-to-noise ratio to enable high marker localisation precision. Blue LED with a 470 nm peak and 20 nm spectral width was used to excite the GFP using a Semrock LED-FI filter with the exciter 474 nm (25 nm spectral width), dichroic 495 nm, and emitter 515 nm (25 nm spectral width) bands. Focus during image acquisition was maintained with the Nikon perfect focus hardware autofocus system (PFS).

2.5.2 Image acquisition

For marker tracking, manually selected fields of view (21 at agarose pad experiments and up to 50 at microfluidics experiments) were scanned, each field of view containing about 30 fluorescent markers. 45 s movies were acquired at a 9.6 frame-per-second frame rate with

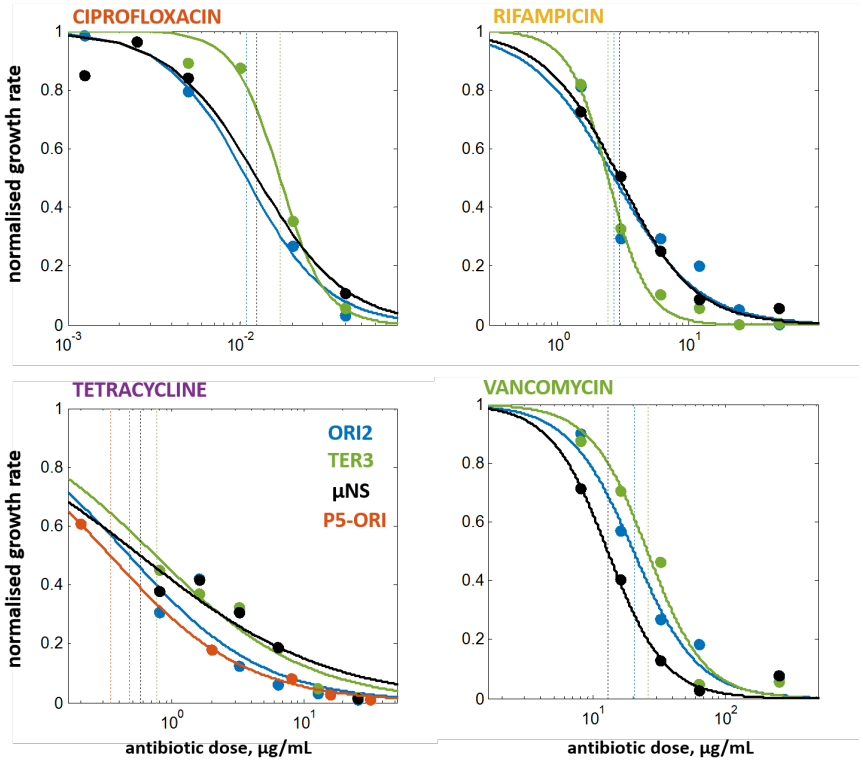

Fig. 2.2 **Dose-response curves used for the IC_{50} concentrations determination.** Slopes of the linear parts of the growth curves obtained at varying concentrations of antibiotics were calculated and the means were used to construct the dose-response curves. After fitting with Equation 2.1, IC_{50} concentrations (*dashed vertical lines*) were selected for microfluidic device experiments (Table 2.1). For loci tracking experiments, Ori2 (*blue*), Ter3 (*green*), and μNS (*black*) strains were tested, while for gene expression experiments, the IC_{50} concentration of tetracycline was determined for the P5-Ori strain (*orange*).

an exposure time of 104 ms. In addition to the movie acquired in the fluoresence mode, a phase contrast image, and a dark frame (acquired immediately before the fluorescent image acquisition using identical settings but no illumination) of each field of view were acquired at every scan. During agarose pad experiments, each field of view was scanned 6 times, 20 min apart (total scanning time 2 h), while at microfluidic experiments each field of view was scanned 7 times, 1 h apart (total scanning time 7 h).

For gene expression level measurements, up to 50 fields of view across whole microfluidic device were manually selected, each field of view containing at least several microchannels loaded with at least one cell. A fluorescence, bright field, and dark frames of each field of view were acquired. After all images at a given measurement time point were collected, the automated stage was idle until the next 5 min mark. Device was scanned 156 times every 5 minutes (total scanning time 13 h). Scanning of individual fields of view and sequential image acquisition were automated with customised software developed by Dr Jurij Kotar. During each experiment, this program stored the positions of manually selected fields of view and sent

appropriate instructions to the microscope stage, camera, heating controller, and illumination system to ensure automated and uninterrupted image acquisition and storage.

2.6 Image processing and data analysis

First, the dark frame was subtracted from all other images. For marker dynamics analysis, image processing methods, tracking analysis, image feature extraction, and MSD fitting algorithms were identical to those previously reported by Javer *et al*. [14]. For gene expression analysis, cell segmentation and feature extraction algorithms were developed by Mia Panlilio (University of Cambridge). All image processing and data analysis including plotting the data were accomplished with custom-written programs using in-built and open-source functions of MATLAB® software, with occasional use of Python programming language. In addition, ImageJ, IrfanView, and Inkscape programmes, and Microsoft Office® package were also used.

2.7 Semi-manual cell size analysis

In addition to using the automated cell segmentation programme, we performed semi-manual measurements of cell lengths (and widths, in specific cases). The length of the long (and short in several conditions to obtain cell width) axis of individual bacteria was measured manually using in-built MATLAB® image display and coordinate marking functions (Figure 2.3). We worked with three different imaging modes (phase contrast, fluorescence, and bright field) and two growth conditions (agarose pads and microfluidic device) (Figure 2.3). In each case, cell length was calculated by determining the distance between two furthest points on the bacterium edge (marked on images in Figure 2.3C). The P1 and P5 *E. coli* strains showed a halo of diffracted fluorescent light around cell boundaries (fluorescence images in Figure 2.3B and C). Consequently, for these strains, furthest points on the edges of the brightest (central) region of the cell were selected. For highest accuracy, all semi-manual measurements were performed by the same person and identical criteria were applied to determine cell boundaries for all measured cells across all treatment conditions.

Semi-manual cell size analysis of phase contrast images was further corroborated with the SuperSegger program designed for automated bacteria segmentation and lineage generation. For SuperSegger software features, capabilities and benchmarks refer to [166], while for gating capabilities refer to [167].

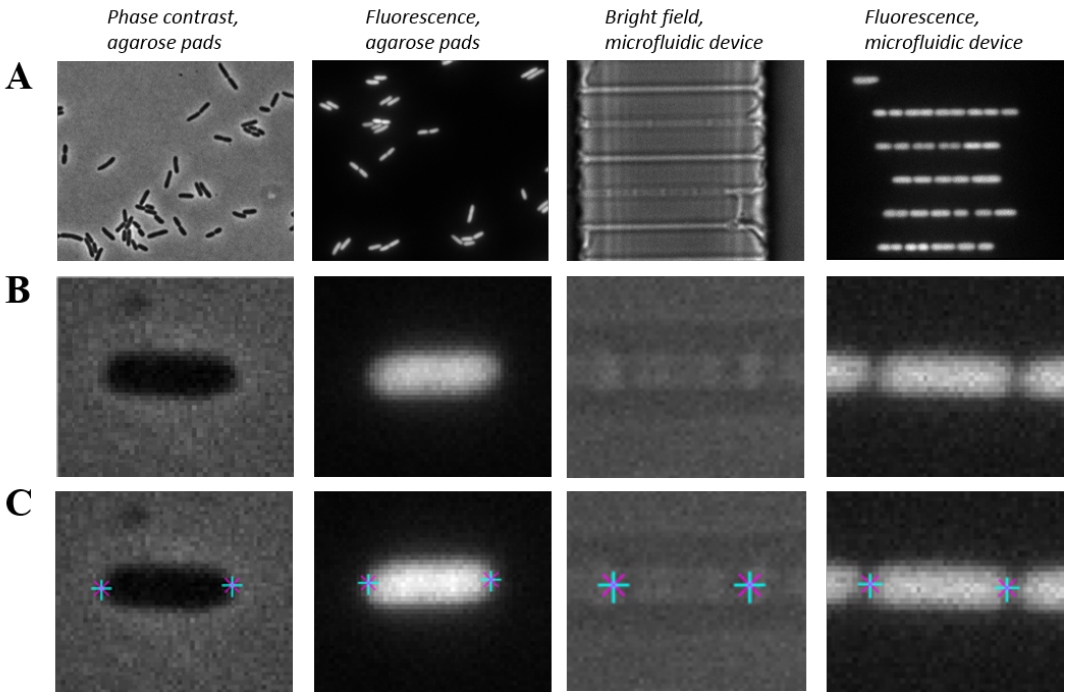

Fig. 2.3 **Semi-manual single-cell level cell size measurements.** (**A**) Example images of *E. coli* in the phase contrast, fluorescence, and bright field mode (on agarose pads or in microfluidic device), as labelled on top of each image column. (**B**) Images of individual cells were enlarged manually for higher measurement accuracy. (**C**) Length of each measured cell was determined by calculating the distance between two furthest points on the bacterium edge (marked on images with star symbols).

Chapter 3

Empirical correction of photo-bleaching effects and marker size-dynamics dependence

3.1 Chapter overview

In this Chapter, we build on the work of Javer *et al.* [14, 22] on short-time chromosomal dynamics in *E. coli* by developing an empirical data treatment procedure to effectively account for marker photo-bleaching effects and size-dynamics dependence. As a result, the procedure enables comparison of dynamics data sets for different treatment conditions and over long measurement times while preserving information about all tracked markers. The purpose of this work is to allow for investigation of long (several hours) short time-scale dynamics measurements in order to accurately measure antibiotics effects on live bacterial cells (Chapter 4).

3.2 Chapter methods

For the purpose of work discussed in this chapter, we performed high-throughput tracking of chromosomal Ori2 and Ter3 loci and rheovirus nonstructural protein cytosolic μNS-GFP aggregates (from here onwards referred to as cytosolic μNS aggregates) collecting in total 34,654 tracks from up to 9 biological replicates per treatment condition (for details refer to the ”control” column of Table B1, Appendix B), growing bacteria in standard agarose pad microcolonies (Figure 3.1A) or as planktonic cultures inside of microchannels of a customised microfluidic chip (Figure 3.1B). Mean cell lengths and elongation rates did not differ significantly between the two growth conditions, however, elongation rates were consistently smaller (by $\sim$1 μm h^{-1}, a factor of $\sim$1.5) on agarose pads (Figure A1, Appendix A). For details of sample preparation and growth conditions refer to Methods chapter (Section 2.3).

3.3 Results

3.3.1 MSD shows dependence on marker size

Chromosomal Ori2 and Ter3 loci (Figure 3.1A, *left* and *middle*) consist of ΔParB-GFP monomers which polymerise at specific *parS* sites in Ori and Ter chromosomal macrodomains (MD) (Figure 3.1C and D), respectively, to form trackable fluorescent markers, stable at 30°C. These loci were previously found to show large (up to 4-fold) differences in MSD [14]. Cytosolic μNS aggregates consist of GFP-labelled proteins of a rheovirus origin foreign to *E. coli* bacteria and capable of self-assembly into trackable particles of variable size (Figure 3.1A, *right*) [15]. The MSD vs lag time curves of the three markers are compatible with a power law with exponent α, with chromosomal loci exploring space slower ($\alpha\sim$0.4) than the cytosolic aggregates ($\alpha\sim$0.6) (Figure 3.1E).

Our markers show wide intensity (size) distributions (100-4,000 AU) and large coefficients of variation (0.87–0.92, depending on the marker), with fainter (having fewer GFP molecules) markers generally having higher MSD compared to brighter ones (having more GFP molecules; Figure 3.1F). In addition, markers photo-bleach when illuminated during image acquisition. This is important because in experiments reported here as the same fields of view are imaged repeatedly over time. In order to precisely quantify the magnitude of changes to marker dynamics, we accounted empirically for photo-bleaching effects, as well as for dependence of MSD on the size of the fluorescent markers.

3.3.2 Empirical correction of marker photo-bleaching effects

Chromosomal loci photo-bleach to a finite baseline value due to a continuous production of ΔParB-GFP molecules (Figure 3.2) while cytosolic aggregates decay to zero (Figure A2, Appendix A) as IPTG-induced μNS-GFP production is stopped by washing the cells directly before experiments. In order to measure the photo-bleaching rate, we consider frequency distributions of recorded loci intensities for individual measurement time points (Figure 3.2A and Equation A1, Appendix A). The decay in the distributions' means (dashed vertical lines in Figure 3.2A and black solid circles in Figure 3.2B) represents a population photo-bleaching profile that can be fitted empirically (Figure 3.2B, blue line) with an exponential function,

$$I_t = I_0 e^{(-\lambda(t-t_0))} + B \,, \tag{3.1}$$

where I_t is locus intensity at time t, I_0 is initial locus intensity at time t_0, t_0 is the initial measurement time (fixed at 20 min for all experiments), and λ and B are free fitting parameters and represent the photo-bleaching rate and the intensity baseline respectively (this is valid for chromosomal loci only, see Equation A2, Appendix A for cytosolic μNS aggregates). Initial intensity is defined as the mean locus intensity as recorded in the first 10 frames of a movie. For each tracked marker, we use its population photo-bleaching rate, λ, to evaluate, using

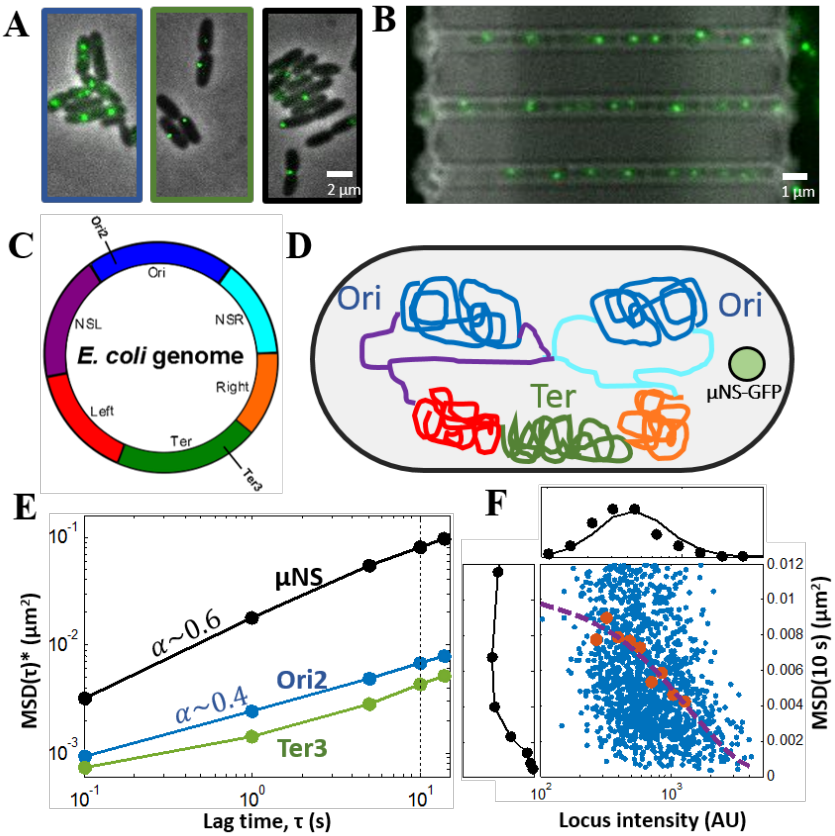

Fig. 3.1 **Illustration of the experiment and basic results**. (**A**) Example phase-contrast images of agarose microcolonies of the three strains, with fluorescent markers (*left*, Ori2; *middle*, Ter3; *right*, μNS) overlaid in *green*. (**B**) Example bright-field image of three microchannels loaded with *E. coli* bacteria with Ori2 loci overlaid in *green*. (**C**) Schematic representation of the *E. coli* genome with colour-coded four macrodomains (MD; Ori, origin of replication; Right; Ter, terminus of replication; and Left MD) and two non-structured regions (NSL, left non-structured region; NSR, right non-structured region), and indicated Ori2 and Ter3 loci relative positions [4]. (**D**) Schematic not-to-scale representation of a dividing *E. coli* chromosome and a cytosolic μNS-GFP aggregate (*green*). Ori MD replicates and segregates first, followed by non-structured regions and then Left and Right MDs, and finishing with Ter MD. The cytosolic μNS-GFP aggregate (foreign to *E. coli*) assembles and suspends in the cytoplasm. (**E**) MSD as a function of a lag time (τ) for the three fluorescent markers tracked in this work. Marker photo-bleaching and size effects are corrected with the data treatment procedure as indicated by a star sign (*). The 10 s lag time selected for analysis is indicated with a dashed line. MSD(τ)* scales as τ^{α} with chromosomal loci exploring space slower ($\alpha \simeq 0.4$) than the cytosolic aggegates ($\alpha \simeq 0.6$). (**F**) "Raw" data MSD(10 s) vs locus intensity, from an example Ori2 loci data set, illustrating the wide MSD (*left*, part of the distribution tail not shown) and intensity (*top*) distributions as well as MSD–intensity (size) dependence (*dashed violet* line; function fitting as in Figure 3.3). Bigger (brighter) loci generally show lower motility compared to smaller (fainter) ones.

Equation 3.1, its original intensity (pre-photo-bleaching, I_0) assuming an exponential decay in intensity.

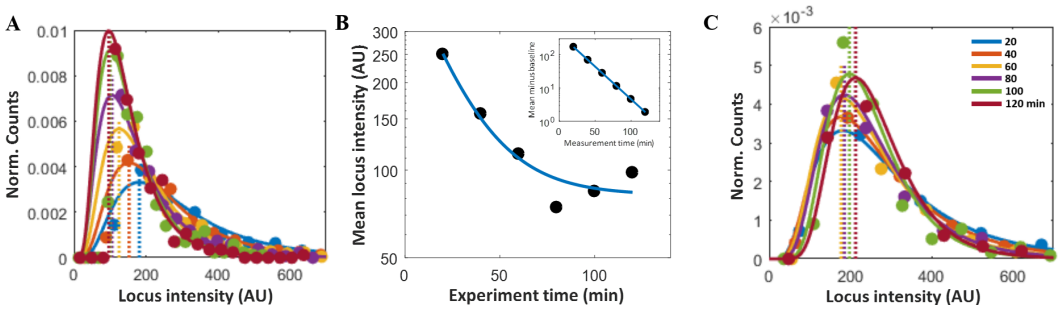

Fig. 3.2 **Correction of marker photo-bleaching**. This procedure evaluates the average marker bleaching rate and uses it to calculate marker intensities. Plots show data for a non-treated Ori2 loci sample as an example. (**A**) Normalised log-normal marker intensity distributions (Equation A1, Appendix A) for different experiment time points (20 – 120 min). Part of the high end of the distribution tails is not shown (full distributions shown in Figure A3, Appendix A). Dashed lines show means of the fitted distributions to demonstrate intensity-time dependence caused by photo-bleaching. (**B**) Distribution mean values from (**A**) over experiment time fitted with an exponential function (Equation 3.1, *blue line*) with a free baseline parameter. Inset: Distributions mean values with subtracted fitted baseline parameter indicating an exponential decay in intensity over experiment time. (**C**) Normalised log-normal marker intensity distributions for different experiment time points as in (**A**) after calculating individual marker intensities.

The pre-photo-bleaching intensity of each locus at each measurement time point is used to correct for marker MSD-size dependence (Figure 3.3). This procedure uses a control (not treated) Ori2 model dataset generated previously by Javer *et al.* [14] consisting of about 2,000 tracks collected using the same experimental set-up and analysis methods. Both Ori2 and Ter3 chromosomal loci data are treated with the same Ori2 model dataset as this approach results in most effective size-dynamics dependence correction (Figure A5, Appendix A). The procedure defines 20 logarithmically-spaced bins along a 100-4,000 AU locus intensity range and evaluates median MSD for each bin. Medians for bins where the number of loci is equal or greater than the mean number of loci per bin (red solid circles in Figure 3.3A) are fitted with a custom exponential function (Figure 3.3A, dashed violet line; Equation A3, Appendix A) that we then use to normalise our data. To flatten this normalisaton curve, we select the statistically strongest ”reference” intensity bin and generate a 20-element correction factor vector that normalises the median MSD values of all other bins to that reference value (black solid circles in Figure 3.3B). This approach minimises locus size effects while including contributions from all tracked loci. We repeat this for five lag times (0.1, 1.0, 5.0, 10, and 14 s; Figure 3.3C) and use the correction vectors to normalise our data.

3.3.3 Empirical correction of marker size effects

To appreciate the effects of the correction procedure on a control Ori2 dataset, compare panels A (before correction) and B (after correction) in Figure 3.4. For correction profiles of Ter3 and μNS control datasets refer to Figure A4, Appendix A. Before correction, there is a strong MSD-intensity (size) dependence as well as a considerable change in median MSD and intensity

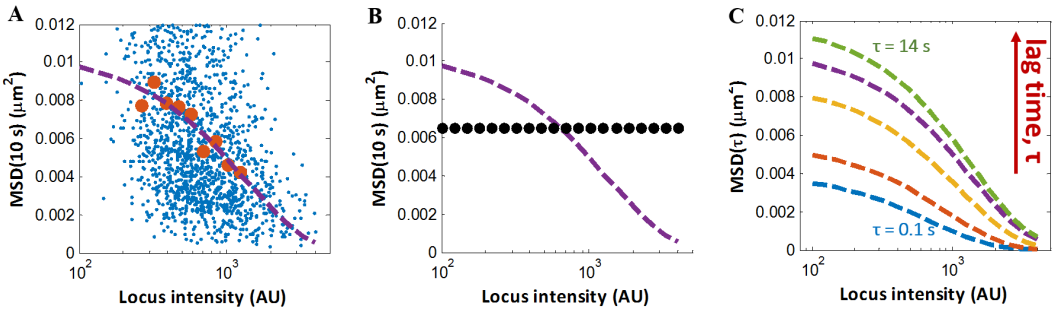

Fig. 3.3 **Correction of marker MSD-size dependence**. Correction factor vectors for MSD at five lag times of our choice (0.1, 1.0, 5.0, 10, and 14 s) based on empirically fitted exponential curves (Equation A3, Appendix A) built on data from the work of Javer *et al.* [14] to correct for MSD–size dependence. **(A)** MSD(10 s) vs marker intensity scatter plot with median MSDs (*red solid circles*) for statistically-strongest bins (containing at least 100 loci). Loci are arbitrarily segregated according their absolute intensities by binning into 20 logarithmically-spaced bins along a 100-4,000 AU range. The medians are used to fit the exponential function (*dashed violet line*). **(B)** For each intensity bin, a correcting factor is calculated to flatten the curve to the reference MSD of the statistically-strongest bin. *Black solid circles* show corrected MSD values for individual bins after correction. **(C)** Exponential curves for the five lag times used for data correction.

over measurement time (Figure 3.4A). Our procedure effectively eliminates photo-bleaching effects (top side plot distribution in Figure 3.4B) and largely reduces MSD-size dependence (generally flat fitted curves in Figure 3.4B) as well as reveals only little change in MSD over measurement time (left side plot distribution in Figure 3.4B).

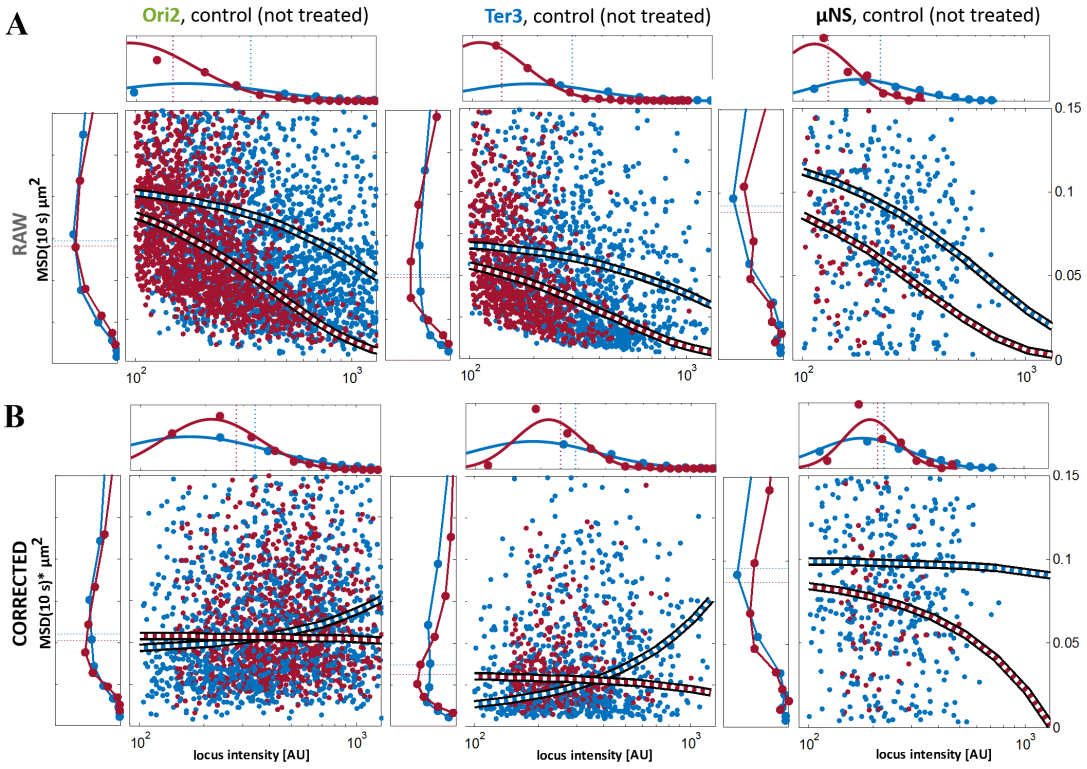

Fig. 3.4 **Effects of correction on the control (not treated) datasets.** Panels (**A**) and (**B**) show scatterplots of the MSD(10 s) over marker intensities with overlaid fitted exponential curves (dashed lines; for function fitting details see Appendix A) and variable distributions in side panels (tails of distributions not shown; agarose data only). Initial measurement time point (20 min) is in *blue* and the final one (120 min) in *red*. Data for Ori2, Ter3, and μNS markers is shown in the *left*, *middle*, and *right* columns as indicated in the figure. (**A**) "Raw" (before correction) data. Fitted curves decrease monotonically with increasing locus intensity and the intensity distribution means shift over time, both indicating photo-bleaching. (**B**) Corrected data. Curves are approximately flat indicating reduced MSD-size dependence and show no time-dependence. Overlapping marker intensity distribution means and median MSD*(10 s) indicate almost no time-dependence in locus intensity and motility, as expected for the control data set.

3.3.4 Short time-scale marker dynamics over several hours of measurements

Our procedure allows to accurately measure long term (several hours) changes to marker dynamics. This is important as it enables investigation of long term responses to antibiotics (Chapter 4), which commonly involve gradual changes to the expression levels of a large number of genes as well as evolutionary adaptations often taking place over tens of generations.

Effects of the data treatment procedure on the MSD(τ) profiles for all tested lag times (0.1-14 s) for chromosomal Ori2 loci and cytosolic μNS aggregates can be appreciated in Figure 3.5 (agarose pad data only). For data treatment effects on MSD(τ) profiles of all markers in both growth conditions, refer to Figures A6 and A7, Appendix A. Correction procedure reduces time-dependent differences in the chromosomal loci motility, especially at shorter ($<$1.1 s) lag times, while the procedure has negligible effects on cytosolic marker motility. By plotting MSD at a lag time of choice (10 s) over measurement times, it is possible to

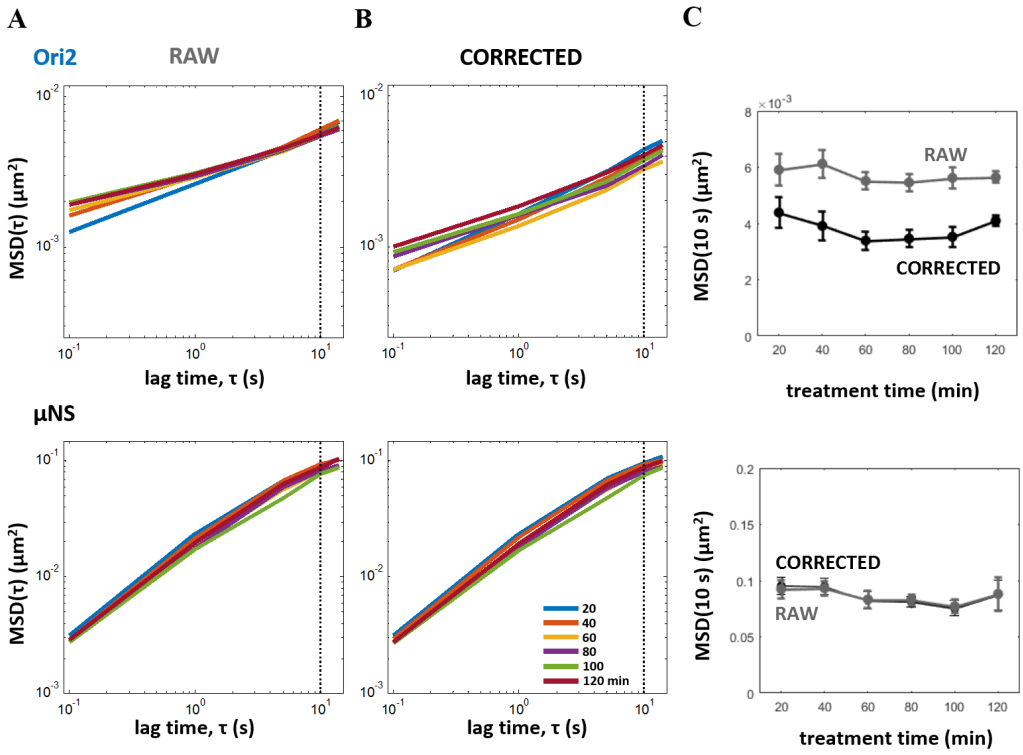

Fig. 3.5 **Photo-bleaching and marker size corrections allows for accurate long (several hours) measurements of short (0.1-14 s) time-scale marker dynamics**. (**A**) Raw and (**B**) photo-bleaching and marker size corrected median ensemble-averaged MSD(τ) for 9 biological replicates for different measurements times (20 - 120 min) for a chromosomal Ori2 locus (*top* panels) and a cytosolic aggregate μNS (*bottom* panels). 10 s lag time indicated with vertical dashed lines. (**C**) Raw (*grey*) and corrected (*black*) MSD(10 s) over 2 h. Agarose pads data only. Error bars show the standard deviations of the medians of the distributions divided by the square root of the number of biological replicates (n = 9 and 6 for chromosomal and cytosolic markers, respectively). For remaining control data sets, Ter3 on agarose pads and all markers in microfluidic device, refer to Figures A6 and A7, Appendix A.

assess changes to marker dynamics over time (Figure 3.5C). We observe that all three markers in control (not treated) conditions show generally stable MSD value throughout the whole experiment time.

In addition, application of our data treatment procedure reveals a transient decrease (40-100 min) in the motility of both chromosomal loci and cytosolic μNS aggregates for agarose pad experiments. This trend is consistent with fluctuations in cell elongation rate (Figure 3.6; for cell elongation profiles for all strains in all conditions refer to Figures B16 and B19, Appendix A), possibly due to bacteria adapting to new growth conditions after the transfer from liquid culture onto solid agarose pads as no such trend is observed in microfluidic device data (Figure A7C, Appendix A).

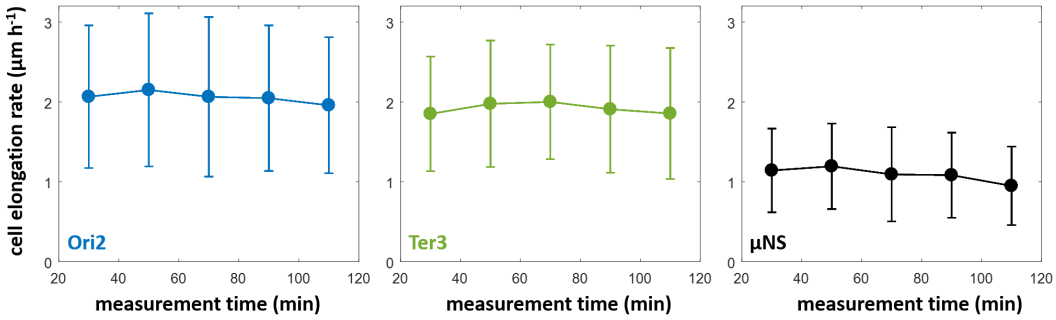

Fig. 3.6 **Control (untreated) cells show characteristic transient increase in elongation rates**. Application of our data treatment procedure reveals a transient decrease (40-100 min) in the motility of both chromosomal loci and cytosolic μNS aggregates for agarose pad experiments (Figure 3.5C). Here we show that this trend is consistent with fluctuations in cell elongation rate: all three tested strains show characteristic small transient increase in mean elongation rate around (40-100 min), possibly due to bacteria adapting to new growth conditions after the transfer from liquid culture onto solid agarose pads. Whiskers indicate the widths of the distributions (specifically, 68.2% of data points, *i.e.* observations within one standard deviation from the mean). We used semi-manual cell length determination method to calculate cell elongation rates (Section 2.7, Methods). Automated analysis with SupperSegger software confirms observed trends (Figure B19, Appendix B).

3.3.5 Faster Ori2 dynamics remains stable for hours

We also confirm higher motility of Ori2 loci compared to Ter3 loci as reported previously [14]. This is an important addition to the pool of evidence demonstrating that the local physical properties of genetic loci are chromosome position dependent. However, we observe a smaller difference in motility between the two loci (by factor of $\sim$1.7) compared to the previously reported factor of 4 [14]. In addition, we demonstrate that this result is stable for hours for exponentially growing cells in two different growth conditions (Figure 3.7). We also reveal that marker motilities measured in the microfluidic device are higher ($\simeq 6.2\times10^{-3}$ and $\simeq 3.9\times10^{-3}$ μm^2 for Ori2 and Ter3 loci, respectively) compared to agarose pads ($\simeq 4.0\times10^{-3}$ μm^2 and $\simeq 2.8\times10^{-3}$ μm^2) for Ori2 and Ter3 loci, respectively. We elaborate on reasons and implications of these differences in Section 4.3.5.

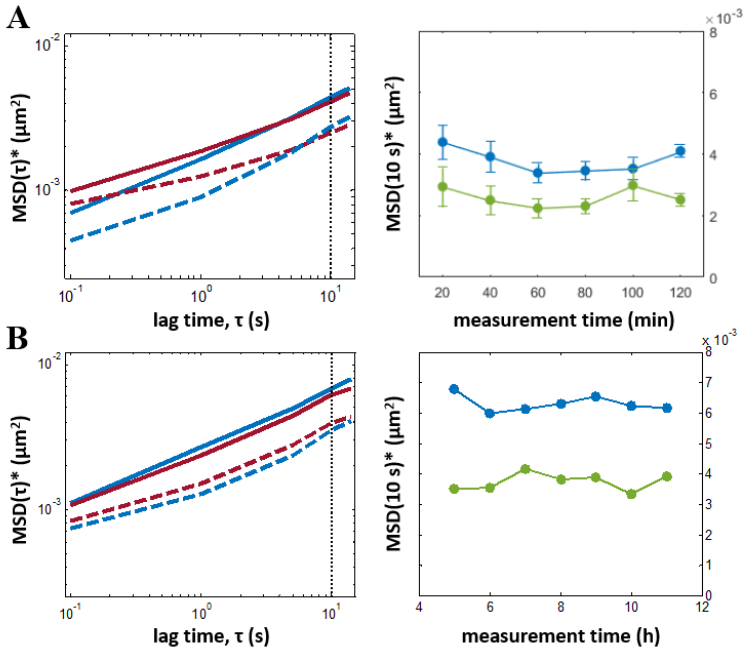

Fig. 3.7 **Chromosomal Ori2 locus shows higher motility than Ter3 and this result is stable for hours in exponentially growing cells in two different growth conditions**. (**A**) Agarose pads data. *Left*: MSD(τ)* for Ori2 (*solid* lines) and Ter3 (*dashed* lines) at 20 (*blue* lines) and 120 min (*red* lines). *Right*: MSD(10 s)* for 20-120 measurement times for Ori2 (*blue*) and Ter3 (*green*). Error bars show the standard deviations of the medians of the distributions divided by the square root of the number of biological replicates (n = 9 and 6 for chromosomal and cytosolic markers, respectively). (**B**) Microfluidic device data. *Left*: MSD(τ)* for Ori2 (*solid* lines) and Ter3 (*dashed* lines) at 1 (*blue* lines) and 7 h (*red* lines). *Right*: MSD(10 s)* for 1-7 h measurement times for Ori2 (*blue*) and Ter3 (*green*). 10 s lag time is indicated with vertical *dashed* lines. Each curve is a single biological replicate.

3.4 Discussion

3.4.1 Empirical approach to data treatment

The empirical approach to data treatment developed here accounts for both marker photo-bleaching and marker size effects, and enables precise quantification of the magnitude of changes to chromosomal and cytosolic marker dynamics. Accounting for photo-bleaching makes it possible to perform long-time (several hours) measurements, necessary to study effects of antibiotics, which often exert measurable effects only after a prolonged exposure (Chapter 4). The correction of marker MSD-size dependence, reduces bias arising from physical effects such as caging and metabolism-dependent contributions to motion, which were shown to depend on marker size [15]. Previous studies on short time-scale genome [42, 21, 14, 13, 22] and cytosol dynamics [15] were limited to single dynamics measurements and did not consider these significant corrections.

3.4.2 Limitations of the data treatment procedure

One limitation of the data treatment procedure presented here is that corrections are computed from population-averages, and hence need a large sample of data. While extracting photobleaching profiles of individual markers is possible, it may be problematic, especially for faster-moving markers such as cytosolic aggregates. Additionally, since a formal physical model describing size-dependent marker motion at short time-scales in live cells has not been developed yet, in the future, a physical model describing tracer size-dependent motions of chromosomal loci and cytosolic aggregates in live cells may further improve the data treatment procedure and highlight aspects of biological and physical significance (refer to Chapter 6).

3.4.3 Ori2 faster than Ter3 over long measurement times

The basic outcome of applying this data treatment procedure is the ability to assess changes to marker dynamics over long measurement times. We were thus able to confirm that chromosomal Ori2 loci show higher motility than Ter3 loci (by a factor of approximately 1.7) and that this does not change (except for small fluctuations, discussed below) over time in a population of exponentially growing cells. This confirms that while allowing for small and transient fluctuations in loci dynamics, these large differences in physical organisation between different regions of the *E. coli* chromosome are a permanent characteristic maintained between generations of cells grown in stable conditions. In addition, relatively small fluctuations in marker dynamics demonstrate that the growth conditions used in this work allow for stable unperturbed exponential growth of bacteria for multiple hours: up to at least 2 h and 11 h on agarose pads and in microfluidic device, respectively.

3.4.4 Faster growth correlates with slower loci dynamics

We explain small fluctuations in chromosomal loci motility such as a transient decrease (during 40-100 min of the experiment) in the motility of both chromosomal loci and cytosolic aggregates for agarose pad experiments with the fact that prior to experiment bacteria were transferred from liquid culture onto solid agarose pads. This trend is consistent with fluctuations in growth rate (Figure 3.6; also refer to Figures B16 and B19, Appendix A), possibly due to bacteria adapting to new growth conditions after the transfer from liquid culture onto solid agarose pads.

Adjusting bacterial physiology to new growth conditions involves changes to the expression rates of multiple genes (reviewed in [168]) and measurable physiological changes may come into effect at time-scales of tens of minutes due to time needed for protein synthesis and folding [169]. Although the compositions of liquid pre-culture medium and solid agarose pads are identical (except for 1.5% w/w agarose in the pads), the change from a planktonic culture to a microcolony on a solid surface is likely to trigger changes to expression of genes responsible for cellular attachment, biofilm formation, and cell-to-cell communication [170]. Supporting these speculations is the fact that although we observe small fluctuations in loci motility for

bacteria grown in the microfluidic device, no systematic transient decrease in MSD is observed in this growth condition (Figure A7C, Appendix A).

The small transient increase in growth rate observed on agarose pads results in an overshoot in global protein and mRNA concentrations, as reported before [25]. Consequently, viscosity of cysotol and macromolecular crowding effects increase during this time leading to a decrease in the motility of cytosolic μNS aggregates and – consequently – chromosomal loci (for speculated causal link between changes to cytosol and chromosomal dynamics, refer to Section 4.4.3, Chapter 4). Similar but very weak correlation between growth rate and locus motility was observed previously by Javer *et al.* [14] for Ori2 loci, however, the effect was too small and highly locus size-dependent to be considered meaningful. Our improved approach allows to quantify these small changes with higher precision.

Chapter 4

E. coli genome and cytosol dynamics under sublethal antibiotic treatments

4.1 Chapter overview

In this chapter we use the empirical data correction method discussed in Chapter 3 to investigate effects of long (several hours) sublethal antibiotic treatments on short time-scale chromosome and cytosole dynamics in two growth conditions: standard agarose pads and a customised microfluidic device. We find that sublethal doses of most of tested antibiotics cause small but consistent effects on motility of both chromosomal loci and cytosolic aggregates. We find that different antibiotics have different effects on genome and cytosol dynamics and that chromosomal and cytosolic responses to each antibiotic are consistent with each other but not between the growth conditions. We speculate on causal mechanisms of the observed effects and possible reasons for differences observed between the growth conditions. We also discuss possible consequences of these physical effects on biological processes of the bacterial cell, and possible consequences for the clinical use of antibiotics.

4.2 Chapter methods

Using experimental and analytical methods identical to those used in Chapter 3, we extended our high-throughput tracking of chromosomal Ori2 and Ter3 loci and cytosolic μNS aggregates to the total of 180,476 tracks across 6 different treatment conditions, with up to 9 biological replicates per treatment condition (for details refer to Table B1, Appendix B). Exponentially growing cells were either not treated (controls) or exposed to sub-lethal antibiotic treatments (ciprofloxacin, rifampicin, teteracycline, vancomycin) or to a hyperosmotic shock inducing dose of sorbitol. For details of treatment conditions refer Methods chapter (Section 2.4). Treatments did not affect the growth rates significantly with an exception of tetracycline (Figures B16 and B19, Appendix B). As previously, we investigated bacteria growing exponentially in two growth conditions: standard agarose pad microcolonies and as planktonic cultures in

microchannels of a customised microfluidic chip as outlined in Section 2.3 and discussed in Chapter 3. To reveal true antibiotic and sorbitol treatment effects on marker dynamics, we applied the data treatment procedure developed in Chapter 3 to empirically account for marker photo-bleaching effects and size-dynamics dependence.

4.3 Results

4.3.1 Sublethal antibiotic treatments cause small but consistent effects on genome and cytosol dynamics

For initial comparison of treatment effects we choose the MSD at an arbitrary lag time of 10 s and look at the agarose pads experiments only. We reveal that in control (not treated) bacteria, motilities of both chromosomal loci and cytosolic μNS aggregates remain stable throughout the experiments (Figure 4.1, blue lines). As expected, cytosolic aggregates show highest motility ($\simeq$0.08 μm^2) while chromosomal loci show the MSD which is an order of magnitude lower, with Ori2 loci exploring space quicker than Ter3 loci ($\simeq 4.0\times10^{-3}$ and $\simeq 2.5\times10^{-3}$ μm^2, respectively).

We find that sublethal doses of most of tested antibiotics and sorbitol cause small changes to short time-scale dynamics of both chromosomal loci and cytosolic μNS aggregates (Figure 4.1). Importantly, the effects are consistent between the three markers and, in most cases, over the entire drug exposure time.

Treatment with ciprofloxacin increases the MSD of both Ori2 and Ter3 loci gradually over the treatment time up to $\simeq 4.0\times10^{-3}$ and $\simeq 2.5\times10^{-3}$ μm^2 at final treatment time point (120 min), respectively. Cytosolic μNS aggregates show an increased MSD already at initial time point (20 min) and gradually decrease motility and reach the control level ($\simeq$0.08 μm^2) at final treatment time point.

We observe a similar trend for rifampicin, however, the effects are smaller and especially minute for Ori2 loci, whose motility increases up to $\simeq 5.0\times10^{-3}$ μm^2 only after 90 min of drug exposure. Ter3 motility remains increased fractionally but consistently at the level of $\simeq 3.5\times10^{-3}$ μm^2 across the whole drug exposure time. Effects are also very small for cytosolic μNS aggregates, whose MSD remains higher by $\sim$0.01 μm^2 throughout the whole treatment time, except the final time point.

Tetracycline is the only treatment agent tested in this work which does not show any consistent effects on the motility of the three markers. In addition, as translation inhibition causes a decease in ΔParB-GFP production, it results in excessive marker photo-bleaching with all trackable Ori2 loci disappearing after the 80^{th} min of experiment.

Vancomycin causes a small decrease in MSD of both chromosomal loci already at the initial treatment time point ($\simeq 3.0\times10^{-3}$ and $\simeq 2.0\times10^{-3}$ μm^2 for Ori2 and Ter3 loci, respectively), and continues to decrease Ori2 loci motility down to $\simeq 2.0\times10^{-3}$ μm^2 while Ter3 motility loci remains relatively constant. Motility of cytosolic μNS aggregates deceases by $\simeq$0.01 μm^2 and

remains at this level till the end of the experiment. In addition, we observed that vancomycin affected visibly cell morphology causing characteristic bending of cells (Figure B21, Appendix B).

Sorbitol also decreases the MSD of both Ori2 and Ter3 loci, however, effects are well pronounced already at the initial treatment time point. Motility is down to $\simeq 1.5\times10^{-3}$ μm^2 for both Ori2 and Ter3 loci at final treatment times. Under hyperosmotic shock conditions, gene expression processes may be impaired [153], resulting in strong marker photo-bleaching and thus inability to collect valid loci tracks after 80 and 60 min for Ori2 and Ter3 loci, respectively. Motilty of cytosolic μNS aggregates remains decreased at $\simeq 0.06$ μm^2.

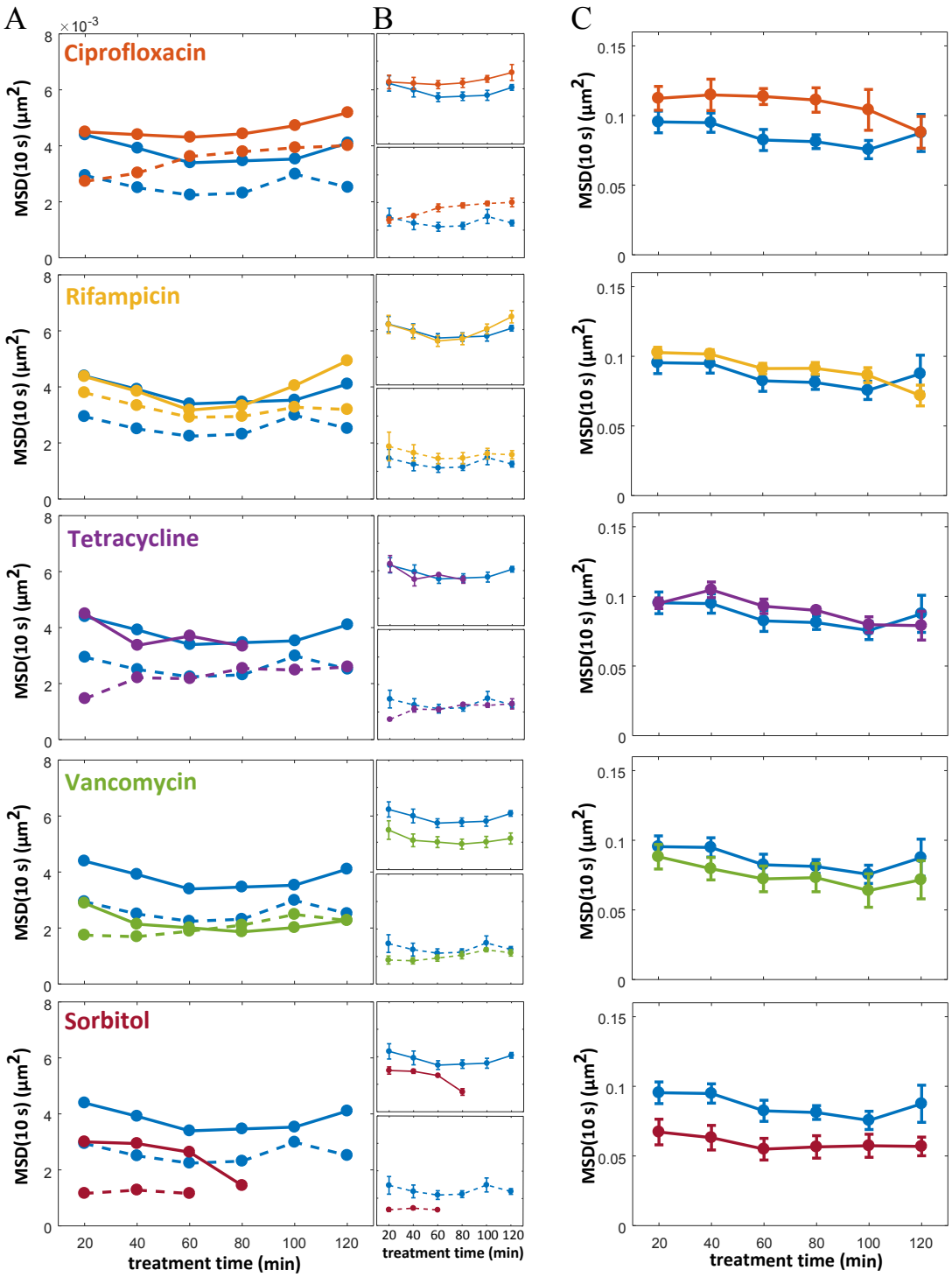

Fig. 4.1 **Sublethal doses of different antibiotics and sorbitol cause small but consistent changes to the short time-scale motility of chromosomal loci and cytosolic aggregates.** (**A**) MSD(10 s)* over 2 h for different antibiotics (in different colours as indicated in the figure) and sorbitol, compared to control (*blue* lines) for Ori2 (*solid* lines) and Ter3 (*dashed* lines) loci. (**C**) Data for cytosolic aggregates μNS. Error bars (in **B** and **C**) show the standard deviations of the medians of the distributions divided by the square root of the number of biological replicates (n = 9 and 6 for chromosomal and cytosolic markers, respectively).

4.3.2 Directions of effects generally correlate between chromosomal Ori2 and Ter3 loci

To compare chromosomal responses directly, we consider relative fold changes in motility, defined as the logarithm of treated-to-control MSD(10 s) ratios, for Ori2 and Ter3 loci for individual treatments and treatment times Figure 4.2). We reveal that the directions of effects are consistent for the two chromosomal loci for each the treatment conditions.

Notably, we show that the initially fast-moving loci, Ori2, increased their motility less when treated with ciprofloxacin and rifampicin (maximal fold changes +0.12 and +0.08, respectively) if compared to the initially slow-moving loci, Ter3 (maximal fold changes +0.2 and +0.1, respectively). Conversely, we show that the initially fast-moving loci, Ter3, decreased their motility less when treated with vancomycin (maximal fold change -0.18) if compared to the initially fast-moving loci, Ori2 (maximal fold change -0.28) and showed comparable magniture in fold change under sorbitol treatment (maximal fold change -0.39 and -0.40 for Ori2 and Ter3, respectively).

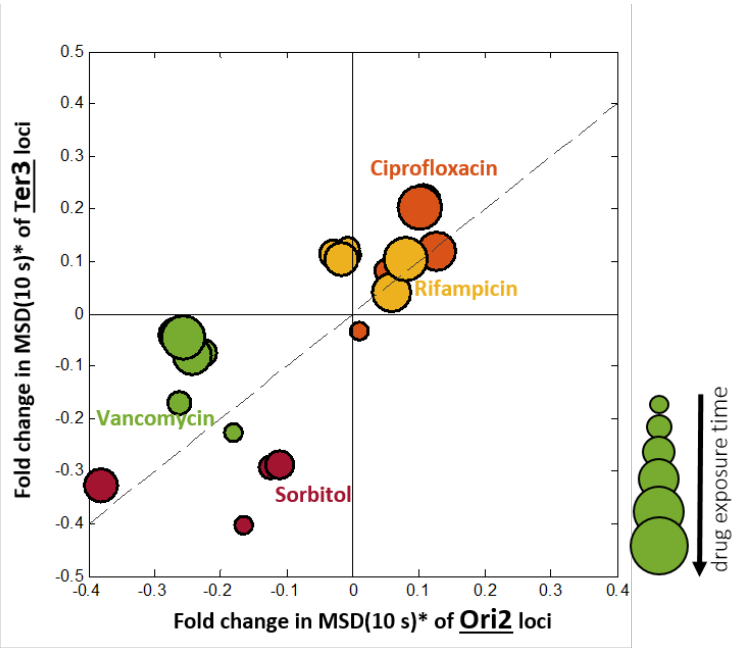

Fig. 4.2 **Directions of effect generally correlate (except for vancomycin) for chromosomal Ori2 and Ter3 loci**. Fold changes in Ori2 vs Ter3 loci motility, defined as the logarithm of treated-to-control MSD(10 s)* ratios, are plotted for ciprofloxacin, rifampicin, vancomycin, and sorbitol (in different colours as indicated in the figure). Plot marker size increases with increasing treatment time (20-120 min). Diagonal dashed line represents a gradient of 1.

4.3.3 Directions of chromosomal and cytosolic effects generally correlate

Analogously, we compare chromosomal and cytosolic responses directly (Figure 4.3) considering relative changes in motility defined again as the logarithm of treated-to-control MSD(10 s) ratios for chromosomal Ori2 and Ter3 loci and cytosolic μNS aggregates for individual treatments and treatment times. We show that directions of responses are generally consistent between chromosomal and cytosolic markers and that the magnitude of fold change for chromosome and cytosol dynamics is generally comparable. In fact, most of the responses lay on or near a straight line with gradient equal to 1 (Figure 4.3, dashed diagonal line). This suggests that changes to the cytosol physical properties generally correlate both in timing and magnitude with changes to the chromosome physical properties. Exceptions to this pattern are Ori2 loci under vancomycin treatment and both chromosomal loci under sorbitol treatment.

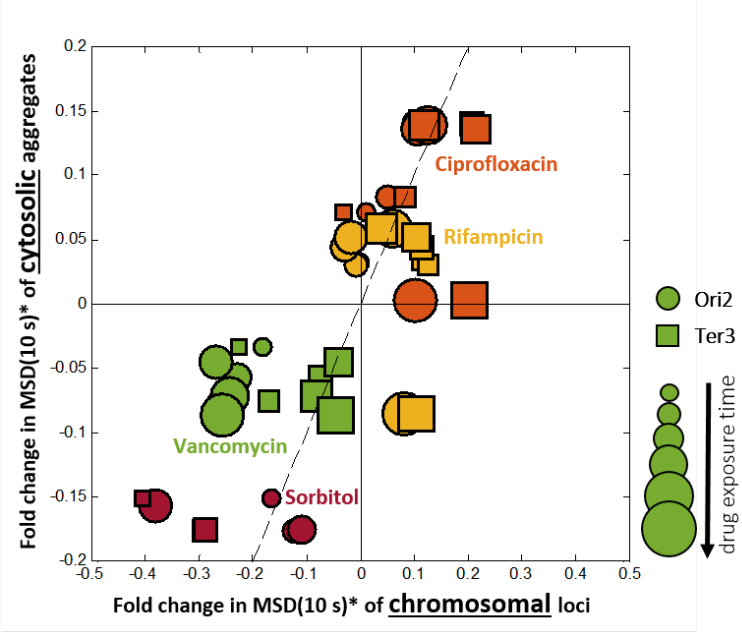

Fig. 4.3 **Direction of effects generally correlate for chromosomal loci and cytosolic aggregates**. Fold changes in chromosomal Ori2 (*circles*) and Ter3 (*squares*) loci vs cytosolic aggregates μNS loci motility, defined as the logarithm of treated-to-control MSD(10 s) ratios, are plotted for ciprofloxacin, rifampicin, vancomycin, and sorbitol (in different colours as indicated in the figure). Plot marker size increases with increasing treatment time (20-120 min). Diagonal dashed line represents a gradient of 1.

4.3.4 Dynamics responses to treatments evolve during lag time

We also looked at how dynamics responses evolve as a function of lag time (Figure 4.4). We plotted fold changes in motility as shown earlier for 5 arbitrary lag times (0.1, 1.0, 5.0, 10, and 14 s) representing full range of tested lag times.

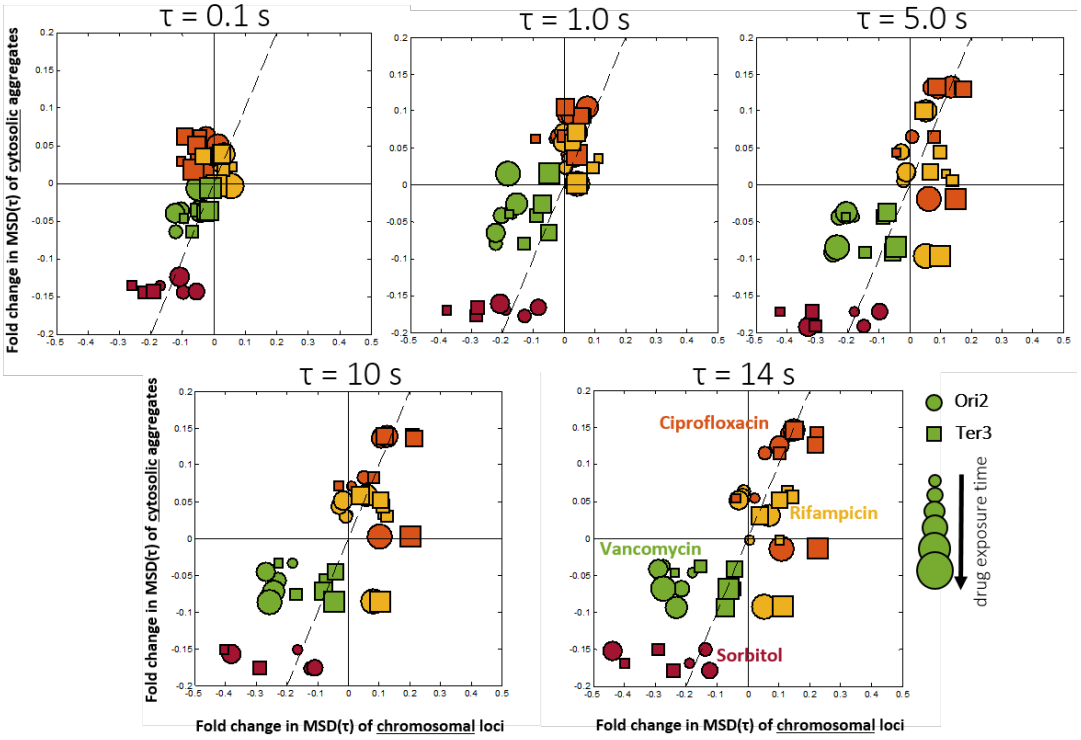

Fig. 4.4 **Responses in marker dynamics to different antibiotics and sorbitol evolve during the lag time.** Fold changes in chromosomal Ori2 (*circles*) and Ter3 (*squares*) loci vs cytosolic μNS aggregates loci motility, defined as the logarithm of treated-to-control MSD(10 s) ratios, are plotted for ciprofloxacin, rifampicin, vancomycin, and sorbitol (in different colours as indicated in the figure) for for 5 arbitrary lag times (0.1, 1.0, 5.0, 10, and 14 s) representing full range of tested lag times as indicated above individual figures. Plot marker size increases with increasing treatment time (20-120 min). Diagonal dashed lines represent gradient of 1.

As expected, dynamics responses for all antibiotics increase in magnitude with increasing lag time, for both chromosomal and cytosolic makers. We reveal however that the differences in responses between all tested antibiotics become apparent after 10 s, with data points for individual treatment conditions forming distinct clouds, especially at longer treatment times. In addition, the difference between Ori2 and Ter3 responses to vancomycin becomes well differentiated only after 5 s and, for ciprofloxacin and rifampicin, only at longer (>40 min) treatment times. Remarkably, sorbitol follows a different pattern, causing distinct effects for both chromosomal and cytosolic makers already at the shortest tested lag time (0.1 s). In addition, the difference between Ori2 and Ter3 responses is apparent already at this lag time and it becomes less noticeable at longer lag times.

4.3.5 Dynamics results for agarose pads and microfluidic device are not consistent

When working with a different fluorescent reporter, *E. coli* strain (MG1655 *rrnBP1-gfp*, refer to Chapter 5) we noticed that cells appear wider after leaving microchannels of our customised microfluidic device than they are when inside of the microchannels (Figure D4).

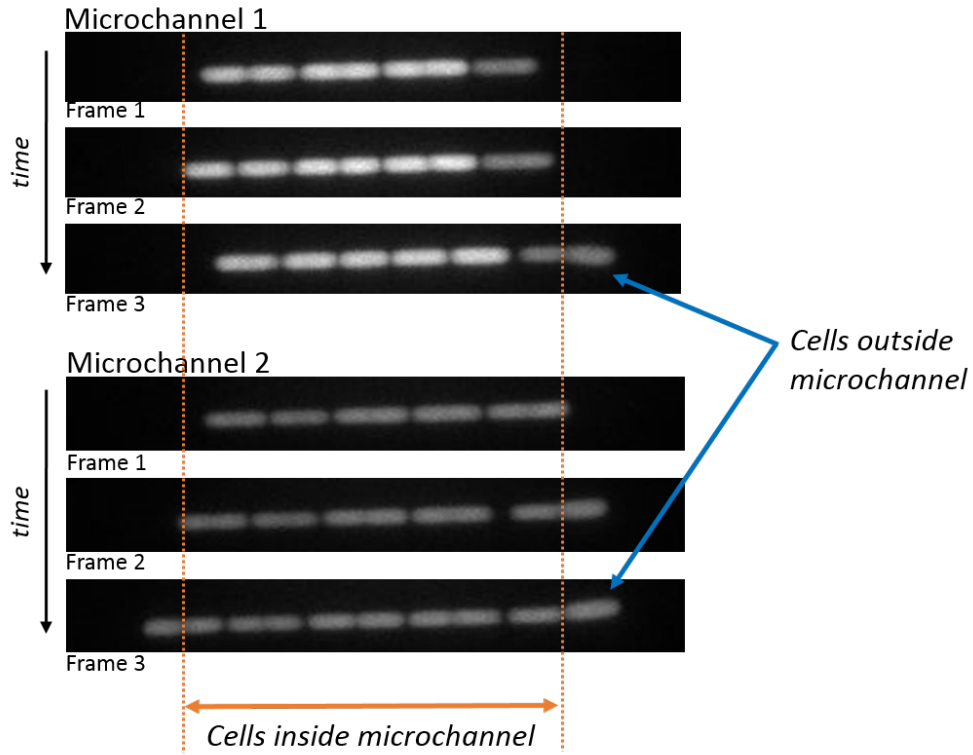

Fig. 4.5 **Cells appear wider when leaving microchannels of our customised chip than they are when inside of microchannels.** Three consecutive frames (5 min apart) showing images in the fluorescence mode of two example microchannels of a customised microfluidic device filled with exponentially growing *E. coli* bacteria (MG1655 *rrnBP1-gfp* fluorescent reporter). Cells leaving the microchannels appear wider than those inside the microchannels suggesting that bacteria may be subjected to significant mechanistic forces when growing inside the microfluidic device.

We compared width distributions between bacteria from agarose pads and microfludicic device and discovered that cells were systematically narrower in the microfluidic device (Figure 4.6). This suggested that bacteria may be subjected to significant mechanistic forces when growing inside of those microchannels, what could in turn affect physical properties of cells and their components.

We observed differences in marker dynamics and in dynamics responses between bacteria grown on agarose pads and in the microfluidic device (Figure D1). While (the long term) responses to ciprofloxacin and rifampicin are at least qualitatively consistent between agarose pads and microfludics device, this it not the case for vancomycin and sorbitol. The latter treatments do not result in a decrease in motility of markers (neither chromosomal nor cytosolic)

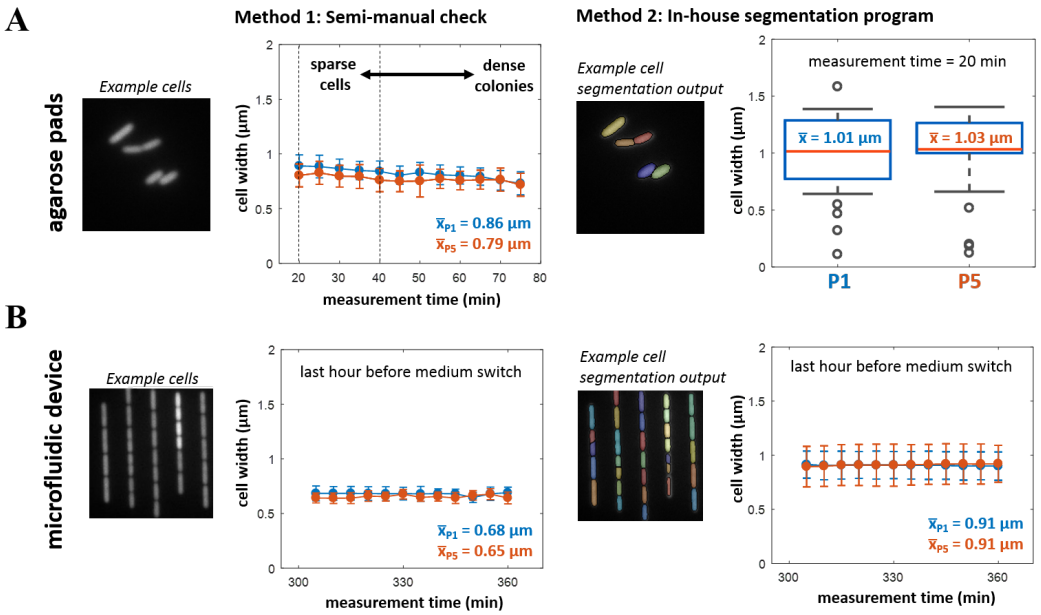

Fig. 4.6 **Bacteria in microfluidic device are systematically narrower compared to agarose pads.** Mean cell widths were calculated for cells growing on (**A**) agarose pads and (**B**) inside of microchannels of the microfluidic device. Two methods were used to determine widths of imaged cells: semi-manual (method 1) and in-house cell segmentation (method 2). For the measurement method details refer to Methods chapter (Section 2.7). When working with images of agarose pad micro-colonies, method 2 was applied to images acquired only at the initial measurement time point (20 min). Whiskers in all four panels indicate the widths of the distributions (specifically, 68.2% of data points, *i.e.* observations within one standard deviation from the mean). Empty points in the *right* panel in row (**A**) indicate outliers data points. While the first method systematically measures smaller widths, both methods show that mean width of cells grown in microfluidic device is smaller by ∼10% (method 1) and ∼20% (method 2) compared to widths of cells grown on agarose pads.

as seen on agarose pads. Conversely, we observe a small increase in the motility of all markers. Notably, and similarly to agarose pads, the initially fast-moving loci, Ori2, increase their motility less if compared to the initially slow-moving loci, Ter3 (maximal fold changes +0.03 and +0.16, respectively).

We speculate that cell squeezing inside microchannels may be the reason for the considerable inconsistency of vancomycin and sorbitol effects seen between agarose pads and microfluidic device experiments. It is possible that as pressure is applied to cells in microchannels, the concentration of their cytosol contents (comprising macromolecules such as protein and nucleid acids) increases compared to ”relaxed” cells. We note that the motilty of cytosolic μNS aggregates in untreated cells in microfluidic device is lower (by a factor of ∼2) compared to agarose pads as shown earlier (Figure 3.7, Section 3.3.5) strongly suggesting changes to the cytosol properties such as an increase in macromolecular crowding. Consequently, applying vancomycin or sorbitol does not result in a further decrease in marker motility. Conversely,

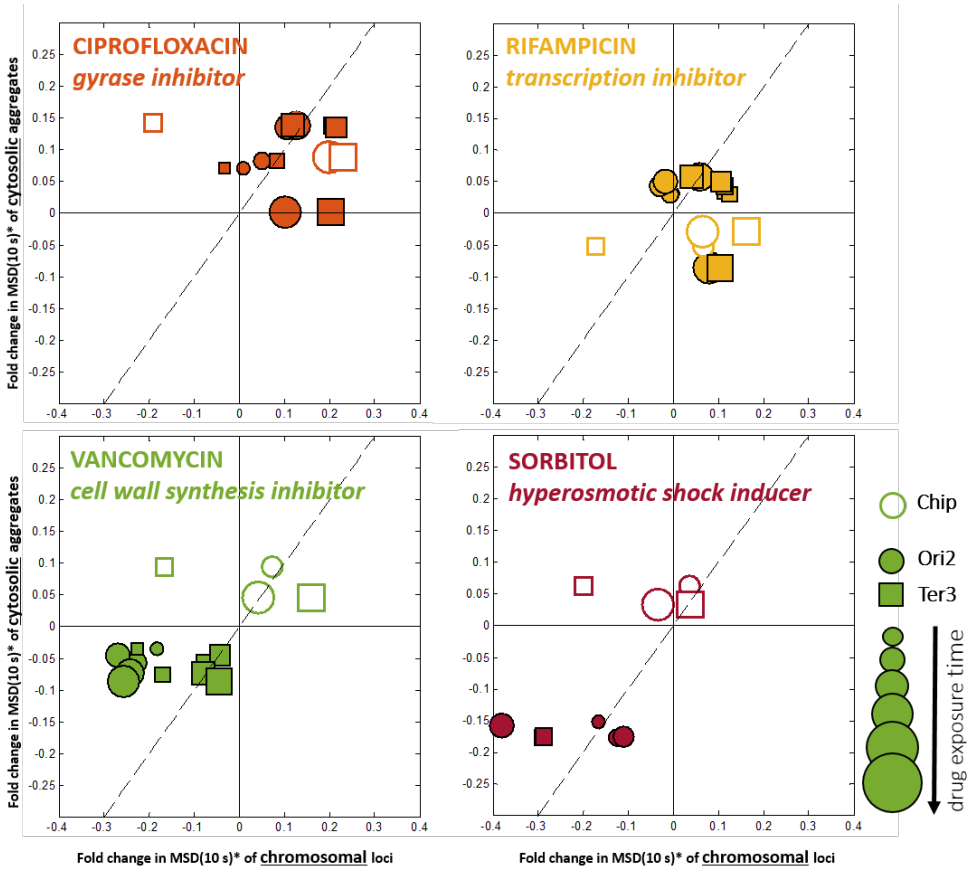

Fig. 4.7 **Dynamics responses to treatments measured on agarose pads and in microfluidic device are not consistent.** Fold changes in chromosomal Ori2 (*circles*) and Ter3 (*squares*) loci vs cytosolic aggregates μNS loci motility, defined as the logarithm of treated-to-control MSD(10 s)* ratios, are plotted for ciprofloxacin, rifampicin, vancomycin, and sorbitol (in different colours as indicated in the figure) for agarose pads (*solid* plot markers) and chip (*empty* plot markers) data for various treatment times (20-120 min for agarose pads and 1 and 2 h for chip). Diagonal dashed lines represent gradient of 1.

as these treatments change cell morphology (Appendix B), they may cause cells to sit in microchannels more loosely, resulting in a small increase in marker motility.

4.4 Discussion

4.4.1 Genome and cytosol dynamics at long (several hours) drug exposure times

Many important aspects of how antibiotics affect bacterial physiology remain unknown. Although attempts have been made to provide a more holistic picture of antibiotic effects (*e.g.*, through DNA microarray studies on global gene expression [35]), systems-level physiological responses such as effects on gene regulatory networks and on the macromolecular composition of cells (*e.g.*, the concentration of ribosomes, protein-DNA ratio) remain largely unexplored. In this Chapter, we addressed some of these response phenotypes as a function of antibiotic class

and growth conditions. Specifically, using fluorescence microscopy we studied spatial short time-scale fluctuations of fluorescently-tagged chromosomal Ori2 and Ter3 loci and cytosolic μNS aggregates.

In order to accurately measure long term (several hours) changes to marker dynamics, we applied the data treatment procedure we developed in Chapter 3. These corrections are critical in order to enable investigation to long-term responses to antibiotics, which commonly can cause gradual and cumulative changes to the expression levels of a large number of genes [35, 120, 121] as well as evolutionary adaptations often taking place over tens of generations [125]. Some of the previous studies on genome and cytosol dynamics included insights on the effects of antibiotic treatments [21, 13, 15], however, they did not consider these important corrections. In addition, these studies were limited to single time-point dynamics measurements and high (above estimated IC_{50}) antibiotic doses.

By addressing these critical considerations, we are able to reveal with high precision that sublethal antibiotic and sorbitol treatments have small but consistent effects on genome and cytosol short time-scale motility. In addition, by selecting sub-lethal antibiotic concentrations, we minimised effects from growth-rate dependent modulations in expression of genes (refer to Section 1.2.1). Furthermore, by studying how antibiotics of different modes of action affect the dynamics of two geographically distant (and physically distinct [14]) chromosomal loci as well as the cytosol, we revealed that antibiotics can have diverse and widespread effects on biophysical properties of the bacterial cell. We discuss these findings and their implications in detail below.

4.4.2 Genomic position affects the degree of response

We observed that almost all (with an exception of tetracycline) tested antibiotics caused small changes to the chromosome dynamics and that these changes persisted for most of the treatment time. We also showed that the directions of effect were generally consistent for both Ori2 and Ter3 loci. Notably, we showed that the change in the amplitude of motion depended on the initial (before treatment) locus motility. The initially fast-moving loci, Ori2, increased their motility less when treated with ciprofloxacin and rifampicin if compared to the initially slow-moving loci, Ter3. The opposite was true for vancomycin.

We hypothesise that the amplitude of these local motions is a measure of the level of genetic locus ”compaction” and macromolecular crowding of the cytosol, respectively. Consequently, limitations to changes in motion may suggest a functional limit to maximal relaxation and compaction of a genetic locus and the ability of a bacterial cell to alter gene physical environment flexibly, not only depending on external stimuli but also on the chromosomal coordinate of a gene. Possible reasons for such limits include, for relaxation: local cytosolic macromolecule crowding and cellular confinement, and for compaction: DNA molecule elasticity and locus-specific NAP density.

4.4.3 Findings support the "polymer in viscoelastic cytosol" model of chromosome

We observed that most of the responses, when plotted as fold changes in chromosomal against cytosolic motility lay on or near a straight line with gradient equal to 1 (Figure 4.3). This general correlation in both timing and magnitude of responses between the chromosome and cytosol is consistent with the physical representation of the chromosome as a "polymer suspended in a viscoelastic medium". In this model, individual parts (*e.g.*, genetic loci) of such polymer explore space by sub-diffusing through a crowded environment of macromolecules, some of which (*e.g.*, nucleic acids and cytoskeletal filaments) possess significant elastic properties. It follows that changes to the elastic moduli of macromolecules or to the viscosity of the surrounding medium will affect the energy states of individual polymer parts [16, 17]. Consequently, we speculate that the treatment-induced chromosomal effects, are a direct consequence of changes to the properties of the cytosol.

Furthermore, since local DNA topology and energy states are key to gene function [16], the antibiotic-induced changes to chromosomal loci dynamics discussed here may at least in part explain global gene expression changes reported previously for many antibiotics [35, 120, 121]. By modulating the "compaction" levels of individual genetic loci, antibiotics can affect the topology and thus physical availability of a gene to the expression machinery proteins as well as its energy levels (negative supercoiling) critical for RNA polymerase activity.

4.4.4 Antibiotics exert biophysical effects

For each treatment agent, we compare our findings to relevant results reported previously and propose a biophysical mechanism that is rooted in the polymer model outlined above and ultimately causes a change in the cystosolic macromolecule concentration.

For ciprofloxacin, we speculate that effects are caused primarily through inhibition of topoisomerase IV, an *E. coli* quinolone target secondary to DNA gyrase. Interference with decatenation of replicated DNA strands causes excessive cell filamentation and significant dilution of cytosol contents. The latter is likely to result in an increase in cytosolic aggregate and chromosomal loci motility. Work of Weber *et al.* also points to the causal role of topoisomerase IV. In their work novobiocin, an aminocoumarin antibiotic which – similarly to ciprofloxacin – targets DNA gyrase but has a significantly lower affinity to topoisomerase IV [171], caused no significant change to loci motility.

Our rifampicin effects are generally consistent with those reported by Weber *et al.*, who showed that after longer ($\geq$5 but $\leq$30 min) treatments, chromosomal loci motility increased and plateaued at an approximately two-fold greater magnitude [13]. While Parry *et al.* [15] reported a small decrease in the motility of cytosolic μNS aggregates under rifampicin treatment, the tested dose was high enough (25 μg/mL, 1.5$\times$expected MIC) to likely cause severe changes to cell physiology (*e.g.*, near complete shut-down of gene expression and significant growth stalling). Following Weber *et al.* [13] and Bakshi *et al.* [17], we speculate that RNAP inhibition

and mRNA pool decay combined with subsequent ribosomal subunit-nucleoid mixing cause a decrease in cytosol viscosity and nucleoid expansion, ultimately increasing cytosolic μNS aggregate and chromosomal loci motility.

Interestingly, the same study reported that treatment with chloramphenicol, a protein synthesis inhibitor which similarly to tetracycline targets the 30S ribosomal subunit to stall translation, resulted in an increase in chromosomal loci motility. This is not consistent with our finding that tetracycline causes no consistent effect on loci motility. However, the chloramphenicol dose used by Weber *et al.* (25 μg/mL, 2,500$\times$expected MIC) was much higher than our tetracycline dose (refer to Section 2.4, Methods). Interestingly, we observed that while tetracycline was the only treatment agent that affected (and decreased) cell lengths (Figures B15 and B18, Appendix B) (and also elongation rates, Figures B16 and B19, Appendix B), it also increased cell widths (Figure B20, Appendix B). We speculate that these two changes to cell size cancelled out (no net change in cell volume) resulting in no net change to cytosol viscosity. It is possible that responses to different doses could be different. It would be particularly useful to establish and test a tetracycline dose that does not affect cell elongation rates as was achieved for all other treatments in this work.

For vancomycin, although we detected only very small and not consistent effects on cell lengths and elongation rates (Figures B16 and B19, Appendix B), we noticed significant changes to cell morphology such as bending of cells (Figure B21). We speculate that inhibited cell wall synthesis resulted in impaired cell elongation and thus morphological defects, possibly creating conditions for condensation of cell contents and reduced motility of tracked markers.

For sorbitol, hyperosmotic shock conditions caused rapid water withdrawal from cells, effectively condensing cytosol components and leading to increased macromolecular crowding effects (*e.g.*, increasing attractive depletion forces between cytosolic proteins and other molecules), what in turn reduced motility of markers. We expected to observe a normalising response to the shock (recovery of pre-shock marker motilities), reported previously in *E. coli* for other parameters such as cytoplasmic osmolarity [156] achieved by import of compatible solutes and ions [172]. Unfortunately, we observed more rapid than typically photo-bleaching of chromosomal markers and were unable to collect valid Ori2 and Ter3 tracks after 80 and 60 min of exposure, respectively. We speculate that the strong shock conditions (sorbitol at 400 mM) impaired the production of ΔParB-GFP proteins. Cytosolic μNS aggregates appeared stable but no response to the initial decrease in motility was observed.

4.4.5 Microfluidics-aided studies of live cells

We observed that bacteria occupying microchannels of our customised microfluidic device are significantly narrower (by $\sim$10-20%) compared to bacteria growing on agarose pads, strongly suggesting bacteria grown in the microfluidic device were exposed to significant mechanistic forces (Figure 4.6). We also observed that dynamics of both genome and cytosol (in untreated cells) and the dynamics responses to treatments differed between those growth conditions,

especially for motility-decreasing treatment agents (vancomycin and sorbitol) (Figure D1). This suggested that physical pressure applied to cells affects the concentration of cytosol contents. This is possible because the elastic bacterial cell wall can be compressed and the cell volume reduced, leading to increased macromolecule concentration and reduced marker motility. Both, changes to cell morphology (without significant changes to physiology) [29] and reduction in cytosolic marker motilty under controlled pressure [*private conversation with Professor Kevin Dorfman and Dr Shi Yu, University of Minnesota*] were observed previously.

More generally, our findings indicate that care should be taken to ensure that microfluidics-aided experiments involving live cells are not biased by the nature of the experiment set-up. Microfluidic devices need to be designed with the investigated organism in mind to enable unbiased inquiry into cell properties and behaviour.

Chapter 5

Single-cell level gene expression under sublethal antibiotic treatments

5.1 Chapter overview

In this Chapter we investigate single-cell level gene expression responses to sublethal doses of tetracycline and chloramphenicol. We measure the levels of GFP production, controlled by either a constitutive or ribosomal promoter (inserted in either Ori3 or Ter3 chromosomal position), over long (7 h) treatment times in exponentially growing bacteria. We explore dose-dependent kinetic responses in cellular resource allocation to translation inhibition and reveal that both the dose and the relative level of antibiotic "reversibility" can affect response kinetics. We discuss the differences in responses from the constitutive and ribosomal promoter in the context of the minimal three-component proteome partitioning model and the gene-length dependent effects on processivity of translation. Finally, we discover that the position of a gene in the genome may affect the response in its activity and that the character of this position-dependence is consistent with the premises of the "polymer in a viscoelastic medium" model of the bacterial chromosome.

5.2 Chapter methods

Exponentially growing bacteria were allowed to populate micro-channels of a customised microfluidic device for 6 h prior to the arrival of a new medium containing either tetracycline (at a "high" 0.9 μM or "low" 0.09 μM dose) or chloramphenicol ("high" 12 μM dose only) (refer to Section 2.4 of the Methods chapter). The "high" tetracycline dose and the chloramphenicol dose appeared to reduce the growth rate by $\sim$30% when measured at a single-cell level, while the "low" tetracycline dose had a negligible effect on the growth rate. Each treatment condition was tested in a single experiment with cells from a single biological replicate. Once equilibrated, the device contained between approximately 2,000 and 3,500 bacteria (refer to Appendix C for details). Cells were segmented using a custom program developed by Mia

Panlilio (University of Cambridge). Cell total fluorescence, area, length, width were computed for all segmented cells. Values smaller or larger than 2 standard deviations from the mean were rejected from analysis. Semi-manual cell size analysis was used to corroborate cell length measurements and to compute cell elongation rates (refer to Section 2.7 of the Methods chapter).

5.3 Results

5.3.1 High dose of tetracycline decreases activity of constitutive and ribosomal promoters

We start by treating bacteria with the "high" dose (0.9 μM) of tetracycline and reveal that activity of both, the constitutive P5 (Figure 5.1) and ribosomal P1 (Figure 5.2) promoters decreases, regardless of their position in the genome. Notably, for both promoter types, the absolute promoter activity (quantified as protein concentration, *i.e.* cell intensity/area) is much higher for Ori (1,700 and 800 AU for P5 and P1, respectively) than for Ter (1,000 and 400 AU, for P5 and P1, respectively), as expected due to the gene copy number and other effects introduced earlier (refer to Section 1.2.3). At this dose, the growth rates decrease by approximately 30% (Figures 5.1C and 5.2C).
Following treatment, activity of the constitutive promoter decreases ($\sim$0.1-fold decrease in protein concentration, defined as the logarithm of ratio between normalised protein concentration before and after the media switch) in first 90 min of treatment and remains at this level for 3 h (Figure 5.1B). Notably, the response in Ori position is consistently stronger than in Ter (Figures 5.1B and 5.1D). Activity of the promoter in both positions returns to the original (pre-treatment) level, however, this recovery is faster for Ori position and it eventually exceeds its original value by $\sim$0.05-fold after 5 hours of treatment. The level is likely not stable at this stage and longer experiment would be necessary to determine equilibrated value. Conversely, the promoter in Ter position recovers much slower and reaches its original value after about 6 hours of treatment.

Response of the P1 promoter follows a similar trend, however, the decrease in protein concentration is faster and stronger (0.22-fold change reached after about 3 hours of treatment; Figures 5.2B and 5.2D) and the activity remains approximately at this level for the duration of the experiment. Similarly to the P5 promoter, response is consistently stronger in Ori position (Figure 5.2D).

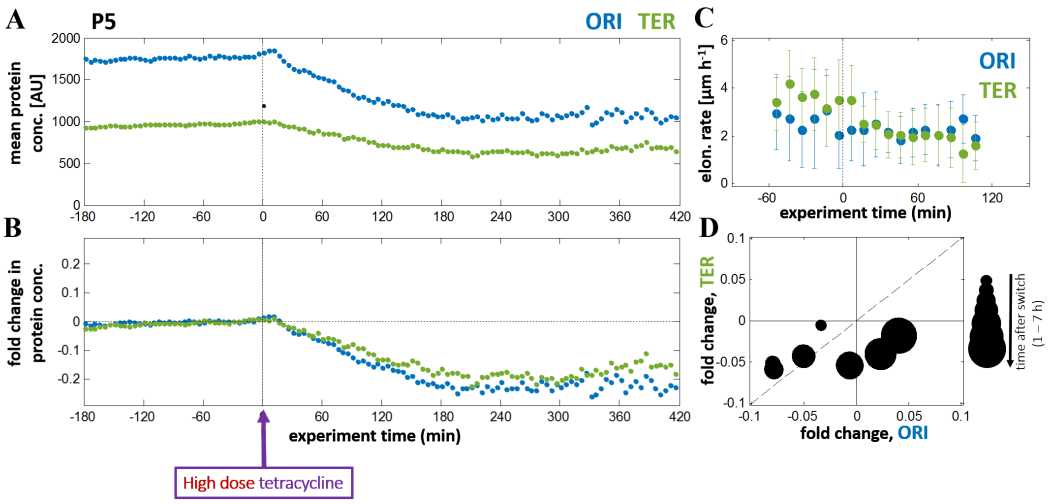

Fig. 5.1 **High dose (0.9 μM) of tetracycline decreases activity of a constitutive promoter.** Panels show (**A**) mean protein concentration (cell intensity/area), (**B**) mean fold change in protein concentration defined as the logarithm of ratio between normalised protein concentration before and after the media switch (indicated with vertical dashed line), (**C**) mean cell elongation rate (refer to Appendix for details) with whiskers indicating the widths of the distributions (specifically, 68.2% of data points, *i.e.* observations within one standard deviation from the mean), and (**D**) mean fold changes from (**B**) for P5-Ori and P5-Ter plotted against each other where each point represents fold change in mean protein concentration for all cells in a given hour (12 measurement time points per hour). Marker point size increases with increasing time (1-7 h after media switch). Straight dashed line represents gradient of 1. High dose (0.9 μM) of tetracycline decreases activity of constitutive P5 in both chromosomal positions: Ori (*blue*) and Ter (*green*).

5.3.2 Low dose tetracycline increases activity of a ribosomal promoter

Next, we decrease tetracycline dose 10-fold to 0.09 μM ("low" dose) and while we do not observe significant effects on the growth rate (Figure 5.3C), activity of the P1 promoter (in Ter position) increases 0.05-fold and fluctuates around this level throughout the experiment (Figure 5.3B). Such an increase is generally consistent with the three component partition of the proteome and global resource allocation through transcription regulation introduced earlier (Section 1.2.1).

In addition, we gathered some evidence that activity of the P1 promoter increases also in Ori position (as indicated with a prominent increase in cell intensity directly after media switch), however, its pre-treatment activity level is not stable and consequently does not allow for valid comparisons (refer to Figure C12, Appendix C).

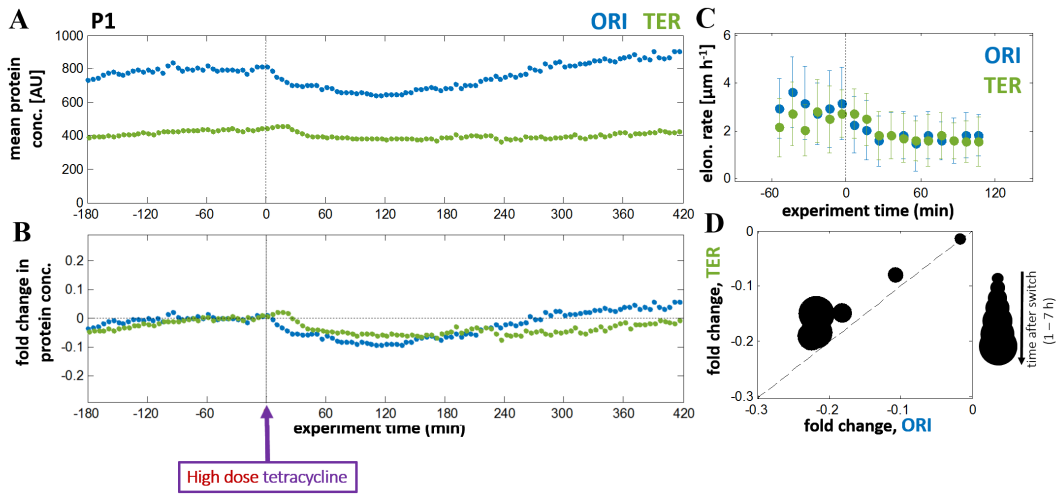

Fig. 5.2 **High dose (0.9 μM) of tetracycline decreases activity of a ribosomal promoters.** Panels show (**A**) mean protein concentration (cell intensity/area), (**B**) fold change in protein concentration defined as the logarithm of ratio between normalised protein concentration before and after the media switch (indicated with vertical dashed line), (**C**) mean cell elongation rate (refer to Appendix for details) with whiskers indicating the widths of the distributions (specifically, 68.2% of data points, *i.e.* observations within one standard deviation from the mean), and (**D**) mean fold changes from (**B**) for P1-Ori and P1-Ter plotted against each other where each point represents fold change in mean protein concentration for all cells in a given hour (12 measurement time points per hour). Marker point size increases with increasing time (1-7 h after media switch). Straight dashed line represents gradient of 1. High dose (0.9 μM) of tetracycline decreases activity of ribosomal P1 in both chromosomal positions: Ori (*blue*) and Ter (*green*).

5.3.3 Low dose tetracycline increases activity also of a constitutive promoter

When treated with the low dose (0.09 μM) of tetracycline, also the P5 promoter shows an increase in its activity and fluctuates around this level for the duration of the experiment, regardless of its position in the genome (Figures 5.4A and 5.4B). Again, at this dose, effects on growth rates are insignificant (Figure 5.4C).

The initial (<2 h of treatment) increase is approximately two times larger in Ori (up to nearly 0.1-fold) position than in Ter (∼0.04-fold) (Figures 5.4B). It should be noted, however, that since measurements are of a single biological replicate and this P1-Ori measurement shows unusually low pre-treatment activity levels (400 AU; Figure 5.4A), this result needs to be interpreted with caution. At longer treatment times responses in Ori and Ter virtually equalise and remain around +0.06, with Ter showing a slightly greater fold change during final 4 h of experiment (Figures 5.4D).

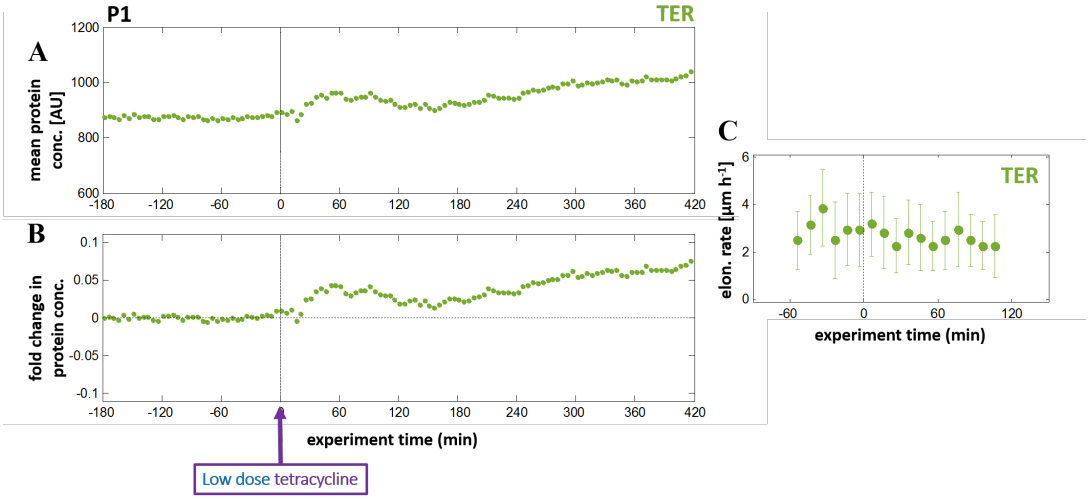

Fig. 5.3 **Low dose (0.09 μM) of tetracycline increases activity of a ribosomal promoter.** Panels show (**A**) protein concentration (cell intensity/area), (**B**) normalised fold change, defined as logarithm of ratio between normalised mean protein concentration before and after the media switch, and (**C**) mean cell elongation rate (refer to Appendix for details) with whiskers indicating the widths of the distributions (specifically, 68.2% of data points, *i.e.* observations within one standard deviation from the mean). Low dose (0.09 μM) of tetracycline causes an increase in the activity of the ribosomal P1 promoter (Ter position shown).

5.3.4 Responses to tetracycline for Ori and Ter positions are generally consistent between all conditions and most treatment times

In order to compare directly responses between different promoter positions across all treatment conditions, we plot mean fold changes in the activity of both promoters during each hour of treatment with ”high” and ”low” doses of tetracycline (Figure 5.5). We reveal that responses to tetracycline from promoters in Ori and Ter positions are generally consistent between all conditions and most treatment times. All responses to low dose tetracycline and all shorter-term responses ($\leq$4 h of treatment) to high dose tetracycline lay on or near a straight line with gradient equal to 1 (Figure 5.5, dashed diagonal line). That is, these responses generally correlate in both magnitude and timing. Longer-term responses ($>$4 h of treatment) under high dose treatment deviate from this pattern: for the P5 promoter, response in Ori position becomes larger (by up to 30%), while for the P1 promoter, response in Ori returns to its original value quicker compared to Ter and then changes sign to reach a fold change of +0.04. Another important observation is that, where responses between positions correlate, response in Ori position is slightly stronger than in Ter, at most treatment times.

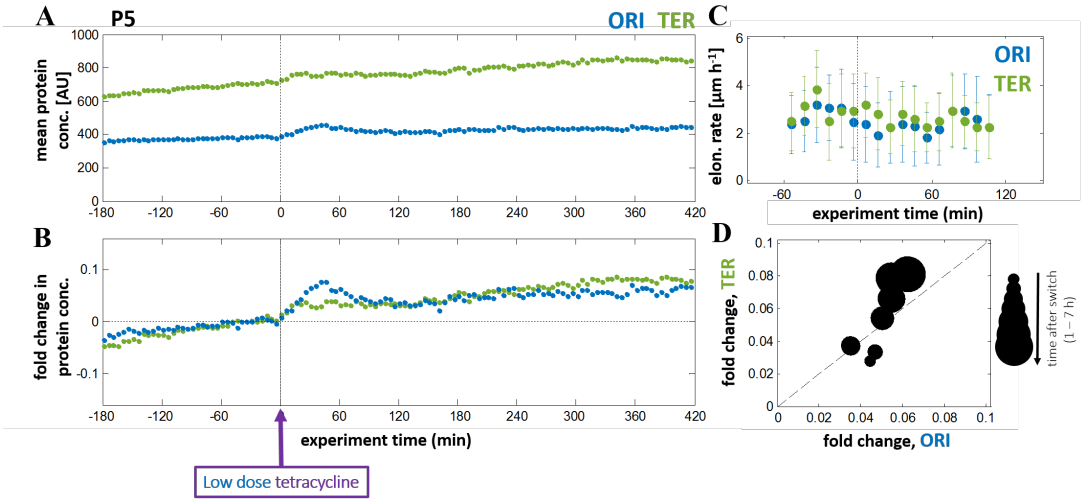

Fig. 5.4 **Low dose (0.09 μM) tetracycline increases activity also of a constitutive promoter, in both chromosomal positions.** Panels show (**A**) mean protein concentration (cell intensity/area), (**B**) normalised fold change, defined as logarithm of ratio between normalised mean protein concentration before and after the media switch, (**C**) mean cell elongation rate (refer to Figure C1, Appendix C for details) with whiskers indicating the widths of the distributions (specifically, 68.2% of data points, *i.e.* observations within one standard deviation from the mean), and (**D**) mean fold changes from (**B**) for P5-Ori and P5-Ter plotted against each other where each point represents fold change in mean protein concentration for all cells in a given hour (12 measurement time points per hour). Marker point size increases with increasing time (1-7 h after media switch). Straight dashed line represents gradient of 1. Low dose (0.09 μM) of tetracycline causes an increase in the activity of the constitutive P5 promoter in both chromosomal positions. The short-term (<1.5 h) is larger for the promoter in Ori position.

5.3.5 Chloramphenicol increases activity of a ribosomal promoter in both positions

We continue by attempting to corroborate the results obtained with tetracycline, using chloramphenicol, another translation inhibitor (refer to Section 1.3.2) with a very similar mode of action to tetracycline whose effects on promoter activity were studied previously [60]. We test effects of a relatively high dose (12 μM) of chloramphenicol, similar to the "high" dose of tetracycline used earlier. Remarkably, we discover that even though both treatments cause similar reductions in the elongation rate (by approximately 30%; Figures 5.2C and 5.6C) and a similar increase in mean cell length (from 2.5-3.0 to 3.2-3.5 μm; Figure C1, Appendix C), chloramphenicol causes an increase in the activity of the ribosomal P1 promoter. This is opposite to the response of this promoter to (an equivalent) "high" dose tetracycline (Figure 5.2). Responses to chloramphenicol in both positions are highly consistent between each other: responses in both Ori and Ter positions increase during the first 2 h of treatment and then stabilise (with some fluctuations), with response in Ori being slightly larger ($\sim$+0.07) compared to Ter ($\sim$+0.06) in the last 5 h of treatment.

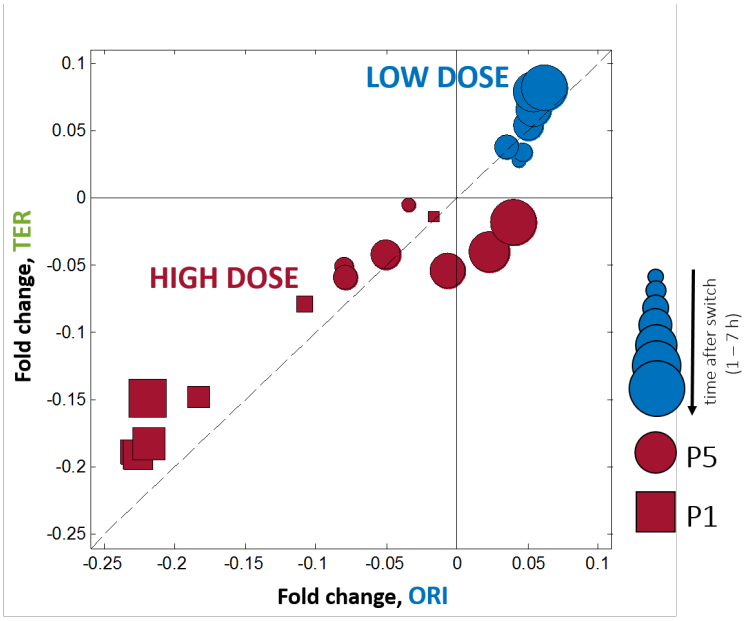

Fig. 5.5 **Responses for Ori and Ter positions are generally consistent between all conditions and most treatment times.** Responses in the activity of P1 (*circles*) and P5 (*squares*) promoters to "low" (*blue* points) and "high" (*red* points) doses of tetracycline lay near the straight dashed line representing gradient of 1. Marker point size increases with increasing time (1-7 h after media switch). Each point represents fold change in mean protein concentration for all cells in a given hour (12 measurement time points per hour). All responses to low dose tetracycline and all shorter-term responses ($\leq$4 h of treatment) to high dose tetracycline lay on or near a straight line with gradient equal to 1 (Figure 5.5, dashed diagonal line). That is, these responses generally correlate in both magnitude and timing. In addition, where responses between positions correlate, response in Ori position is slightly stronger than in Ter, at most treatment times.

5.3.6 Similar antibiotics can have comparable effects on a promoter activity but different on cell size and elongation rate

Our final observation is that, remarkably, tetracycline and chloramphenicol – when used at doses exerting comparable effects on promoter activity (Figure 5.7D) – cause drastically different effects on cell size and elongation rates (Figure 5.7). Chloramphenicol causes significant cell filamentation (by up to +0.15-fold; 2.8-3.9 μm in cell length) and a $\sim$30% reduction in the cell elongation rate while tetracycline causes a small decrease in cell length (by only up to -0.05-fold) and a very small and practically negligible change in the cell elongation rate. It is important to point out that the semi-manual cell size analysis did not corroborate effects of tetracycline: no effect on cell length was measured there (Figure C1, Appendix C).

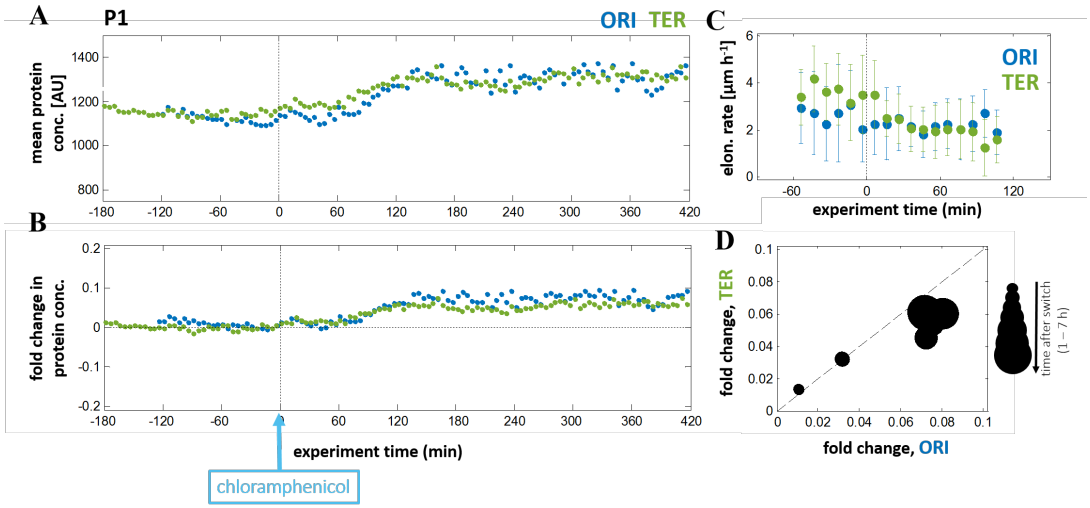

Fig. 5.6 **"High" dose (12 μM) chloramphenicol increases activity of ribosomal promoter in both positions.** Panels show (**A**) mean protein concentration (cell intensity/area), (**B**) normalised fold change, defined as the logarithm of ratio between normalised mean protein concentration before and after the media switch, (**C**) mean cell elongation rate (refer to Appendix for details) with whiskers indicating the widths of the distributions (specifically, 68.2% of data points, *i.e.* observations within one standard deviation from the mean), and (**D**) mean fold changes from (**B**) for P1-ori and P1-ter plotted against each other where each point represents fold change in mean protein concentration for all cells in a given hour (12 measurement time points per hour). Marker point size increases with increasing time (1-7 h after media switch). Straight dashed line represents gradient of 1. "High" dose (12 μM) chloramphenicol causes an increase in the activity of the ribosomal P1 promoter. Responses are comparable for both Ori and Ter position.

5.4 Discussion

5.4.1 Resource allocation at translation inhibition

Bacteria evolved efficient mechanisms of response to changes in their environment. One of these mechanisms is global transcription regulation where stimuli-sensitive fluctuations in metabolites such as ppGpp can cause widespread and differential effects on the activity of a variety of genetic promoters. At translation inhibition, transcription machinery is directed mostly to ribosomal promoters to compensate for lowered translation rates and thus reduce the intracellular build-up of amino acids. Consequently, constitutive promoters can experience changes in their activity caused by intracellular competition for transcription resources as predicted by the minimal three-component proteome partitioning model.

We observed these effects by monitoring GFP production under control of constitutive and ribosomal promoters. Following treatment with the "low" dose of tetracycline, we observed an increase in the activity of the ribosomal P1 promoter and – to our knowledge, for the first time – revealed the kinetics of this response in exponentially growing cells. The activity increased 0.05-fold over the first 60 min of treatment and then showed marked fluctuations around this level (from +0.02 to +0.07-fold) during the next 6 hours of treatment, suggesting prolonged

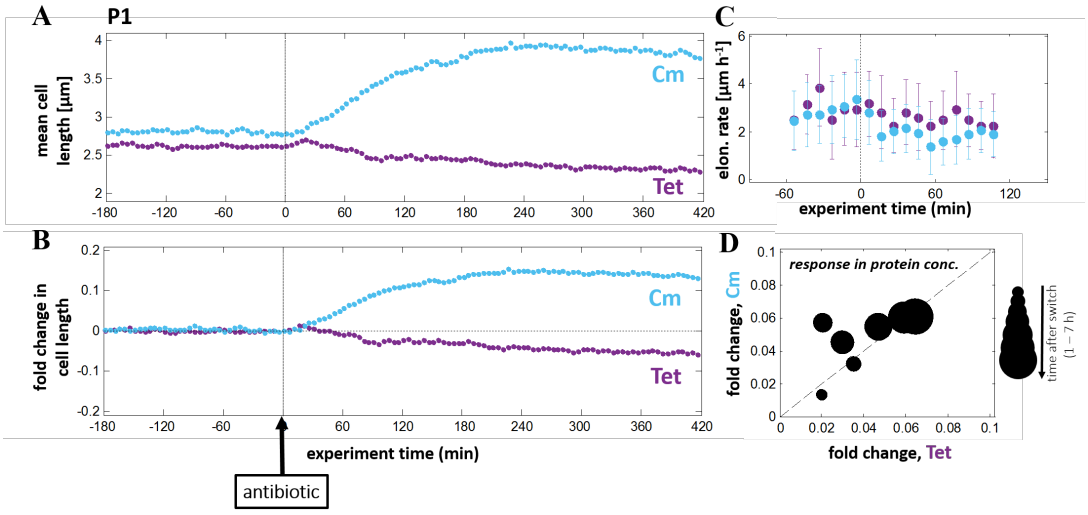

Fig. 5.7 **Similar antibiotics can have comparable effects on a promoter activity but different on cell size and elongation rate.** Panels show (**A**) mean cell length of all cells at each measurement time point and (**B**) normalised fold change in mean cell length, defined as logarithm of ratio between normalised mean cell length before and after the media switch, (**C**) mean cell elongation rate (refer to Figure C1 Appendix C) with whiskers indicating the widths of the distributions (specifically, 68.2% of data points, *i.e.* observations within one standard deviation from the mean), and (**D**) mean fold changes from (**B**) for P1-Ter under tetracycline and chloramphenicol treatment plotted against each other where each point represents fold change in mean protein concentration for all cells in a given hour (12 measurement time points per hour). Marker point size increases with increasing time (1-7 h after media switch). Straight dashed line represents gradient of 1. Low dose (0.09 μM) of tetracycline and a relatively high dose (12 μM) of chloramphenicol both cause a comparable increase in the activity of the P1 promoter (in Ter position) but radically different changes in cell length.

adaptation to translation inhibition (Figure 5.3). The highly reversible nature of permeation of tetracycline through bacterial membranes and of binding to its target, can at least partially explain the delayed onset of effects and fluctuations in the response. In agreement with these findings, we observed similar kinetics of response also to chloramphenicol, another reversible translation inhibitor.

By normalising responses by dose potency (antibiotic-induced reduction in growth rate or cell elongation rate), we compared the effects of tetracycline to the effects of chloramphenicol reported by Hwa *et al.*, who used the latter antibiotic to inhibit translation and measured (in bulk) the RNA/protein ratio, which directly reported for the mass fraction of ribosomes in the cell. We revealed that tetracycline and chloramphenicol (at equivalent doses) caused comparable increases ($\sim$0.05-fold and $\sim$0.03-fold, respectively) in the ribosome concentration. We speculate on the origins of this small difference in Section 5.4.3.

In order to compare directly our findings to literature, we challenged bacteria with a 12 μM dose of chloramphenicol and observed an increase in the activity of the P1 promoter of up to 0.08-fold. By normalising responses by the dose potency, we revealed that Hwa *et al.* observed, at an equivalent dose, a $\sim$0.16-fold increase in the RNA/protein ratio. This difference

between our studies may originate from the fact that our measurements were performed on exponentially growing cells while the cited work used values averaged along the growth curve (total RNA and protein assayed across a range of OD_{600}).

5.4.2 Effects of gene length and the processivity of translation

Generally, activity of a constitutive promoter is expected to decrease in response to translation inhibition as predicted by the three component partition of the proteome model and as shown previously for β-galactosidase production under chloramphenicol treatment [60]. Seemingly contradicting this prediction, we observed a tetracycline-induced increase (up to 0.08-fold) in the P5 promoter activity. This apparent contradiction can be explained with translation effects. As the processivity of translation (number of codons successfully translated into amino acids per unit time) decreases exponentially with increasing gene length [173], the probability to finish translation of a long gene is lower compared to a shorter gene. Consequently, translation inhibition will decrease the rate of expression of the longer gene to a greater extent.

This was recently demonstrated experimentally for two reporter proteins (a GFP and β-galactosidase), characterised by a $\sim$4-fold difference in their amino acid length and whose expression was under control of the constitutive P5 promoter. Despite competition for transcription resources at translation inhibition, the shorter reporter protein (GFP) still showed an increase in its intracellular concentration as its production rate was higher than its dilution rate. The opposite was true for the longer reporter protein [*private conversation with Dr Bianca Sclavi, ENS Cachan, Université Paris-Saclay*].

5.4.3 Response kinetics may be affected by antibiotic reversibility

Despite the consistent effects discussed above and a general similarity in the pharmacology, tetracycline and chloramphenicol showed a number of striking differences in their effects. We observed that equivalent doses (limiting growth to a comparable degree) of the two antibiotics caused drastically different effects on promoter activity. Tetracycline decreased significantly the GFP production rates, regardless of which promoter type controlled its transcription (Figures 5.1 and 5.2), while chlorampenicol caused an increase in the P1 promoter activity (Figure 5.6).

Although reversible translation inhibitors such as tetracycline and chloramphenicol cause a gradual decline in translation rates as a function of dose (in contrast to irreversible translation inhibitors, which cause a sharp decline above a critical dose) [114], a sufficiently high intracellular antibiotic concentration may effectively shut down the compensatory ribosome production. The ability to elicit such a compensatory response depends also on the degree of antibiotic reversibility. For two antibiotics of higher and lower reversibility present at the same concentration in the cell, the fraction of free (not inhibitor-bound) ribosomes capable of compensatory production will be higher at any moment for the relatively more reversible one, speeding up the compensatory response. Further, since transport of molecules such as antibiotics across bacterial membranes may be metabolically regulated [113], change in

nutrient quality may affect the degree of antibiotic reversibility. Scott *et al.* showed that a reduction in nutrient quality caused an increase in the critical reversibility of chloramphenicol (factoring in its transport across the cell membrane and binding to ribosomes) [114].

Consequently, since our experiments involving chloramphenicol used media without casamino acids (CAAs) and tetracyline experiments used media with CAAs (not affecting pre-treatment growth rates significantly), it is possible that this difference resulted in a relatively lower reversibility of tetracycline action and the observed decrease in the activity of both promoters in response to the high tetracycline dose during the experiment. At this dose, tetracycline saturated most ribosomes (lower reversibility) shutting down most of protein synthesis and caused a slow compensatory ribosome production while an equivalent dose of chloramphenicol was far from saturating most ribosomes (higher reversibility) resulting in a quicker compensatory ribosome production, as observed experimentally in this work.

As a result, only after we lowered the tetracycline dose (10-fold), we observed comparable response kinetics and measured an increase in the P1 promoter activity caused by both antibiotics (discussed earlier; refer to Section 5.4.1). While the two antibiotics when used at different doses caused similar changes to the promoter activity, they affected the cell elongation rates and sizes differently, as expected: chloramphenicol caused a significant reduction in the elongation rate and considerable cell filamentation while tetracycline caused very small reductions in the elongation rate and cell size. Chloramphenicol-induced filamentation of bacterial cells was reported before and although its mechanism is not fully understood, it can be a result of erroneous synthesis of the divisome proteins [174].

5.4.4 Responses from promoters in different genomic positions are generally consistent but responses from Ori tend to be larger than from Ter

The fundamental question asked in this PhD work was how different antibiotics can affect the physical properties (Chapter 3 and 4) of the genetic loci (and the cytosol) and whether these effects may affect their biological function. In this Chapter, we discovered that responses to various doses of tetracycline in the activity of ribosomal and constitutive promoters generally correlated between the promoter positions in the genome, in both response magnitude and timing. At the same time, we noticed that wherever there was a general consistency in effects from both positions, responses from the Ori position were (by a small degree but consistently) larger than from Ter.

We speculate that the observed general genome-wide consistency in effects reflects the global structure of the chromosome as a compacted ”polymer in a viscoelastic medium”, while the systematic differences in the magnitude of responses from individual loci originate from the combined effect of several local factors: higher gene copy number and DNA gyrase concentration in the Ori half of the genome, and an uneven NAPs distribution along the genome: for example, preferential clustering of upregulated genes (including the rRNA operons) around

the OriC site by HU and the preferential formation of gene-silencing extensive binding domains in the Ter half of the genome by H-NS.

Chapter 6

Conclusions and future work

This PhD work contributed to the much needed systems-level understanding of bacterial responses to antibiotics. First, we improved the precision of "microrheology" measurements developing a novel data treatment procedure. This way we empirically accounted for marker photo-bleaching and size-displacement dependence and, as a result, enabled comparisons of long term (several hours) effects of different antibiotics. Similar studies in the past [13–15, 21, 22, 42] were limited to single time-point measurements and did not consider these significant corrections. Applying the procedure to control (not treated) data sets revealed, for the first time, the stable nature (over several hours in exponentially growing cells) of position-dependent differences in the physical organisation of the chromosome reported previously [14] and possible growth-rate dependent effects on loci motility.

Second, by performing high-throughput and high-precision intracellular marker tracking, we discovered that sublethal doses of ciprofloxacin, rifampicin, and vancomycin as well as hyperosmotic shock conditions caused small but consistent changes (unique to each treatment agent) to the physical organisation of chromosomal Ori2 and Ter3 loci and the cytosol. We revealed strong correlations between the effects in different parts of the chromosome and between the chromosome and cytosol, and proposed specific mechanisms – consistent with the current physical view of the bacterial chromosome – on how different antibiotics can exert observed effects. It is for the first time that the physical chromosomal and cytosolic responses to a range of sublethal treatments were characterised systematically.

Finally, we linked the biophysical observations with gene expression effects. By performing high-throughput single-cell level promoter activity measurements during exposure to antibiotics, we revealed that the relationship between position of a gene and response in its activity to treatment may reflect the globally consistent but locally modulated structure of the chromosome. In addition, we compared responses from constitutive and ribosomal promoters over long (7 h) treatment times in exponentially growing bacteria and revealed, for the first time, the kinetics of cellular resource allocation at translation inhibition. We then proposed how differences in the "reversibility" of different translation inhibitors may account for differences in response kinetics.

Despite the novel and important insights delivered in this work, further research is needed to gain a more complete understanding of how antibiotics affect bacterial physiology and behaviour to eventually devise improved methods of infection control. We briefly discuss possible directions of future research originating from each segment of this work and outline relevant examples of work already in progress.

Although our empirical data procedure is useful for comparing different data sets and improves measurement precision, it does not take into account the underlying physics of marker motion. In the future, a physical model describing tracer size-dependent motions of chromosomal loci and cytosolic aggregates in live cells may further improve the data treatment procedure and highlight aspects of biological and physical significance. Ground work in this field has already been completed by J. Theriot *et al.* and A. Spakowitz *et al.*, among others, with recent publications discussing physical models of motion for both chromosomal loci [13, 175] and cytosolic molecules [15, 176]).

Since bacterial growth and susceptibility to treatments depend heavily on the growth conditions, future work on the genome and cytosol dynamics needs to include measurements in bacteria grown in a variety of environments. Such experiments may include microfluidic growth platforms (*e.g.*, [141, 177, 178]), however, device designs must ensure minimal or no impact on the bacterial physiology, as explained earlier (refer to Section 4.4.5). Further, alternative approaches, for example agarose pads systems with permeable membranes for fresh medium supply and waste removal, can be considered. Moreover, in order to further foster development of novel antimicrobial therapeutics, studies need to emulate closely clinically relevant treatment conditions, for example, by enabling monitoring of responses to dynamically modulated concentrations of a variety of antibiotics, including novel peptide antibiotics (reviewed in [179]), and their combinations. Use of antibiotic gradients in agarose pads [125] and microfluidic devices [180] have been explored recently while the recent work of T. Bollenbach *et al.*, and other groups, offered improved understanding of the effects of combinatorial antibiotic therapies (*e.g.*, [117]).

In addition, in order to better understand relationships between the structures and functions of the genome and cytosol, fluorescent tagging of multiple markers per cell is necessary to reduce strain-dependent bias and to provide insights on real-time interactions between different cellular components. This has been achieved in bacteria using modern genetic engineering and automated high-resolution microscopy methods (*e.g.*, [181]). Moreover, researchers should aim for complete characterisation of marker motion and thus compute – in addition to the MSD and where relevant – the radius of gyration, length of confinement, eccentricity levels, and elastic properties of individual markers. Robust analytical workflows for the analysis of single-particle trajectories have been developed (*e.g.*, [182]). Furthermore, other loci tagging techniques such as the ParB-$parS_{pMT1}$ system [183] can be explored to minimise label-dependent effects. Additionally, changes to local physical properties should be complemented with measurements of the global macromolecular composition of the cell such as changes to the total protein concentration and – where relevant – total RNA and ribosome concentrations. Methods for

measuring macromolecular composition in bulk cultures have long been established (*e.g.*, [184, 185]) and novel approaches of single-molecule sensitivity are emerging (*e.g.*, [186]).

Single-cell level gene expression studies should take into account the above considerations regarding growth and treatment conditions and, ultimately, aim for correlating directly "biological" effects with the "physical" ones. For example, characterising gene expression kinetics as a function of the genome and cytosol dynamics will provide a more holistic understanding of gene regulation mechanisms. This can be achieved directly, with real-time reporting on promoter activity and marker dynamics using multi-colour labelling and automated microscopy systems and indirectly with single-cell level '-omics' measurements (reviewed in [187]), ideally performed on selected cells whose physical properties were previously measured (for example, in a microfluidic device). Another approach, where heterogeneous populations of bacteria with pre-determined (fluorescently-labelled) genotypes are investigated at a single-cell level has been recently explored [188].

Studies should include resistant strains and, ideally, measure changes in variables as a function of resistance levels. Experimental techniques for controlled resistance development have been explored (*e.g.*, [125]). Understanding how resistance emerges and spreads in temporal and spatial dimensions should remain key area of microbiological research. In addition to resistance however, future experiments should focus on responses from 'tolerant' (or 'persistent') bacterial subpopulations. N. Balaban *et al.* and K. Gerdes *et al.*, among others, have completed ground work on the experimental methods of tolerant bacteria determination [129] and the characterisation of some of the molecular mechanisms underlying tolerance emergence [77, 132, 111, 189, 190], including the causal relationship between tolerance and resistance [191].

References

[1] Jay K. Fisher, Aude Bourniquel, Guillaume Witz, Beth Weiner, Mara Prentiss, and Nancy Kleckner. Four-dimensional imaging of E. coli nucleoid organization and dynamics in living cells. *Cell*, 153(4):882–895, 2013.

[2] Suckjoon Jun and Bela Mulder. Entropy-driven spatial organization of highly confined polymers: lessons for the bacterial chromosome. *Proc. Natl. Acad. Sci. U. S. A.*, 103(33):12388–93, 2006.

[3] Henrik J. Nielsen, Brenda Youngren, Flemming G. Hansen, and Stuart Austin. Dynamics of Escherichia coli chromosome segregation during multifork replication. *J. Bacteriol.*, 189(23):8660–8666, 2007.

[4] Olivier Espéli and Frédéric Boccard. Organization of the Escherichia coli chromosome into macrodomains and its possible functional implications. *J. Struct. Biol.*, 156(2):304–10, 2006.

[5] Jack Bryant, Laura E Sellars, Stephen J W Busby, and David J Lee. Chromosome position effects on gene expression in Escherichia coli K-12. *Nucleic Acids Res.*, 42(18):11383–92, 2014.

[6] Thomas E Kuhlman and Edward C Cox. Gene location and DNA density determine transcription factor distributions in Escherichia coli. *Mol. Syst. Biol.*, 8(610):1–13, 2012.

[7] Patrick Sobetzko, Andrew Travers, and Georgi Muskhelishvili. Gene order and chromosome dynamics coordinate spatiotemporal gene expression during the bacterial growth cycle. *Proc. Natl. Acad. Sci. U. S. A.*, 109(2):42–50, 2012.

[8] Patrick N. Higgins. RNA polymerase: chromosome domain boundary maker and regulator of supercoil density. *Curr. Opin. Microbiol.*, 22:138–143, 2014.

[9] Ramanan Laxminarayan, Adriano Duse, Chand Wattal, Anita K M Zaidi, Heiman F L Wertheim, Nithima Sumpradit, Erika Vlieghe, Gabriel Levy Hara, Ian M Gould, Herman Goossens, Christina Greko, Anthony D So, Maryam Bigdeli, Göran Tomson, Will Woodhouse, Eva Ombaka, Arturo Quizhpe Peralta, Farah Naz Qamar, Fatima Mir, Sam Kariuki, Zulfiqar a Bhutta, Anthony Coates, Richard Bergstrom, Gerard D Wright, Eric D Brown, and Otto Cars. Antibiotic resistance-the need for global solutions. *Lancet Infect. Dis.*, 13(12):1057–98, 2013.

[10] Nancy Kleckner, Jay K Fisher, Mathieu Stouf, Martin A White, David Bates, and Guillaume Witz. The bacterial nucleoid: nature, dynamics and sister segregation. *Curr. Opin. Microbiol.*, 22:127–137, 2014.

[11] Julio E Cabrera, Cedric Cagliero, Selwyn Quan, Catherine L Squires, and Ding Jun Jin. Active transcription of rRNA operons condenses the nucleoid in Escherichia coli: examining the effect of transcription on nucleoid structure in the absence of transertion. *J. Bacteriol.*, 191(13):4180–5, 2009.

[12] Somenath Bakshi, Renée M Dalrymple, Wenting Li, Heejun Choi, and James C Weisshaar. Partitioning of RNA polymerase activity in live Escherichia coli from analysis of single-molecule diffusive trajectories. *Biophys. J.*, 105(12):2676–86, 2013.

[13] Stephanie C Weber, Andrew J Spakowitz, and Julie A Theriot. Nonthermal ATP-dependent fluctuations contribute to the in vivo motion of chromosomal loci. *Proc. Natl. Acad. Sci. U. S. A.*, 109(19):7338–43, 2012.

[14] Avelino Javer, Zhicheng Long, Eileen Nugent, Marco Grisi, Kamin Siriwatwetchakul, Kevin D Dorfman, Pietro Cicuta, and Marco Cosentino Lagomarsino. Short-time movement of E. coli chromosomal loci depends on coordinate and subcellular localization. *Nat. Commun.*, 4:3003, 2013.

[15] Bradley R Parry, Ivan V Surovtsev, Matthew T Cabeen, Corey S O'Hern, Eric R Dufresne, and Christine Jacobs-Wagner. The bacterial cytoplasm has glass-like properties and is fluidized by metabolic activity. *Cell*, 156(1-2):183–94, 2014.

[16] Vincenzo G. Benza, Bruno Bassetti, Kevin D. Dorfman, Vittore F. Scolari, Krystyna Bromek, Pietro Cicuta, and Marco Cosentino Lagomarsino. Physical descriptions of the bacterial nucleoid at large scales, and their biological implications. *Reports Prog. Phys.*, 75(076602), 2012.

[17] Somenath Bakshi, Heejun Choi, Jagannath Mondal, and James C Weisshaar. Time-dependent Effects of Transcription- and Translation-halting Drugs on the Spatial Distributions of the E. coli Chromosome and Ribosomes. *Mol. Microbiol.*, 94(4):871–887, 2014.

[18] Remus T. Dame. The role of nucleoid-associated proteins in the organization and compaction of bacterial chromatin. *Mol. Microbiol.*, 56(4):858–870, 2005.

[19] Martijn S. Luijsterburg, Maarten C. Noom, G. J L Wuite, and Remus Th Dame. The architectural role of nucleoid-associated proteins in the organization of bacterial chromatin: A molecular perspective. *J. Struct. Biol.*, 156(2):262–272, 2006.

[20] Renko De Vries. DNA condensation in bacteria: Interplay between macromolecular crowding and nucleoid proteins. *Biochimie*, 92(12):1715–1721, 2010.

[21] Stephanie C. Weber, Andrew J Spakowitz, and Julie A Theriot. Bacterial chromosomal loci move subdiffusively through a viscoelastic cytoplasm. *Phys. Rev. Lett.*, 104(23):27–30, 2010.

[22] Avelino Javer, Nathan J Kuwada, Zhicheng Long, Vincenzo G Benza, Kevin D Dorfman, Paul a Wiggins, Pietro Cicuta, and Marco Cosentino Lagomarsino. Persistent super-diffusive motion of Escherichia coli chromosomal loci. *Nat. Commun.*, 5:3854, 2014.

[23] Carl R. Woese, Otto Kandler, and Mark L. Wheelis. Towards a natural system of organisms: proposal for the domains Archaea, Bacteria, and Eucarya. *Proc. Natl. Acad. Sci. U. S. A.*, 87(12):4576–4579, 1990.

[24] Stefan Klumpp and Terence Hwa. Bacterial growth: global effects on gene expression, growth feedback and proteome partition. *Curr. Opin. Biotechnol.*, 28:96–102, 2014.

[25] Stefan Klumpp, Zhongge Zhang, and Terence Hwa. Growth Rate-Dependent Global Effects on Gene Expression in Bacteria. *Cell*, 139(7):1366–1375, 2009.

[26] Jue D. Wang and Petra A. Levin. Metabolism, cell growth and the bacterial cell cycle. *Nat. Rev. Microbiol.*, 7(11):822–7, 2009.

[27] Luanne Hall-Stoodley, William J Costerton, and Paul Stoodley. Bacterial biofilms: from the natural environment to infectious diseases. *Nat. Rev. Microbiol.*, 2(2):95–108, 2004.

[28] David Davies. Understanding biofilm resistance to antibacterial agents. *Nat. Rev. Drug Discov.*, 2(2):114–122, 2003.

[29] Fangwei Si, Bo Li, William Margolin, and Sean X Sun. Bacterial growth and form under mechanical compression. *Sci. Rep.*, 5:11367, 2015.

[30] Ana Flores-Meireles, Jennifer Walker, Michael Caparon, and Scott Hultgren. Urinary tract infections: epidemiology, mechanisms of infection and treatment options. *Nat. Rev. Microbiol.*, 13(5):269–284, 2015.

[31] Stefano C. M. Picozzi, Stefan Casellato, and Luca Carmignani. Extended-spectrum beta-lactamase-positive Escherichia coli causing complicated upper urinary tract infection: Urologist should act in time. *Urol. Ann.*, 6(2):107–112, 2014.

[32] Richard D Smith and Joanna Coast. Antimicrobial resistance: a global response. *Bull. World Health Organ.*, 80(2):126–33, 2002.

[33] Stephen R. Palumbi. Humans as the world's greatest evolutionary force. *Science*, 293(5536):1786–90, 2001.

[34] Alfonso J Alanis. Resistance to antibiotics: are we in the post-antibiotic era? *Arch. Med. Res.*, 36(6):697–705, 2005.

[35] Janine T Lin, Mariah Bindel Connelly, Chris Amolo, Debbie S Yaver, and Suzie Otani. Global Transcriptional Response of Bacillus subtilis to Treatment with Subinhibitory Concentrations of Antibiotics That Inhibit Protein Synthesis Global Transcriptional Response of Bacillus subtilis to Treatment with Subinhibitory Concentrations of Antibi. *Antimicrob. Agents Chemother.*, 49(5):1915–1926, 2005.

[36] Wang Xindan, Llopis Paula Montero, and Z. Rudner David. Organization and segregation of bacterial chromosomes. *Nat Rev Genet*, 86(12):3279–3288, 2008.

[37] Joel Stavans and Amos Oppenheim. DNA-protein interactions and bacterial chromosome architecture. *Phys. Biol.*, 3(4):1–10, 2006.

[38] James D Watson and Francis H C Crick. Molecular structure of nucleic acids. *Nature*, 171(4356):737–738, 1953.

[39] John F Marko and Simona Cocco. The micromechanics of DNA. *Phys. World*, 3:37–41, 2003.

[40] Lisa Postow, Christine D Hardy, Javier Arsuaga, and Nicholas R Cozzarelli. Topological domain structure of the Escherichia coli chromosome. *Genes Dev.*, 18:1766–1779, 2004.

[41] Hironori Niki, Yoshiharu Yamaichi, and Sota Hiraga. Dynamic organization of chromosomal DNA in Escherichia coli. *Genes Dev*, 14:212–223, 2000.

[42] Olivier Espeli, Romain Mercier, and Frédéric Boccard. DNA dynamics vary according to macrodomain topography in the E. coli chromosome. *Mol. Microbiol.*, 68(6):1418–1427, 2008.

[43] Remus T. Dame, Olga J. Kalmykowa, and David C. Grainger. Chromosomal macrodomains and associated proteins: Implications for DNA organization and replication in gram negative bacteria. *PLoS Genet.*, 7(6), 2011.

[44] Charles J Dorman. Genome architecture and global gene regulation in bacteria: making progress towards a unified model? *Nat. Rev. Microbiol.*, 11(5):349–55, 2013.

[45] Sarah M. McLeod and Reid C. Johnson. Control of transcription by nucleoid proteins. *Curr. Opin. Microbiol.*, 4(2):152–159, 2001.

[46] Shane C. Dillon and Charles J. Dorman. Bacterial nucleoid-associated proteins, nucleoid structure and gene expression. *Nat. Rev. Microbiol.*, 8(3):185–195, 2010.

[47] Sylvie Rimsky and Andrew Travers. Pervasive regulation of nucleoid structure and function by nucleoid-associated proteins. *Curr. Opin. Microbiol.*, 14(2):136–41, 2011.

[48] Julio E. Cabrera and Ding J. Jin. Active transcription of rRNA operons is a driving force for the distribution of RNA polymerase in bacteria: Effect of extrachromosomal copies of rrnB on the in vivo localization of RNA polymerase. *J. Bacteriol.*, 188(11):4007–4014, 2006.

[49] Andrew Travers and Georgi Muskhelishvili. DNA supercoiling - a global transcriptional regulator for enterobacterial growth? *Nat. Rev. Microbiol.*, 3(2):157–69, 2005.

[50] Nastaran Hadizadeh Yazdi, Calin C. Guet, Reid C. Johnson, and John F Marko. Variation of the folding and dynamics of the Escherichia coli chromosome with growth conditions. *Mol. Microbiol.*, 86(6):1318–1333, 2013.

[51] Kathrine P. Lemon and Alan D. Grossman. Localization of bacterial DNA polymerase: evidence for a factory model of replication. *Science*, 282(5393):1516–1519, 1998.

[52] Conrad L. Woldringh. The role of co-transcriptional translation and protein translocation (transertion) in bacterial chromosome segregation. *Mol. Microbiol.*, 45(1):17–29, 2002.

[53] Julio E. Cabrera and Ding J. Jin. The distribution of RNA polymerase in Escherichia coli is dynamic and sensitive to environmental cues. *Mol. Microbiol.*, 50(5):1493–1505, 2003.

[54] Arash Sanamrad, Fredrik Persson, Ebba G Lundius, David Fange, Arvid H Gynnå, and Johan Elf. Single-particle tracking reveals that free ribosomal subunits are not excluded from the Escherichia coli nucleoid. *Proc. Natl. Acad. Sci. U. S. A.*, 111(31):1–6, 2014.

[55] Brian J Paul, Wilma Ross, Tamas Gall, and Richard L Gourse. rRNA transcription rate in Escherichia coli. *J. Bacteriol.*, 173(20):6647–6649, 2004.

[56] Douglas F. Browning and Stephen J. W. Busby. Local and global regulation of transcription initiation in bacteria. *Nat. Rev. Microbiol.*, 14(10):638–650, 2016.

[57] O. Maaløe. Regulation of the Protein-Synthesizing Machinery—Ribosomes, tRNA, Factors, and So On. *Biol. Regul. Dev.*, 1:487–542, 1979.

[58] F.C. Neidhardt and M. Ingraham, J.L. Schaechter. *Physiology of the Bacterial Cell: A Molecular Approach*. Sunderland, UK: Sinauer Nilsson, 1990.

[59] Hans Bremer and Patrick P Dennis. Modulation of Chemical Composition and Other Parameters of the Cell by Growth Rate. *ASM Press*, 2(93):1553–1569, 1996.

[60] Matthew Scott, Carl W Gunderson, Eduard M Mateescu, Zhongge Zhang, and Terence Hwa. Interdependence of cell growth and gene expression: origins and consequences. *Science*, 330(6007):1099–102, 2010.

[61] Zachary D. Dalebroux and Michele S. Swanson. ppGpp: magic beyond RNA polymerase. *Nat. Rev. Microbiol.*, 10(3):203–212, 2012.

[62] Lisa U. Magnusson, Anne Farewell, and Thomas Nyström. ppGpp: A global regulator in Escherichia coli. *Trends Microbiol.*, 13(5):236–242, 2005.

[63] Wilma Ross, Catherine E. Vrentas, Patricia Sanchez-Vazquez, Tamas Gaal, and Richard L. Gourse. The magic spot: A ppGpp binding site on E. coli RNA polymerase responsible for regulation of transcription initiation. *Mol. Cell*, 50(3):420–429, 2013.

[64] S. Klumpp and T. Hwa. Growth-rate-dependent partitioning of RNA polymerases in bacteria. *Proc. Natl. Acad. Sci.*, 105(51):20245–20250, 2008.

[65] Matthew Scott and Terence Hwa. Bacterial growth laws and their applications. *Curr Opin Biotechnol*, 37(1):62–70, 2012.

[66] Matthew Scott, Stefan Klumpp, Eduard M. Mateescu, and Terence Hwa. Emergence of robust growth laws from optimal regulation of ribosome synthesis. *Mol. Syst. Biol.*, 10(8):747, 2014.

[67] Julie A. Cass, Nathan J. Kuwada, Beth Traxler, and Paul A. Wiggins. Escherichia coli Chromosomal Loci Segregate from Midcell with Universal Dynamics. *Biophys. J.*, 110(12):2597–2609, 2016.

[68] Kerren K Swinger and Phoebe A Rice. IHF and HU: flexible architects of bent DNA. *Curr. Opin. Struct. Biol.*, 14(1):28–35, 2004.

[69] Michael Berger, Anca Farcas, Marcel Geertz, Petya Zhelyazkova, Klaudia Brix, Andrew Travers, and Georgi Muskhelishvili. Coordination of genomic structure and transcription by the main bacterial nucleoid-associated protein HU. *EMBO Rep.*, 11(1):59–64, 2010.

[70] Georgi Muskhelishvili and Andrew Travers. Transcription factor as a topological homeostat. *Front. Biosci.*, 8:279–285, 2003.

[71] Christina Kahramanoglou, Aswin S N Seshasayee, Ana I. Prieto, David Ibberson, Sabine Schmidt, Jurgen Zimmermann, Vladimir Benes, Gillian M. Fraser, and Nicholas M. Luscombe. Direct and indirect effects of H-NS and Fis on global gene expression control in Escherichia coli. *Nucleic Acids Res.*, 39(6):2073–2091, 2011.

[72] Tiffany Vora, Alison K. Hottes, and Saeed Tavazoie. Protein Occupancy Landscape of a Bacterial Genome. *Mol. Cell*, 35(2):247–253, 2009.

[73] Rajalakshmi Srinivasan, Deepti Chandraprakash, Revathy Krishnamurthi, Parul Singh, Vittore F Scolari, Sandeep Krishna, and Aswin Sai Narain Seshasayee. Genomic analysis reveals epistatic silencing of "expensive" genes in Escherichia coli K-12. *Mol. Biosyst.*, 9:2021–33, 2013.

[74] Nikolaus Sonnenschein, Marcel Geertz, Georgi Muskhelishvili, and Marc-Thorsten Hütt. Analog regulation of metabolic demand. *BMC Syst. Biol.*, 5(1):40, 2011.

[75] Anne Liu, Lillian Tran, Elinne Becket, Kim Lee, Laney Chinn, Eunice Park, Katherine Tran, and Jeffrey H Miller. Antibiotic sensitivity profiles determined with an Escherichia coli gene knockout collection: generating an antibiotic bar code. *Antimicrob. Agents Chemother.*, 54(4):1393–403, 2010.

[76] Sonja Hansen, Kim Lewis, and Marin Vulić. Role of global regulators and nucleotide metabolism in antibiotic tolerance in Escherichia coli. *Antimicrob. Agents Chemother.*, 52(8):2718–26, 2008.

[77] Daria Leszczynska, Ewelina Matuszewska, Dorota Kuczynska-Wisnik, Beata Furmanek-Blaszk, and Ewa Laskowska. The Formation of Persister Cells in Stationary-Phase Cultures of Escherichia Coli Is Associated with the Aggregation of Endogenous Proteins. *PLoS One*, 8(1):e54737, 2013.

[78] Kyeong Soo Jeong, Jaeyong Ahn, and Arkady B Khodursky. Spatial patterns of transcriptional activity in the chromosome of Escherichia coli. *Genome Biol.*, 5(11):86, 2004.

[79] Brian J Peter, Javier Arsuaga, Adam M Breier, Arkady B Khodursky, Patrick O Brown, and Nicholas R Cozzarelli. Genomic transcriptional response to loss of chromosomal supercoiling in Escherichia coli. *Genome Biol.*, 5(11):87, 2004.

[80] Karl Drlica and Xilin Zhao. DNA Gyrase , Topoisomerase IV , and the 4-Quinolones. *Microbiol. Mol. Biol. Rev.*, 61(3):377–392, 1997.

[81] Eduardo P C Rocha. The organization of the bacterial genome. *Annu. Rev. Genet.*, 42:211–233, 2008.

[82] Sara Berthoumieux, Hidde de Jong, Guillaume Baptist, Corinne Pinel, Caroline Ranquet, Delphine Ropers, and Johannes Geiselmann. Shared control of gene expression in bacteria by transcription factors and global physiology of the cell. *Mol. Syst. Biol.*, 9(634):634, 2013.

[83] Charles L. Turnbough. Regulation of bacterial gene expression by the NTP substrates of transcription initiation. *Mol. Microbiol.*, 69(1):10–14, 2008.

[84] Kuanqing Liu, Alycia N. Bittner, and Jue D. Wang. Diversity in (p)ppGpp metabolism and effectors. *Curr. Opin. Microbiol.*, 24:72–79, 2015.

[85] Charles E. Helmstetter. Origin and sequence of chromosome replication in Escherichia coli. *J. Mol. Biol.*, 95(5):1634–1641, 1968.

[86] Shasha Chong, Chongyi Chen, Hao Ge, and X. Sunney Xie. Mechanism of Transcriptional Bursting in Bacteria. *Cell*, 158(2):314–326, 2014.

[87] Patrick Sobetzko, Monika Glinkowska, Andrew Traversb, and Georgi Muskhelishvili. DNA thermodynamic stability and supercoil dynamics determine the gene expression program during the bacterial growth cycle. *Mol. BioSyst.*, 9:1643–1651, 2013.

[88] Werner Arber. Horizontal Gene Transfer among Bacteria and its Role in Biological Evolution. *Life*, 4(2):217–224, 2014.

[89] Keith E Shearwin, Benjamin P Callen, and J Barry Egan. Transcriptional interference – a crash course. *Trends Genet.*, 21(6):339–345, 2010.

[90] Kim Sneppen, Ian B. Dodd, Keith E. Shearwin, Adam C. Palmer, Rachel A. Schubert, Benjamin P. Callen, and J. Barry Egan. A mathematical model for transcriptional interference by RNA polymerase traffic in Escherichia coli. *J. Mol. Biol.*, 346(2):399–409, 2005.

[91] Jie Ma and Michelle Wang. Interplay between DNA supercoiling and transcription elongation. *Transcription*, 5(3):e28636, 2014.

[92] Patrick Sobetzko. Transcription-coupled DNA supercoiling dictates the chromosomal arrangement of bacterial genes. *Nucleic Acids Res.*, 44(4):1514–1524, 2016.

[93] Stewart B. Levy. The challenge of antibiotic resistance. *Sci. Am.*, 278(3):46–53, 1998.

[94] Julian Davies and Dorothy Davies. Origins and evolution of antibiotic resistance. *Microbiol. Mol. Biol. Rev.*, 74(3):417–33, 2010.

[95] Wiltshire Clinical Commissioning Group. NHS Wiltshire CCG, BANES CCG & Swindon CCG: Guidelines for Antibiotic Prescribing in the Community 2013-15, 2013.

[96] Anne K Vidaver. Uses of antimicrobials in plant agriculture. *Clin. Infect. Dis.*, 34(3):107–10, 2002.

[97] Jacqui Wise. Call for global action on antibiotic resistance. *BMJ*, 341:4957, 2010.

[98] Brad Spellberg, Robert Guidos, David Gilbert, John Bradley, Helen W Boucher, Michael W Scheld, John G Bartlett, and John Edwards. The epidemic of antibiotic-resistant infections: a call to action for the medical community from the Infectious Diseases Society of America. *Clin. Infect. Dis.*, 46(2):155–64, 2008.

[99] Mark S Butler, Mark Blaskovich, and Matthew Cooper. Antibiotics in the clinical pipeline in 2013. *J. Antibiot.*, 66(10):571–91, 2013.

[100] Humphrey P. Rang, Maureen M. Dale, James M. Ritter, and Rod J. Flower. *Rang and Dale's Pharmacology*. Churchill Livingstone, 7 edition, 2012.

[101] B. Fournier, X. Zhao, T. Lu, K. Drlica, and D. C. Hooper. Selective Targeting of Topoisomerase IV and DNA Gyrase in Staphylococcus aureus: Different Patterns of Quinolone- Induced Inhibition of DNA Synthesis. *Antimicrob. Agents Chemother.*, 44(8):2160–2165, 2000.

[102] A B Khodursky, E L Zechiedrich, and N R Cozzarelli. Topoisomerase IV is a target of quinolones in Escherichia coli. *Pr. Natl. Acad. Sci. USA*, 92:11801–11805, 1995.

[103] Michael A Kohanski, Daniel J Dwyer, and James J Collins. How antibiotics kill bacteria: from targets to networks. *Nat. Rev. Microbiol.*, 8(6):423–435, 2010.

[104] *British National Formulary (Online)*. BMJ Group and Pharmaceutical Press, London.

[105] Ian Chopra and Marilyn Roberts. Tetracycline Antibiotics: Mode of Action, Applications, Molecular Biology, and Epidemiology of Bacterial Resistance. *Microbiol. Mol. Biol. Rev.*, 65(2):232–260, 2001.

[106] Cristina Rodriguez-Fonseca, Ricardo Amils, and Roger A Garrett. Fine Structure of the Peptidyl Transferase Centre on 23 S-like rRNAs Deduced from Chemical Probing of Antibiotic-Ribosome Complexes. *J. Mol. Biol.*, 247(2):224–235, 1995.

[107] Richard Goering, Hazel Dockrell, Mark Zuckerman, Ivan Roitt, and Peter Chiodini. *Mims' Medical Microbiology*. Mosby Elsevier, 2008.

[108] Patrice Courvalin. Vancomycin resistance in gram-positive cocci. *Clin. Infect. Dis.*, 42:S25–34, 2006.

[109] Lawrence P. Garrod. The action of penicillin on bacteria. *Br. Med. J.*, 1945.

[110] George A. Pankey and L D Sabath. Clinical relevance of bacteriostatic versus bactericidal mechanisms of action in the treatment of Gram-positive bacterial infections. *Clin. Infect. Dis.*, 38(6):864–870, 2004.

[111] Thomas K. Wood, Stephen J. Knabel, and Brian W. Kwan. Bacterial persister cell formation and dormancy. *Appl. Environ. Microbiol.*, 79(23):7116–7121, 2013.

[112] Kim Lewis. Persister cells. *Annu. Rev. Microbiol.*, 64:357–72, 2010.

[113] Kyle R Allison, Mark P Brynildsen, and James J Collins. Metabolite-enabled eradication of bacterial persisters by aminoglycosides. *Nature*, 473:216–220, 2011.

[114] Philip Greulich, Matthew Scott, Martin R. Evans, and Rosalind J. Allen. Growth-dependent bacterial susceptibility to ribosome-targeting antibiotics. *Mol. Syst. Biol.*, 11(3):796–796, 2015.

[115] Myriam Vincent, Laura S. England, and Jack T. Trevors. Cytoplasmic membrane polarization in Gram-positive and Gram-negative bacteria grown in the absence and presence of tetracycline. *Biochim. Biophys. Acta - Gen. Subj.*, 1672(3):131–134, 2004.

[116] Michael Kohanski, Daniel Dwyer, Boris Hayete, Carolyn Lawrence, and James Collins. A Common Mechanism of Cellular Death Induced by Bactericidal Antibiotics. *Cell*, 130(5):797–810, 2007.

[117] Karin Mitosch and Tobias Bollenbach. Bacterial responses to antibiotics and their combinations. *Environ. Microbiol. Rev.*, 6(6):545–557, 2014.

[118] Borut Jerman, Matej Butala, and Darja Zgur-Bertok. Sublethal Concentrations of Ciprofloxacin Induce Bacteriocin Synthesis in Escherichia coli. *Antimicrob. Agents Chemother.*, 49(7):3087–3090, 2005.

[119] Lucas R. Hoffman, David A. D'Argenio, Michael J. MacCoss, Zhaoying Zhang, Roger A. Jones, and Samuel I. Miller. Aminoglycoside antibiotics induce bacterial biofilm formation. *Nature*, 436(7054):1171–1175, 2005.

[120] Pavel P. Khil and R. Daniel Camerini-Otero. Over 1000 genes are involved in the DNA damage response of Escherichia coli. *Mol. Microbiol.*, 44(1):89–105, 2002.

[121] K J Shaw, N Miller, X Liu, D Lerner, J Wam, A Bittner, and BJ Morrow. Comparison of the changes in global gene expression of Escherichia coli induced by four bactericidal agents. *J. Mol. Microbiol. Biotechnol.*, 5(2), 2003.

[122] Tobias Bollenbach, Selwyn Quan, Remy Chait, and Roy Kishony. Nonoptimal Microbial Response to Antibiotics Underlies Suppressive Drug Interactions. *Cell*, 139(4):707–718, 2009.

[123] Bénédicte Michel. After 30 years of study, the bacterial SOS response still surprises us. *PLoS Biol.*, 3(7):1174–1176, 2005.

[124] Christine Miller, Line Elnif Thomsen, Carina Gaggero, Ronen Mosseri, Hanne Ingmer, and Stanley N Cohen. SOS response induction by beta-lactams and bacterial defense against antibiotic lethality. *Science*, 305(5690):1629–31, 2004.

[125] Baym Michael, Tami D. Lieberman, Eric D. Kelsic, Remy Chait, Rotem Gross, Idan Yelin, and Roy Kishony. Spatiotemporal microbial evolution on antibiotic landscapes. *Science*, 353(6304):1147–1152, 2016.

[126] Jessica M. A. Blair, Mark A. Webber, Alison J. Baylay, David O. Ogbolu, and Laura J. V. Piddock. Molecular mechanisms of antibiotic resistance. *Nat. Rev. Microbiol.*, 13(1):42–51, 2014.

[127] Guillaume Chevereau, Marta Dravecká, Tugce Batur, Aysegul Guvenek, Dilay Hazal Ayhan, Erdal Toprak, and Tobias Bollenbach. Quantifying the Determinants of Evolutionary Dynamics Leading to Drug Resistance. *PLoS Biol.*, 13(11):1–18, 2015.

[128] Orit Gefen and Nathalie Q Balaban. The importance of being persistent: heterogeneity of bacterial populations under antibiotic stress. *FEMS Microbiol. Rev.*, 33(4):704–17, 2009.

[129] Asher Brauner, Ofer Fridman, Orit Gefen, and Nathalie Q. Balaban. Distinguishing between resistance, tolerance and persistence to antibiotic treatment. *Nat. Rev. Microbiol.*, 14(5):320–330, 2016.

[130] Kim Lewis. Persister Cells and the Paradox of Chronic Infections. *Microbe Mag.*, 5(10):429–437, 2010.

[131] Etienne Maisonneuve, Manuela Castro-Camargo, and Kenn Gerdes. (p)ppGpp controls bacterial persistence by stochastic induction of toxin-antitoxin activity. *Cell*, 154(5):1140–50, 2013.

[132] Etienne Maisonneuve and Kenn Gerdes. Molecular Mechanisms Underlying Bacterial Persisters. *Cell*, 157(3):539–548, 2014.

[133] Michael B Elowitz, Arnold J Levine, Eric D Siggia, and Peter S Swain. Stochastic gene expression in a single cell. *Science*, 297(5584):1183–6, aug 2002.

[134] Martin Ackermann. Microbial individuality in the natural environment. *ISME J.*, 7(3):465–7, 2013.

[135] Martin Ackermann, Bärbel Stecher, Nikki E Freed, Pascal Songhet, Wolf-Dietrich Hardt, and Michael Doebeli. Self-destructive cooperation mediated by phenotypic noise. *Nature*, 454(7207):987–90, 2008.

[136] Gert-Jan Kremers, Sarah G. Gilbert, Paula. J. Cranfill, Michael W. Davidson, and David W. Piston. Fluorescent proteins at a glance. *J. Cell Sci.*, 124(15):2676–2676, jul 2011.

[137] Xuening Fei and Yingchun Gu. Progress in modifications and applications of fluorescent dye probe. *Prog. Nat. Sci.*, 19(1):1–7, 2009.

[138] Viki J Allan. *Protein localisation by Fluorescence Microscopy: A Practical Approach*. PAS, 2000.

[139] Dale Muzzey and Alexander van Oudenaarden. Quantitative Time-Lapse Fluorescence Microscopy in Single Cells. *Annu Rev Cell Dev Biol.*, 25:301–327, 2009.

[140] Jonathan W Young, James C W Locke, Alphan Altinok, Nitzan Rosenfeld, Tigran Bacarian, Peter S Swain, Eric Mjolsness, and Michael B Elowitz. Measuring single-cell gene expression dynamics in bacteria using fluorescence time-lapse microscopy. *Nat. Protoc.*, 7(1):80–8, jan 2012.

[141] Zhicheng Long, Eileen Nugent, Avelino Javer, Pietro Cicuta, Bianca Sclavi, Marco Cosentino Lagomarsino, and Kevin D Dorfman. Microfluidic chemostat for measuring single cell dynamics in bacteria. *Lab Chip*, 13(5):947–54, 2013.

[142] Lingling Yang, Yingxing Zhou, Shaobin Zhu, Tianxun Huang, Lina Wu, and Xiaomei Yan. Detection and quantification of bacterial autofluorescence at the single-cell level by a laboratory-built high-sensitivity flow cytometer. *Anal. Chem.*, 84(3):1526–1532, 2012.

[143] Anat Lipovsky, Yeshayahu Nitzan, Aharon Gedanken, and Rachel Lubart. Visible light-induced killing of bacteria as a function of wavelength: Implication for wound healing. *Lasers Surg. Med.*, 42(6):467–472, 2010.

[144] Mohan C Joshi, Aude Bourniquel, Jay Fisher, Brian T Ho, David Magnan, Nancy Kleckner, and David Bates. Escherichia coli sister chromosome separation includes an abrupt global transition with concomitant release of late-splitting intersister snaps. *Proc. Natl. Acad. Sci. U. S. A.*, 108(7):2765–2770, 2011.

[145] Romain Koszul and Nancy Kleckner. Dynamic chromosome movements during meiosis: a way to eliminate unwanted connections? *Trends Cell Biol.*, 19(12):716–724, 2009.

[146] Ido Golding and Edward C. Cox. Physical nature of bacterial cytoplasm. *Phys. Rev. Lett.*, 96(9):14–17, 2006.

[147] Iva Marija Tolić-Nørrelykke, Emilia Laura Munteanu, Genevieve Thon, Lene Oddershede, and Kirstine Berg-Sørensen. Anomalous diffusion in living yeast cells. *Phys. Rev. Lett.*, 93(7):1–4, 2004.

[148] Thomas A Waigh. Microrheology of complex fluids. *Reports Prog. Phys.*, 68(3):685–742, 2005.

[149] Pietro Cicuta and Athene M. Donald. Microrheology: a review of the method and applications. *Soft Matter*, 3(12):1449, 2007.

[150] Jean-Philippe Bouchaud and Antoine Georges. Anomalous diffusion in disordered media: Statistical mechanisms, models and physical applications. *Phys. Rep.*, 195(4-5):127–293, 1990.

[151] Fred C. MacKintosh. Active diffusion: The erratic dance of chromosomal loci. *Proc. Natl. Acad. Sci.*, 109(19):7138–7139, 2012.

[152] Olivier Espéli, Romain Borne, Pauline Dupaigne, Axel Thiel, Emmanuelle Gigant, Romain Mercier, and Frédéric Boccard. A MatP-divisome interaction coordinates chromosome segregation with cell division in E. coli. *EMBO J.*, 31(14):3198–3211, 2012.

[153] Jonas van den Berg, Arnold J. Boersma, and Bert Poolman. Microorganisms maintain crowding homeostasis. *Nat. Rev. Microbiol.*, 15(5):309–318, 2017.

[154] Kem A. Sochacki, Irina A. Shkel, M. Thomas Record, and James C. Weisshaar. Protein diffusion in the periplasm of E. coli under osmotic stress. *Biophys. J.*, 100(1):22–31, 2011.

[155] Robert S Fuller, Jon M Kaguni, and Arthur Kornberg. Enzymatic replication of the origin of the Escherichia coli chromosome (oriC plasmids/dnaA gene/DNA replication). *Biochemistry*, 78(12):7370–7374, 1981.

[156] Janet M Wood. Osmosensing by Bacteria. *Sci. Signal.*, 2006(357):pe43–pe43, 2006.

[157] Enrique Rojas, Julie A Theriot, and Kerwyn Casey Huang. Response of Escherichia coli growth rate to osmotic shock. *Proc Natl Acad Sci U S A*, 111(21):7807–7812, 2014.

[158] Teuta Pilizota and Joshua W. Shaevitz. Fast, multiphase volume adaptation to hyperosmotic shock by escherichia coli. *PLoS One*, 7(4):1–10, 2012.

[159] Michael C. Konopka, Irina A. Shkel, Scott Cayley, M. Thomas Record, and James C. Weisshaar. Crowding and confinement effects on protein diffusion in vivo. *J. Bacteriol.*, 188(17):6115–6123, 2006.

[160] Teresa. J. Broering, John. S. L. Parker, Patricia. L. Joyce, Jonghwa. Kim, and Max. L. Nibert. Mammalian Reovirus Nonstructural Protein NS Forms Large Inclusions and Colocalizes with Reovirus Microtubule-Associated Protein 2 in Transfected Cells. *J. Virol.*, 76(16):8285–8297, 2002.

[161] Teresa J Broering, Michelle M Arnold, Cathy L Miller, Jessica A Hurt, Patricia L Joyce, and Max L Nibert. Carboxyl-Proximal Regions of Reovirus Nonstructural Protein μ NS Necessary and Sufficient for Forming Factory-Like Inclusions. *J. Virol.*, 79(10):6194–6206, 2005.

[162] David J Lee, Lewis EH Bingle, Karin Heurlier, Mark J Pallen, Charles W Penn, Stephen JW Busby, and Jon L Hobman. Gene doctoring: a method for recombineering in laboratory and pathogenic Escherichia coli strains. *BMC Microbiol.*, 9(1):252, 2009.

[163] Kirill A Datsenko and Barry L Wanner. One-step inactivation of chromosomal genes in Escherichia coli K-12 using PCR products. *Proc. Natl. Acad. Sci. U. S. A.*, 97(12):6640–5, 2000.

[164] Ingrid M. Keseler, Amanda Mackie, Martin Peralta-Gil, Alberto Santos-Zavaleta, Socorro Gama-Castro, César Bonavides-Martínez, Carol Fulcher, Araceli M. Huerta, Anamika Kothari, Markus Krummenacker, Mario Latendresse, Luis Muñiz-Rascado, Quang Ong, Suzanne Paley, Imke Schröder, Alexander G. Shearer, Pallavi Subhraveti, Mike Travers, Deepika Weerasinghe, Verena Weiss, Julio Collado-Vides, Robert P. Gunsalus, Ian Paulsen, and Peter D. Karp. EcoCyc: Fusing model organism databases with systems biology. *Nucleic Acids Res.*, 41:605–612, 2013.

[165] Irith Wiegand, Kai Hilpert, and Robert E W Hancock. Agar and broth dilution methods to determine the minimal inhibitory concentration (MIC) of antimicrobial substances. *Nat. Protoc.*, 3(2):163–75, 2008.

[166] Stella Stylianidou, Connor Brennan, Silas B. Nissen, Nathan J. Kuwada, and Paul A. Wiggins. SuperSegger: robust image segmentation, analysis and lineage tracking of bacterial cells. *Mol. Microbiol.*, 102(4):690–700, 2016.

[167] Julie A. Cass, Stella Stylianidou, Nathan J. Kuwada, Beth Traxler, and Paul A. Wiggins. Probing bacterial cell biology using image cytometry. *Mol. Microbiol.*, 103(5):818–828, 2017.

[168] Luis López-Maury, Samuel Marguerat, and Jürg Bähler. Tuning gene expression to changing environments: from rapid responses to evolutionary adaptation. *Nat. Rev. Genet.*, 10(1):68–68, 2009.

[169] Alexey N. Fedorov and Thomas O. Baldwin. Cotranslational Protein Folding - Minireview. *J. Biol. Chem.*, 272(52):32715–32718, 1997.

[170] David G Davies, Matthew R Parsek, James P Pearson, Barbara H Iglewski, J W Costerton, and E P Greenberg. The Involvement of Cell-to-Cell Signals in the Development of a Bacterial Biofilm. *Science*, 280(5361):295–298, 1998.

[171] Christine D Hardy and Nicholas R Cozzarelli. Alteration of Escherichia coli Topoisomerase IV to Novobiocin Resistance Alteration of Escherichia coli Topoisomerase IV to Novobiocin Resistance. *Antimicrob. Agents Chemother.*, 47(3):941–947, 2003.

[172] Ihmhoff Johannes. Osmoregulation and compatible solutes in eubacteria. *FEMS Microbiol. Rev.*, 2(1-2), 1986.

[173] Kangla Tsung, Sumiko Inouye, and Masayori Inouye. Factors affecting the efficiency of protein synthesis in Escherichia coli. *J Biol Chem*, 264(8):4428–4433, 1989.

[174] Christina Steel, Qian Wan, and Xiao-Hong Nancy Xu. Single live cell imaging of chromosomes in chloramphenicol-induced filamentous Pseudomonas aeruginosa. *Biochemistry*, 43:175–182, 2004.

[175] Thomas J. Lampo, Andrew S. Kennard, and Andrew J. Spakowitz. Physical Modeling of Dynamic Coupling between Chromosomal Loci. *Biophys. J.*, 110(2):338–347, 2016.

[176] Thomas J. Lampo, Stella Stylianidou, Mikael P. Backlund, Paul A. Wiggins, and Andrew J. Spakowitz. Cytoplasmic RNA-Protein Particles Exhibit Non-Gaussian Subdiffusive Behavior. *Biophys. J.*, 112(3):532–542, 2017.

[177] Ping Wang, Lydia Robert, James Pelletier, Wei Lien Dang, Francois Taddei, Andrew Wright, and Suckjoon Jun. Robust growth of escherichia coli. *Curr. Biol.*, 20(12):1099–1103, 2010.

[178] Matthias Kaiser, Florian Jug, Olin Silander, Siddharth Deshpande, Thomas Julou, Gene Myers, and Erik Van Nimwegen. Tracking single-cell gene regulation in dynamically controlled environments using an integrated microfluidic and computational setup. *Pending peer-review*, 2016.

[179] Jerold Y. Gordon, Eric G. Romanowski, and Alison M. McDermott. Mini review: A review of antimicrobial peptides and their therapeutic potential as anti-infective drugs. *Curr. Eye Res.*, 30(7):505–515, 2005.

[180] Christer Malmberg, Pikkei Yuen, Johanna Spaak, Otto Cars, Thomas Tängdén, and Pernilla Lagerbäck. A novel microfluidic assay for rapid phenotypic antibiotic susceptibility testing of bacteria detected in clinical blood cultures. *PLoS One*, 11(12):1–15, 2016.

[181] Britta Barlag, Oliver Beutel, Dennis Janning, Frederik Czarniak, Christian P. Richter, Carina Kommnick, Vera Göser, Rainer Kurre, Florian Fabiani, Marc Erhardt, Jacob Piehler, and Michael Hensel. Single molecule super-resolution imaging of proteins in living Salmonella enterica using self-labelling enzymes. *Sci. Rep.*, 6(1):31601, 2016.

[182] Assaf Amitai, Andrew Seeber, Susan M. Gasser, and David Holcman. Visualization of Chromatin Decompaction and Break Site Extrusion as Predicted by Statistical Polymer Modeling of Single-Locus Trajectories. *Cell Rep.*, 18(5):1200–1214, 2017.

[183] Henrik J. Nielsen, Jesper R. Ottesen, Brenda Youngren, Stuart J. Austin, and Flemming G. Hansen. The Escherichia coli chromosome is organized with the left and right chromosome arms in separate cell halves. *Mol. Microbiol.*, 62(2):331–338, 2006.

[184] Marion M Bradford. A rapid and sensitive method for the quantitation of microgram quantities of protein utilizing the principle of protein-dye binding. *Anal Biochem.*, 72(248):54, 1976.

[185] John M Walker. The bicinchoninic acid (BCA) assay for protein quantitation. *Methods Mol. Biol.*, 32:5(8), 1994.

[186] Yuichi Taniguchi, Paul J Choi, Gene-wei Li, Huiyi Chen, Mohan Babu, Jeremy Hearn, Andrew Emili, and X Sunney Xie. Quantifying E. coli proteome and transcriptome with single- molecule sensitivity in single cells. *Most*, 329(5991):533–538, 2010.

[187] Christoph Bock, Matthias Farlik, and Nathan C. Sheffield. Multi-Omics of Single Cells: Strategies and Applications. *Trends Biotechnol.*, 34(8):605–608, 2016.

[188] Kalle Kipper, Ebba G. Lundius, Vladimir Ćurić, Ivana Nikić, Manfred Wiessler, Edward A. Lemke, and Johan Elf. Application of Noncanonical Amino Acids for Protein Labeling in a Genomically Recoded Escherichia coli. *ACS Synth. Biol.*, 6(2):233–255, 2017.

[189] Stephanie M Amato, Christopher H Fazen, Theresa C Henry, Wendy W K Mok, Mehmet a Orman, Elizabeth L Sandvik, Katherine G Volzing, and Mark P Brynildsen. The role of metabolism in bacterial persistence. *Front. Microbiol.*, 5(March):70, 2014.

[190] Stephanie M Amato and Mark P Brynildsen. Nutrient transitions are a source of persisters in Escherichia coli biofilms. *PLoS One*, 9(3), 2014.

[191] Irine Levin-Reisman, Orit Irit, Ilan Braniss Gefen, Noam Shoresh, and Nathalie Q. Balaban. Antibiotic tolerance facilitates the evolution of resistance. *Science*, 355(6327):826–830, 2017.

Appendices

Appendix A

Supplementary materials for Chapter 3

Comparison of cell length and elongation rate between the two growth conditions

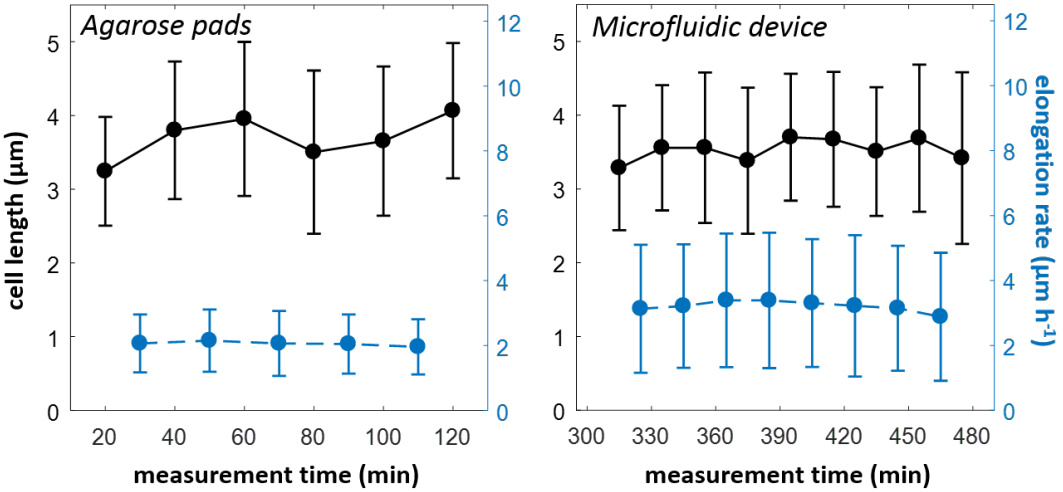

Fig. A1 **Comparison of cell length and elongation rate between the two growth conditions**. Mean cell lengths (*black solid lines*) and elongation rates (*blue dashed lines*) are plotted over experiment time. Cell lengths were measured semi-manually for not treated (control) Ori2 cells grown on agarose pads (*left*; 691 cells measured from 3 biological replicates) and in microfluidic device (*right*; 519 cells measured from a single biological replicate). For microfluidic device, measurements were performed only from 1 h before and up to 2 h after media switch time. Cell lengths and elongation rates are generally comparable between the two growth conditions, however, cells grown in microfluidic device consistently appear to have larger ($\sim$1.3 μm h^{-1}) elongation rates compared to agarose pads ($\sim$1.0 μm h^{-1}).

Photo-bleaching profile of an example cytosolic aggregate data set

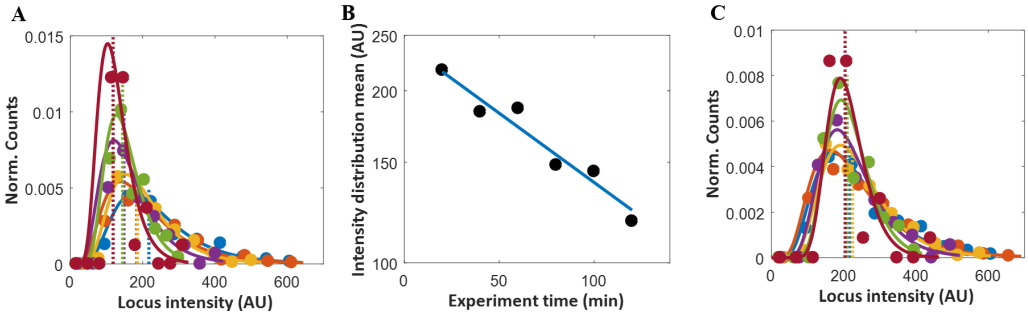

Fig. A2 **Example data set of μNS-GFP cytosolic aggregates before and after photo-bleaching correction.** We calculate marker population bleaching rate and use it to calculate marker intensities. Plots show data for an example control (no drug) μNS-GFP sample. (**A**) Normalised log-normal marker intensity distributions for different experiment time points (20-120 min) (for function fitting details see Supplementary Materials). Part of the high end of the distribution tails is not shown. Dashed lines show means of the fitted distributions to demonstrate intensity-time dependence caused by photo-bleaching. (**B**) Distribution mean values from (**A**) over experiment time fitted with an exponential function (Equation A2, *blue line*). (**C**) Normalised log-normal marker intensity distributions for different experiment time points after calculating individual marker intensities.

Function fitting for data treatment

Marker intensity distribution and photo-bleaching profile fitting

To compare loci dynamics at various measurement times, effects of photo-bleaching must be accounted for first. We start by plotting frequency distributions of recorded loci intensities for individual measurement time points. We apply a cut-off to our intensity data at 100 AU as markers below this intensity value show significant static resolution errors, as shown previously. For this reason, we fit the data by generating maximum likelihood estimates of mean (μ) and standard deviation (σ) and then fit a log-normal probability density function, truncated at 100 AU, and then renormalized so that it integrates to one:

$$f(x) = \frac{\frac{1}{\sqrt{2\pi}\sigma x} e^{-(\log(x)-\mu)^2/2\sigma^2}}{1 - \frac{1}{\sigma\sqrt{2\pi}} \int_0^x \frac{e^{\frac{-(ln(t)-\mu)^2)}{2\sigma^2}}}{t} dt}, \tag{A1}$$

The decay in distribution means (dashed vertical lines in Figure 2A and black solid circles in Figure 2B in main text) represents population photo-bleaching profile that can be fitted (Figure 2B) with an exponential function with a free baseline parameter for chromosomal loci (Equation 2, *main text*) or without a baseline parameter (for cytosolic aggregates to determine photo-bleaching rate):

$$I_t = I_0 e^{(-\lambda(t-t_0))}, \tag{A2}$$

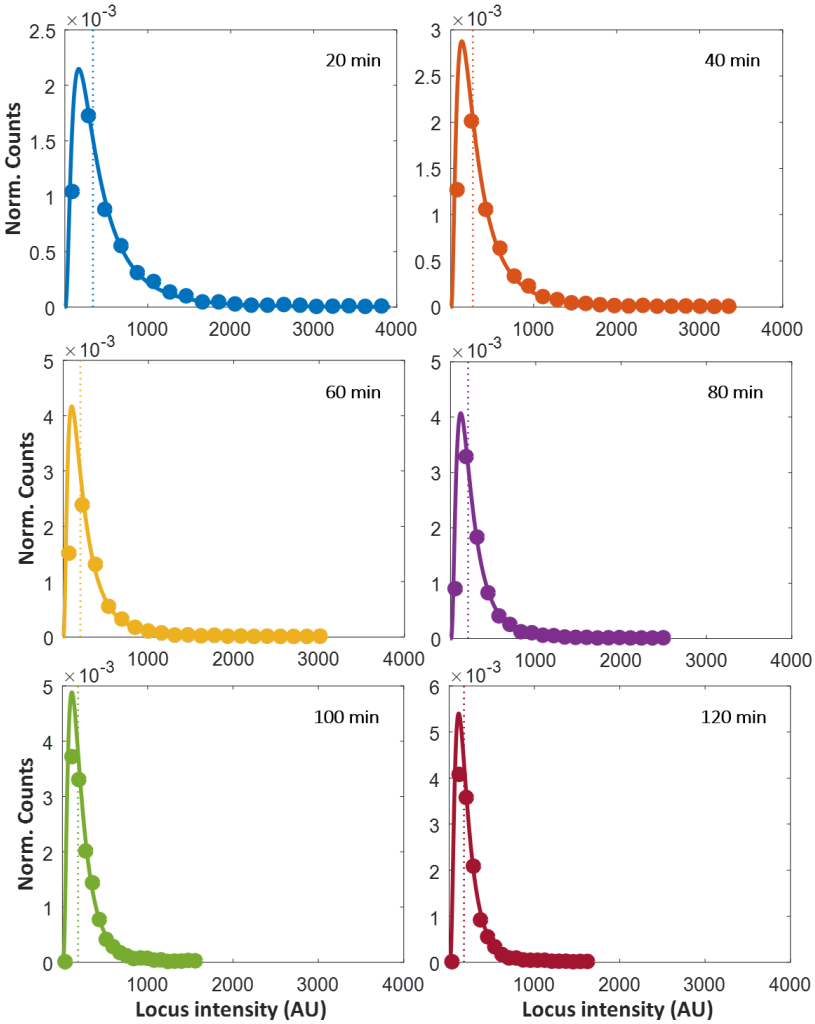

Fig. A3 **Locus intensity distributions of an example Ori2 loci sample for individual measurement time points.** Distribution means are represented with dashed vertical lines.

where I_t is locus intensity at time t, I_0 is initial locus intensity at time t_0, t_0 is the initial measurement time (fixed at 20 min for all experiments), and λ is a free fitting parameter representing the photo-bleaching rate. For each tracked locus, we use its population photo-bleaching rate, λ, to evaluate, using either Equation 2 (for chromosomal loci) or Equation A2 (for cytosolic aggregates), its original intensity (pre-photo-bleaching, I_0) assuming exponential decay in intensity.

Marker MSD–size dependence fitting

Once pre-photo-bleaching intensity of each locus at each measurement time point is determined, we proceed to correct for locus MSD–size dependence. Procedure is applied to MSDs at five arbitrary lag times (0.1, 1.0, 5.0, 10, and 14 s). For each lag time, we first arbitrarily segregate loci according their intensities by binning into 20 logarithmically-spaced bins along a 100-4,000 AU range and evaluate median MSD for each bin. We select medians for bins where

the number of loci is equal of larger than the mean number of loci per bin (red solid circles in Figure 3A, *main text*) and fit those medians with a custom exponential function:

$$MSD_\tau(I) = p_1 e^{p_2 I}, \tag{A3}$$

where MSD_τ is MSD at one of the five lag times, τ, as a function of median binned locus intensity, I, and p_{1-2} are free fitting parameters.

Effects of photo-beaching and marker size correction on the three markers in control condition

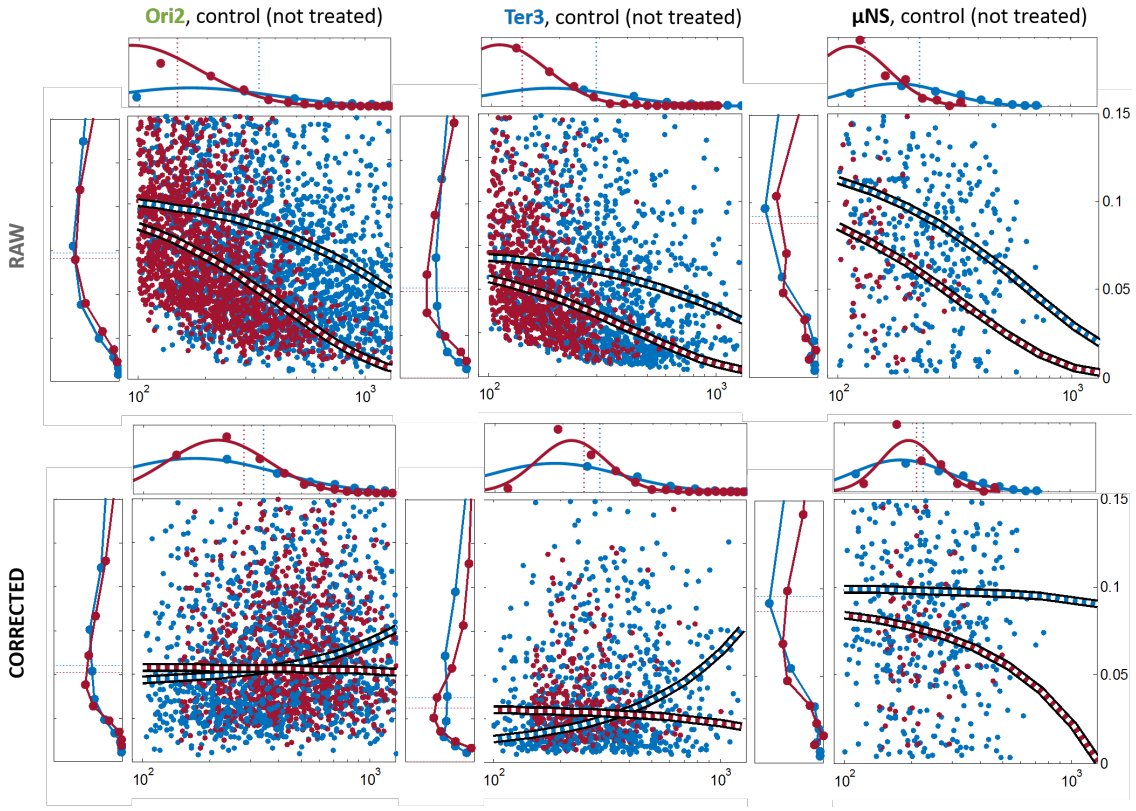

Fig. A4 **Effects of correction on the control data sets.** Panels show scatter-plots of the MSD(10 s) over loci intensities with overlaid fitted exponential curves (for function fitting details see Supplementary Materials) and variable distributions in side panels (tails of distributions not shown; agarose pads data only) for control (not treated) (**A**) Ori2, (**B**) Ter3, and (**C**) μNS data sets as indicated in the figure. Initial measurement time point (20 min) is in *blue* and the final one (120 min) in *red*. Corrected variables are indicated with a star sign (*). *Top*: "Raw" (before correction) data. Fitted curves decrease monotonically with increasing locus intensity and the intensity distribution peaks shift over time, both indicating photo-bleaching. *Bottom*: Corrected data. Curves are approximately flat indicating reduced MSD-size dependence and show no time-dependence. Overlapping locus intensity distribution peaks and median MSD*(10 s) indicate almost no time-dependence in locus intensity and motility.

Marker size corrections performed on Ter3 loci data with Ori2 model data is more effective than if performed with Ter3 model data

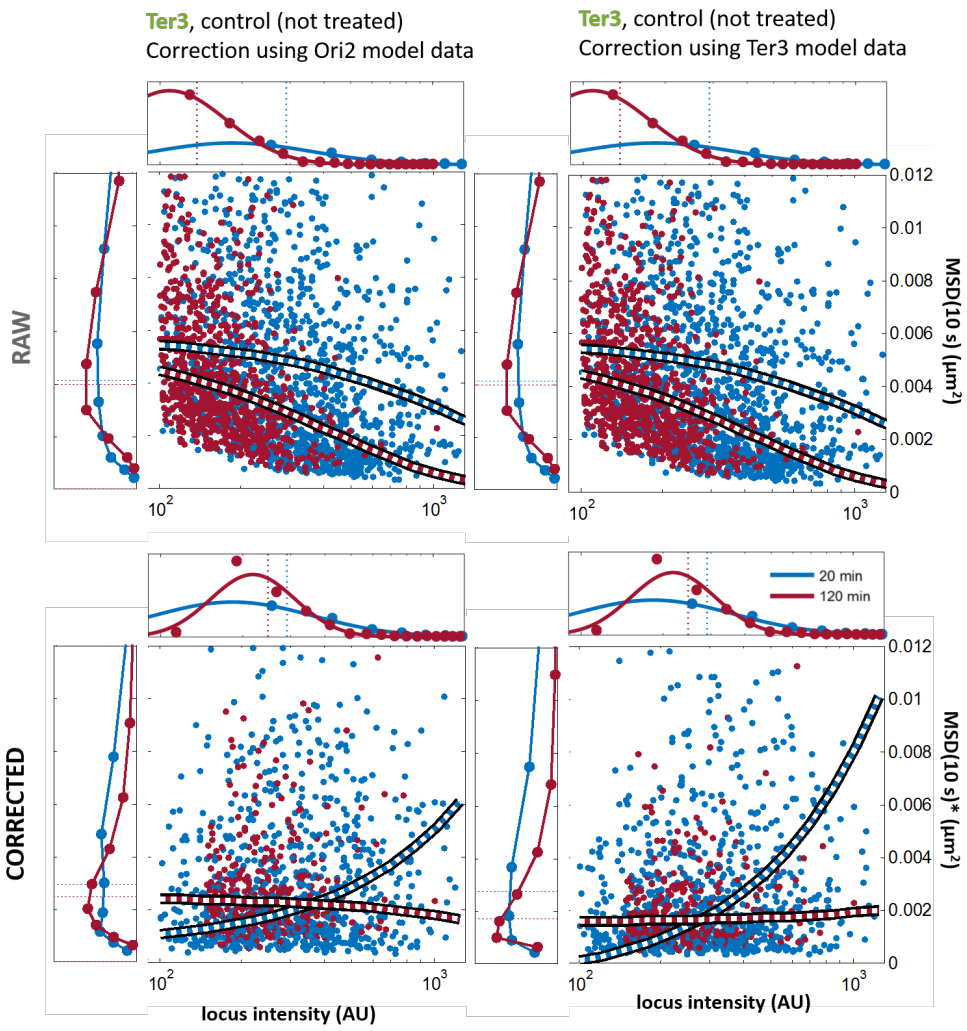

Fig. A5 **Marker size corrections performed on Ter3 loci data with Ori2 model is more effective than if performed with Ter3 model data.**

Photo-bleaching and marker size correction effects on MSD(τ) for control (not treated) samples for all lag times, measurement time points, markers, and growth conditions.

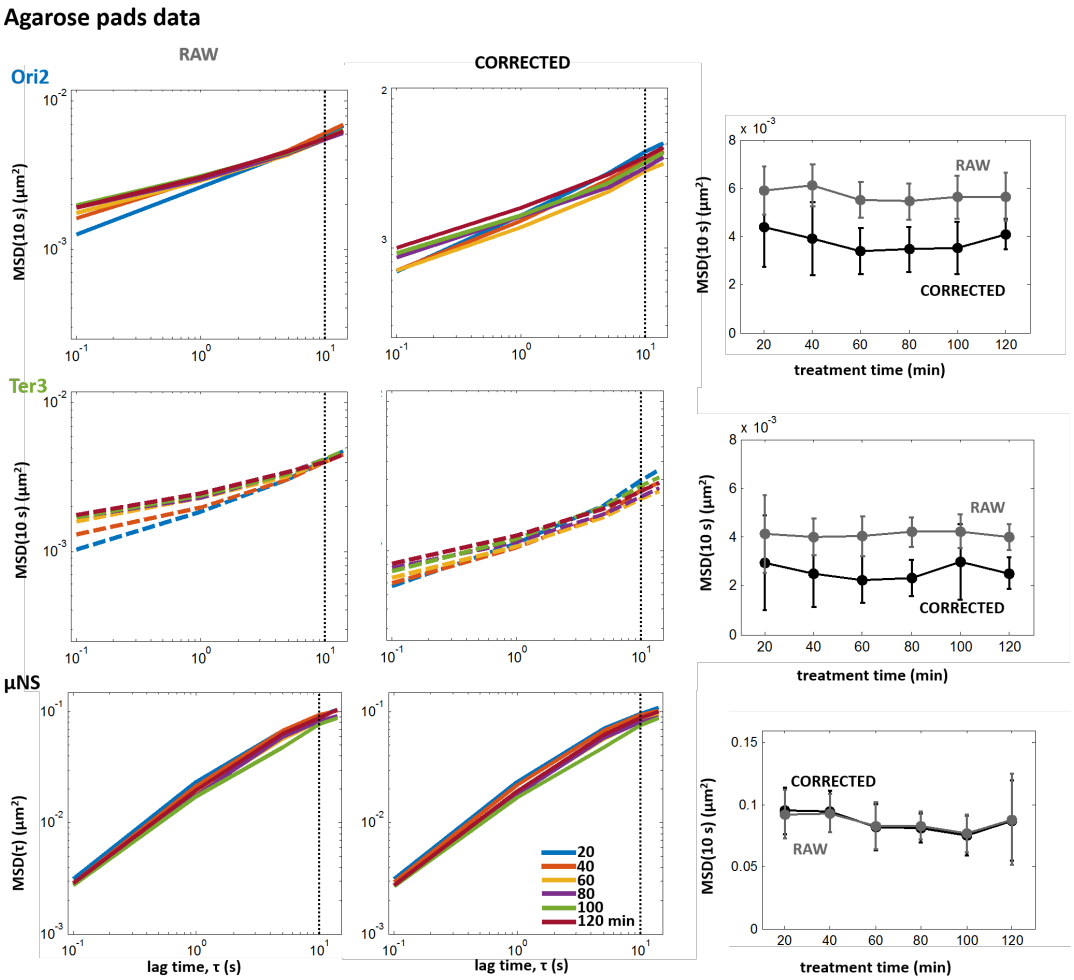

Fig. A6 **Photo-bleaching and marker size corrections allows for accurate long (several hours) measurements of short time-scale marker dynamics.** (**A**) Raw and (**B**) photo-bleaching and marker size corrected median ensemble-averaged MSD(τ) for 9 biological replicates for different measurements times (20 - 120 min) for chromosomal Ori2 loci (*top* panels), Ter3 loci (*middle* panels), and a cytosolic aggregate μNS (*bottom* panels). 10 s lag time indicated with vertical dashed lines. (**C**) Raw (*grey*) and corrected (*black*) MSD(10 s) over 2 h.

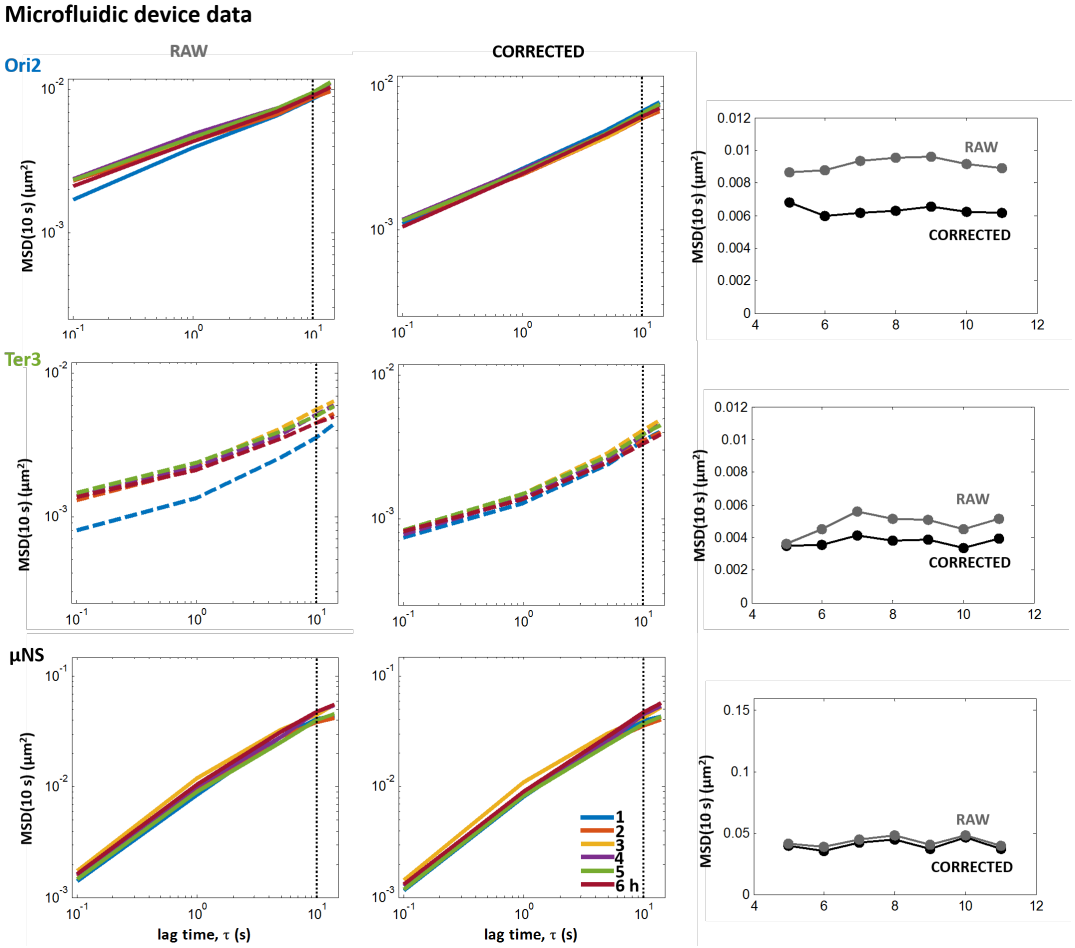

Fig. A7 **Photo-bleaching and marker size corrections allows for accurate long (several hours) measurements of short time-scale marker dynamics.** (**A**) Raw and (**B**) photo-bleaching and marker size corrected median ensemble-averaged MSD(τ) for 9 biological replicates for different measurements times (1 - 7 h) for chromosomal Ori2 loci (*top* panels), Ter3 loci (*middle* panels), and cytosolic aggregates μNS (*bottom* panels). 10 s lag time indicated with vertical dashed lines. (**C**) Raw (*grey*) and corrected (*black*) MSD(10 s) over 7 h.

Appendix B

Supplementary materials for Chapter 4

Track and biological replicate statistics

Agarose pads experiments										
	experiment #	bio. repl.	control	ciprofloxacin	rifampicin	tetracycline	vancomycin	sorbitol		
Ori2	1.	3	7,985	5,015	1,986	451	2,608	1,356		
	2.	3	4,051	2,556	3,443	712	2,110	338		
	3.	3	1,728	1,977	2,528	2,768	1,356	2,001		
	subtotals	***9***	***13,764***	***9,548***	***7,957***	***3,931***	***6,074***	***3,695***		
Ter3	4.	3	1,456	3,387	4,718	1,440	1,342	868		
	5.	3	3,214	3,199	3,499	2,560	2,698	454		
	6.	3	1,694	1,813	2,649	1,243	3,601	888		
	subtotals	***9***	***6,364***	***8,399***	***10,866***	***5,243***	***7,641***	***2,210***		
GFP-µNS	7.	3	1,230	841	784	10,66	746	1,837		
	8.	3	760	743	1,127	298	1,078	948		
	subtotals	***6***	***1,990***	***1,584***	***1,911***	***1,364***	***1,824***	***2,785***		
	TOTALS	***24***	***22,118***	***19,531***	***20,734***	***10,538***	***15,539***	***8,690***	***97,150***	
Microfluidic device experiments										
Ori2	1.	1	6,273	5,480	4,371	7,960	6,443	3,761		
Ter3	2.	1	4,502	3,142	5,130	3,789	3,527	9,376		
GFP-µNS	3.	1	1,761	8,150	1,315	1,035	3,592	3,719		
	TOTALS	***3***	***12,536***	***16,772***	***10,816***	***12,784***	***13,562***	***16,856***	***83,326***	
	GRAND TOTALS	**11**	**27**	**34,654**	**36,303**	**31,550**	**23,322**	**29,101**	**25,546**	**180,476**

Table B1 **Number of collected and analysed tracks and biological replicates for individual experiments.** Numbers represent sums of tracks acquired at all measurement time points (6 every 20 min for agarose pads and 7 for microfluidic device every 1 h). At agarose pads experiments, for each marker, three experiments, each for 3 (chromosomal loci) or 2 (cytosolic aggregates) biological replicates (refer to Methods for details) In total, at least 23,322 (rifampicin) and up to 36,303 (ciprofloxacin) tracks were collected per treatment condition in both growth conditions. The total of 180,476 tracks were collected and analysed for entire work.

Photo-bleaching profiles of all data sets

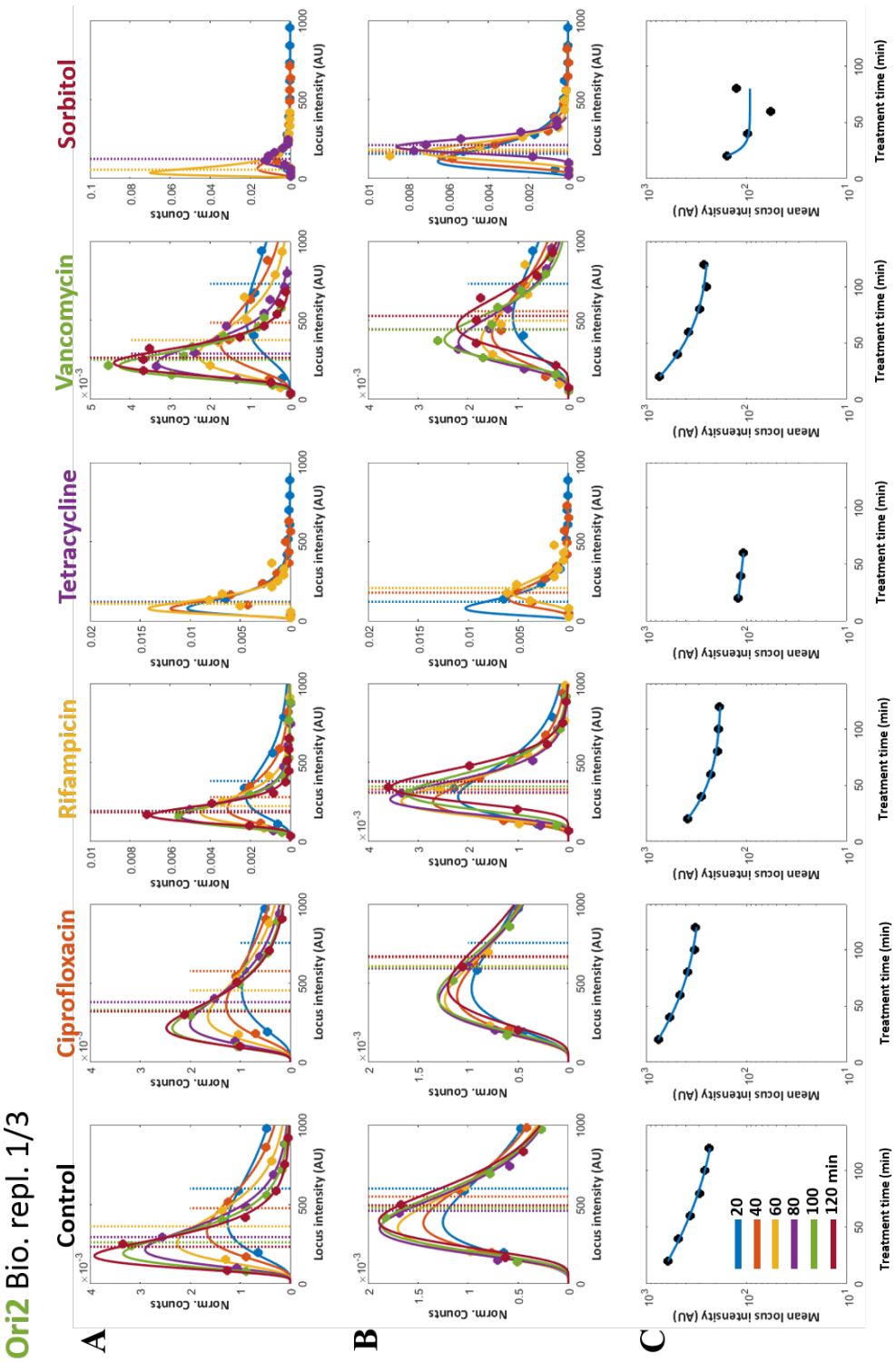

Fig. B1 **Photo-bleaching profiles of Ori2 loci, biological replicate 1/3, in all treatment conditions.**

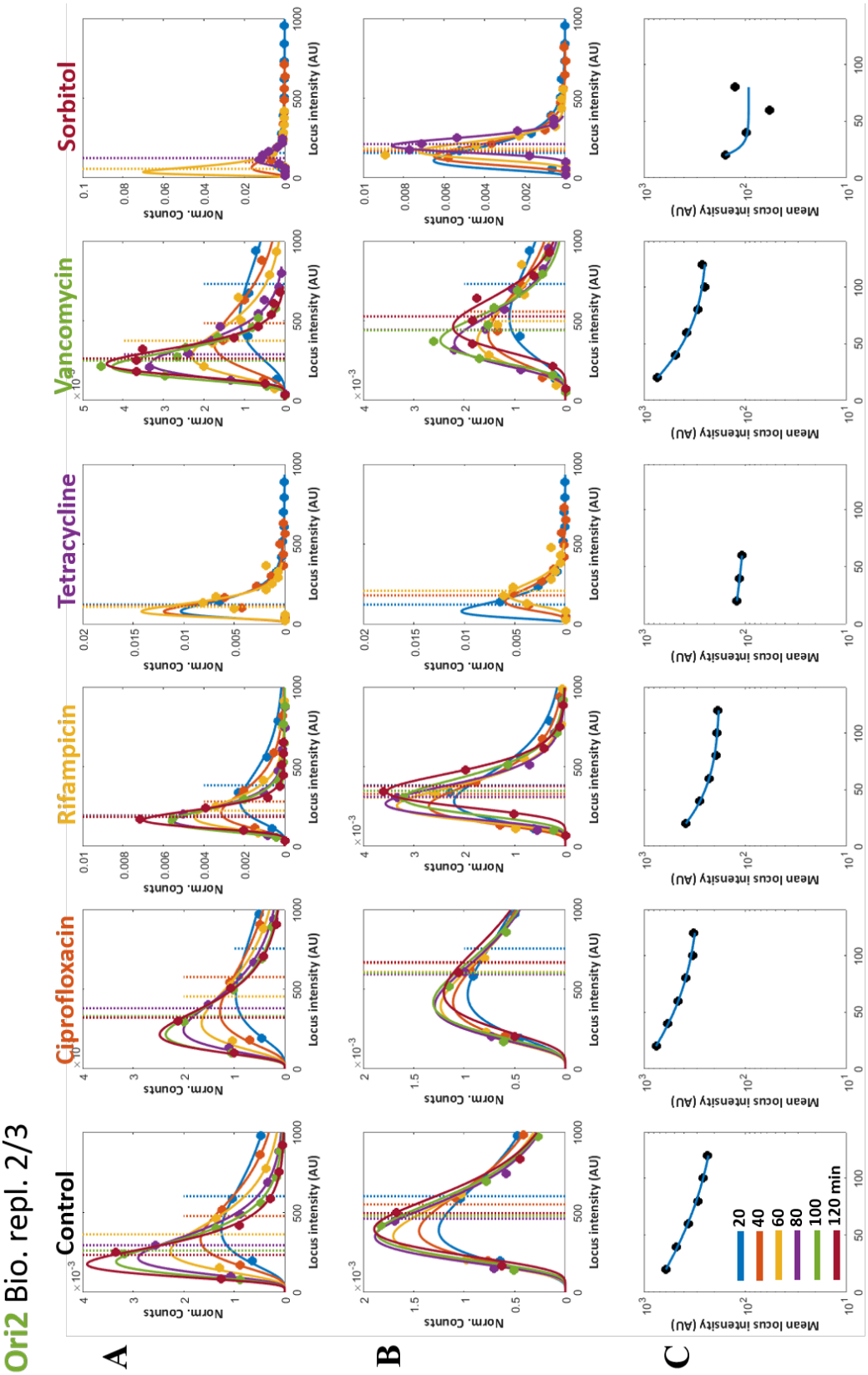

Fig. B2 **Photo-bleaching profiles of Ori2 loci, biological replicate 2/3, in all treatment conditions.**

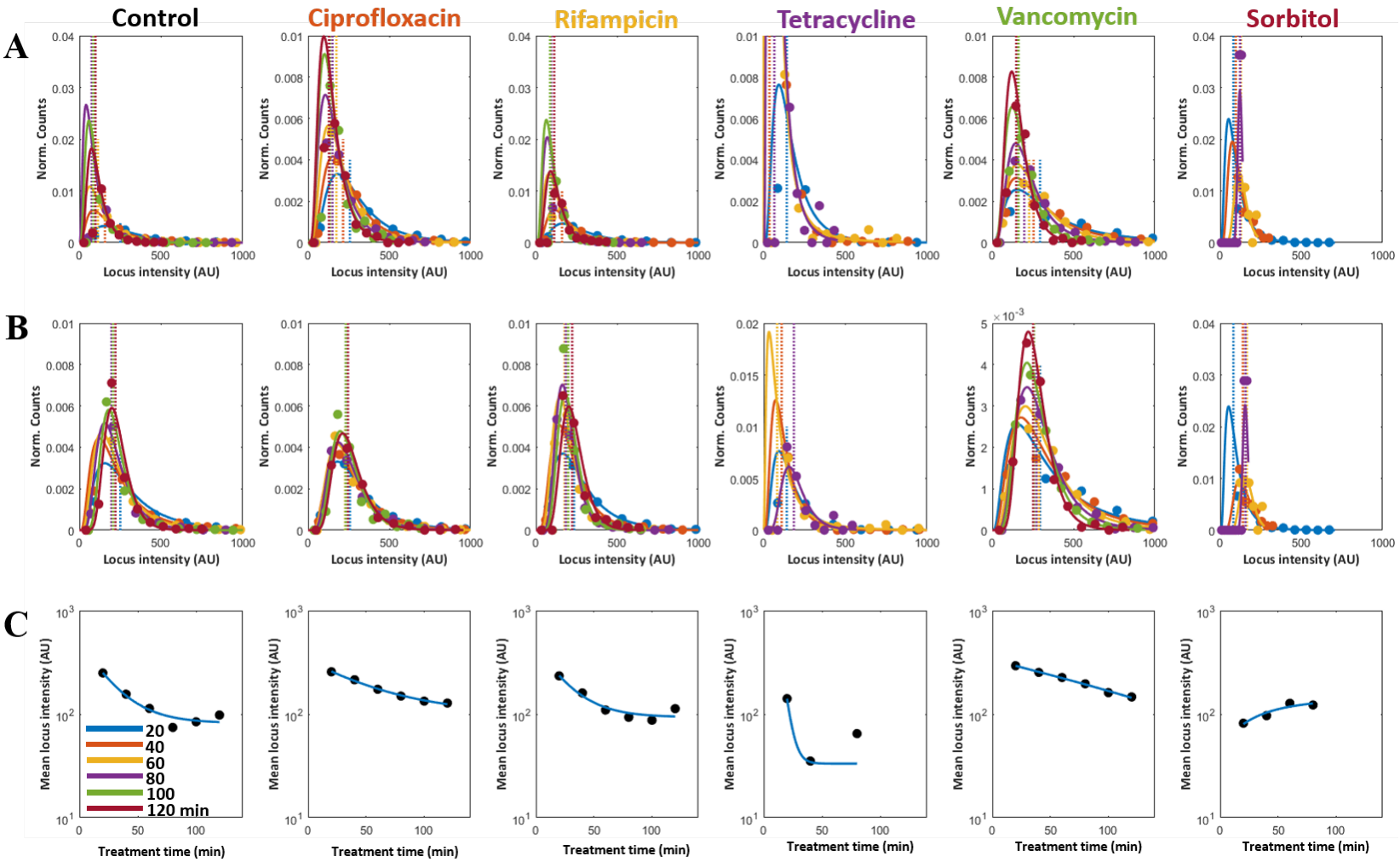

Fig. B3 **Photo-bleaching profiles of Ori2 loci, biological replicate 3/3, in all treatment conditions.**

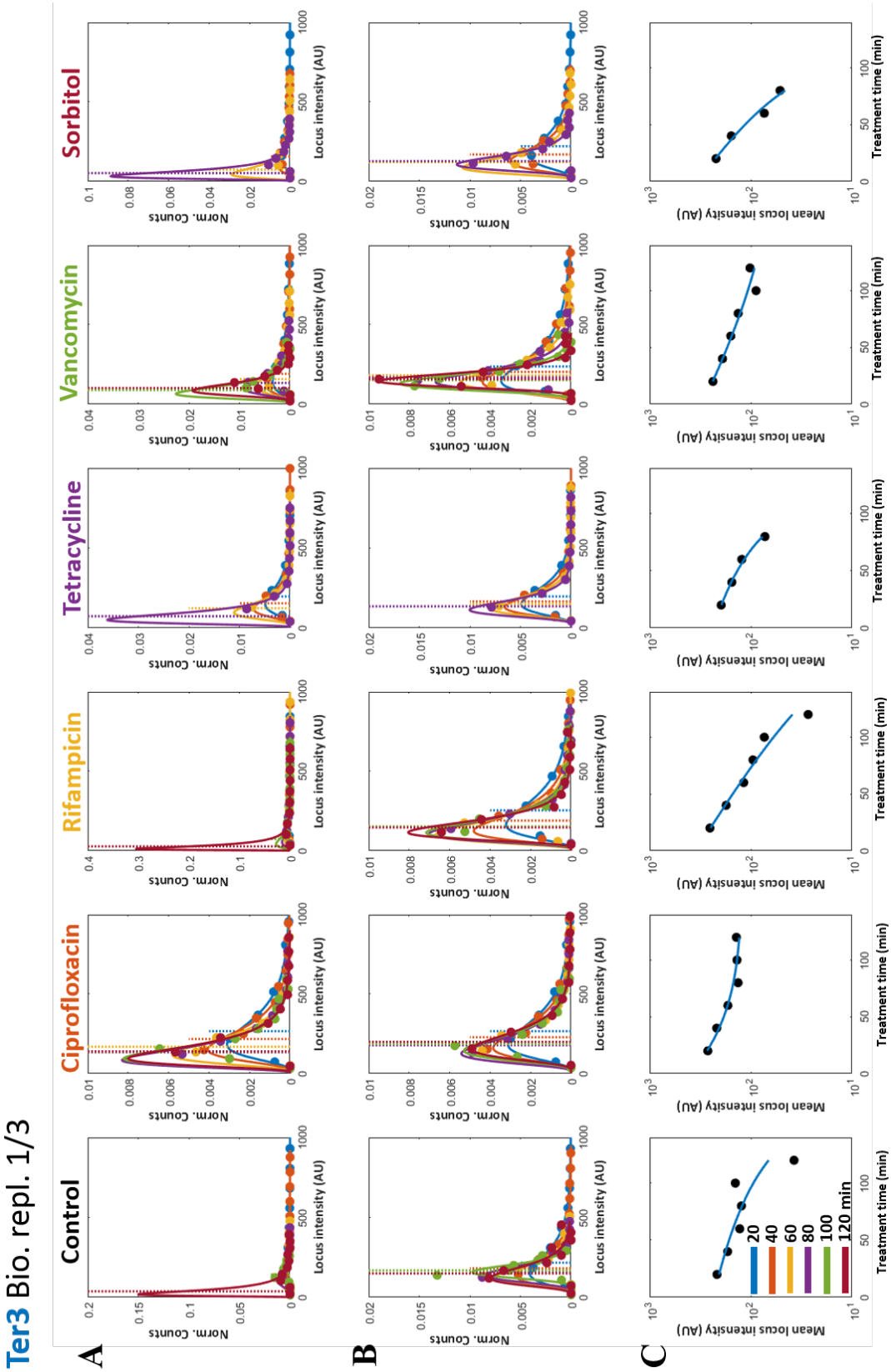

Fig. B4 **Photo-bleaching profiles of Ter3 loci, biological replicate 1/3, in all treatment conditions.**

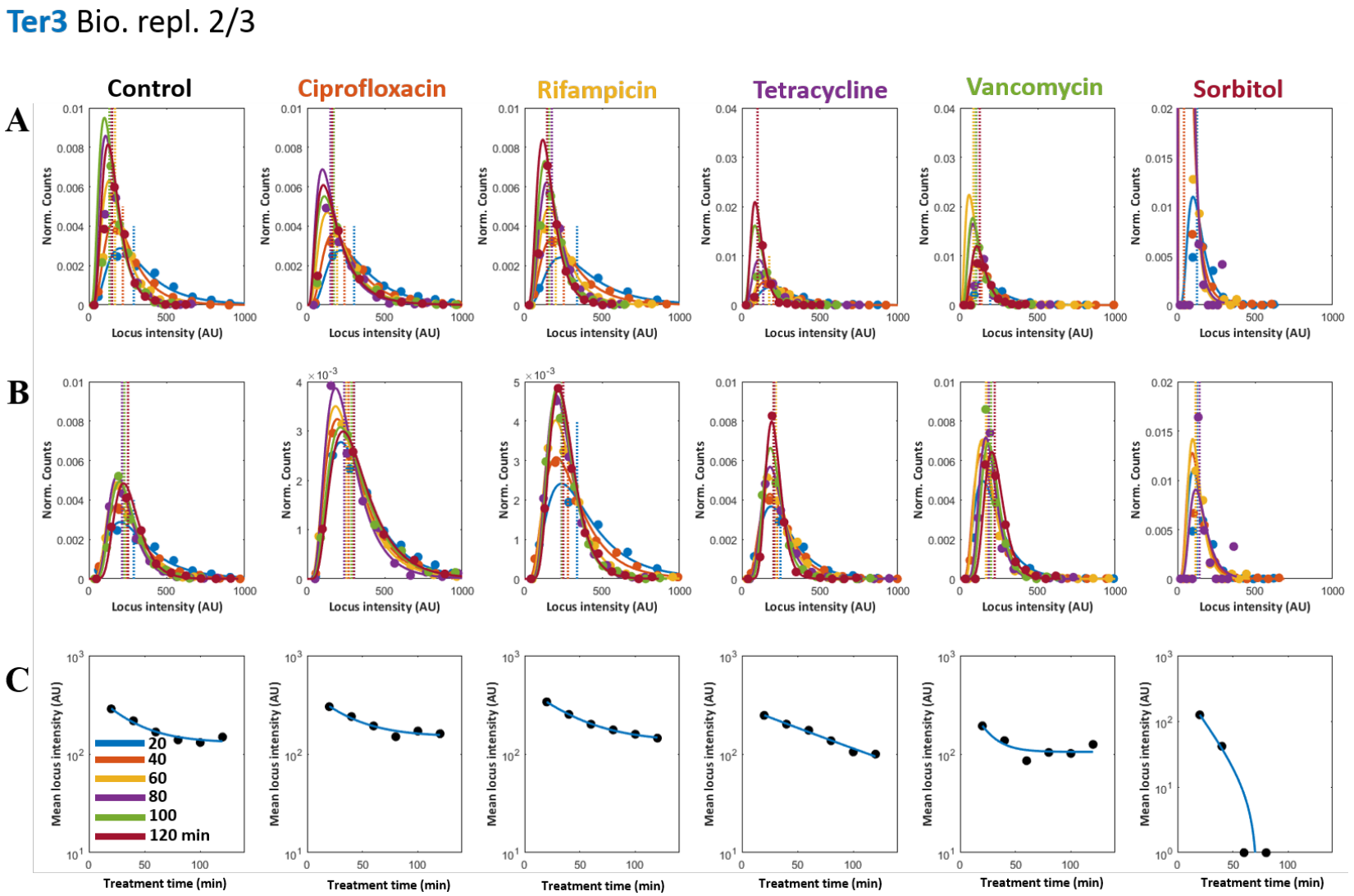

Fig. B5 **Photo-bleaching profiles of Ter3 loci, biological replicate 2/3, in all treatment conditions.**

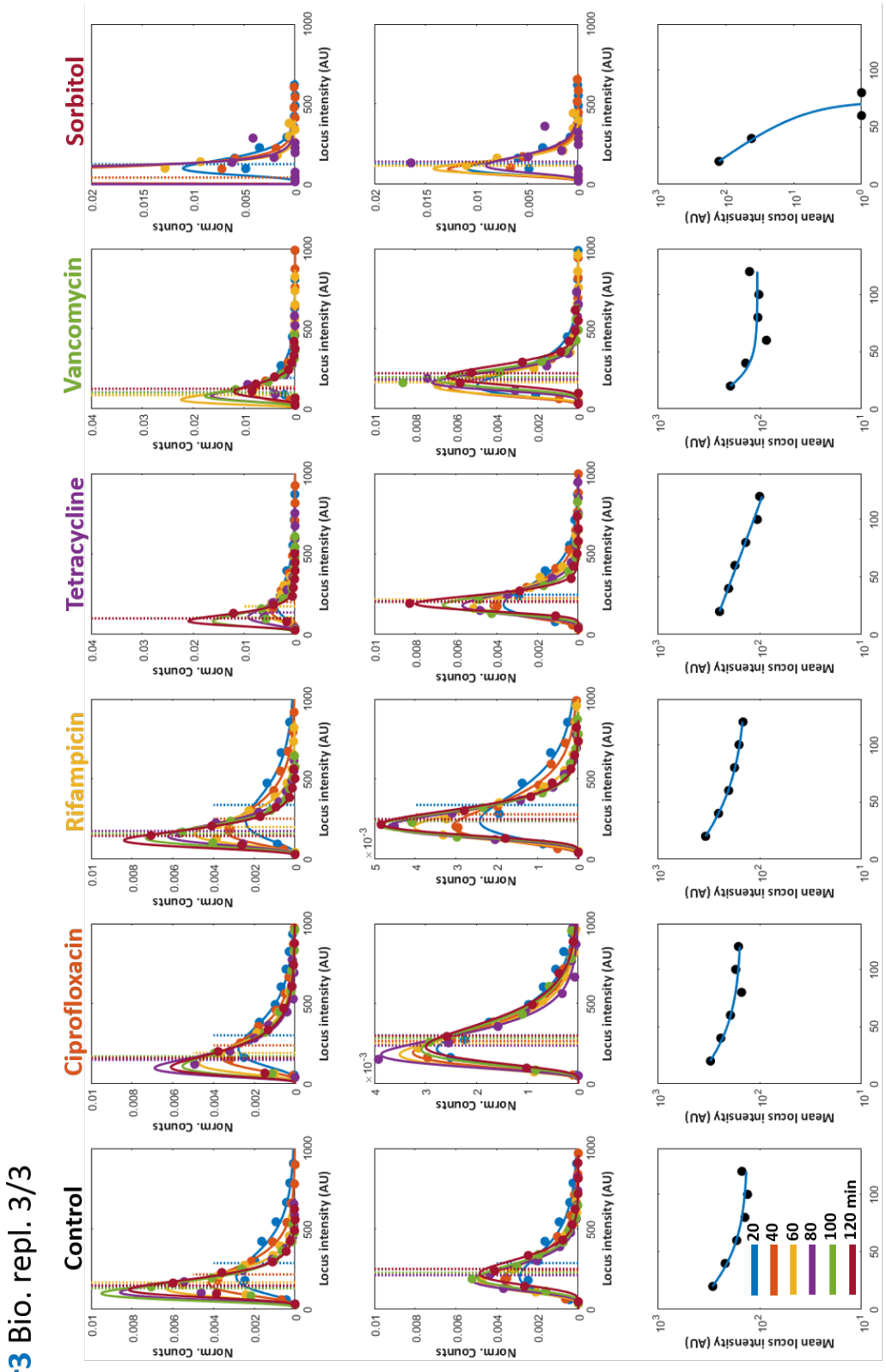

Fig. B6 **Photo-bleaching profiles of Ter3 loci, biological replicate 3/3, in all treatment conditions.**

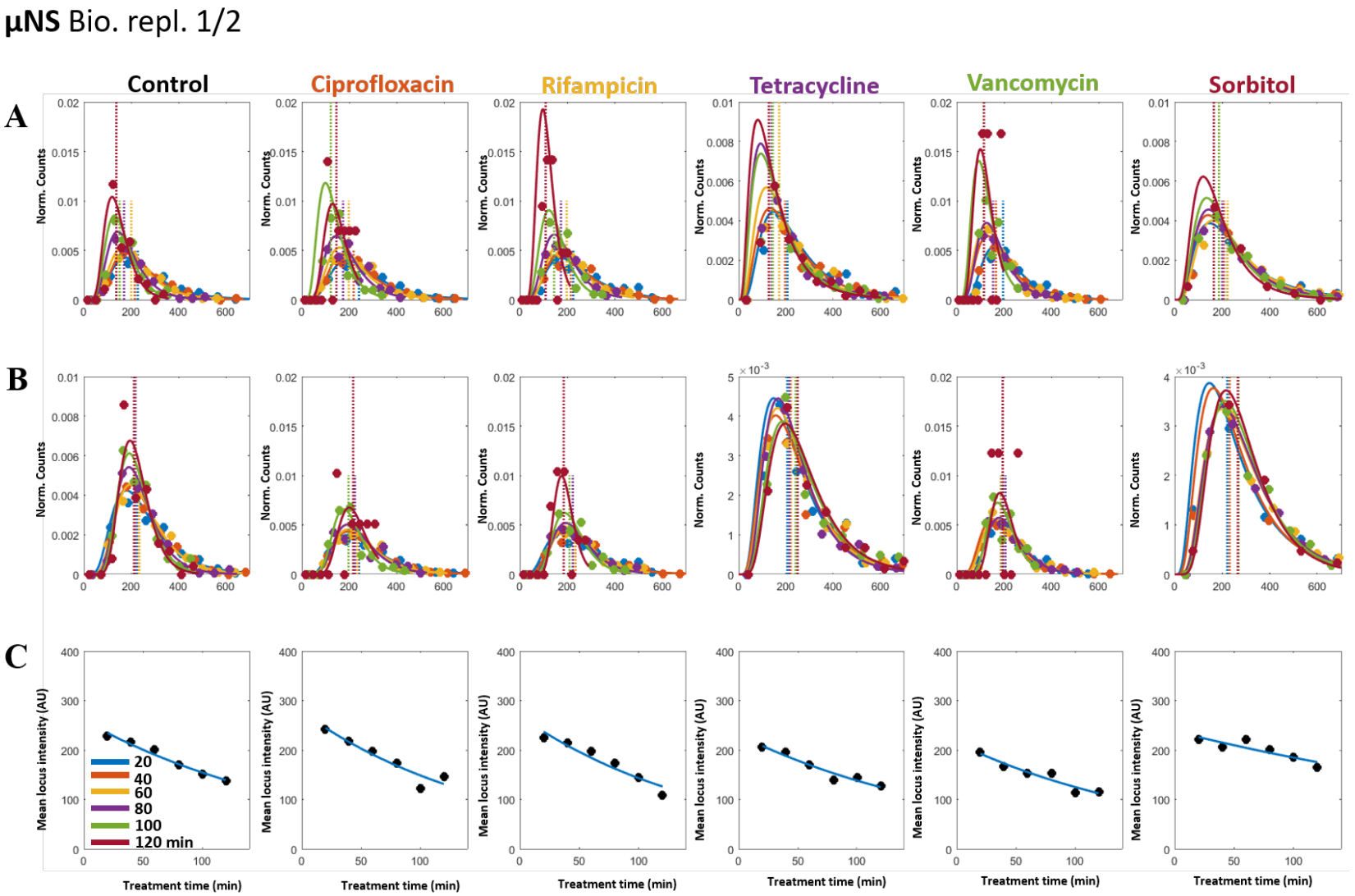

Fig. B7 **Photo-bleaching profiles of μNS loci, biological replicate 1/3, in all treatment conditions.**

µNS Bio. repl. 2/2

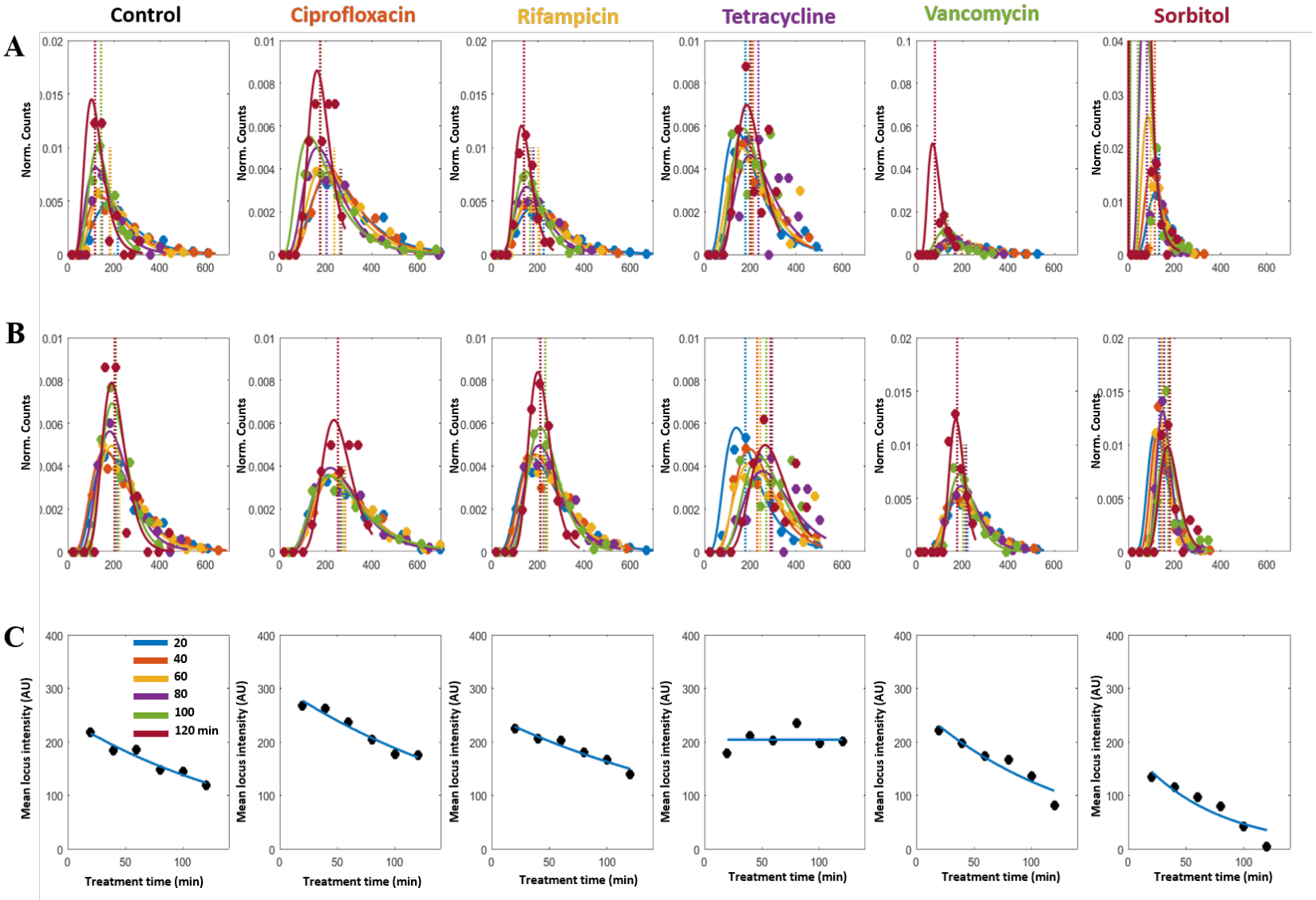

Fig. B8 **Photo-bleaching profiles of μNS loci, biological replicate 2/3, in all treatment conditions.**

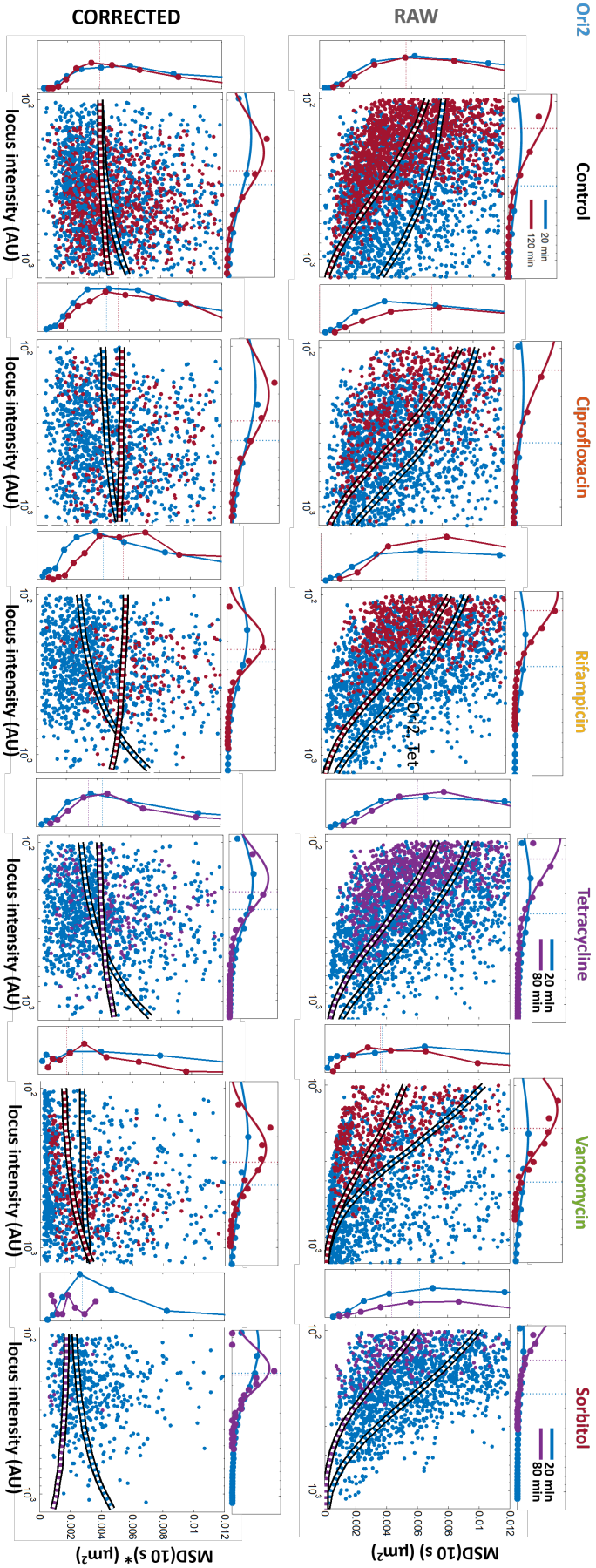

Fig. B9 **Correction profiles for Ori2 loci for all treatment conditions for agarose pads data.**

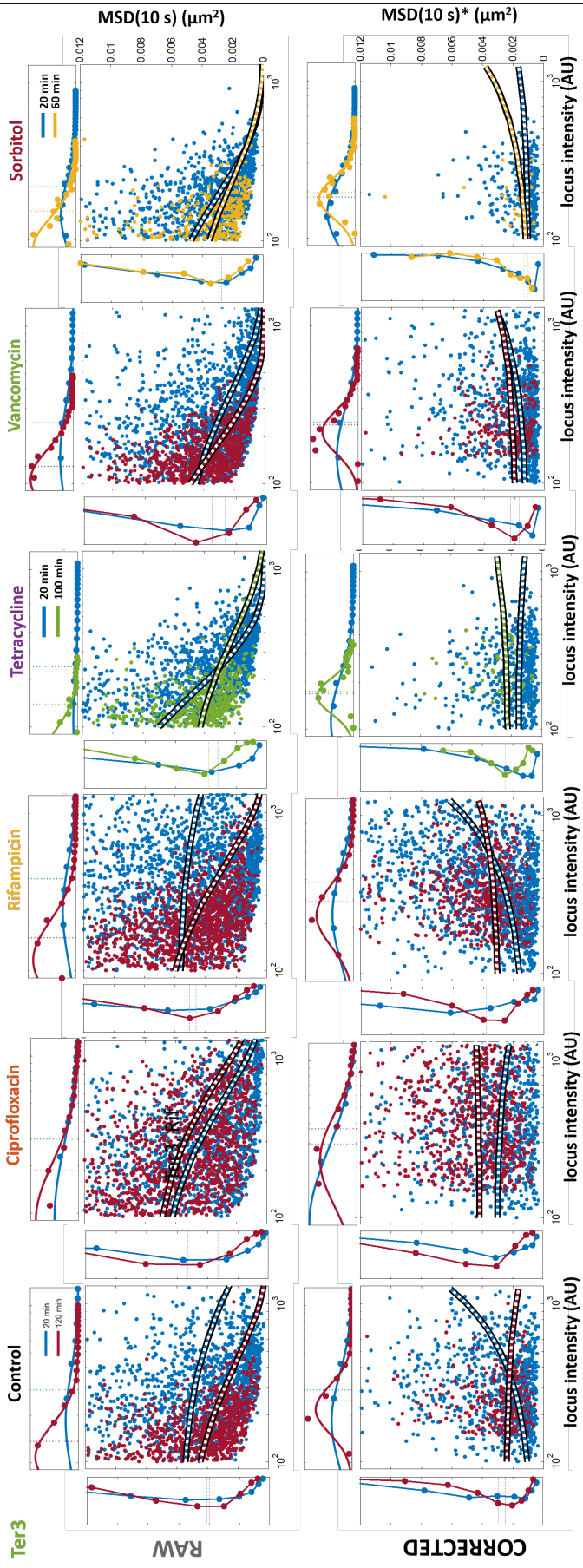

Fig. B10 **Correction profiles for Ter3 loci for all treatment conditions for agarose pads data.**

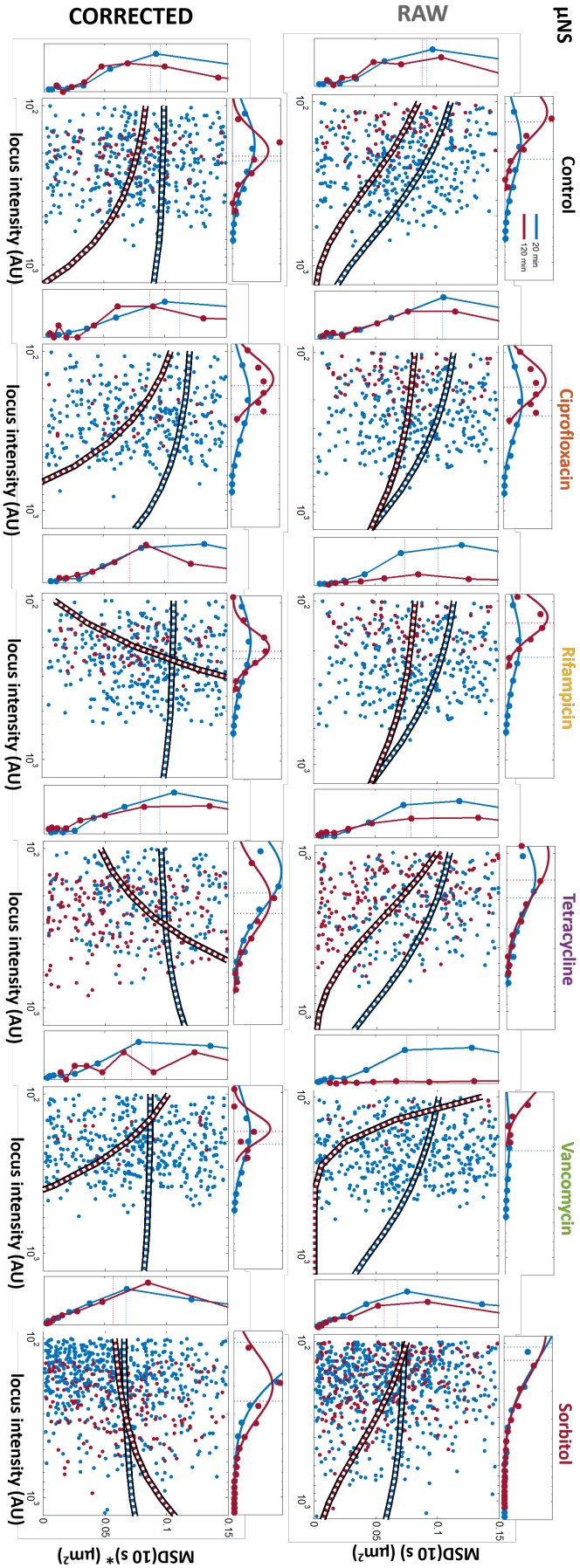

Fig. B11 **Correction profiles for μNS loci for all treatment conditions for agarose pads data.**

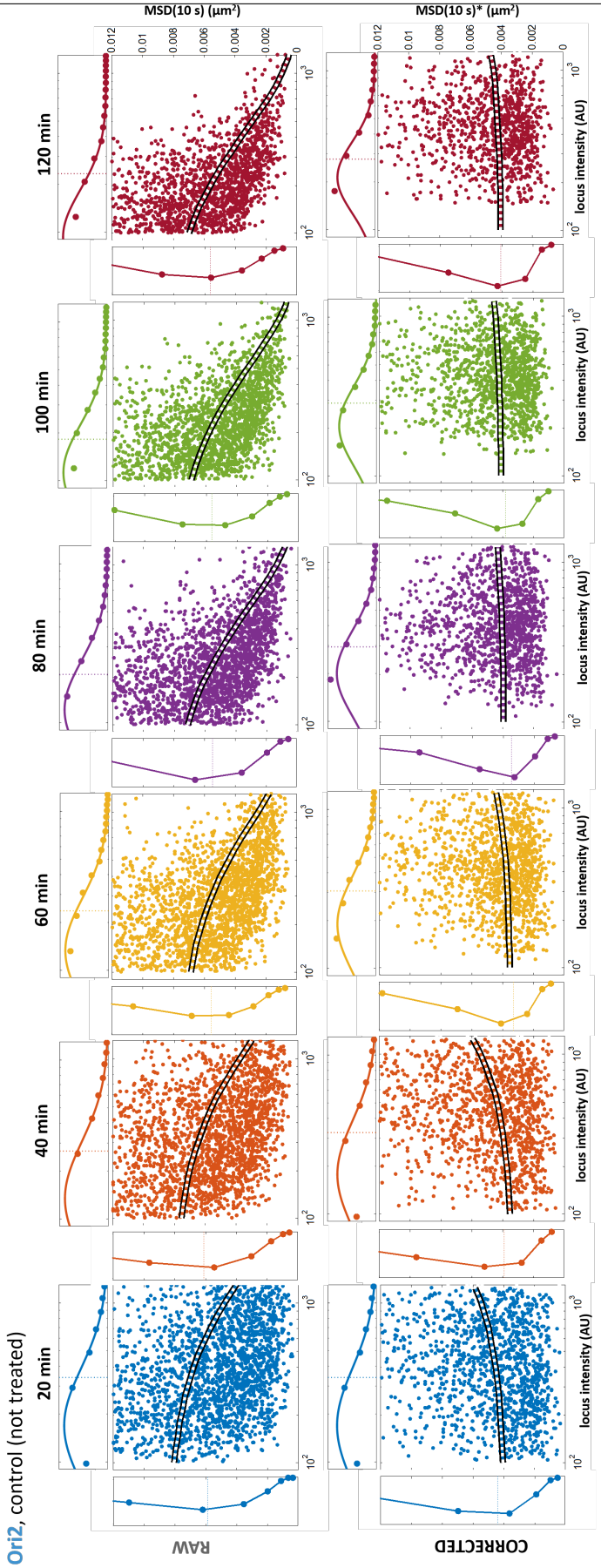

Fig. B12 Correction profiles for Ori2 loci in control (not treated) condition for all measurement times (20-120 min) for agarose pads data.

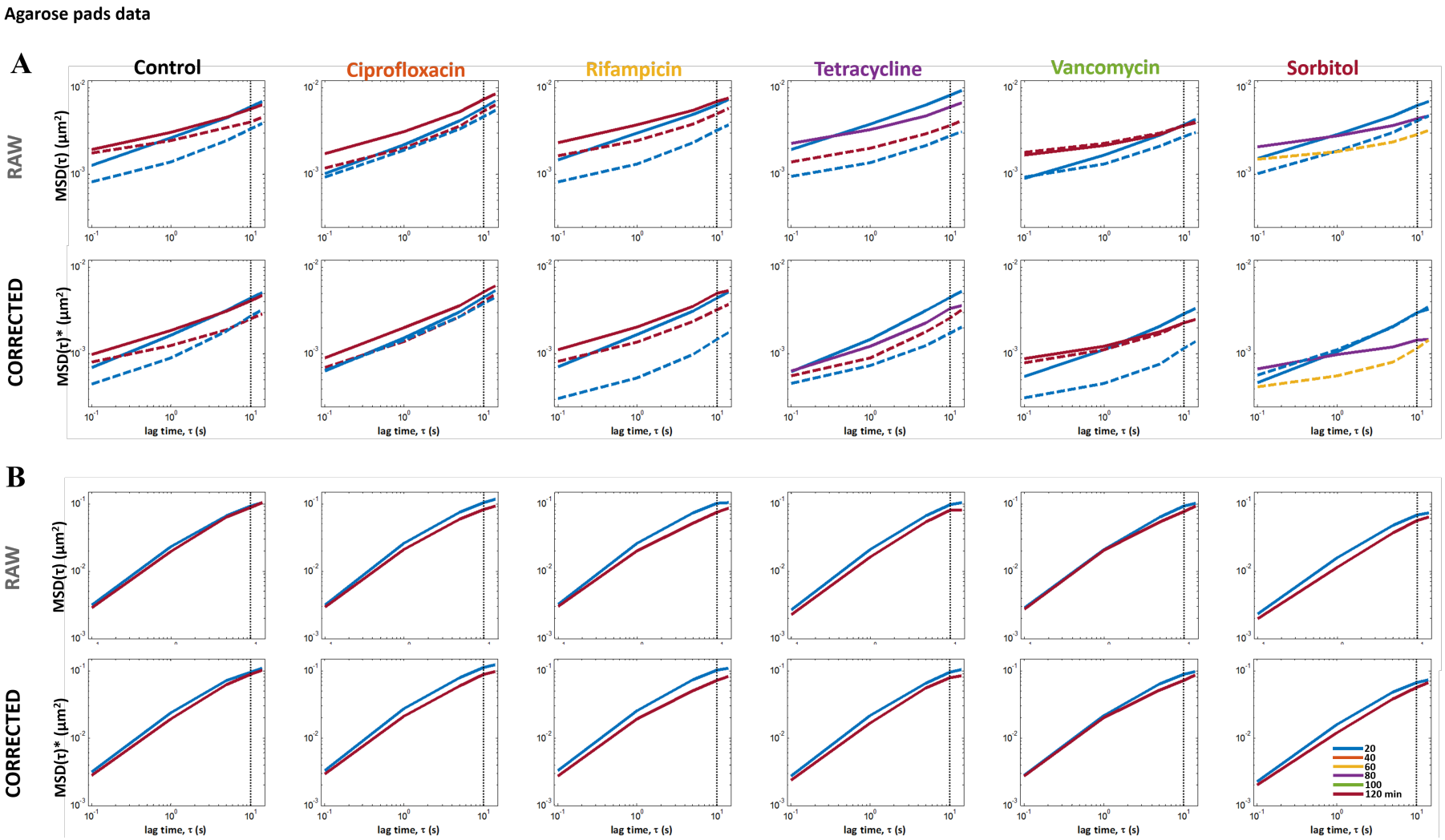

Fig. B13 **MSD(τ) for raw and corrected data sets for initial and final measurement times for all treatment conditions (as labelled on top of individual figure columns) for (A) Ori2 (*solid* lines) and Ter3 (*dashed* lines) loci and (B) μNS cytosolic aggregates. Agarose pads data only.**

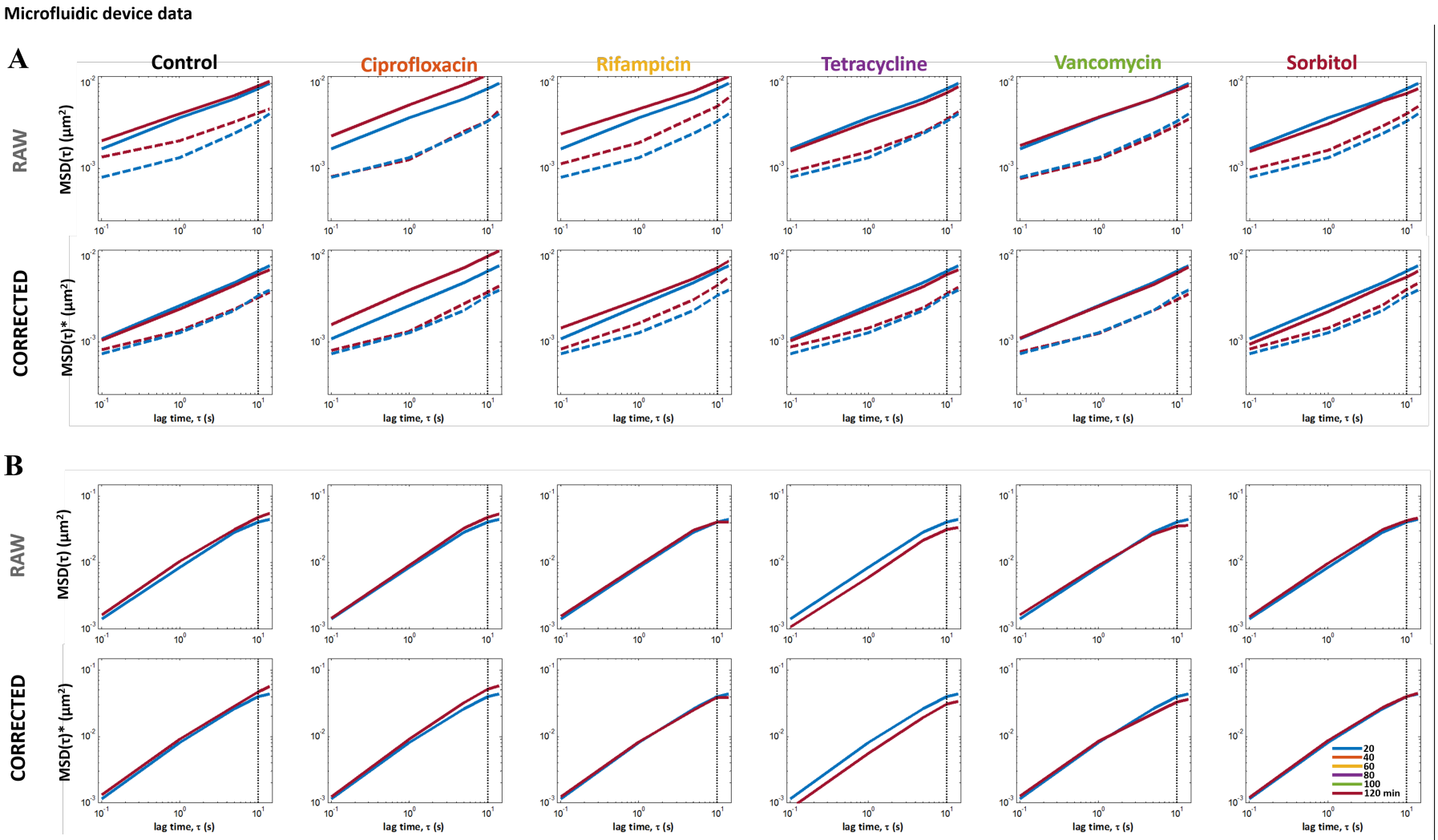

Fig. B14 **MSD(τ) for raw and corrected data sets for initial and final measurement times for all treatment conditions (as labelled on top of individual figure columns) for (A) Ori2 (*solid* lines) and Ter3 (*dashed* lines) loci and (B) μNS cytosolic aggregates. Microfluidic device data only.**

Cell lengths, elongation rates, and widths for all strains and treatment conditions using two measurement methods (semi-manual and SuperSegger software)

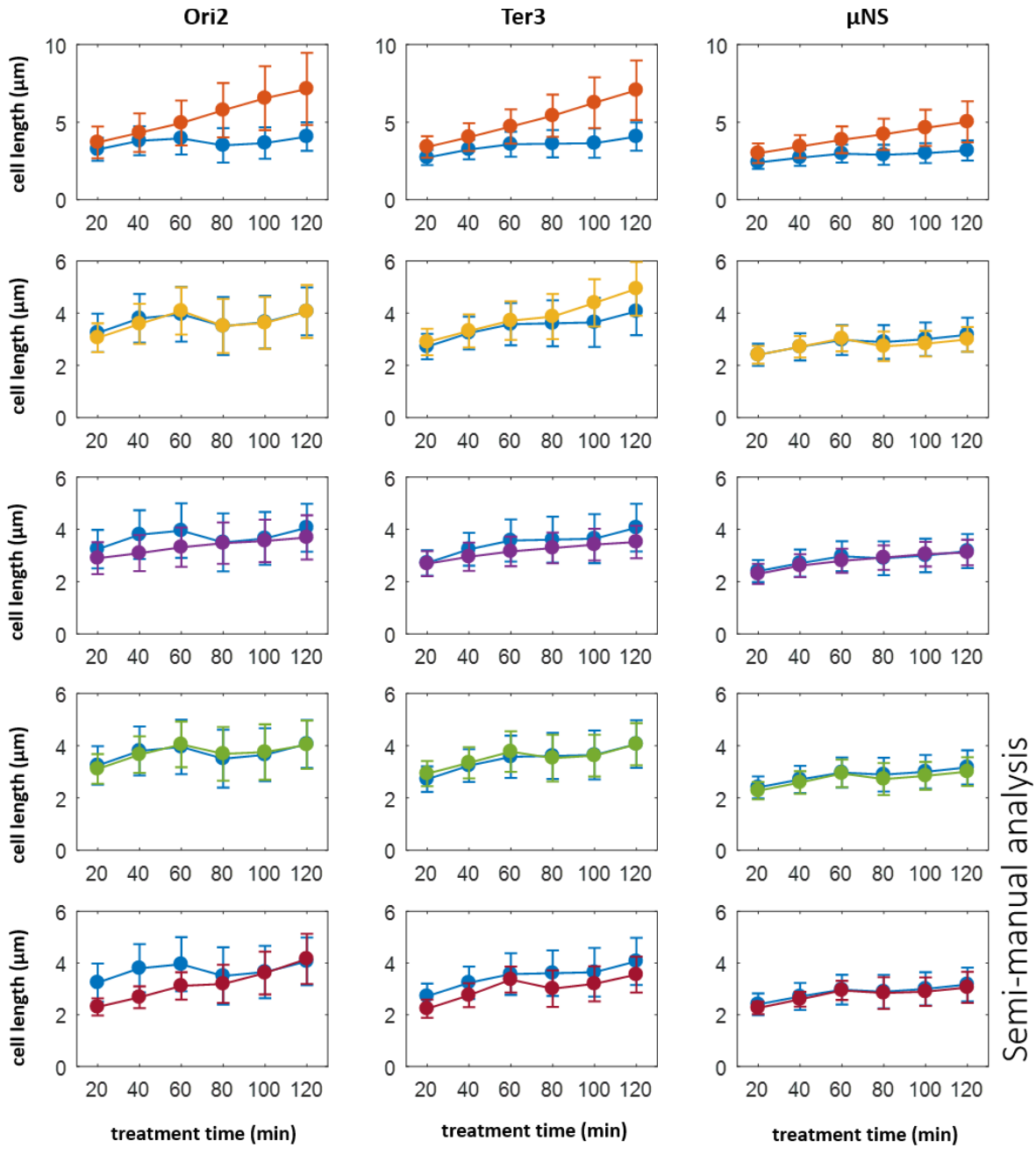

Fig. B15 **Cell lengths measured semi-manually.** Strains are indicated at the top of each column of plots; treated with ciprofloxacin (*orange*), rifampicin (*yellow*), tetracycline (*violet*), vancomycin (*green*), and sorbitol (*red*); and the controls (*blue*).

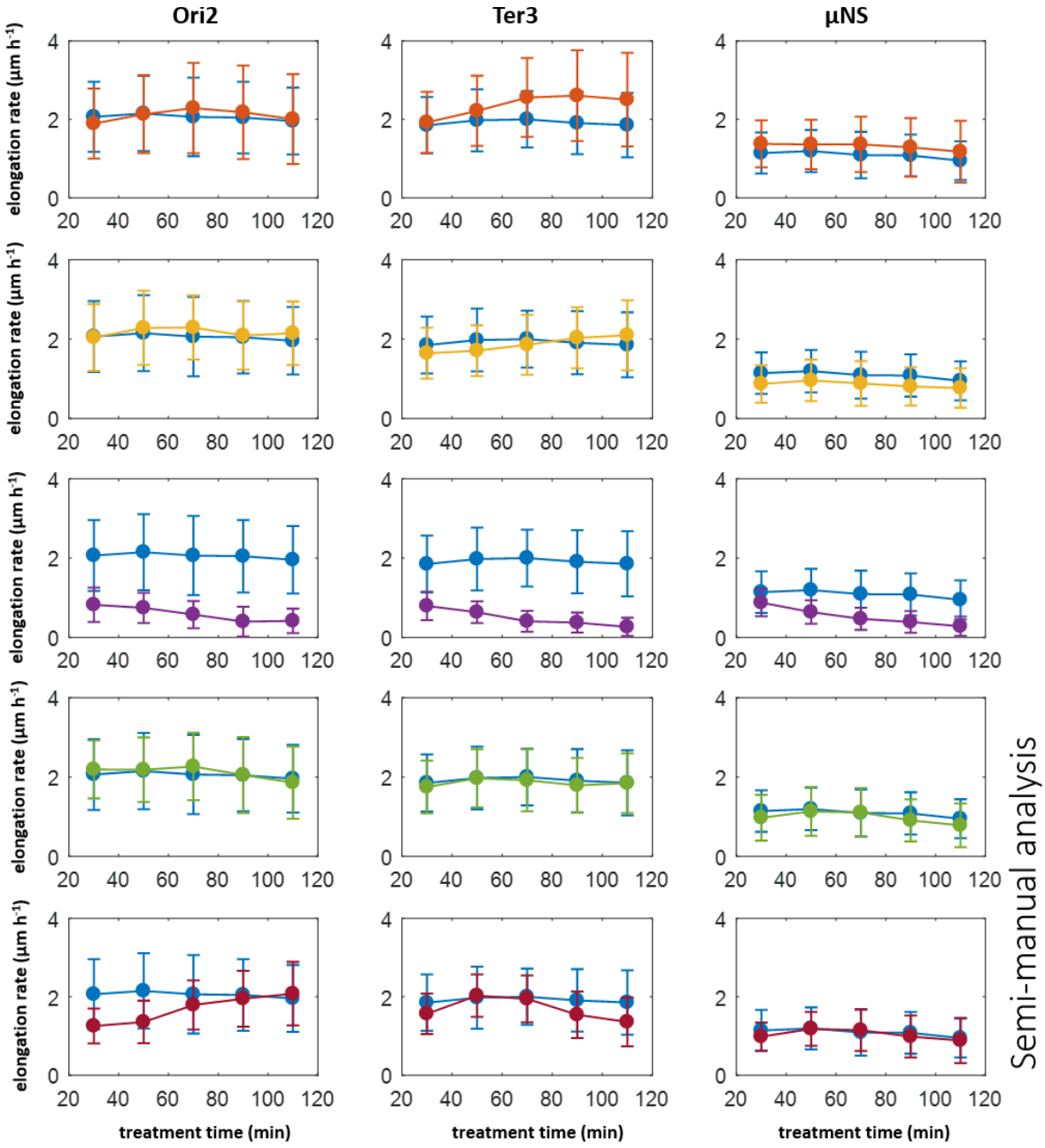

Fig. B16 **Cell elongation rates measured semi-manually.** Strains are indicated at the top of each column of plots; treated with ciprofloxacin (*orange*), rifampicin (*yellow*), tetracycline (*violet*), vancomycin (*green*), and sorbitol (*red*); and the controls (*blue*).

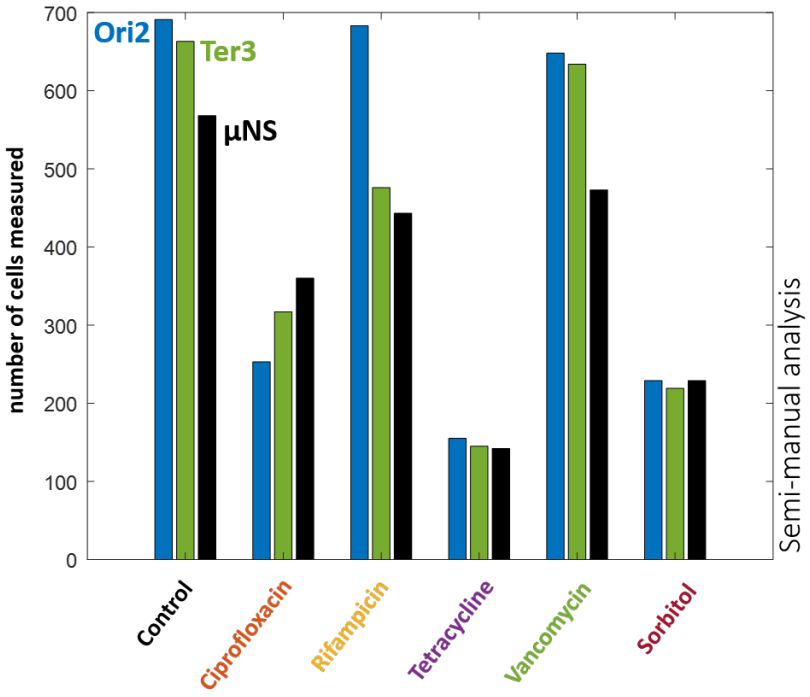

Fig. B17 **Numbers of cells measured semi-manually for cell size analysis of phase contrast images (cells grown on agarose pads).**

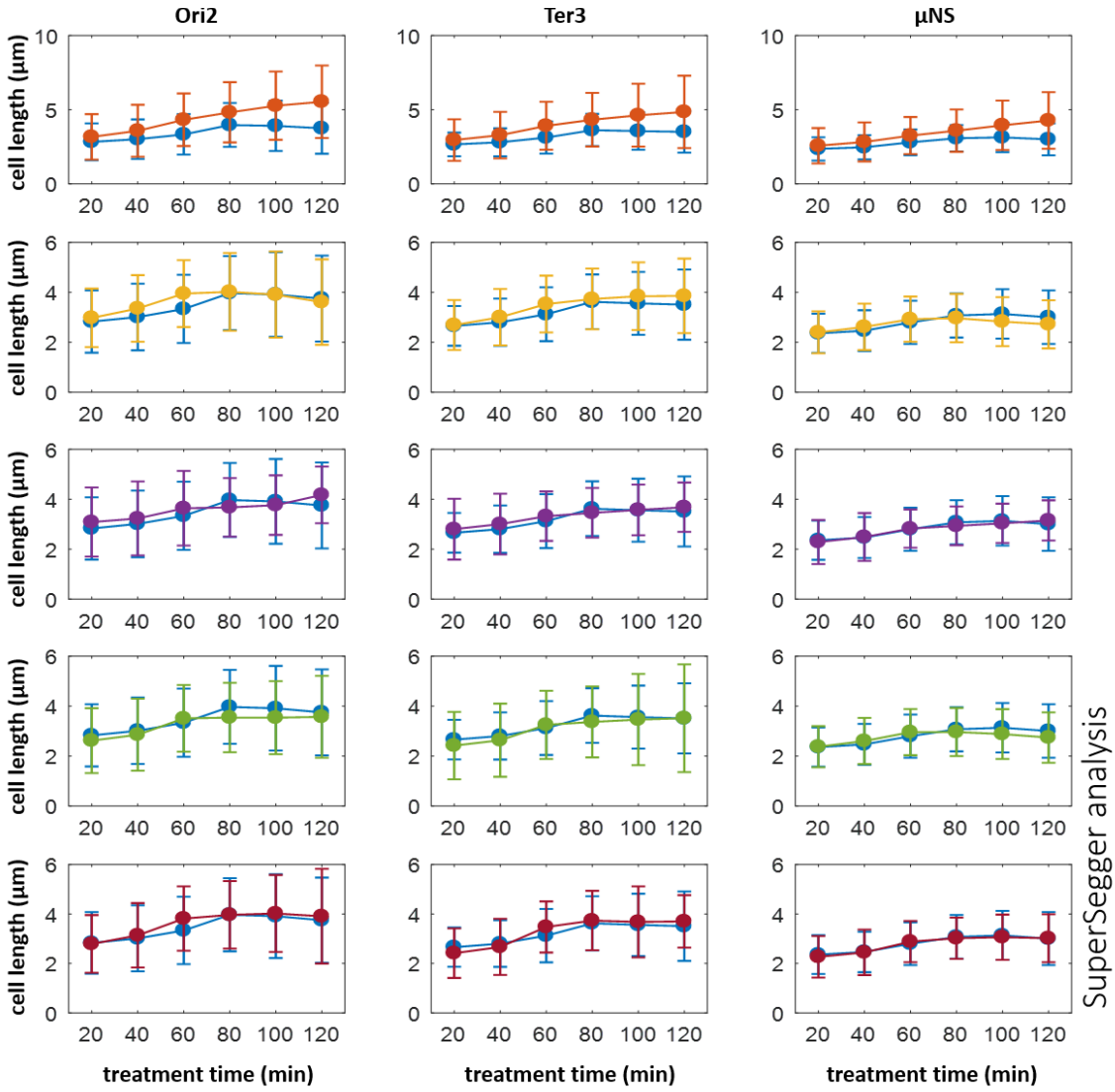

Fig. B18 **Cell lengths measured with SupperSegger software.** Strains are indicated at the top of each column of plots; treated with ciprofloxacin (*orange*), rifampicin (*yellow*), tetracycline (*violet*), vancomycin (*green*), and sorbitol (*red*); and the controls (*blue*).

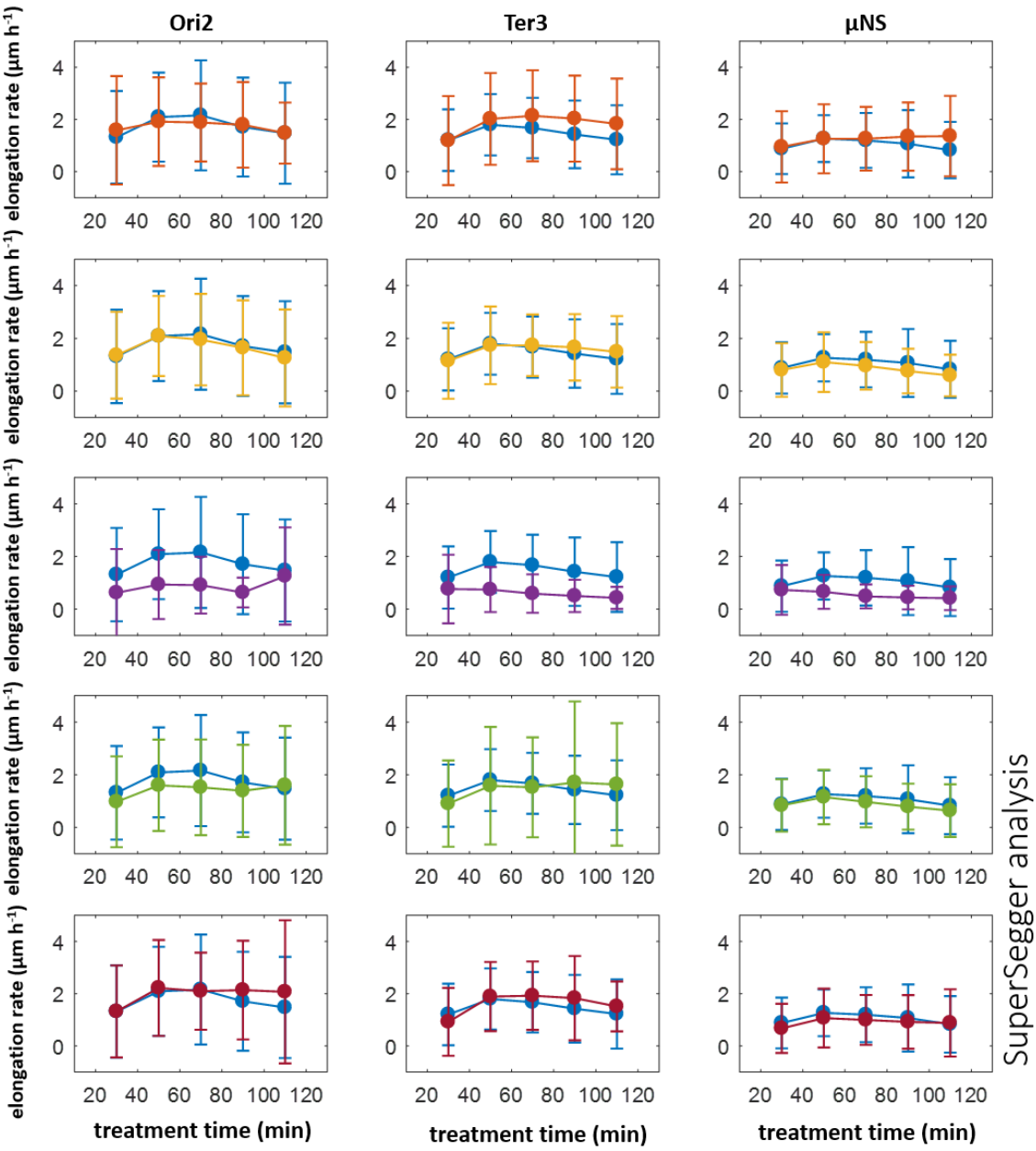

Fig. B19 **Cell elongation rates measured with SupperSegger software.** Strains are indicated at the top of each column of plots; treated with ciprofloxacin (*orange*), rifampicin (*yellow*), tetracycline (*violet*), vancomycin (*green*), and sorbitol (*red*); and the controls (*blue*).

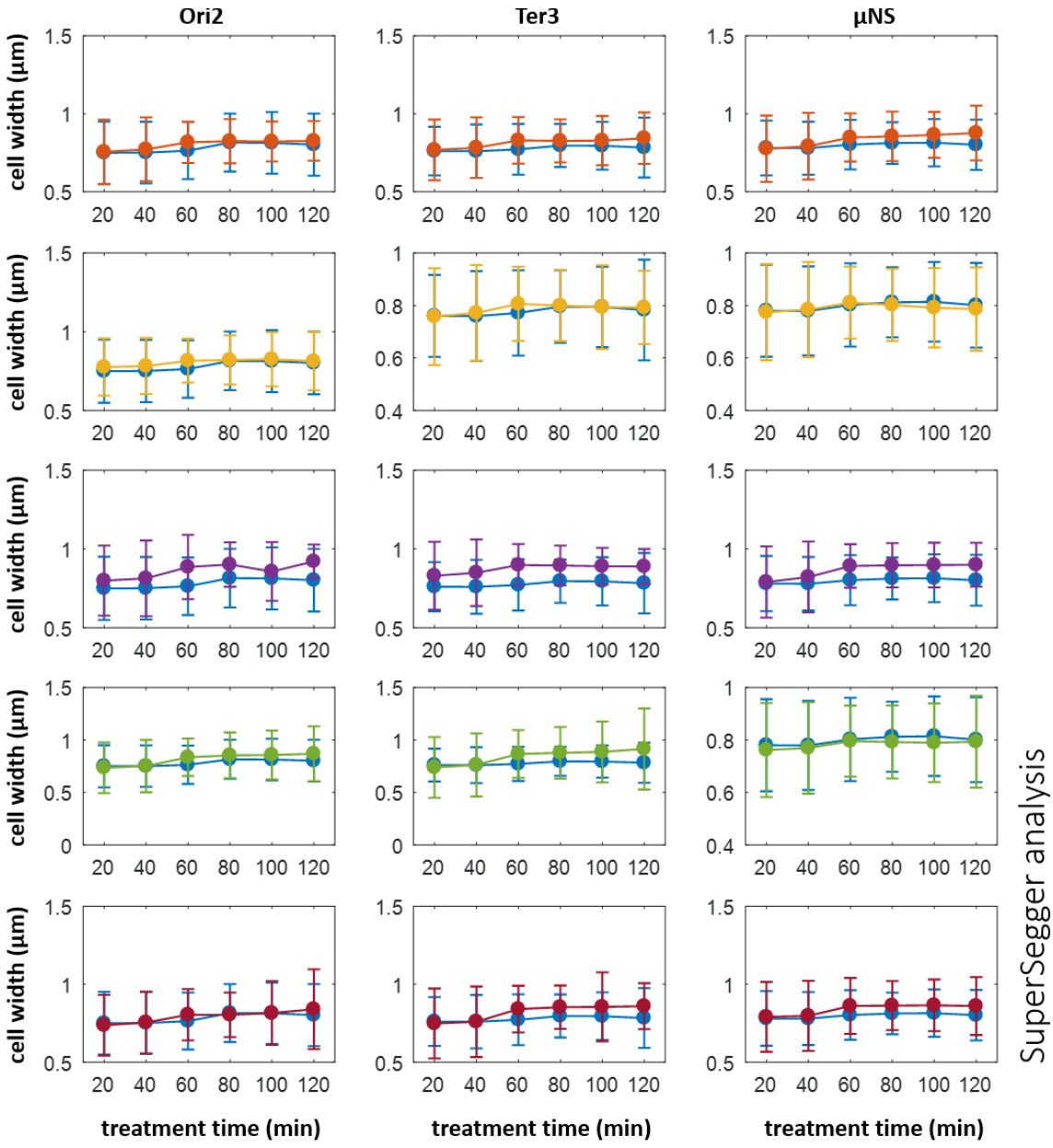

Fig. B20 **Cell widths measured with SupperSegger software.** Strains are indicated at the top of each column of plots; treated with ciprofloxacin (*orange*), rifampicin (*yellow*), tetracycline (*violet*), vancomycin (*green*), and sorbitol (*red*); and the controls (*blue*).

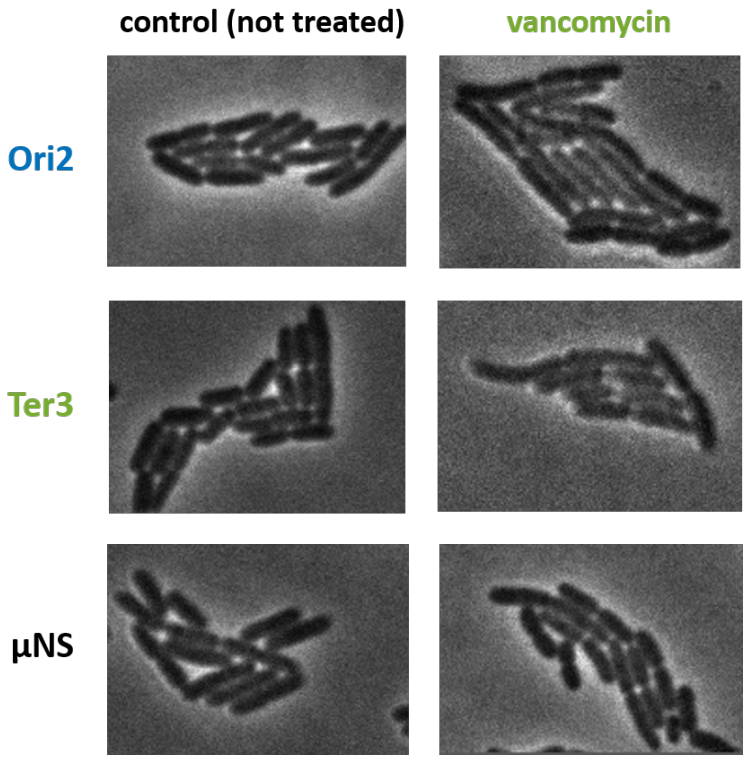

Fig. B21 **Vancomycin changes cell morphology.** Example phase contrast images of three *E. coli* strains under no treatment and sub-lethal vancomycin. Treatment with vancomycin affects cell shape causing unusual bending of cells.

Appendix C

Supplementary materials for Chapter 5

Semi-manual analysis of cell lengths and elongation rates (for cells grown in microfluidic device)

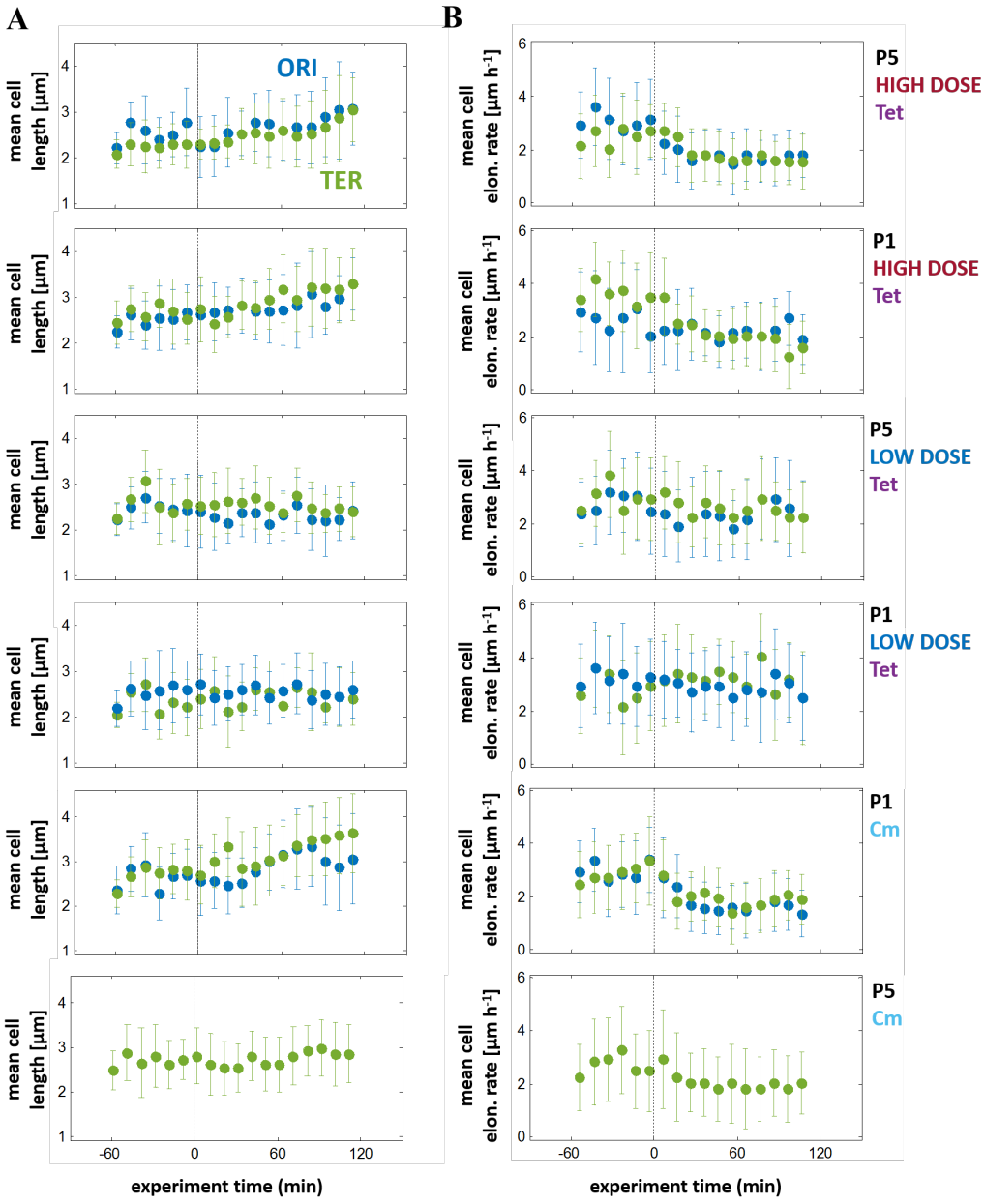

Fig. C1 **Semi-manual analysis of cell lengths and elongation rates.** Effects on (**A**) cell length and (**B**) elongation rate of all treatment conditions. Cell lengths were measured manually at 36 frames (1 h before and 2 h after the media switch), as detailed in Methods. Elongation rate is the difference in cell length between two consecutive frames. Mean cell length and elongation rates for two closest data points were plotted for clarity.

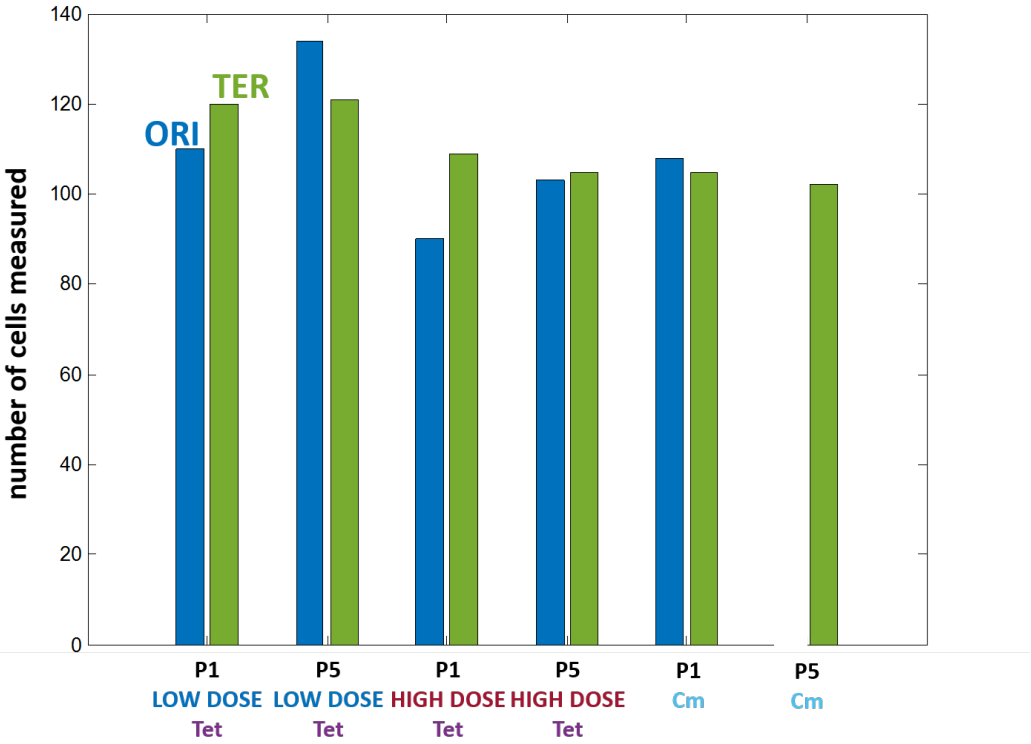

Fig. C2 **Number of cells measured semi-manually for cell size analysis in each treatment condition (for cells grown in microfluidic device).**

All variables (cell intensity, protein concentration, area, length, width, and count) for all promoter types, chromosomal positions, and treatment conditions

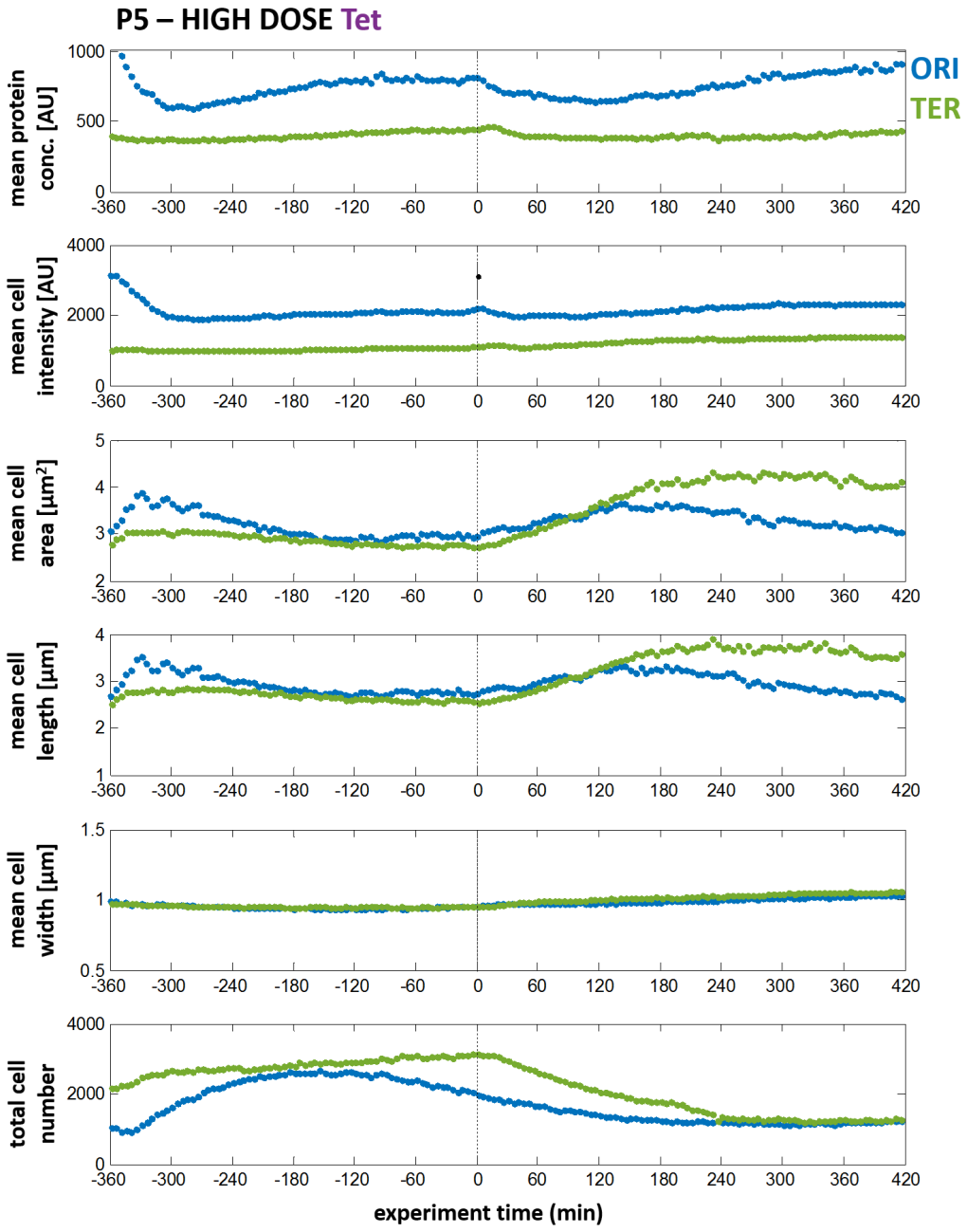

Fig. C3 **Response of the P5 strain to a high dose of tetracycline**. Absolute values of cell intensity, protein concentration, area, length, width, and count for all chromosomal positions are shown across full experiment time.

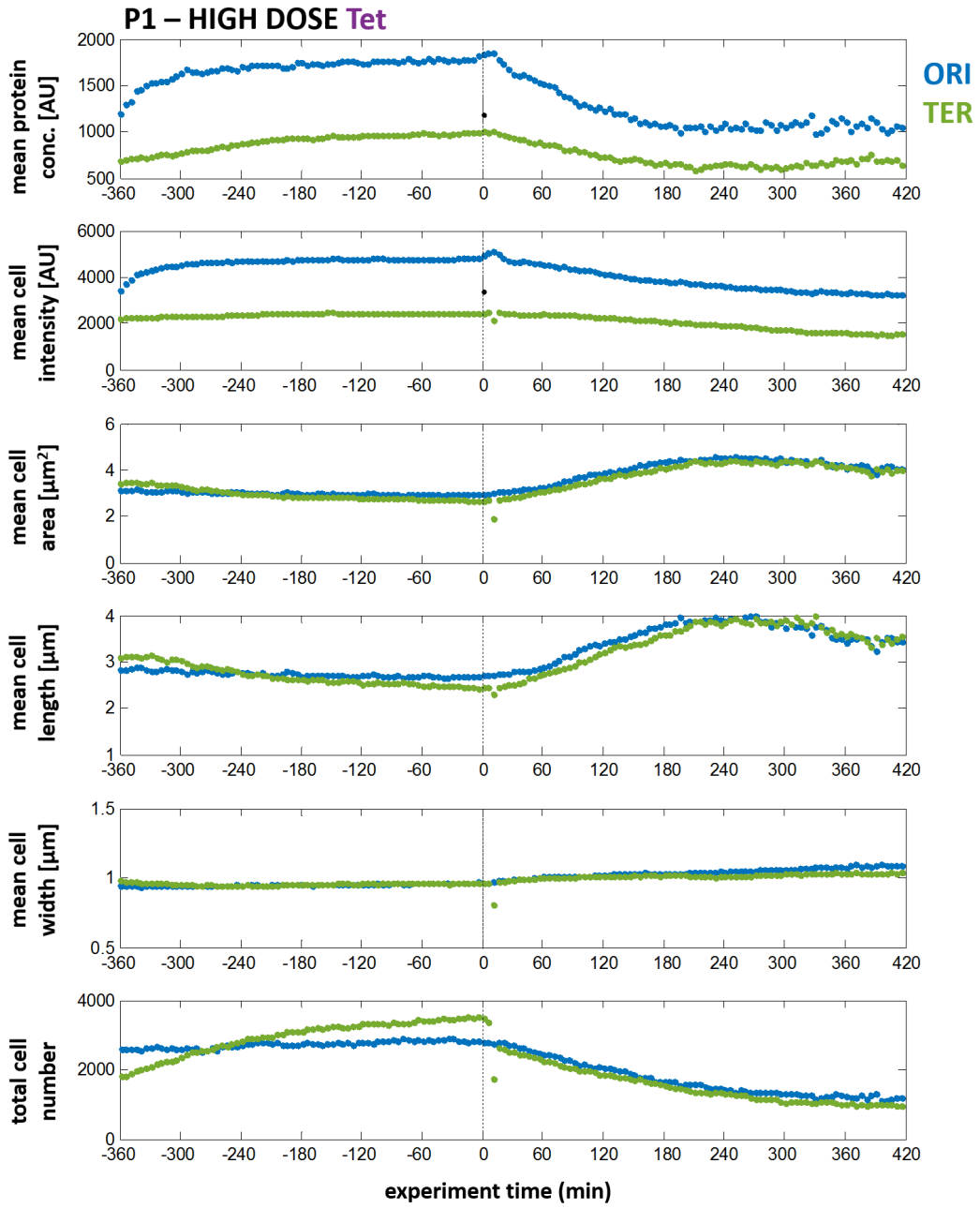

Fig. C4 **Response of the P1 strain to a high dose of tetracycline**. Absolute values of cell intensity, protein concentration, area, length, width, and count for all chromosomal positions are shown across full experiment time.

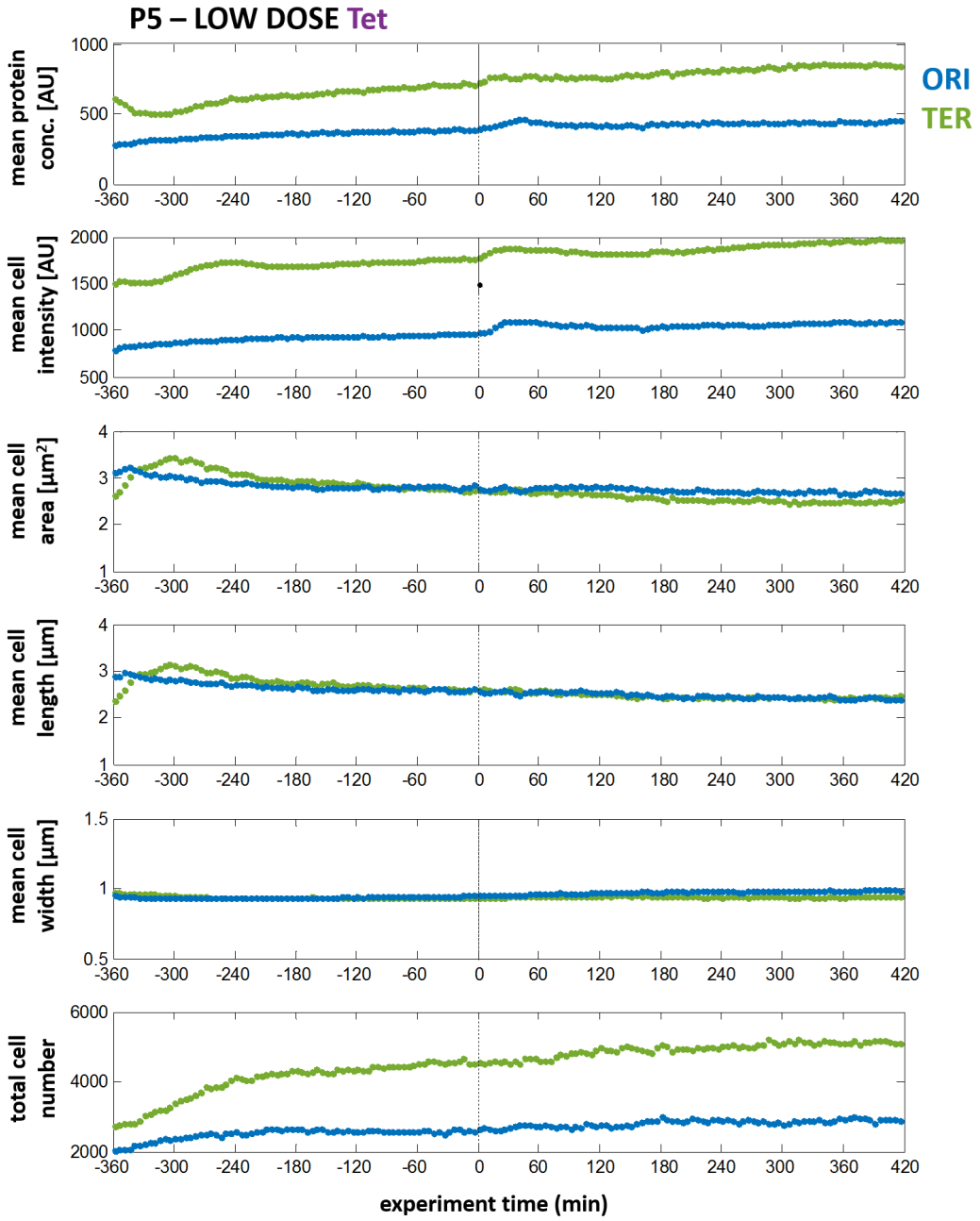

Fig. C5 **Response of the P5 strain to a low dose of tetracycline**. Absolute values of cell intensity, protein concentration, area, length, width, and count for all chromosomal positions are shown across full experiment time.

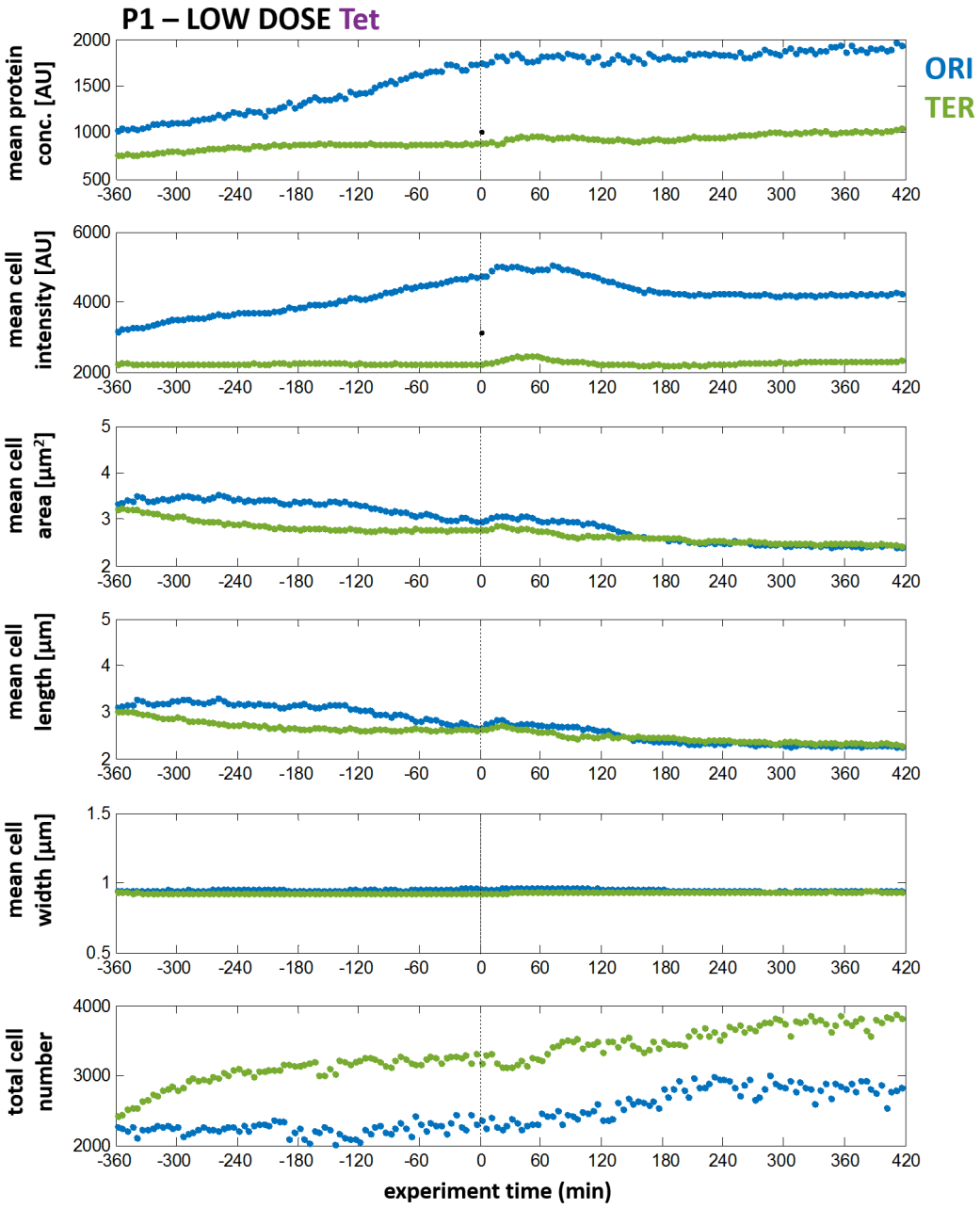

Fig. C6 **Response of the P1 strain to a low dose of tetracycline**. Absolute values of cell intensity, protein concentration, area, length, width, and count for all chromosomal positions are shown across full experiment time.

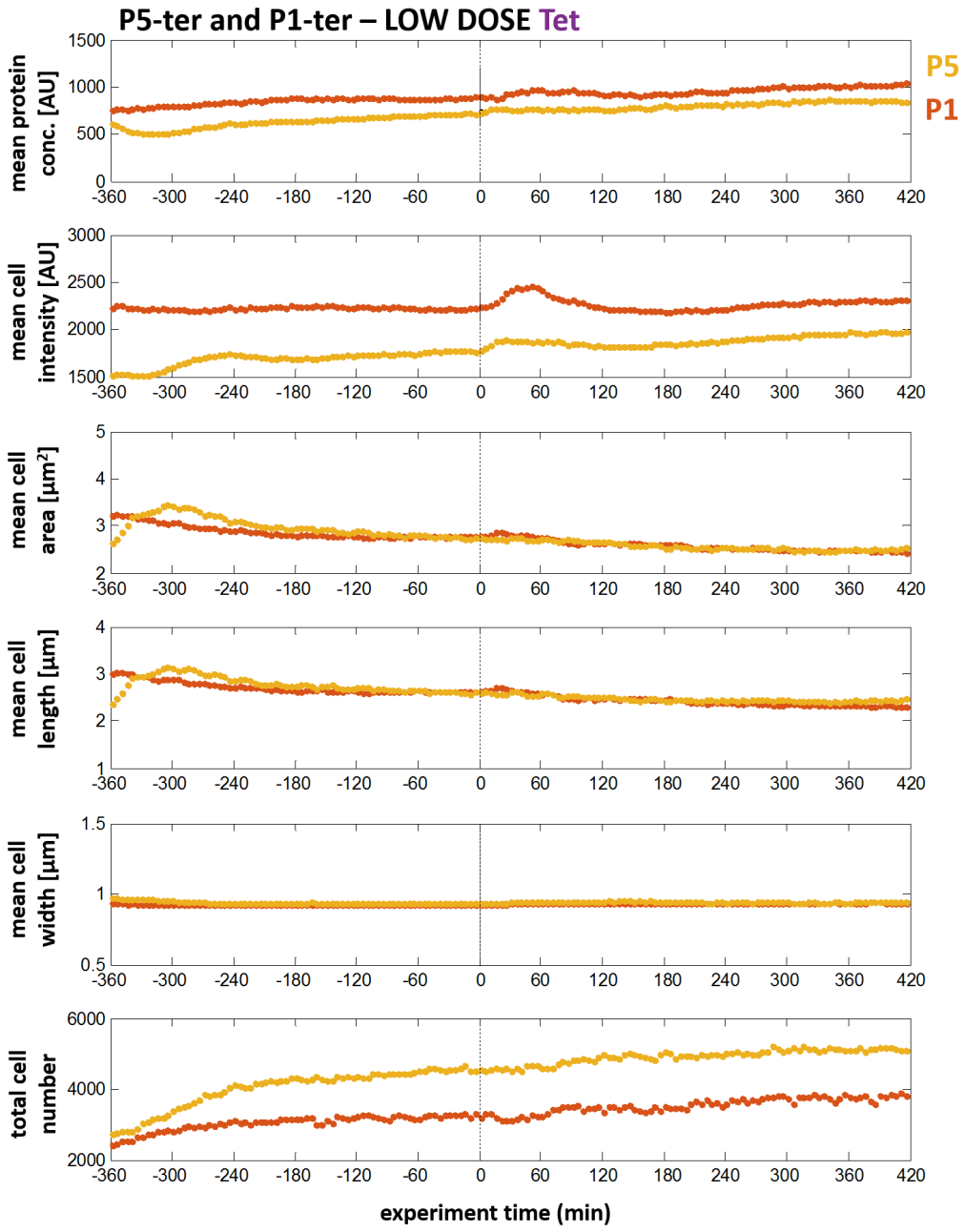

Fig. C7 **Response of the P5 and P1 strains with promoters in Ter positions to a low dose of tetracycline**. Absolute values of cell intensity, protein concentration, area, length, width, and count are shown across full experiment time.

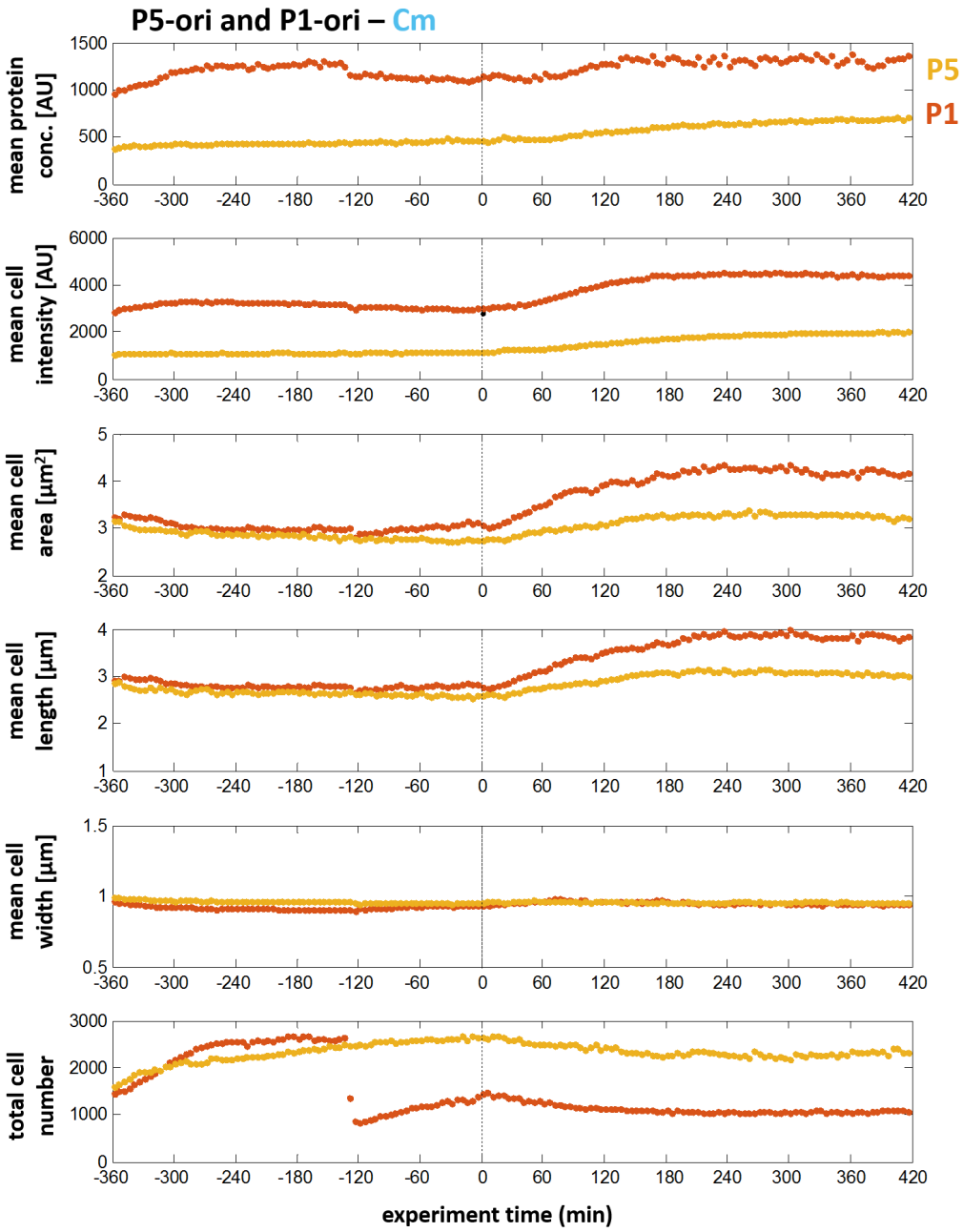

Fig. C8 **Response of the P5 and P1 strains with promoters in Ori positions to chloramphenicol**. Absolute values of cell intensity, protein concentration, area, length, width, and count for are shown across full experiment time.

Fold change in all variables (cell intensity, protein concentration, area, length, and width) for all promoter types, chromosomal positions, and treatment conditions

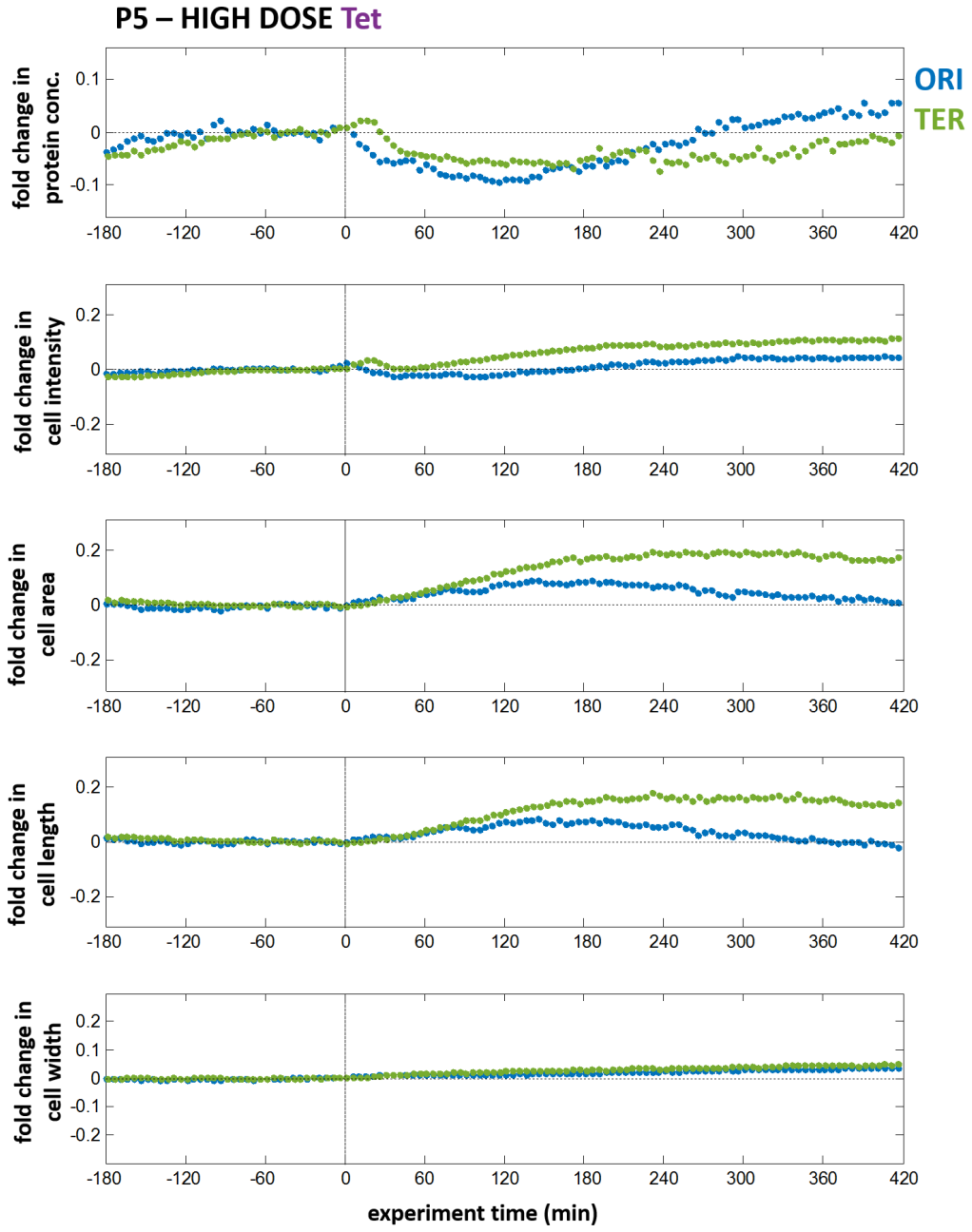

Fig. C9 **Response of the P5 strain to a high dose of tetracycline**. Fold change in cell intensity, protein concentration, area, length, width, and count for all chromosomal positions are shown across full experiment time.

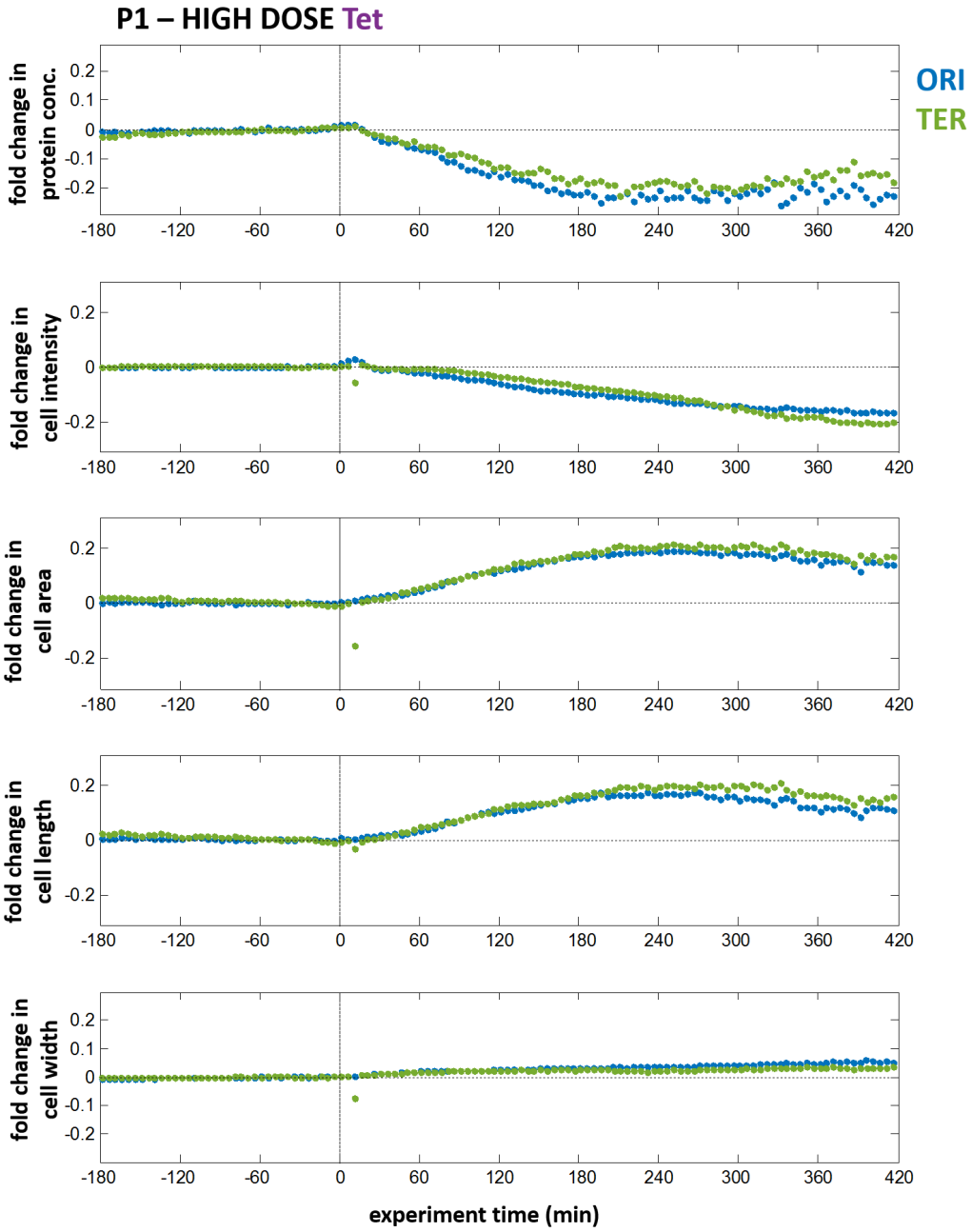

Fig. C10 **Response of the P1 strain to a high dose of tetracycline**. Fold change in cell intensity, protein concentration, area, length, width, and count for all chromosomal positions are shown across full experiment time.

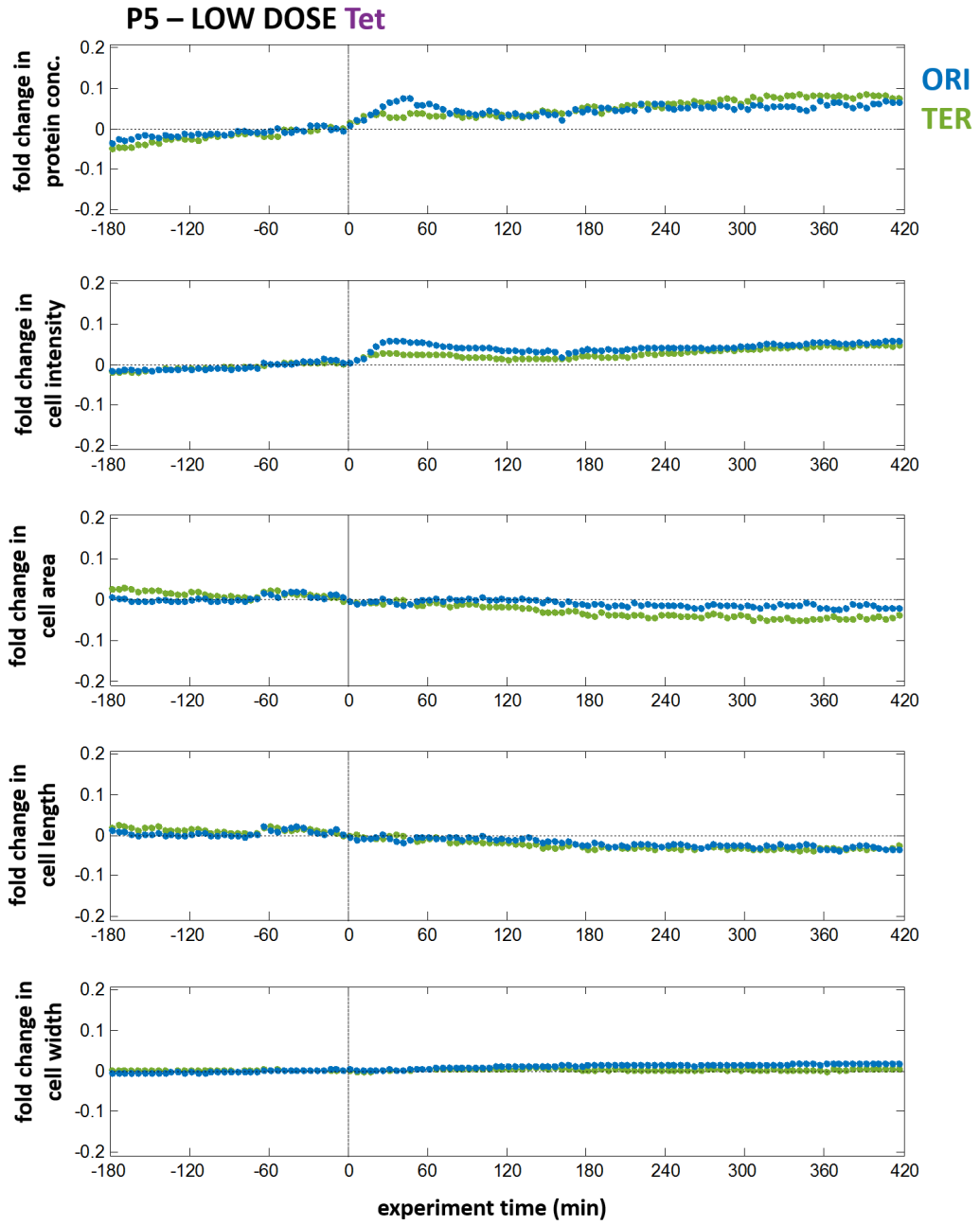

Fig. C11 **Response of the P5 strain to a low dose of tetracycline**. Fold change in cell intensity, protein concentration, area, length, width, and count for all chromosomal positions are shown across full experiment time.

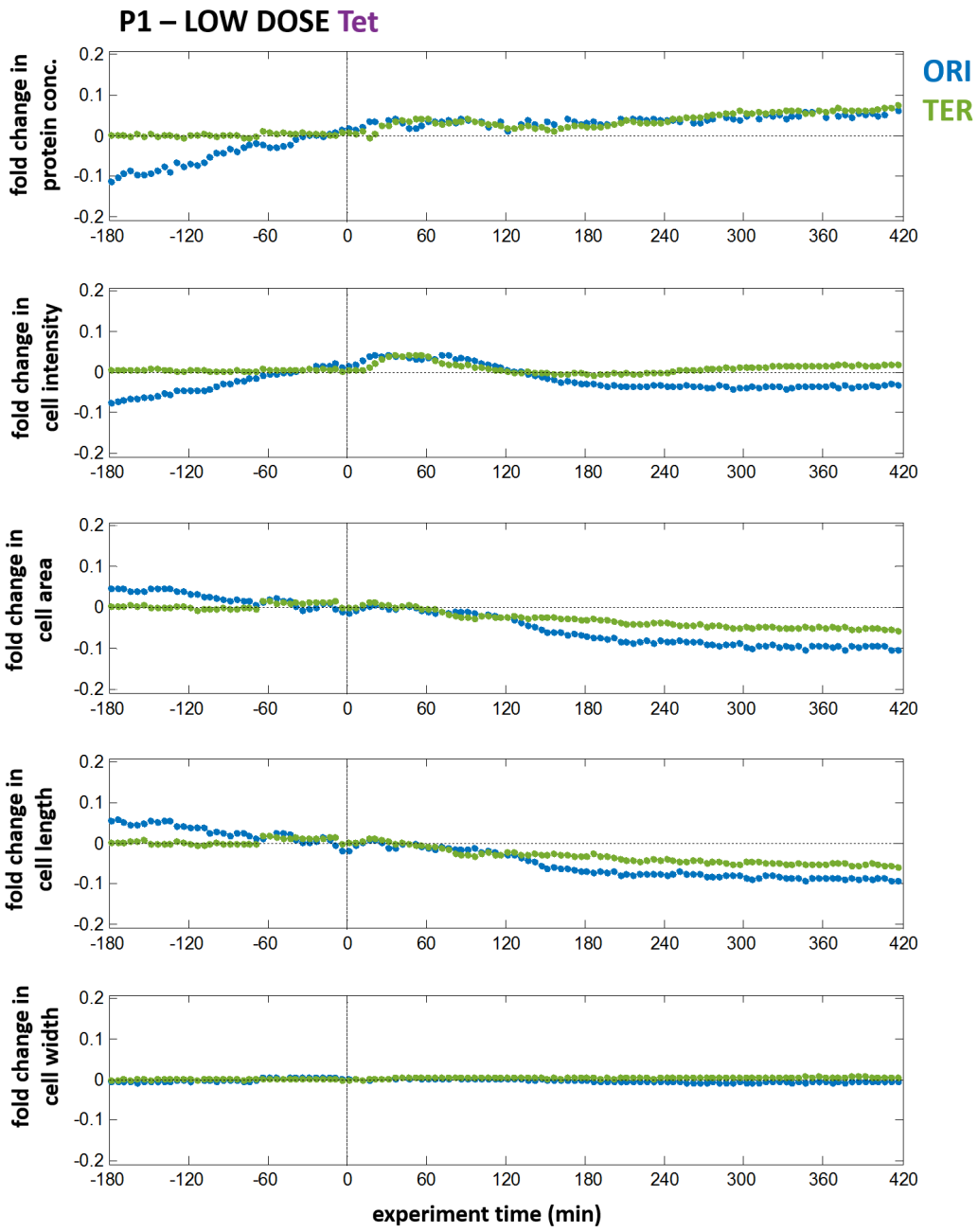

Fig. C12 **Response of the P1 strain to a low dose of tetracycline**. Fold change in cell intensity, protein concentration, area, length, width, and count for all chromosomal positions are shown across full experiment time.

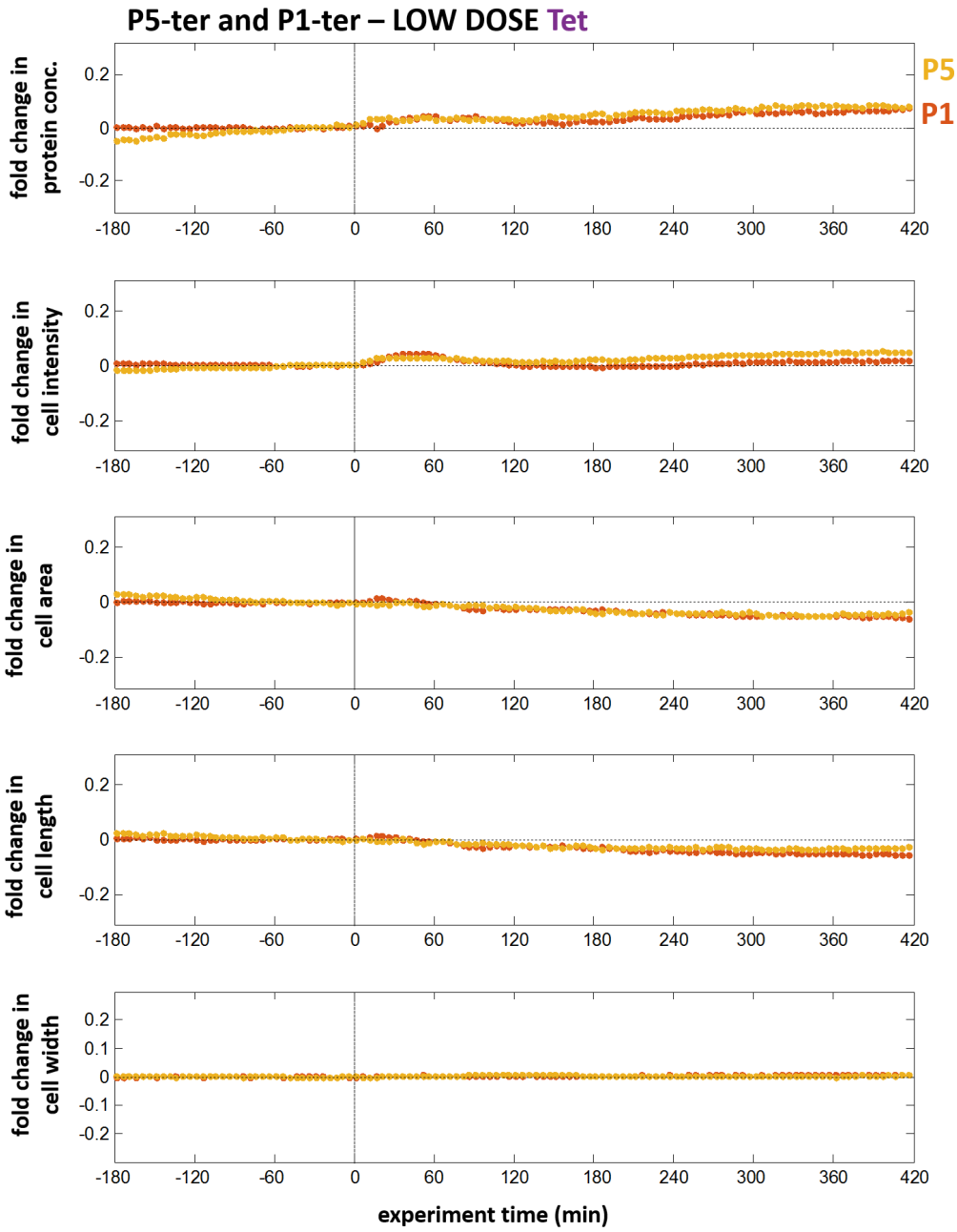

Fig. C13 **Response of the P5 and P1 strains with promoters in Ter positions to tetracycline**. Absolute values of cell intensity, protein concentration, area, length, width, and count for are shown across full experiment time.

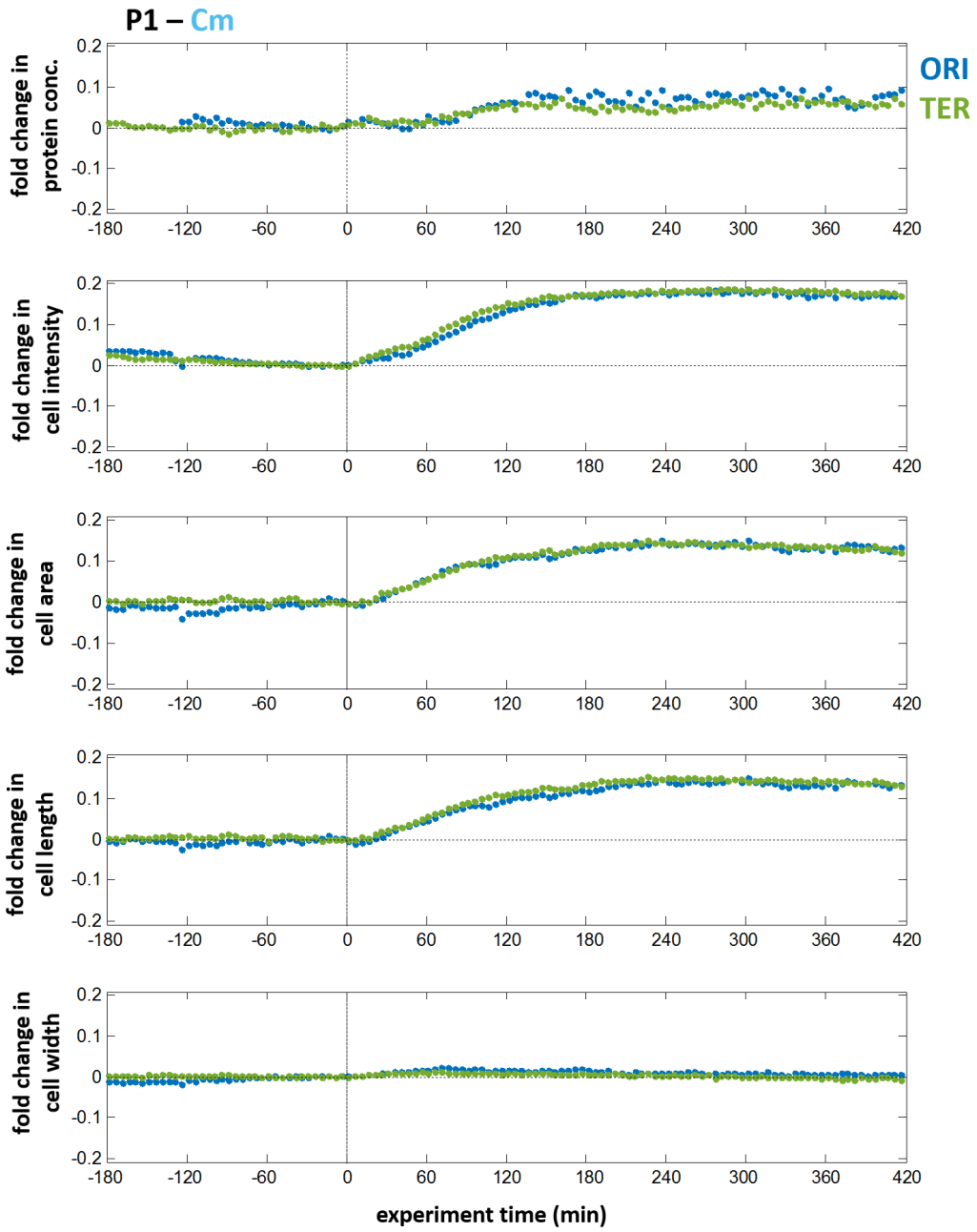

Fig. C14 **Response of the P1 strain to chloramphenicol**. Fold change in cell intensity, protein concentration, area, length, width, and count for all chromosomal positions are shown across full experiment time.

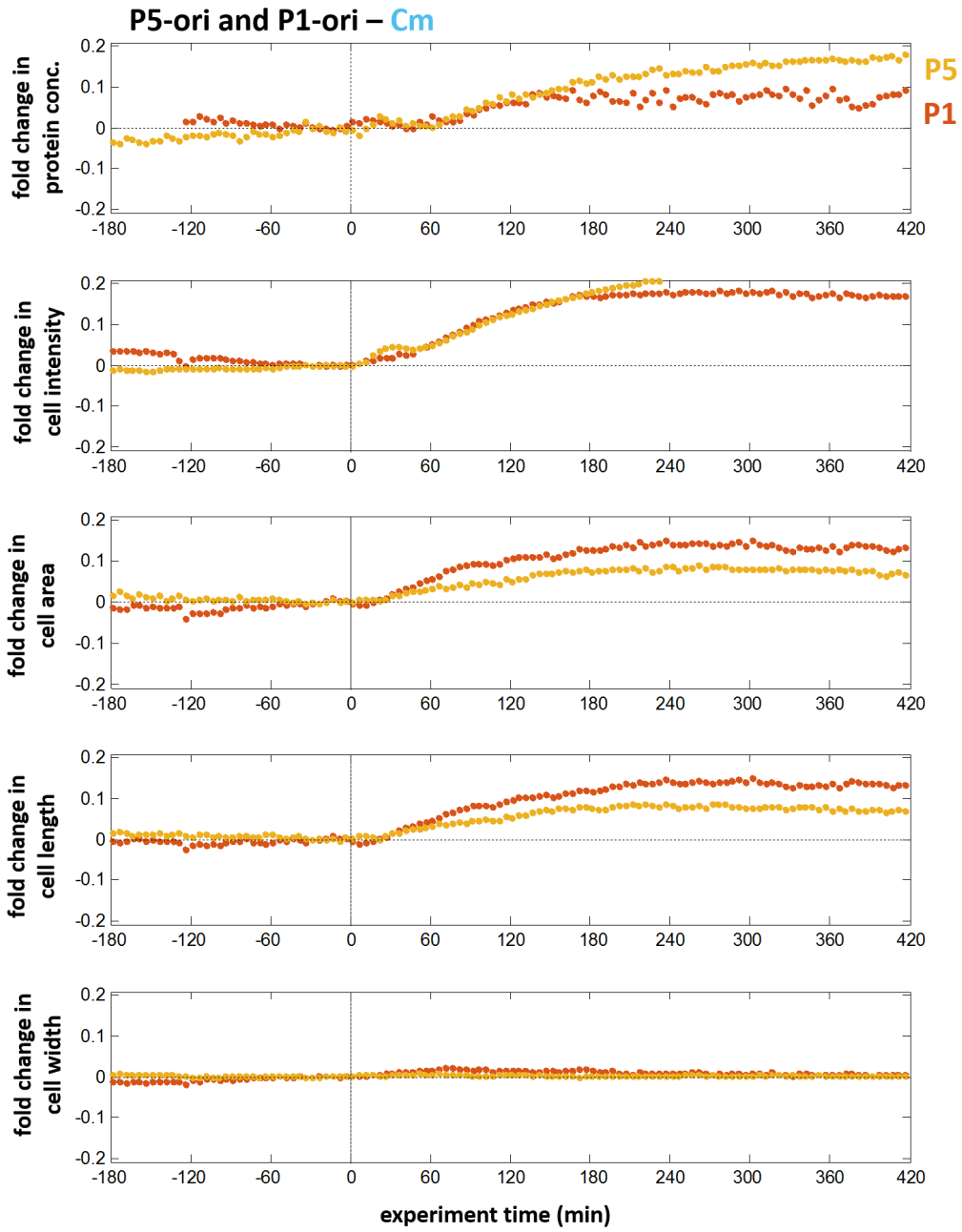

Fig. C15 **Response of the P5 and P1 strains with promoters in Ori positions to chloramphenicol**. Absolute values of cell intensity, protein concentration, area, length, width, and count for are shown across full experiment time.

All variables (cell intensity, protein concentration, area, length, width, and count) for all promoter types, chromosomal positions, and treatment conditions with standard deviations of the mean plotted as errorbars

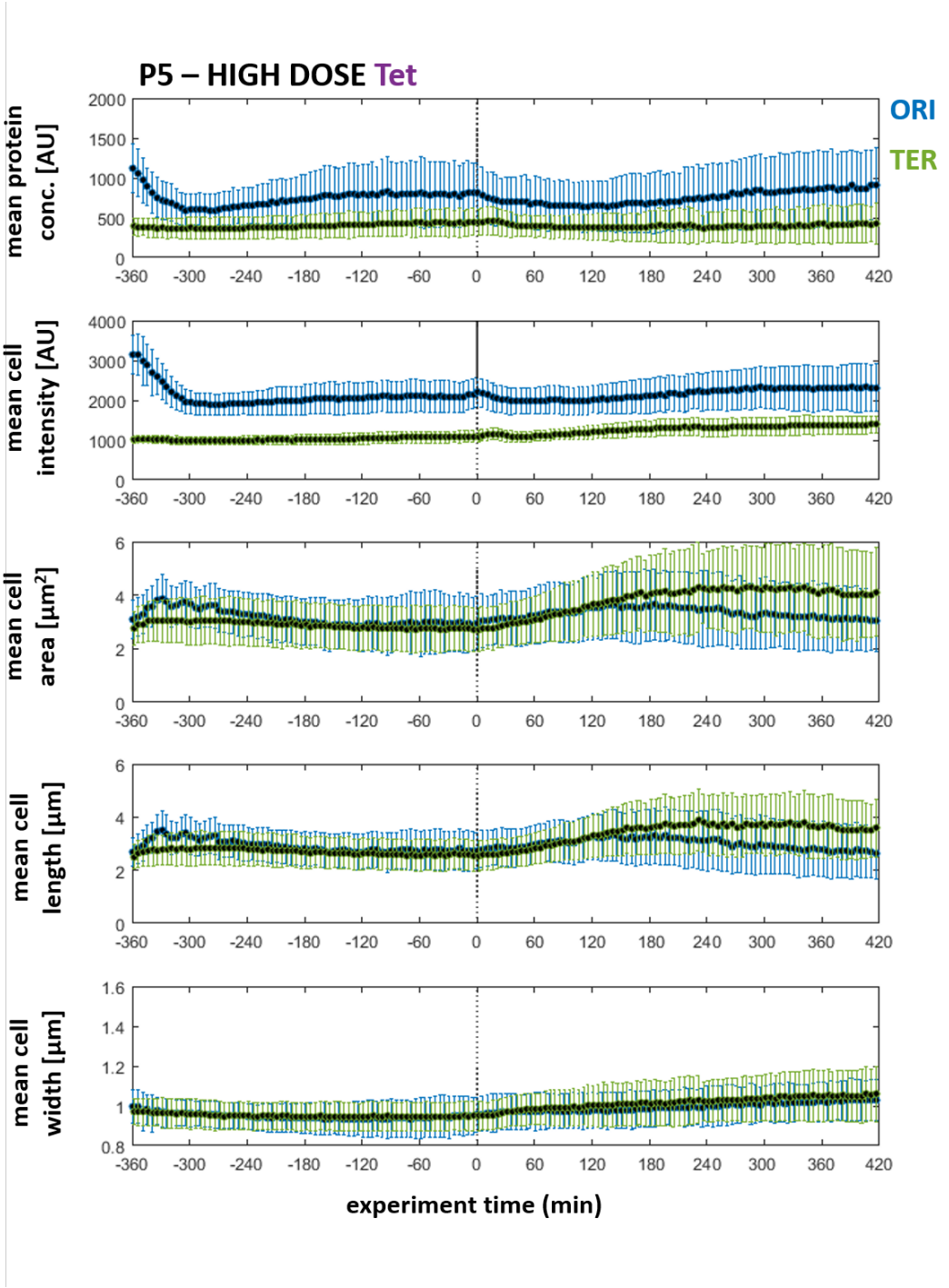

Fig. C16 **Response of the P5 strain to a high dose of tetracycline**. Absolute values of cell intensity, protein concentration, area, length, width, and count for all chromosomal positions are shown across full experiment time with standard deviations of the mean plotted as errorbars.

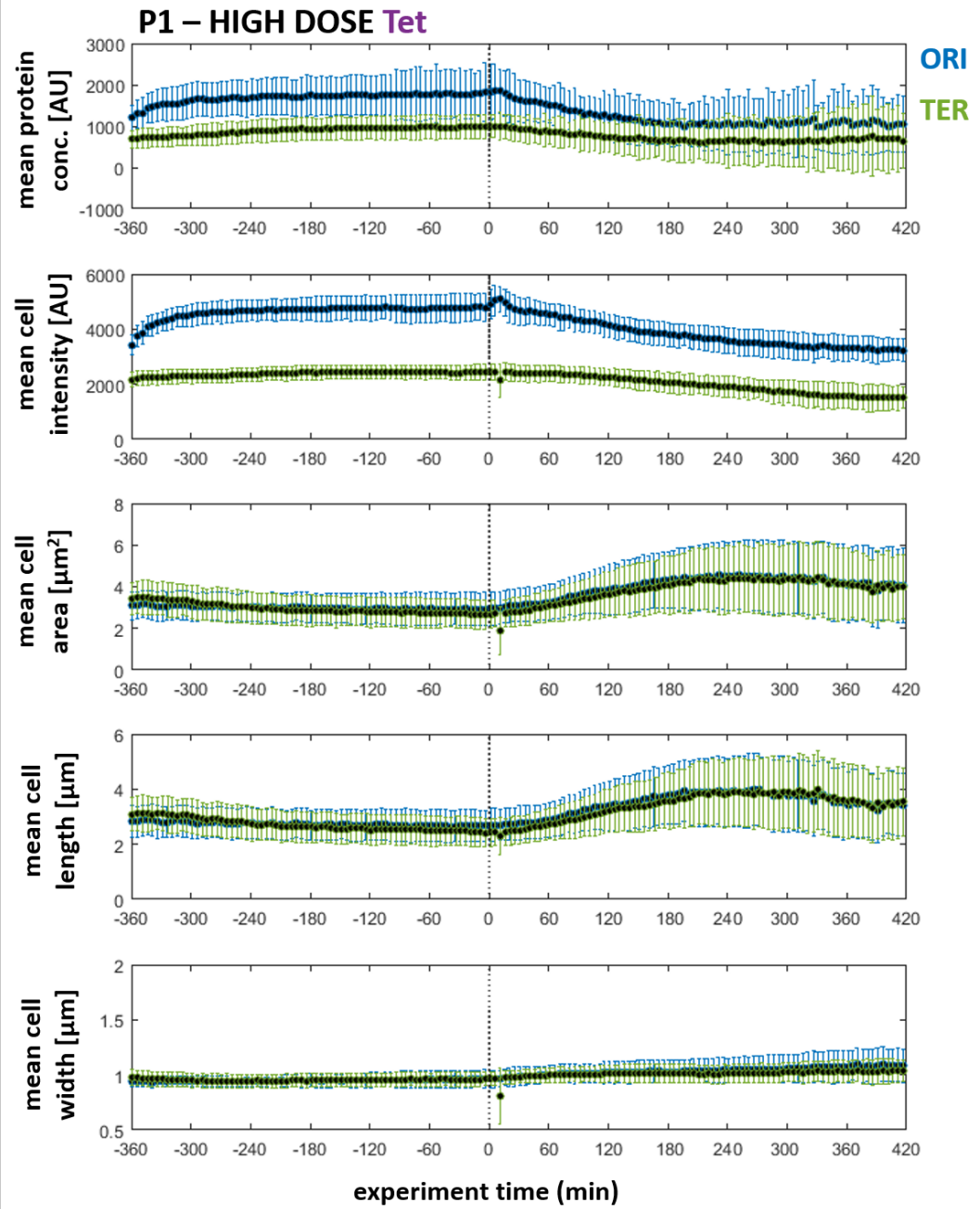

Fig. C17 **Response of the P1 strain to a high dose of tetracycline**. Absolute values of cell intensity, protein concentration, area, length, width, and count for all chromosomal positions are shown across full experiment time with standard deviations of the mean plotted as errorbars.

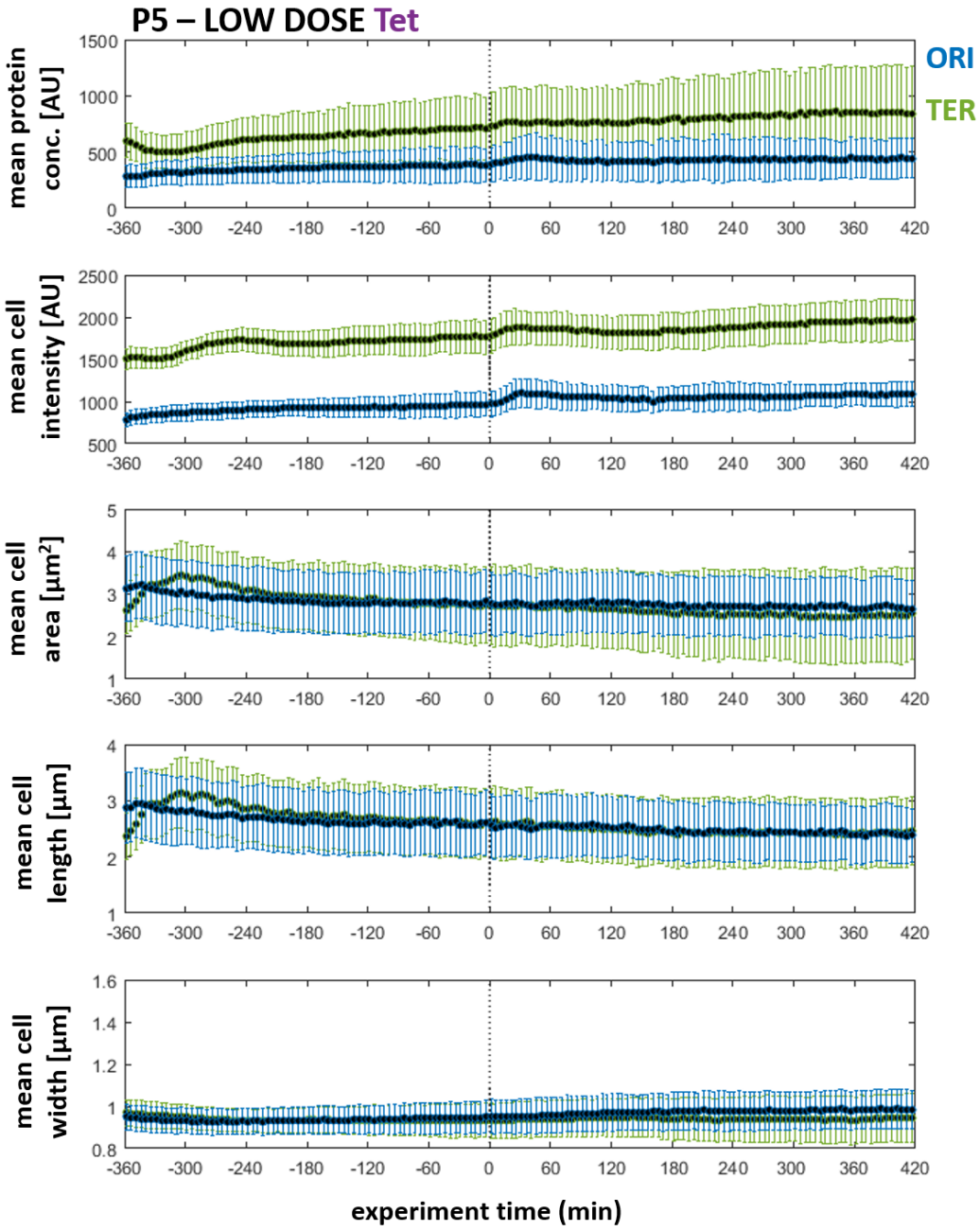

Fig. C18 **Response of the P5 strain to a low dose of tetracycline**. Absolute values of cell intensity, protein concentration, area, length, width, and count for all chromosomal positions are shown across full experiment time with standard deviations of the mean plotted as errorbars.

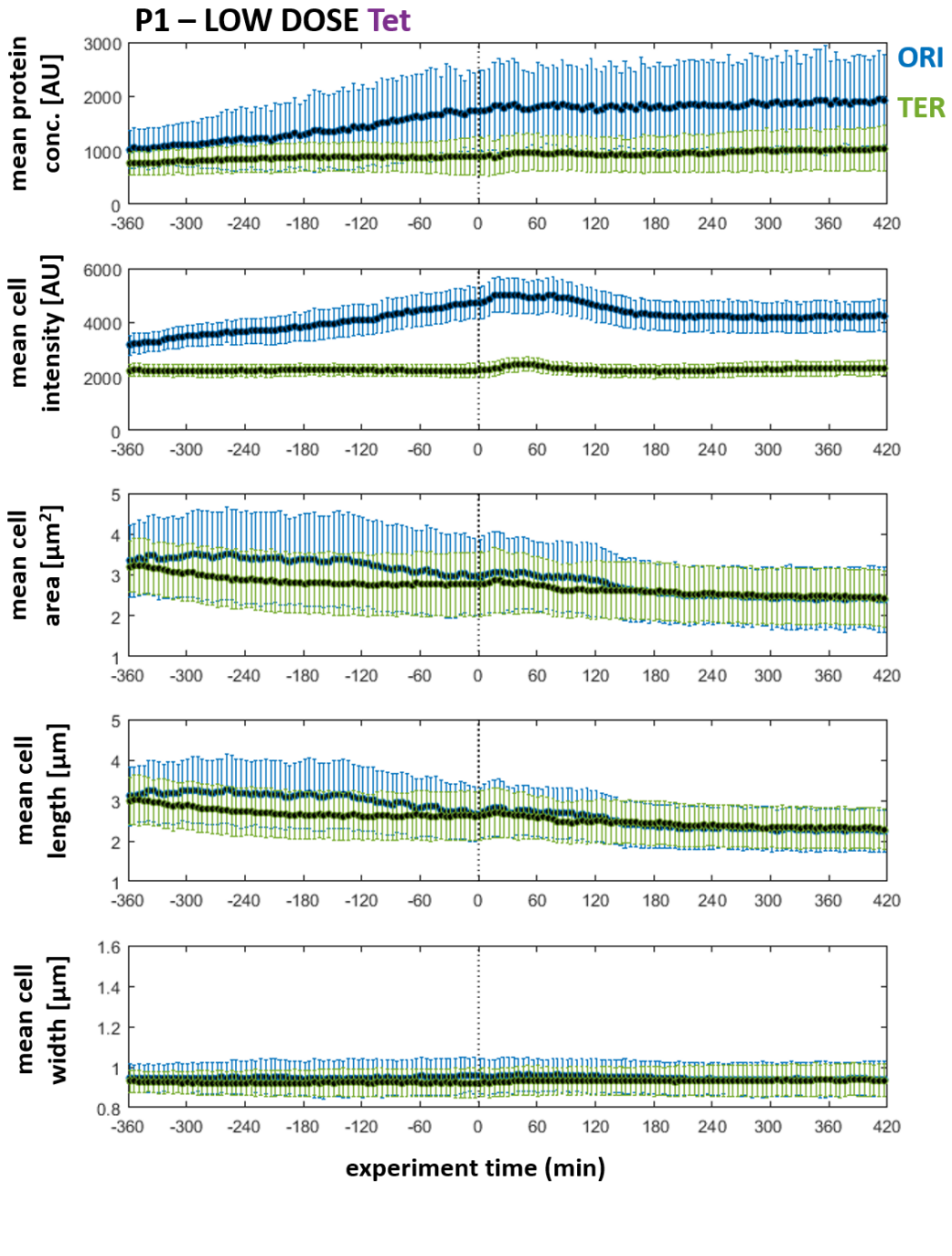

Fig. C19 **Response of the P1 strain to a low dose of tetracycline**. Absolute values of cell intensity, protein concentration, area, length, width, and count for all chromosomal positions are shown across full experiment time with standard deviations of the mean plotted as errorbars.

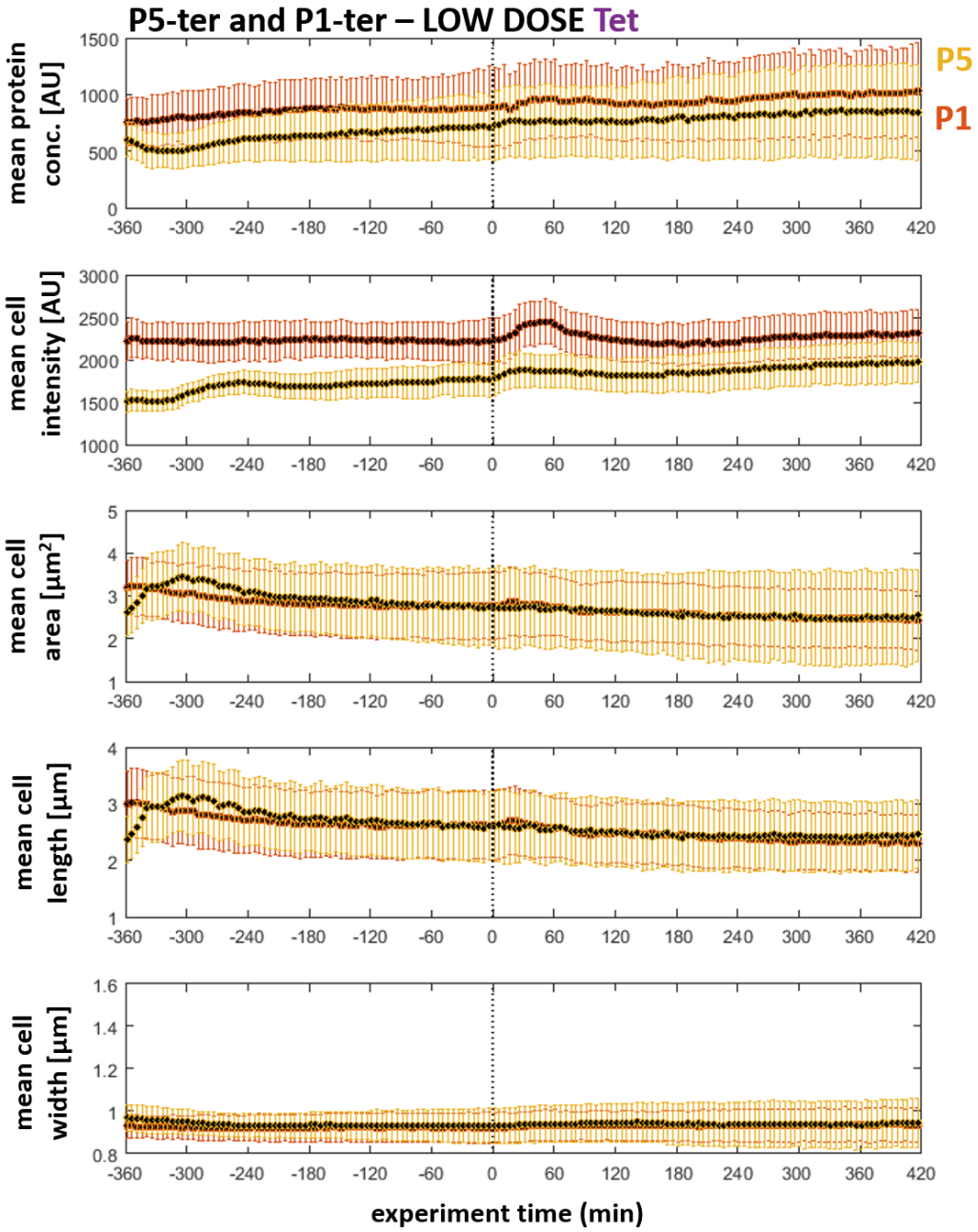

Fig. C20 **Response of the P5 and P1 strains with promoters in Ter positions to a low dose of tetracycline**. Absolute values of cell intensity, protein concentration, area, length, width, and count are shown across full experiment time with standard deviations of the mean plotted as errorbars.

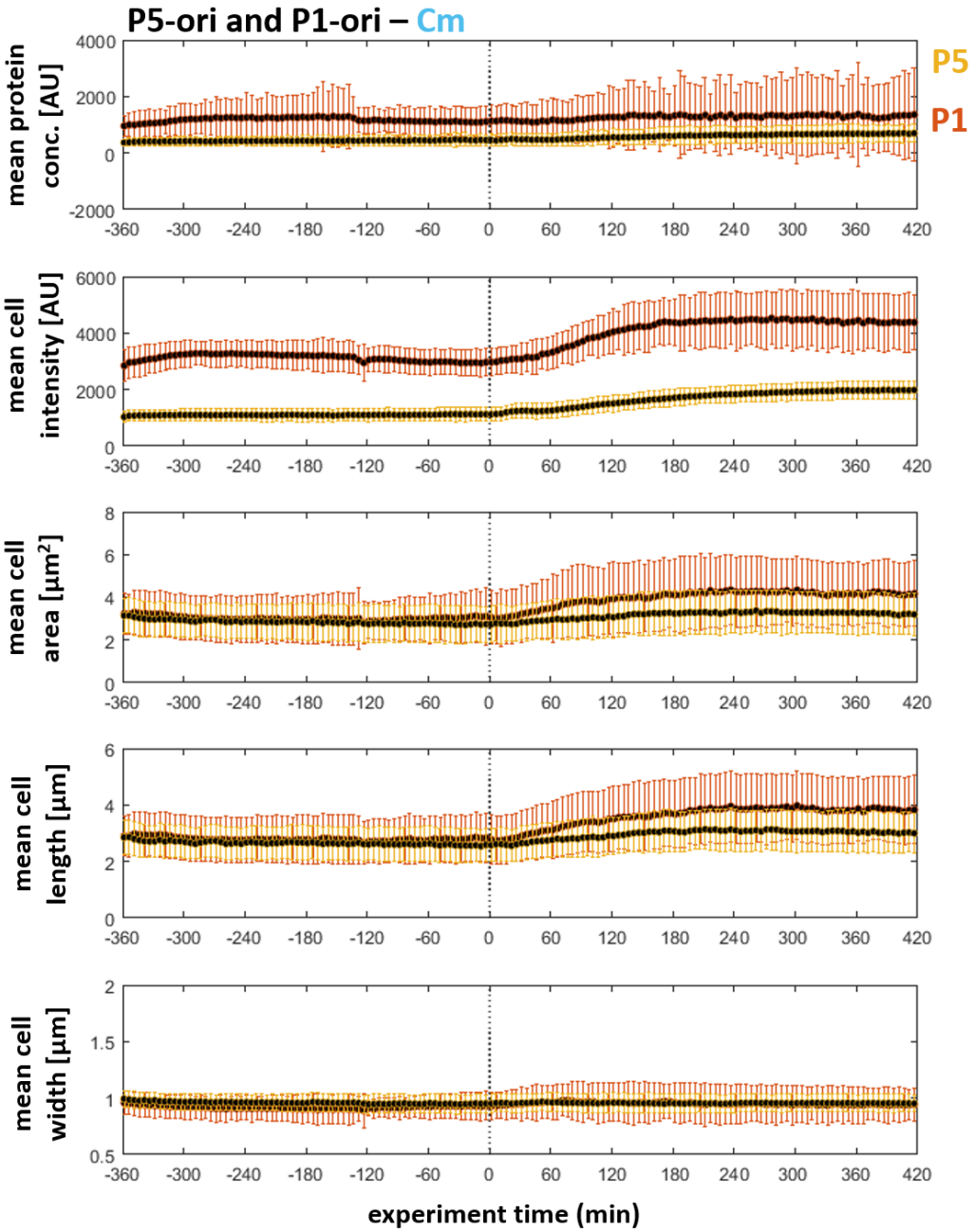

Fig. C21 **Response of the P5 and P1 strains with promoters in Ori positions to chloramphenicol**. Absolute values of cell intensity, protein concentration, area, length, width, and count are shown across full experiment time with standard deviations of the mean plotted as errorbars.

Appendix D

Work completed post PhD thesis submission

1. Growth condition dependent effects

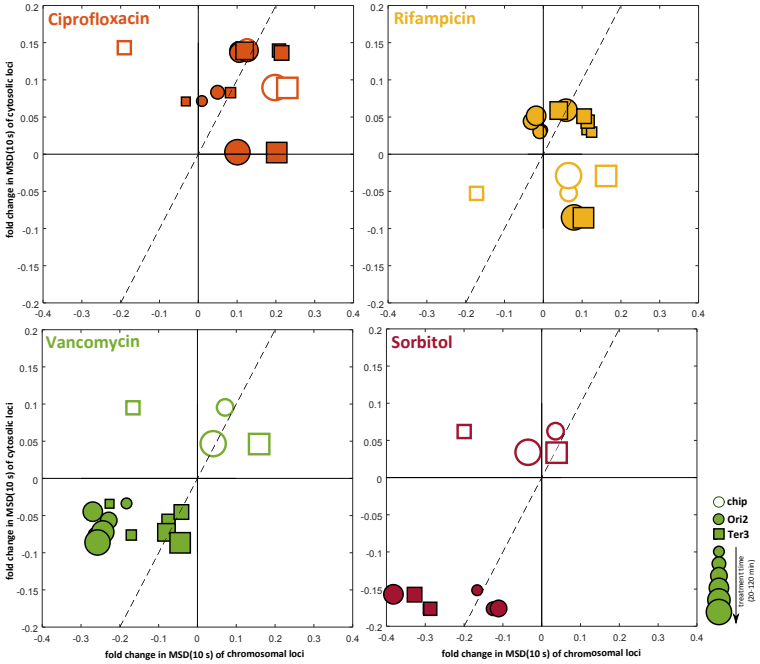

Fig. D1 **Dynamics responses to treatments measured on agarose pads and in microfluidic device are not consistent.** Fold changes in chromosomal Ori2 (*circles*) and Ter3 (*squares*) loci vs cytosolic aggregates μNS loci motility, defined as the logarithm of treated-to-control MSD(10 s)* ratios, are plotted for ciprofloxacin, rifampicin, vancomycin, and sorbitol (in different colours as indicated in the figure) for agarose pads (*solid* plot markers) and chip (*empty* plot markers) data for various treatment times (T_{treat} = 20-120 min for agarose pads and T_{treat} = 1 and 2 h for chip). Diagonal dashed lines represent gradient of 1.

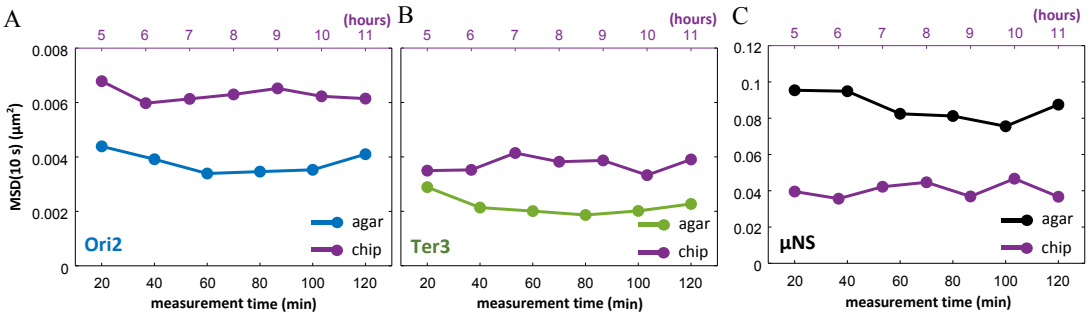

Fig. D2 **Marker dynamics is affected by the growth conditions.** Panels show mean MSD(10 s) of **(A)** Ori2 and **(B)** Ter3 chromosomal loci, and **(C)** cytosolic μNS aggregates for agarose pads (in *blue*, *green*, and *black* as labelled in panels) and the microfluidic device (in *magenta*) over measurement time (for agarose pads in min (*bottom* axes) and for microfluidic device in hours (*top* axes)). In microfluidic device, chromosomal loci show a small increase in MSD caused by a slightly higher temperature in this growth condition compared to agarose pads (due to less optimal temperature control in agarose pad experiments). Conversely, cytosolic μNS aggregates show a significant $\sim$2-fold decrease in MSD in the microfluidic device, likely due to cell compression by the walls of the micrchannels. Similar reduction in motility of the cytosolic μNS aggregates has also been observed recently by Yu *et al.* under 10 psi compression.

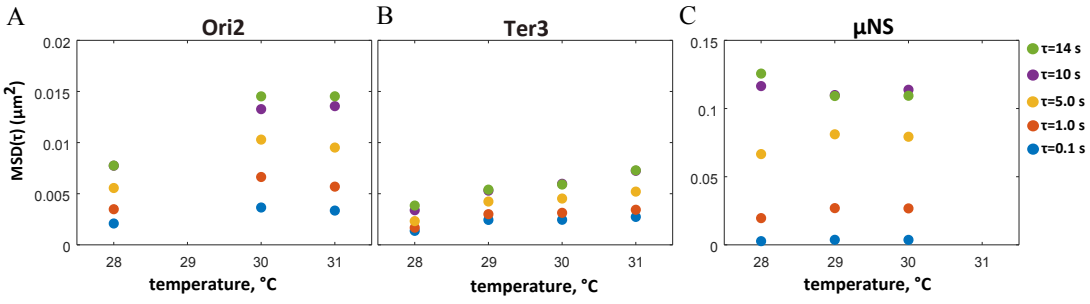

Fig. D3 **Motility of chromosomal loci and cytosolic aggregates generally increases as a function of temperature.** Each point represents the mean MSD of 100-260 makers for five different lag times.

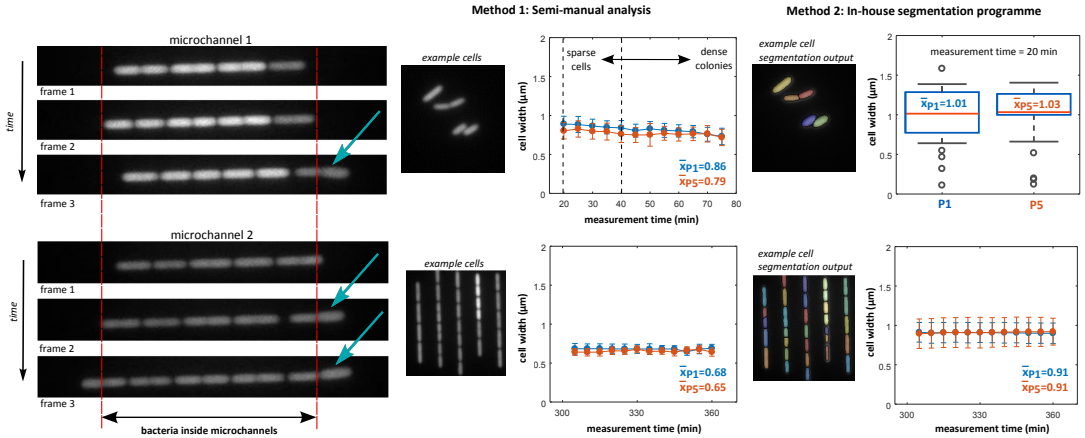

Fig. D4 **Bacteria in microfluidic device are systematically narrower compared to agarose pads.** (**A**) Three consecutive frames (5 min apart) showing images in the fluorescence mode of two example microchannels of a customised microfluidic device filled with exponentially growing *E. coli* bacteria (MG1655 rrnBP1-*gfp*). Cells leaving the microchannels (indicated with *blue* arrows) appear wider that those inside the microchannels suggesting that bacteria may be subjected to significant mechanistic forces when growing inside the microfluidic device. Mean cell widths were calculated for cells growing on (**B**) agarose pads (for first 20 min experiment before bacteria formed dense microcolonies) and (**C**) inside the microchannels of the microfluidic device (for the 6^{th} hour of experiment, after 5 h of equilibration inside the device). Two methods were used to determine widths of imaged cells: semi-manual (method 1) and in-house cell segmentation (method 2). For the measurement method details refer to Methods. When working with images of agarose pad micro-colonies, method 2 was applied to images acquired only at the initial measurement time point (T_{treat} = 20 min). While the first method systematically measures smaller widths, both methods show that mean width of cells grown in microfluidic deveice is smaller by ∼10% (method 1) and ∼20% (method 2) compared to widths of cells grown on agarose pads.

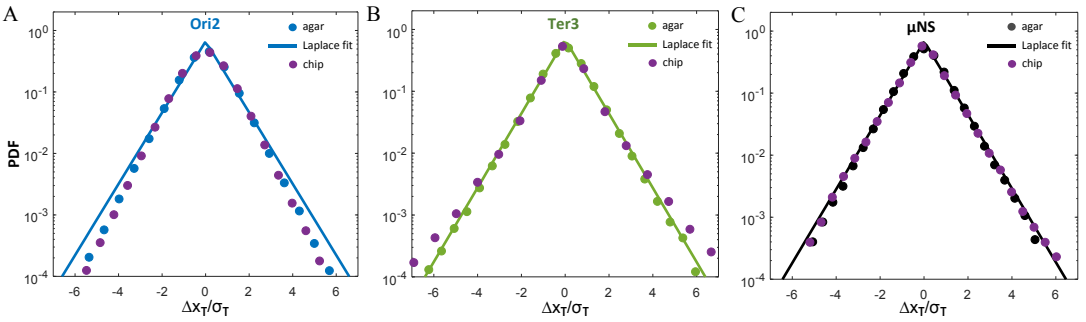

Fig. D5 **Step size distributions show evidence of cell compression inside microfluidic device.** Panels show normalised probability distributions of step sizes at τ=1 s along a fixed x-direction normalised by standard deviation for **(A)** Ori2 and **(B)** Ter3 chromosomal loci, and **(C)** cytosolic μNS aggregates, tracked on agar and in microfluidic device (*magenta*). Data is binned into an arbitrary number of 32 linearly spaced out bins; bins containing at least 50 steps are shown. The solid lines represent Laplacian fits of agar data. In microfluidic device, the fraction of longer steps increases (and the fraction of shorter steps decreases) for Ter3 and also – to some extent – for cytosolic μNS aggregates, suggesting significant cell compression in the microchannels. Similar effect on step-size distribution of cytosolic μNS aggregates has been observed recently by Yu *et al*. No characteristic effects on the step-size distribution of Ori2 markers was observed.

2. Crowding levels under treatment conditions measured in bulk

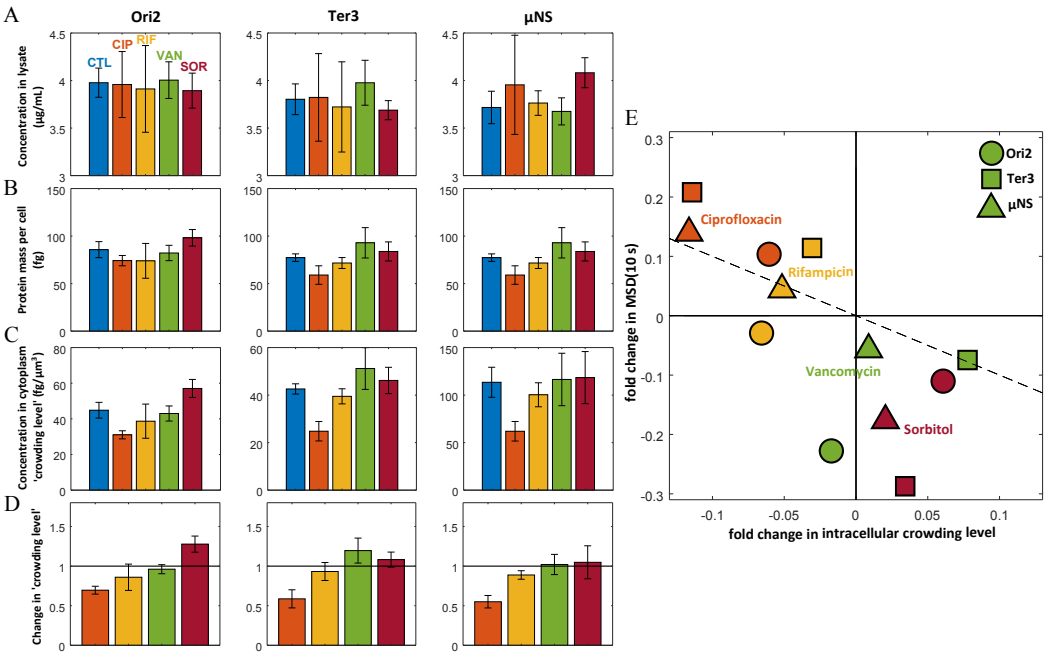

Fig. D6 **Treatment-induced changes to crowding levels of cytosol are consistent with dynamics responses.** **(A)** Total soluble protein concentration in cell lysate after 1 h of antibiotic treatment measured with Bradford test. Treatment conditions include: CTL, control (not treated); CIP, ciprofloxacin; RIF, rifampicin; VAN, vancomycin; and SOR, sorbitol. **(B)** Total protein mass per cell. Assuming 10^8 cells in culture of OD=1 and using mean cell volume calculated from the cell dimensions from microscopy images acquired in each condition after 1 h of treatment on agarose pads (Supplementary Materials, Figures B15 and B20), total number of cells in each sample was calculated to obtain total soluble protein mass per cell. **(C)** Total protein concentration as mass of protein per μm^3 of cell, representing the intracellular crowding level. Using total protein mass per cell and mean cell volume, protein mass per μm^3 of cell was calculated for each condition. **(D)** Change in the crowding level relative to the control (not treated) sample. Error bars represent standard deviation from the mean for 5 biological replicates (refer to Methods for details). **(E)** Scatter plot of the logarithm of fold change in MSD(10 s) after 1 h of treatment vs fold change in crowding levels for the three tested strains (Ori2, *circles*; Ter, *squares*; μNS, *triangles*) under the four treatments. The dashed diagonal line represents a gradient of -1. Changes to the crowding levels are generally consistent with the dynamics responses shown earlier (Figure 4.3). That is, marker motility is generally inversely proportional to the crowding level.

Appendix E

Work communications and completed courses

External communications

1. Gordon Research Conference: Chromosome Dynamics, 21-26 May 2017, Lucca (Barga), Italy (poster presentation)
2. Gordon Research Seminar: Chromosome Dynamics, 20-21 May 2017, Lucca (Barga), Italy (speaker)
3. ”BioPhysChrom2016: The Biology and Physics of Bacterial Chromosome Organization”, 5-8 September 2016, Collège de France, Paris, France (speaker)
4. IOP Topical Research Meeting: ”Physical Principles of Biological and Active Systems”, 6-7 January 2016, University of Edinburgh, Edinburgh, UK (speaker)
5. EMBO | EMBL Symposium: ”New Approaches and Concepts in Microbiology”, 11-14 October 2015, Heidelberg, Germany (poster presentation)
6. ”Emerging Methods and Technologies for Medical Research”, 1-2 September 2015, Karolinska Institutet, Stockholm, Sweden (poster presentation)
7. ”Physics of Microorganisms” Institute of Physics conference, 23 March 2015, London, UK (poster presentation)
8. ”Physics Meets Biology, Institute of Physics conference, 3-5 September 2014, Oxford, UK (poster presentation)

Internal communications

1. Biological and Soft Systems Research Day, Cavendish Laboratory, Cambridge, UK, 12 June 2015 (speaker)
2. BBSRC Doctoral Training Programme internal event, 17 November 2014, Cambridge, UK (poster presentation)

Educational events

1. ”MATLAB® Programming Techniques”, MathWorks® event, 14-15 July 2015, Cambridge, UK
2. ”MATLAB® for Data Processing and Visualization”, MathWorks® event, 13 July 2015, Cambridge, UK
3. ”Understanding the Physics of Life: Summer School”, 14-18 July 2014, Lancaster, UK